



University of Kentucky
UKnowledge

Theses and Dissertations--Plant and Soil
Sciences

Plant and Soil Sciences

2014

UNDERSTANDING THE ROLE OF MEMBRANE LOCALIZED UGT80B1 ENCODING FOR UDP-GLUCOSE: STEROL GLUCOSYLTRANSFERASE IN PLANT DEVELOPMENT

Meera Nair

University of Kentucky, meer.rocks23@gmail.com

[Right click to open a feedback form in a new tab to let us know how this document benefits you.](#)

Recommended Citation

Nair, Meera, "UNDERSTANDING THE ROLE OF MEMBRANE LOCALIZED UGT80B1 ENCODING FOR UDP-GLUCOSE: STEROL GLUCOSYLTRANSFERASE IN PLANT DEVELOPMENT" (2014). *Theses and Dissertations--Plant and Soil Sciences*. 54.
https://uknowledge.uky.edu/pss_etds/54

This Doctoral Dissertation is brought to you for free and open access by the Plant and Soil Sciences at UKnowledge. It has been accepted for inclusion in Theses and Dissertations--Plant and Soil Sciences by an authorized administrator of UKnowledge. For more information, please contact UKnowledge@lsv.uky.edu.

STUDENT AGREEMENT:

I represent that my thesis or dissertation and abstract are my original work. Proper attribution has been given to all outside sources. I understand that I am solely responsible for obtaining any needed copyright permissions. I have obtained needed written permission statement(s) from the owner(s) of each third-party copyrighted matter to be included in my work, allowing electronic distribution (if such use is not permitted by the fair use doctrine) which will be submitted to UKnowledge as Additional File.

I hereby grant to The University of Kentucky and its agents the irrevocable, non-exclusive, and royalty-free license to archive and make accessible my work in whole or in part in all forms of media, now or hereafter known. I agree that the document mentioned above may be made available immediately for worldwide access unless an embargo applies.

I retain all other ownership rights to the copyright of my work. I also retain the right to use in future works (such as articles or books) all or part of my work. I understand that I am free to register the copyright to my work.

REVIEW, APPROVAL AND ACCEPTANCE

The document mentioned above has been reviewed and accepted by the student's advisor, on behalf of the advisory committee, and by the Director of Graduate Studies (DGS), on behalf of the program; we verify that this is the final, approved version of the student's thesis including all changes required by the advisory committee. The undersigned agree to abide by the statements above.

Meera Nair, Student

Dr. Seth DeBolt, Major Professor

Dr. Arthur G. Hunt, Director of Graduate Studies

UNDERSTANDING THE ROLE OF MEMBRANE LOCALIZED UGT80B1
ENCODING FOR UDP-GLUCOSE: STEROL GLUCOSYLTRANSFERASE IN
PLANT DEVELOPMENT

DISSERTATION

A dissertation submitted in partial fulfillment of the
requirements for the degree of Doctor of Philosophy in the
College of Agriculture
at the University of Kentucky

By

Meera Nair

Director: Dr. Seth DeBolt, Professor of Plant Physiology/Biochemistry/Molecular
Biology

Lexington, Kentucky

2014

Copyright © Meera Nair 2014

ABSTRACT OF DISSERTATION

UNDERSTANDING THE ROLE OF MEMBRANE LOCALIZED UGT80B1 ENCODING FOR UDP-GLUCOSE: STEROL GLUCOSYLTRANSFERASE IN PLANT DEVELOPMENT

Sterols have been identified as major components of membrane lipids that are part of specialized membrane domains necessary for organizing events such as polar protein targeting and signal transduction in plants, fungi and animals. However a common modification of sterols is the addition of sugar moieties via glycosylation abundantly found in plants. An exact physiological role for such diversification of sterols in plants is still unknown. Using reverse genetics and transcriptomics we show that UDP-glucose: sterol glucosyltransferase encoded by UGT80B1 is necessary for correct epidermal patterning in *Arabidopsis* root. Patterning of hair cells (trichoblasts) and non-hair cells (atrachoblasts) in the epidermis of the *Arabidopsis* root involves signaling through SCRAMBLED (SCM), a plasma membrane localized LRR-RL kinase. Feedback regulation via the transcriptional regulatory complex containing R2R3-MYB transcription factor WEREWOLF (WER) represses *SCM* and activates the homeodomain-leucine-zipper protein GLABRA2 (GL2) in atrichoblasts. Evidence suggests symplastic connections between cells, known as plasmodesmata, establish passage ways for single-repeat R3-MYB transcription factors to activate *SCM* expression in trichoblasts. Mutations in *UGT80B1* cause atypical localization patterns of *GL2*, *WER*, and *SCM* in the root epidermis. The *ugt80B1* formed fewer trichoblasts in comparison to wild-type. A translational fusion of UGT80B1 to GFP localizes to the ER, plasma membrane and to sites that appear to be plasmodesmata-associated desmotubules. Ultrastructural analysis revealed abnormalities in plasmodesmata formation and morphology in *ugt80B1* mutants. Steryl glucoside profiling indicated deficiencies in specific glycosylated sterol compounds in roots. This study identifies UGT80B1 as a novel membrane component that is critical for plasmodesmata morphogenesis and cell-fate determination in the root epidermis. A model is proposed in which UGT80B1 activity provides spatially discrete sterol and steryl glucoside architecture within the plasma membrane to

anchor the SCM receptor and within plasmodesmata to facilitate intercellular movement of R3-MYB regulatory proteins underlying proper differentiation of trichoblasts versus atrichoblasts. Moreover, evidence from reverse genetics, proteomics and live cell imaging point to an actin dependent localization of UGT80B1 at the vesicle rich zone of root hair tip. This localization actively supports root hair elongation via tip growth, possibly by membrane modifications required for vesicle trafficking.

KEYWORDS: UGT80B1, Sterol Glycosylation, Epidermal
Patterning, Plasmodesmata, Symplastic
Continuum

MUTIMEDIA ELEMENTS USED: JPEG (.jpg); TIFF (.tif); VIDEO (.avi)

Meera Nair

Students Signature

12-15-2014

Date

UNDERSTANDING THE ROLE OF MEMBRANE LOCALIZED UGT80B1
ENCODING FOR UDP-GLUCOSE: STEROL GLUCOSYLTRANSFERASE IN
PLANT DEVELOPMENT

By

Meera Nair

Dr. Seth DeBolt

Director of Dissertation

Dr. Arthur G. Hunt

Director of Graduate Studies

12-15-2014

ACKNOWLEDGEMENTS

It is with deepest regard that I thank, my advisor and mentor Dr. Seth DeBolt for taking a chance on someone half way across the globe. I sincerely appreciate his time, effort and funding for this project and for me to live and continue my work in his lab. Most of all I appreciate the scientific discussions that we had and led to some breakthrough discoveries in the project. His motivation and positive energy is best described as infectious and gave me the courage to carry on my PhD work in the toughest of times. I commend him for setting an excellent example for my future as I embark on a journey towards becoming an educator and scientist.

It would have been impossible for me to finish this work without the consistent support and love from DeBolt lab group. First and foremost I would like to thank my dearest Jozsef Stork, our lab manager who is next to my kin in the Lab. Jozsef was there as I struggled through life situations and experiments that failed to work as a supportive shoulder and technical assistance. He enriched my experience in Kentucky through camping, fishing and long drives through country roads. The opportunity to see the scenic beauty in Kentucky will remain in my heart forever. My work would be incomplete if it hadn't been for the constant push from my friends, fellow lab members and fellow PhD students Andrea Sanchez and Chad Brabham. Being with them in lab and outside has been the best time of my life. I would like to thank my dear friend and fellow PhD student in Department of Horticulture, Sutapa Roy. She not only supported me mentally through some of my roughest times in life but also was my link to my Indian culture in a foreign land. They are part of my extended international family whom I will cherish for the rest of my life.

I would like to thank my committee members, Dr. Douglas Archbold, Dr. Sharyn Perry and Dr. Rebecca Dutch for ensuring that I achieve success in this endeavour and I would like to thank Dr. Hsin-Sheng Yang for being on my defense committee.

With regards to working with genetic crosses with epidermal patterning reporter lines, sterol reporter lines and lipid analysis that have added clarity and depth to the work, I would like to thank Dr. John Schiefelbein, University of Michigan and Dr. Kathrin Schrick from Kansas State University. They have not only contributed to the experimentation but have provided with fruitful discussions towards completion of this work.

I would also like to thank Mary Gail Engle, Jim Begley and Cindy Meier at the University of Kentucky Imaging center, for the assistance needed with ultrathin sections and transmission electron microscope. Without their expert knowledge and positive interactions this work would not be possible.

Pursuing a PhD has not only provided an impetus to learn more in science but also in life. As the member of Soka Gakkai Buddhist group, my degree has become part of my human revolution. And this human revolution is incomplete

without the love of my life Joseph Deas, whom I met while pursuing this PhD here in University of Kentucky. I thank him for being a compassionate individual and being patient with me through this strenuous process. I would like to appreciate the love and care he provides me and from time to time challenges my intellectual potential through introducing me to new ideas. As I extend my presence in this world through being with Joseph, I cannot help but mention our lovely pets that make me a complete human being. Stella who is our wonderful tabby cat gives us our daily dose of cuteness with mischief and Tamale, our bearded dragon whose presence is awesome enough.

Lastly I would like to thank my parents, Sobhana and Narayanan Nair for bringing me up as a liberated individual in a society that is oppressive towards women. They gave me the courage to look at myself as a contributing member to the society no matter what. They have supported me in all the pursuits in my life. I cannot help but feel indebted to them for being such loving parents and I feel honored to be their child. I would also like to thank my little sister Preeti Nair and for being so patient and forgiving to me for not being at her wedding as I was completing this dissertation. Thank you.

TABLE OF CONTENTS

Acknowledgements	iii
Table of Contents	v
List of Tables	xi
List of Figures	xii
List of Files	xiv
Chapter1: Introduction	1
1.1 Outline of this dissertation.....	1
1.2 Sterols.....	1
1.3 Steryl glycosides and sterol glycosyltransferases	3
1.4 Role of steryl glycosides	5
Membrane microdomains and steryl glycosides	5
Role of SGs in membrane fluidity and cold stress.....	7
Role of SG in stress induced signal transduction	8
SGs and neurodegeneration	8
SG and plant development.....	10
Proposed role of SGs in cellulose biosynthesis	10
1.5 Aims of this dissertation	11
Chapter 2: A complex role for membrane sterol glycosylation uncovered by global transcript analysis in the Arabidopsis mutant <i>ugt80B1</i>	13
2.1 Introduction.....	13
2.2 Results.....	14
Analysis of transcriptional change in <i>ugt80B1</i>	14
Functional Categorization of Differentially Expressed Genes	15
Differential genes expression linked to phenotypes of <i>ugt80B1</i>	24
Transcriptional and proteomic analysis of seed storage proteins in <i>ugt80B1</i>	26

Stress responsive gene expression and stress responsive UGT80B1 expression: assaying heat, cold and salt stress response using transgenic plants expressing <i>proUGT80B1::GUS</i>	27
2.3 Discussion	28
UGT80B1 and implicated its SG transport mediator for SSP, flavanoids, aliphatic monomers and stress response.....	29
Transcription factors and Cell Fate Patterning	31
2.4 Methods	35
Generation and growth of <i>Arabidopsis thaliana</i> plants and mutant <i>ugt80B1</i> line	35
Systematic and integrative analysis of genes responding to depletion of SG	36
Chapter 3: A Membrane-Associated UDP-Glc:Steryl Glucosyltransferase 80B1 (UGT80B1) is Required for Plasmodesmata Function and Morphogenesis Underlying Cell Fate Determination in the <i>Arabidopsis</i> Root Epidermis.....	37
3.1 Introduction.....	37
3.2 Results.....	39
Randomized cell files in <i>ugt80B1</i> roots	39
Aberrant expression of root epidermal cell TFs in <i>ugt80B1</i>	42
Subcellular localization defects of the SCM receptor in <i>ugt80B1</i> ..	44
UGT80B1 protein is localized to ER, PM and PD in root epidermal cells.....	45
Aberrant PD structure and morphology in <i>ugt80B1</i>	49
Sterol glucoside profiling reveals reduction of stigmasteryl glucosides in <i>ugt80B1</i> roots	53
3.3 Discussion.....	55
UGT80B1 is a novel membrane component required for epidermal cell fate in the root.....	55
Membrane modules at PM and PD are required for root epidermal patterning	56
<i>ugt80B1</i> mutants provide evidence for the role of plasmodesmata in the root epidermal patterning	57

Common mechanisms underlying epidermal patterning in the root and leaf	58
3.4 Methods	60
Plant material and growth conditions	60
Constructs	61
Laser scanning confocal microscopy and fluorescence stereomicroscopy	61
Plasmolysis	62
Quantification of epidermal patterning.....	62
Resin Embedding and Sectioning	62
TEM of 5-day-old Arabidopsis seedling roots.....	63
Global analysis of genes responding to <i>ugt80B1</i>	63
Lipid Extraction and Electrospray Ionization Tandem (ESI-MS/MS) Mass Spectrometry.....	63
Chapter 4: Steryl glycoside biosynthesis is necessary for sustained root hair growth during Arabidopsis development.....	65
4.1 Introduction.....	65
4.2 Results.....	66
<i>UGT80B1</i> is required for correct root hair elongation.....	66
<i>UGT80B1::GFP</i> localizes to the growing tip of root hairs	68
Perturbation of actin disrupts root hair development and pre-bulge localization of <i>UGT80B1</i>	74
4.3 Discussion	76
4.4 Methods and materials.....	78
Plant material and growth conditions	78
Constructs	78
Laser scanning confocal microscopy and fluorescence stereomicroscopy	79

Quantification of root hair phenotype	80
Drug treatments	80
Chapter 5: Membrane proteomics in steryl glycoside mutants reveals alteration in GPI anchored proteins.....	81
5.1 Introduction	81
5.2 Results and discussion	82
Proteomics analysis of UGT80B1 mutants.....	82
Identification of SG regulated membrane proteins using proteomics.....	88
5.3 Methods and Materials.....	93
Plant material and growth conditions	93
Total membrane protein extraction.....	93
Proteomics	94
LC-MS/MS Analysis	94
Chapter 6: Conclusion	96
6.1 SG is involved in membrane processes that rely on both symplastic isolation and symplastic continuum in plant cells.....	96
Appendix A: The involvement of J-protein AtDjC17 in root development in Arabidopsis.....	99
A.1 Introduction.....	99
A.2 Results	100
Mutations in <i>Atdjc17</i> caused altered organization of root hair position in atrichoblast versus trichoblast cell files	100
Visual examination of <i>proAtDjC17::GUS</i> transcript revealed localization to the stele cells.....	106
Transcript analysis reveals differential expression in root patterning genes in <i>Atdjc17-1</i> and <i>35S::AtDjC17</i> roots versus WT	107
Cortical and endodermal cell layers display aberrant divisions in <i>Atdjc17</i> but not in <i>35S::AtDjC17</i>	111
A.3 Discussion	112
A.4 Material and Methods.....	113

Plant material and Growth conditions.....	113
Genotyping of the mutant lines.....	114
Microscopy.....	114
Construction of reporter and overexpression lines. Selection and expression analysis of transgenic lines.....	115
Gene expression studies.....	115
Appendix B: Analyzing cellulose biosynthesis with confocal microscopy	119
B.1 Introduction.....	119
Vector selection.....	120
Promoter	120
Where to fuse your AFP: Amino (N), Carboxy (C) or internal.....	121
Choice of AFP.....	121
Transformation of your AFP fusion into a plant.....	122
B.2 Materials.....	122
Polymerase chain reaction (PCR) to amplify gene of interest with promoter and subcloning into an entry vector.....	122
Cloning of your gene of interest into a compatible destination vector to make AFP fusions and introducing this into the plant by <i>Agrobacterium</i> mediated transformation.....	122
SDS-Polyacrylamide gel electrophoresis (SDS-PAGE).....	122
Western Blotting for YFP	123
Imaging analysis	123
B.3 Methods.....	123
Polymerase chain reaction (PCR) to amplify gene of interest and subcloning into an entry vector	124
Cloning of your gene of interest with promoter into a compatible destination vector to make AFP fusions and introducing this into the plant by <i>Agrobacterium</i> mediated transformation	124
SDS Page and Western Blotting for detection of YFP in Plant Tissue.....	125
Preparation of plants for imaging.....	125
Imaging Analysis.....	126
B.4 Notes.....	126

Appendix C: UGT80B1 is enriched in detergent resistant membrane fraction..	129
C.1 Introduction	129
C.2 Results	129
C.3 Method for extraction of lipid raft	130
References	132
Vita	162

LIST OF TABLES

Table 2.1 Downregulated genes in <i>ugt80B1</i> , fold change expressed as wild-type versus <i>ugt80B1</i> . P-value<0.005	17
Table 2.2 Upregulated genes in <i>ugt80B1</i> , fold change expressed as <i>ugt80B1</i> versus wild-type. P-value<0.005.....	18
Table 2.3 Auxin responsive genes upregulated in <i>ugt80B1</i> P<0.1 based on T-TEST	24
Table 2.4 Upregulated genes putatively involved in Flavanoid biosynthesis in <i>ugt80B1</i>	25
Table 2.5 Upregulated ABC transporters in <i>ugt80B1</i> excluded for T-TEST at P<0.005 but included in P<0.01 in <i>ugt80B1</i>	31
Table 2.6 List of genes that are related to cell fate and patterning	33
Table 2.7 List of genes associated with plasmodesmata.....	34
Table 2.8 Circadian rhythm genes differentially regulated in <i>ugt80B1</i> versus wild-type.....	35
Table 3.1 Percentage emergence of hair and non-hair cells in H and N cell files for wild-type and <i>ugt80B1</i> alleles. Averages and SE are indicated for each genotype. Asterisk represents P<0.05 based on Mann Whitney U test, n=40.	41
Table 3.2 Number of root hairs, distance between adjacent root hairs and trichoblast cell areas in both <i>ugt80B1-1</i> and <i>ugt80B1-2</i>	42
Table 3.3 Pattern of the <i>GL2::GUS</i> expression in the root epidermis	44
Table 3.4 SG and ASG quantification in roots	54
Table 4.1 List of cytoskeleton genes upregulated in <i>ugt80B1</i> , P<0.01	78
Table 5.1 Differentially expressed spots from 2D gel comparison of Arabidopsis COL-O WT versus Arabidopsis 35S:UGT80B1 and <i>UGT80B1</i> KO	83
Table 5.2 Core list of proteins identified as steryl glycoside responsive in at least two biological replicate experimental datasets.....	87
Table 5.3 Core metrics for proteins identified as steryl glycoside responsive in at least two biological replicate experimental datasets	88

LIST OF FIGURES

Figure 1.1 Enzyme reaction catalyzing conversion of a sterol moiety into sterol glucoside	5
Figure 2.1 565 genes were differentially expressed in <i>ugt80B1</i> compared to wild-type.....	16
Figure 2.2 SDS-PAGE and MS results for identification of CRUCIFERIN	26
Figure 2.3 Effect of temperature variation and osmotic stress on <i>proUGT80B1::GUS</i>	28
Figure 3.1 <i>UGT80B1</i> expresses ubiquitously in Arabidopsis roots	40
Figure 3.2 T-DNA insertion alleles for <i>UGT80B1</i>	40
Figure 3.3 Mutations in <i>UGT80B1</i> cause aberrant epidermal root hair distribution	41
Figure 3.4 Localization of the <i>pGL2::GUS</i> , <i>pWER::WER::GFP</i> and <i>pSCM::SCM::GFP</i> reporter fusions in four-day-old <i>ugt80B1</i> versus wild-type roots	43
Figure 3.5 Localization of UGT80B::GFP reporter fusion in the root epidermis ...	46
Figure 3.6 Desmotubule localization of UGT80B::GFP reporter fusion in the root epidermal cells.....	47
Figure 3.7 Localization of UGT80B1::GFP reporter in four-day-old Arabidopsis cotyledon cells	48
Figure 3.8 <i>ugt80B1</i> mutant is impaired in PD morphology	51
Figure 3.9 PD phenotype is present in the <i>fackel</i> allele <i>fk-3158</i>	52
Figure 3.10 Steryl glucoside (SG) and asyl steryl glucoside (ASG) content in wild-type and mutant roots.....	54
Figure 3.11 Model illustrating membrane SG requirement for epidermal patterning	60
Figure 4.1 UGT80B1 is required for correct elongation of root hairs in Arabidopsis.....	67
Figure 4.2 GUS expression data: Histochemical analysis of β -glucuronidase....	68
Figure 4.3 Fluorescence localization of UGT80B1::GFP in Arabidopsis root by stereomicroscopy and laser scanning confocal microscopy	71
Figure 4.4 UGT80B1::GFP localization in epidermal cell types	73

Figure 4.5 Depolymerization of actin cytoskeleton perturbs pre-bulge and root hair tip localization of UGT80B1::GFP	75
Figure 5.1 2-dimensional gel electrophoresis (silver stain and false color overlay for protein identification) of the membrane proteome derived from wild-type and SG mutant genetic backgrounds	86
Figure 5.2 Cellular localization and quantitative assessment of SG responsive GPI anchored proteins identified by 2DGE	92

LIST OF FILES

Movie 3.1 UGT80B1:GFP localizes to the ER	48
Movie 3.2 UGT80B1:GFP labeled ER tubules show symplastic continuum	48
Movie 3.3 UGT80B1:GFP localizes as a punctate at the PM	48
Movie 3.4 UGT80B1:GFP labeled ER tubules show symplastic continuum during plasmolysis	49
Movie 4.1: Documents a time lapse confocal examination of Figure A1.3B	72
Movie 4.2: Fluorescence plot of the entire apical basal division between trichoblast cells	72

Chapter 1: Introduction

1.1 Outline of this dissertation

The overarching goals of this dissertation were to investigate the effect of membrane modifications via monoglycosylated sterols on plant development. Despite 30-50% of membrane sterols being glycosylated in plant membranes an obvious function in plant development is unknown. A developmental study on the effect of integral membrane lipid is laborious and difficult at best, however a sincere effort to understating steryl glycosides (SGs) in nature is made using Arabidopsis as a model organism. **Sections 1.2** until **1.4** explore the current status of literature, elucidating the various roles of SGs found in several organisms as well as the proteins encoding for UDP-glucose: sterol glucosyltransferase. **Section 1.5** discusses the aims of this dissertation.

Focus is placed on elucidating the role of UGT80B1 encoding for UDP-glucose: sterol glucosyltransferase in Arabidopsis and its SG. **Chapter 2** explores the genes and gene regulatory networks affected via mutations in *UGT80B1*, providing hints to a developmental pathway affected in *ugt80B1*.

Results of transcriptional data from **Chapter 2** revealed differential expression of epidermal pathway genes. Based on these results, **Chapter 3** provides evidence for the role of UGT80B1 in epidermal patterning via maintaining plasma membrane (PM) and plasmodesmata structure necessary for cell-to-cell communication for developmental pathways such as epidermal patterning. **Chapter 4** explores the role of UGT80B1 and SG in root hair tip growth. Furthermore, a role for SG and UGT80B1 in vesicle trafficking is explored in **Chapter 5** through proteins affected due to *UGT80B1* knockout and overexpression. Moreover, developmental role for SG via supporting a membrane structure for protein localization and vesicle trafficking is concluded in **Chapter 6**.

Appended into the dissertation work are chapters that emerged as a consequence of a broad screen to investigate the role of SGs and UGT80B1 in plant development via proteomics, transcriptomics, biochemical fractionation and live cell imaging. Each appendix chapter is a complete work in itself and adds to the wealth of knowledge for SGs. One of the appendix chapters has been published in peer-reviewed journal and another chapter forms a book chapter for Springer protocols "Methods in Molecular Biology" series "The Plant Cell Wall".

1.2 Sterols

The plasma membrane (PM) surrounding the protoplast is an essential component to the survival of all cells and allows the cell to communicate to the outside environment by forming a semi-permeable barrier. Phospholipids, glycerolipids and sterols are the characteristic components of all PMs. Despite the diverse variety of lipid species, the plant PM is enriched in sphingolipids and sterols forming lipid pools that give rise to structural as well as signaling lipid molecules (Furt et al., 2011). Sterol compounds are found as membrane lipids in many species of plants, mosses, fungi and animals (Esders and Light, 1972;

Haque et al., 1996; Mayberry and Smith, 1983; Murakami-Murafushi et al., 1987) Where ergosterol and cholesterol are the main sterol components of fungal and animal membranes respectively, plants possess diverse sterols and their derivatives. The divergence in basic membrane composition at the kingdom level implies a physical function for this adaptation.

Typical plant membrane sterols are isoprenoid compounds made of four condensed aliphatic rings hydroxylated at the C3 carbon and a hydrocarbon chain on C17 position. Sterols play a major role in morphogenesis, cell differentiation and patterning (Lindsey et al. 2003). Further, by live cell imaging, sterols have been shown to be central to the acquisition of cell polarity by modulating endocytosis after cell division in root cells of Arabidopsis (Men et al., 2008; Jaillais and Gaude, 2008) and can be divided into two primary metabolic fates; one branch forming sitosterol and stigmasterol, and the other branch forming campesterol and brassinosteroid. Sitosterol, stigmasterol and campesterol form the bulk of membrane sterols whereas brassinosteroid is the only known steroidogenic hormone in plants. An example of the complexity and non-linearity of the sterol pathway is demonstrated by the various mutants in the pathway (Carland et al., 2010; Diener et al., 2000; Schrick et al., 2002). Mutations in genes involved in sterol biosynthesis such as *FACKEL* (sterol-C-14 reductase), *CEPHALOPOD* (sterol methyltransferase), *HYDRA1* (sterol $\Delta 8$ - $\Delta 7$ isomerase) and *COTYLEDON VASCULAR PATTERN1* (C-24 methyltransferase) all were found to cause severe developmental phenotypes (Carland et al., 2002; Schrick et al., 2000; Schrick et al., 2002; Souter et al., 2002). The mutants accumulated unusual sterols with deficiency in sitosterols and non-compromised brassinosteroid levels. However the phenotypes demonstrated were not rescued by addition of sitosterols or brassinosteroid. These phenotypes can be explained by plant sterols having roles analogous to cholesterol in animals. An interaction between cholesterol and protein such as the interaction between HEDGEHOG protein and cholesterol was shown for patterning and development in embryogenesis and growth in animals (Porter et al., 1996; Simpson et al., 2009). A similar role in plants is expected of sterols for protein-lipid interaction for plant development (Lindsey et al., 2003; Jang et al., 2000). This is further exemplified by the presence of steroidogenic acute regulatory protein (StAR)-related lipid transfer or START domain containing proteins in plants (Schrack et al., 2004). These domains are conserved among animals and plants and have been shown to function in animals by binding to cholesterol and regulating downstream signaling in mammals (Ponting and Aravind, 1999; Schrick et al., 2004). Members of the class of proteins containing the homeodomain-leucine zipper (HD-ZIP) domain have been known to contain START domains in Arabidopsis and are likely candidates for sterol or lipid binding (Schrack et al., 2004). Some members of this class have been implicated in maintaining embryogenesis, plant morphogenesis especially the meristems and epidermal patterning (Prigge et al., 2005; Kubo et al., 1999; McConnell et al., 2001; Rerie et al., 1994; Ohashi-Ito and Fukuda, 2003). This is further augmented by the suggested overlap in some of the phenotypes in sterol mutants and the mutants of the *HD-START* family of

genes (Carand et al., 2010; Prigge et al., 2005). However a comparison between the phenotypes and restricting the function of sterol moieties as possible protein ligands undermines its complexity and that of the sterol metabolic pathway.

1.3 Steryl glycosides and sterol glycosyltransferases

Among the various sterol derivatives the most abundant are steryl glycosides (SG) with 33-50% of total sterols in plants being SGs (Bush and Grunwald, 1974; Potocka and Zimowski, 2008). First discovered as 'ipuranol' from the bark of olive tree and *Ipomoea purpurea* (Power and Tutin, 1908; Power and Salway, 1913), SGs are membrane sterols that have sugar attached to the 3 β -hydroxy group at the C3 position. SGs are regarded as pathway end products, as *in vitro* experiments showed maximum glycosylation with sitosterol and 22-oxycholesterol (Potocka and Zimowski, 2008). Apart from end product sterols a few intermediates can be glycosylated albeit at lower rates. However *in vitro* experiments with purified steryl glycosyltransferases from various plant species have come to a common consensus about planar sterol backbone requirements by the glycosylating enzyme. Accordingly maximum glycosylation is acquired with typical sterol molecules with the C3 atom hydroxylated and hydrocarbon attached at C17. Apart from that there are double bond requirements in ring B, with higher rates of glycosylation with Δ -5 sterols than Δ -7 sterols. Furthermore saturated sterols, Δ -25 sterols and sterols that carry methyl groups at C4 atom are poor substrates for glycosylation (Wojciechowski and Von Uon, 1975; Potocka and Zimowski, 2008; Grille et al., 2010). These *in vitro* experiments also brought forth the requirement for a nucleoside diphosphate sugar as the sugar donor, where UDP-glucose has been found to be the best sugar donor along with UDP-galactose, TDP-glucose and CDP-glucose (Wojciechowski et al., 1979; Warnecke et al., 1997; Potocka and Zimowski, 2008). Although the most common sugar observed is D-glucose, sugars such as D-mannose, D-galactose, L-rhamnose, D-xylose, D-ribose, D-glucuronic acid and D-xyluronic acid have been observed in lower abundance (Wojciechowski, 1991; Kovganko and Kashkan, 1999). Although rare in occurrence, SGs with di-, tri-, and tetraglucoside residues have also been reported (Kojima et al., 1989). SGs can be acylated, polyhydroxylated or sulfated, however acylation with fatty acid attachment to the C6 position of the attached sugar moiety with palmitic acid or linoleic acid as the most common fatty acids to form acylated SGs (ASGs) are the most common modifications (Lepage, 1964).

The biosynthesis of SG is catalyzed by the membrane-bound UDP-glucose:sterol glucosyltransferase that attaches a sugar moiety to the 3 β -hydroxy group at the C-3 carbon atom on sterol (Warnecke and Heinz, 1994; Wojciechowski, A. and Zimoski, J. 1975) (**Figure 1.1**). Hou et al. (1968) first showed glycosylation of β -sitosterol with UDP-glucose in plants using a crude particulate preparation from soybean seeds. The enzyme responsible for glycosylation is membrane bound as solubilization with non-ionic detergent such as Triton X-100 in the case of *Calendula officinalis* (Wojciechowski and Von Uon, 1975), *Sinapis alba* (Wojciechowski et al., 1979), maize coleoptiles (Ullmann et

al., 1993) *Solanum tuberosum* leaves (Zimowski, 1992) and eggplant leaves (Potocka and Zimowski, 2008); whereas n-octyl- β -D-thioglucopyranoside in the case of etiolated oat shoots (Warnecke and Heinz, 1994) was achieved along with an increase in activity from 20-12500 fold. An inhibition of the reaction by UDP and the end product steryl glycoside as well as phospholipids dependence of UDP-glucose:sterol glucosyltransferase is shown in above mentioned studies. Purification of sterol glucosyltransferase enzyme from etiolated oat seedlings by Warnecke and Heinz (1994) resulted in the identification and functional expression in *Escherichia coli* of genes encoding for the enzyme from *Avena sativa* and *Arabidopsis thaliana* (Warnecke et al., 1999). *Arabidopsis thaliana* gene identified was named *UGT80A2* following the nomenclature for the glucosyltransferases UGT family (Mackenzie et al., 1997; Mackenzie et al., 2005; Ross et al., 2001; Warnecke et al., 1999). Following the completion of genome sequencing for *Arabidopsis*, a second gene named *UGT80B1* was identified (DeBolt et al., 2009). Both *UGT80A2* and *UGT80B1* genes have 14 exons and 13 introns, with *UGT80B1* showing 61.5% amino acid similarity and 51.2% amino acid identity to *UGT80A2* (DeBolt et al., 2009). Apart from genes in *Arabidopsis* and *Avena sativa*, three putative genes in *Oryza sativa* and five in *Physcomitrella patens* have been identified (Grille et al., 2010).

Consisting of 54 families and spanning multiple organisms from bacteria to humans, glucosyltransferases are enzymes that utilize an activated sugar to transfer glycosyl moieties to various non-carbohydrate small molecules such as proteins, lipids and sterols (Paquette et al., 2003). Sterol glucosyltransferases belong to glucosyltransferase family 1 or GT1 that is a subfamily under the UDP glucosyltransferase family (UGT) (<http://www.cazy.org/>). Phylogenetic analysis of all the UGTs found in different organisms included members from *Arabidopsis* genome. *Arabidopsis* has 120 members that are UGTs with 112 full-length genes and the rest are regarded as putative. Phylogenetic analysis with protein sequences resulted in plants dividing into three clades, with the majority falling in one clade and two minor clades that included *UGT80A2* (Ross et al., 2001; Paquette et al., 2003). Being a feature of eukaryotic membranes *UGT80A2* was expected to group with fungal UGTs that also glycosylate sterols (*UGT51* and *UGT52* (Warnecke et al., 1999)) (Paquette et al., 2003). The lack of homology with fungal UGTs was concluded as specialization of SG function in plants (Paquette et al., 2003). Moreover considering the abundance of sterol glucosyltransferase in plants compared to other organisms where sterol glucosyltransferase is found only in a few instances and being the only membrane bound enzyme in the GT1 family, a specialization of SGs in plants cannot be denied. Members of the UGT family including the plant family have a conserved PROSITE consensus motif (Li et al., 2001). Apart from the PROSITE consensus motif, a Putative Secondary Plant Glucosyltransferase (PSPG) motif exists that is unique to plant UGTs (Hughes and Hughes, 1994). This PSPG motif is thought to bind activated sugar and transfer it to sterol moiety. Furthermore, conserved amino acid residues in the PSPG motif essential to its function were identified in sterol glucosyltransferase from *Solanum* species by Potocka and Zimowski (2008). In plants subcellular fractionation of *UGT80A2*

activity has indicated that these enzymes are commonly distributed in the plasma membrane (PM), Golgi vesicles, the endoplasmic reticulum (ER) membrane and occasionally the tonoplast (Palta et al., 1993; Uemura and Steponkus, 1994; Ulmann et al., 1993). UGT80B1's activity in SG biosynthesis was characterized genetically (DeBolt et al., 2009). It has also been reported that a UDP-glucose-dependent glucosylceramide synthase localized on the apoplastic side of the plasma membrane from cotton is capable of synthesizing SG in plants (Hillig et al., 2003).

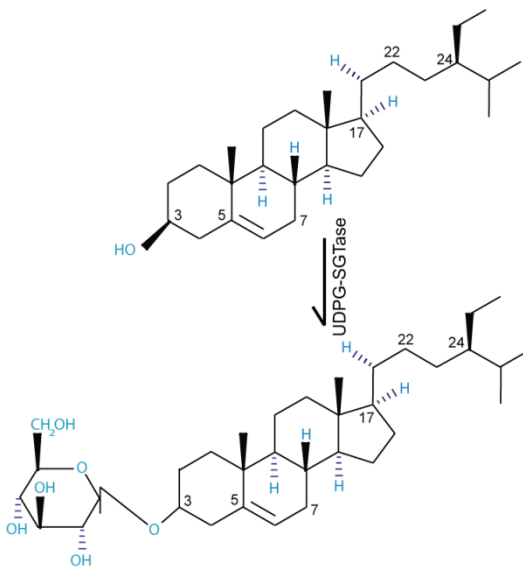


Figure 1.1 Enzyme reaction catalyzing conversion of a sterol moiety into sterol glucoside UDP-glucose: sterol glucosyltransferase (UDPG-SGTase) (abbreviation adapted from Warnecke and Heinz, 1994) catalyzes the addition of a sugar moiety to the 3 β -hydroxy group of C3 carbon atom of sterol backbone. Typical sterol moiety consists of four condensed aliphatic rings.

1.4 Role of steryl glycosides

Membrane microdomains and steryl glycosides

Singer and Nicholson (1972) gave a gross explanation of how the cell membranes are structured. Described as the “fluid mosaic model” where lipids and globular proteins form a two-dimensional liquid with proteins free to diffuse and form certain interactions with lipids. However, recent evolution in the study of membrane biology suggests heterogeneity of biological membranes arising from differential properties of lipids it consists of. Lipids in biological membranes exist in a constant state of exchange between liquid ordered and disordered phases. Depending on the hydrocarbon chain length and saturation levels certain lipids have a tendency to reside in liquid ordered or disordered phase. This property also decides the transition temperature of gel to liquid crystalline state of the biological membrane as deduced from experiments with artificial membranes.

Saturation of phospholipid chains allows the tight packaging of membranes and thereby increases the gel to liquid crystalline temperature (Brown and London, 1998). Taking into account the complexity of biological membranes, cholesterol (or membrane sterols in case of plants), sphingolipids and phospholipids with saturated and unsaturated hydrocarbons make up the membrane. Due to the structure of cholesterol molecules, the mixing of phospholipid and cholesterol allows the tight packing of the membrane thereby forming liquid ordered phases or domains among the liquid disordered phases formed mainly by the phospholipids with unsaturated hydrocarbons that allows for a kink in the structure of the phospholipid molecule thereby allowing loose packaging (Brown and London, 1998; Simons and Toomre, 2000). Lipid rafts, also defined as detergent insoluble membranes (DIMs) or detergent resistant membranes (DRMs), are *in vitro* biochemical counterparts to liquid ordered phases or domains mentioned above and emerged as a possible explanation to the asymmetry in the lipid species in the apical and basal membranes of the bilayer (Simons and Ikonen, 1997, Lingwood and Simons, 2010).

Lipid rafts are defined as small 10-200nm heterogeneous structures that are highly dynamic and are enriched in sterols and sphingolipids (Pike, 2006). Biochemical fractionation based on their insolubility in non-ionic detergents such as Triton-X 100 under cold conditions led to naming of lipid rafts as DRMs or DIMs. Due to the low density of DRMs, they are further isolated by floating on a density gradient (Simons and Ikonen, 1997). Although, Shogomori and Brown (2003) argue that the insolubility of DRMs does not come as a surprise, since detergents solubilize the membranes by inserting themselves within the membrane bilayer. Tight packaging of ordered domains rich in sphingolipids and sterols do not allow insertion of detergent molecules thus making them insoluble. Thereby as the detergent solubilizes the rest of the disordered domains, the ordered domains are left out which are floated on density gradients.

Sterols and SGs are components of the plant cell membrane architecture. The distribution of sterols and SGs in the membrane may be of functional significance. A thorough lipid analysis for instance, of detergent resistant membranes (DRM) from higher plants such as tobacco (*Nicotiana tabacum*) and *Arabidopsis thaliana* revealed enrichment of sterols (Borner et al., 2005; Mongrand et al., 2004). Furthermore, characterization of DRM composition in *A. thaliana*, *N. tabacum* and Leek (*Allium ampeloprasum* var. *porrum* (L.)) membranes showed that SGs were significantly enriched in DRM fractions (Mongrand et al., 2004; Laloi et al., 2007; Lefebvre et al., 2007). Thus it is plausible that like sterols, SGs may further diversify membrane architecture. Previous studies have analyzed the proteomic element of DRMs. Peskan et al. (2000) extracted DRMs from tobacco and showed an overlap of proteins studied previously from mammalian cell types, namely GPI-anchored proteins and heterotrimeric G proteins. DRMs and their functional significance in the cell membrane are looked upon with caution. This is partly due to the extraction procedures involved in extracting microdomains from cell membranes. It was pointed out as early as the idea emerged in early 1990's that sterols and

sphingolipids have the tendency to clump together under cold conditions and detergent treatment (Borner et al., 2005; Simons and Ikonen, 1997; Bhat and Panstruga, 2005; Grennan, 2007; Kierszniowska et al., 2009). Studies performed in plant cells on DRMs have been using these conditions to report associated proteins however the actual dependence on sterols for these proteins is missing (Kierszniowska et al., 2009). Thus, Kierszniowska *et al.* (2009) depleted the cells of sterols using a drug methyl- β -cyclodextrin used in animal systems to deplete cholesterol to study raft-associated proteins. They found no differences in the signaling proteins in contrast to previous studies but an enrichment of cell wall associated, lipid modifying and vesicular transport proteins in sterol-enriched lipid rafts. These data leave a need to characterize proteins associated with the membrane in a genetic background where a putative DRM enriched component was altered.

Role of SGs in membrane fluidity and cold stress

Association of sterols and SG with plant DRMs raises a question on its functionality for membrane property and physiological implications for plant adaptation. Membrane fluidity is often associated with the ability for membranes to adapt to cold conditions as membrane bilayer toggle between the states of liquid ordered and liquid disordered state as discussed in previous section. A definitive answer to the effects of plant sterols on membrane fluidity is difficult to conclude based on the existing literature as contradictions arise in these reports. Different methods to test such an effect involved exogenous addition of plant sterols on plant tissues or the introduction of plant sterols in artificial membrane vesicles and then testing membrane permeability based on methods such as electrolyte leakage. Studies such as the one conducted by Grunwald (1971), where barley roots from etiolated seedling were used to measure the effect of free sterols, steryl esters and steryl glycosides on the permeability of membrane based on ethanol induced electrolyte leakage. Exogenously added cholesterol and campesterol reduced the permeability of barley root membranes while stigmasterol, sitosterol and cholesterol glucoside were ineffective in changing the permeability of the membrane. This was concluded to be due to structural interference caused due to a large group such as the glucoside in cholesterol glucoside at the C-3 carbon and ethyl group in stigmaterol and sitosterol at C-24, making it difficult for these molecules to penetrate effectively into the phospholipid.

However, *In vitro* studies involving lipid membrane vesicles that have sitosterol, SG or ASG added show contrasting results. Perhaps, as pointed out by Grille et al., (2010) this is due to differences in composition of lipids in the membrane vesicles being tested. An example of the effect of different lipid compositions is illustrated in study by Halling et al., (2008) where cholesterol glycosides were as effective as cholesterol in increasing the order of bilayers made of palmitoyl oleoyl phosphatidyl choline (POPC); however when bilayers are made of sphingomyelin, in contrast to cholesterol alone cholesterol glycoside is unable to increase the order of these bilayers when temperatures are above

phase transition temperature for gel to liquid crystalline phase. The authors attributed it to the fact that POPC lipids have highly ordered acyl chains. In a similar study both free sterols and SGs reduced the fluidity of membranes made of phosphatidylcholine by increasing the order however less efficiently as free sterols (Muramatsu et al., 1994). In contrast Mudd and McManus (1980) concluded that SGs increase the fluidity of membrane consisting of dipalmitoyl lecithin. Thus, the effect of SGs on membrane property and fluidity remains inconclusive.

Due to the speculation of the involvement of sterols in membrane fluidity and permeability (Schaller, 2003; Warnecke et al., 1999; Warnecke and Heinz, 1994) and the phospholipids dependence of UDP-glucose:sterol glucosyltransferase (Bouvier-Nave et al., 1984), it has been postulated that SGs may have a role in adaptation to temperature stress (Palta et al., 1993). A difference in the proportions of glycosylated versus acylated sterols were reported in two different Solanaceous species under the same cold acclimation experiment (Palta et al., 1993). The study seemed inconclusive since one species showed that an increase in SG was correlated with decreased ASG and in the other SG and ASG levels did not change with temperature. Using *ugt80A2*, *ugt80B1* and double knockout mutants in Arabidopsis, considerable effort was spent looking for hypersensitivity to cold stress, but based on electrolyte leakage, and morphological differences as quantitative measures no response to temperature shock was determined (DeBolt et al., 2009).

Role of SG in stress induced signal transduction

Changes in SG levels in response to heat stress induction in *Pysarum polycephalum* (slime mold) (Murakami-Murofushi et al., 1987, Kunimoto et al., 2000) suggested that SG may have a dedicated role in signal transduction Tabata et al., (2008). Studies on human fibroblast cells show rapid activation of heat shock protein 70 (HSP70) occurred upon treatment with steryl glycosides (Kunimoto et al., 2000). However, it was unclear whether the sterol or glycosides was active in inducing the activation of HSP70 proteins when exogenously added to the fibroblast cells. The inconsistency with this model is that SGs are not mobile signaling agents since they are invariably membrane structures (Warnecke et al., 1997, 1999, Lefebvre et al., 2007); additionally, in comparison to normal sterols, SG and ASG exchange more slowly between the monolayer halves of a bilayer (Warnecke et al., 1997). Alternatively, this opens a new avenue where indirect affect of SG via its membrane presence through supporting specific membrane proteins can be explored.

SGs and neurodegeneration

Interestingly, in the same study where exogenously added SGs induce HSP70 activation in cultured neuron cells (Tabata et al., 2008); the authors also discovered dose dependent neuronal cell death. Similarly their *in vivo* study in mice uncovered a similar phenomenon where spinal cord sections reveal neuronal death and increase in CASPASE-3 protein labeling in neurons that is a

cell death activated protease. Furthermore, consumption of seeds of the cycad palm (*Cycas micronesica*) containing high SG levels have been linked to unusual human neurological disorder, ALS-Parkinsonism dementia complex (ALS-PDC) in the people of Guam (Khabazian et al., 2002; Tabata et al., 2008). Laboratory mice fed SGs faithfully produce either ALS or Parkinsonism pathologies (Ly et al., 2007). However, SG is a dominant moiety of all plant membranes, and some of the most widely consumed plant products in the United States, for example soybeans (*Glycine max*), have concentrations well within the dose range of cycad. Some studies have postulated that populations such as Japan, Kii Peninsula and West New Guinea, where high incidence epicenters for ALS-PDC occur are linked to dietary dependence on SG containing foods such as udamame and soybean proteins (Karamyan and Speth, 2008).

As data remains lacking in the manner in which SG crosses the blood brain barrier (Tabata et al., 2008), alternative reasoning to a direct link between SG and neurotoxicity can be imagined. Neurodegenerative diseases, ALS and PD are characterized by selective loss of specific neurons. PD is characterized as loss in dopaminergic neurons which manifests itself with muscle rigidity, tremors and slowed movement. While, ALS characterized as loss in motoneurons leads to progressive muscle wasting. Like all neurodegenerative disorders these disorders are caused due to accumulation of misfolded proteins in neuronal cells (Turturici et al., 2011). Heat shock proteins (HSPs) are molecular chaperones that assist cells in proper folding of proteins and are induced naturally in response to injuries including neurodegeneration. An elevation in the levels of HSP70 has been seen with ALS and PD pathologies in neurons (Chen and Brown, 2007; Chow and Brown, 2007). In the alternative reasoning SG causes induction of cellular stress via signal transduction due to its membrane presence. In the alternative reasoning neurotoxicity is not necessarily due to SG directly, but rather a consequence of a buildup of misfolded proteins because of the onset of cellular stress. The induction of HSP70 represents a secondary effect where molecular chaperones are induced as a consequence of cellular stress. In support of this reasoning, Kunimoto et al., (2000) found upregulation of HSP70 in human fibroblasts cells upon treatment with SG, indicating the involvement of SGs in stress response.

Furthering our interest in SG and neurodegenerative disorders is the speculation that human pathogen *Helicobacter pylori* can cause neurodegenerative disorders (Ly et al., 2007; Schulz et al., 2006). Although a conclusive answer to this speculation has not been found, nevertheless *Helicobacter pylori* is an interesting human pathogen with the ability to elude host immune system and causes gastric ulcers and carcinoma (Wunder et al., 2006). Although *Helicobacter pylori* requires cholesterol (Testerman et al., 2001) for survival, it lacks the ability to produce cholesterol and thus depends on the gastric mucosal epithelial cells where it colonizes for the cholesterol (Schreiber et al., 2004). *Helicobacter pylori* possesses *HP0421* encoding for cholesterol- α -glucosyltransferase that glycosylates cholesterol using α -glycosidic bonding (Lebrun et al., 2006) as compared to β -glycosidic bonding in other

organisms (Grille et al., 2010). Although unclear, this difference in glycosylation was suggested to protect *Helicobacter pylori* from phagocytosis antigen presenting cells (APCs) by avoidance of T-cell activation and thus avoiding an immune response by the human body (Bouic et al., 1996; Grille et al., 2010; Wunder et al., 2006).

SG and plant development

Using *ugt80A2*, *ugt80B1* single mutants and *ugt80A2 ugt80B1* double mutants, DeBolt et al., (2009) showed marked defects perhaps arising due to aberrant cellular elongation. Defects were marked in embryogenesis whereby torpedo through bent cotyledon stages displayed marked dwarfing. However, these changes were limited to embryogenesis and mature plant displays only minor growth phenotypes. Conversely the authors also found depletion of cutin and suberin from the seed coat and transparent testa phenotype in the seeds. It should be noted that the defects were more prominent in *ugt80B1* single mutants and double mutant than *ugt80A2* mutant alone. Although both genes encode for UDP-glucose: sterol glucosyltransferase, they seem to spacially differ in function yet seem to overlap in some. This is evident in promoter GUS fusions for *UGT80A2* and *UGT80B1* (DeBolt et al., 2009; Grille et al., 2010). Using TEM data as well as lipid monomer analysis on seed coat cells of the *ugt80B1* and double mutants, the authors (DeBolt et al., 2009) speculate a defect in membrane integrity leading to a defect in transport of lipophilic monomers from the cytoplasm of epidermal cell to the apoplast outside as well as transport and storage of flavanoids in the epidermal cell of seed coat in *ugt80B1* and double mutants. Since ATP binding cassette (ABC) transporters such as the ABCG12/CER5 and ABCG11/WBC11 transport cuticular wax in epidermal cells of Arabidopsis (Pighin et al., 2004; Panikashvili et al., 2007; McFarlane et al., 2010). Simultaneously considering the membrane presence of SGs and the speculative function of membrane in supporting transporters for lipophilic monomers; a specific ABC transporter responding to a depletion in *ugt80B1* and thereby SGs could be responsible for seed phenotypes observed for *ugt80B1*. Results from Choi et al., (2014) conclude that ABC transporters ABCG9 and ABCG31 transport SGs from tapetum to pollen coat. A depletion in either *ABCG9* *ABCG31* or *ugt80A2 ugt80B1* lead to incomplete pollen coat deposition, furthermore in *abcg9 abcg31* SGs were reduced to more than half of wild type levels leading to a conclusion that ABCG9 and ABCG31 transport SGs to pollen coat. However considering the DRM aspect of SGs and the presence of transporters in DRM fractions (Peskan et al., 2000) it could be that depleting ABC transporters from DRM causes a collapse in the general structure of DRM in Arabidopsis. Further work will elucidate the exact function of SGs in transport of lipophilic monomers in Arabidopsis.

Proposed role of SGs in cellulose biosynthesis

An alternative role for SGs was proposed based on a laborious study of cellulose synthesis in herbicide-treated cotton fibers. These authors found that SG co-purified with cellulose fragments (Peng et al., 2002), leading to

speculation that SGs act as a primer for cellulose biosynthesis in higher plants (Peng et al., 2002). In support of the hypothesis, SG biosynthesis was reported to be pharmacologically inhibited by the known cellulose biosynthesis inhibitor 2-6-dichlorobenzonitrile (DCB) (Peng et al., 2002) which could be reversed by addition of SG, thus suggesting that DCB inhibited cellulose synthesis by inhibiting SG synthesis. Further genetic studies that knocked out single *UGT80B1* and *UGT80A2* genes as well as the combination double mutant have been unable to show any tangible link between cellulose biosynthesis and the SG pool despite a dramatic decrease in SG levels (DeBolt et al., 2009). Through the use of live cell imaging and YFP::CESA6 in Arabidopsis, DeBolt et al., (2007) show that following DCB treatment there is a hyperaccumulation of non-motile CESA at the plasma membrane which appears as punctae in the images which were taken as time averaged projections of 61 frames spaced 5 seconds apart. The result by Peng et al., (2002) that exogenous addition of SG could reverse the inhibitory effect of 25 μ M DCB in cotton fibers, was repeated by DeBolt et al., (2007) using YFP::CESA6. However even after using a range of DCB concentration, 0.5 to 25 μ M and 7-21 μ M of SG there was no difference in particle velocity. It is likely that the effects of DCB on cellulose synthesis were so rapid that the turnover of SGs would need to be very fast to account for the effects of DCB on cellulose synthesis (DeBolt et al., 2007).

Schrack et al. (2002; 2004) reported that sterol biosynthesis mutants *fackel*, *hydra1* and *sterol methyltransferase1/cephalopod* have reduced levels of cellulose. Since SGs are downstream products in the sterol pathway, whether the cellulose deficiency in sterol mutants was due to SG deficiency was not inferred. Although an accumulation of unusual sterols was suggested to cause deficiency in cellulose in sterol mutants (Schrack et al., 2000; Schrack et al., 2012). An attempt to biochemically characterize cellulose synthase (CESA) enzyme led to the observation that specific lipid environment is necessary to maintain CESA activity *in vitro* (Schrack et al., 2012) as detergents used to extract CESA from PM leads to loss in its activity (Delmer, 1999; Bessueille and Bulone, 2008). The recent identification of cellulose biosynthetic machinery in sterol rich detergent resistant membranes (DRM) suggests sterols may support cellulose biosynthesis through their role in DRM formation (Bessueille et al., 2009). This could also be true for SGs, as SGs further enrich DRM fractions in plant membrane. However further work needs to be done to prove an actual association of CESA proteins with SG enriched DRM fraction.

1.5 Aims of this dissertation

The overall aim of this dissertation was to elucidate the physiological role of SG in plant development. SGs are abundant membrane lipid in plants (Hartmann and Benveniste, 1978) and are enriched in DRM fractions or microdomains in PM (Mongrand et al., 2004; Laloi et al., 2007; Lefebvre et al., 2007). As DRMs in plants support the localization of certain membrane proteins (Kierszniowska et al., 2009), thus in our working model SG is a diversification element of the plant membrane that directly or indirectly regulates a suite of

metabolic processes from the transcriptional to structural level. Consequently, it was expected that membrane proteins that specifically require SG for their membrane localization could be discovered. Furthermore, a physiological role for SG dependent membrane protein could be uncovered.

Reverse genetics, proteomics, transcriptional and biochemical approach were used utilizing *ugt80B1* knockout mutant and *UGT80B1* overexpression lines to investigate this hypothesis. Moreover, *UGT80B1*:beta-glucuronidase (GUS) promoter fusions and green fluorescent protein (GFP) fusion lines were generated to provide a range of molecular genetics tools to study SG functionality. Whole genome transcriptional array and 2-D proteomics pieced together molecular events associated with *UGT80B1*. As biochemical data on UGT80B1 enzymatic reaction is lacking, an effort to understating which SG species are affected in *ugt80B1* has been made via LC-MS technique. Moreover, genetic crosses with reporter lines and TEM were utilized to amalgamate molecular events from transcriptional data to discover a mechanism via which UGT80B1 and its SG play a role in plant development.

Chapter 2: A complex role for membrane sterol glycosylation uncovered by global transcript analysis in the *Arabidopsis* mutant *ugt80B1*

2.1 Introduction

Sterols are abundant isoprenoid derived compounds found across kingdoms from mammals to bacteria (Dufourc, 2008). Sterols form part of membrane microdomains and modulate membrane properties such as fluidity and permeability (Schaller, 2003; Carland et al., 2010). All eukaryotic cells start sterol biosynthesis from the mevalonate pathway, however plants add complexity and diversity to the biosynthetic steps to create a suite of sterol moieties (He et al., 2003). Where cholesterol and ergosterol are sterol moieties in mammals and yeast respectively, 61 sterol moieties have been identified in maize seedlings (Guo et al., 1995). What separates plants from other organisms is the ability to first cyclize its starting substrate 2,3-oxidosqualene and further metabolize intermediary compounds to get obtusifoliol (He et al., 2003; Schaller, 2003). The key to plant sterol pathway is the branch point where 24-methylene lophenol is converted to 24-ethylidene lophenol. These two create branch points for the production of 24-methyl sterols and 24-ethyl sterols, where 24-ethyl sterols form the majority in plants (Schaller, 2003). In *Arabidopsis* three key enzymes have been uncovered facilitating the addition of a methyl group called sterol methyltransferase (Diener et al., 2000). The positioning of these enzymes in the pathway is vital as SMT1 encoding for sterol methyltransferase 1 is in the beginning of the pathway converting cycloartenol to 24-methylene cycloartenol. SMT2 and SMT3 encoding for sterol methyltransferase 2 and 3 respectively position themselves at the above mentioned branch point (Diener et al., 2000; He et al., 2003; Schaller, 2003). The branch for 24-methylene sterols gives rise to membrane sterols stigmasterol and sitosterol whereas 24-ethylene branch point gives rise to another minor membrane sterol campesterol and phytohormone brassinosteroid (Husselstein et al., 1996; Bouvier-Navé et al., 1997; Nes et al., 1999). Brassinosteroids play an important role in postembryonic development via cellular expansion and morphogenesis, thus mutations in genes that lead to brassinosteroids result in dwarf syndrome in plants (Schaller, 2003; Carland et al., 2010). Sterols were considered as having a role in membrane structural organization as depleting sterols has structural consequences on PM microdomain fractions (Roche et al., 2008; Hartmann and Benveniste, 1978). However with the studies on mutants in sterol pathway such as *hydra2/fackel*, *hydra1*, *smt1*, *smt2/cvp1* and *smt3* both embryonic and postembryonic developmental roles, for sterols in plants have been discovered (Jang et al., 2000; Schrick et al., 2000; Schrick et al., 2002; Souter et al., 2002; Souter et al., 2004; Diener et al., 2000; Carland et al., 2002). It is imperative to note that mutants mentioned above have a depletion in different sterols as well as brassinosteroids (*hydra2/fackel* and *hydra1*) that cannot be overcome via supplementing these compounds externally, thus pointing to a specific role of different sterol moieties in plants. One such example is the requirement of a specific ratio of sitosterol to campesterol for reproduction in plants (Benveniste, 2004). Although an exact mechanism of sterol action in plant development is not

known, mutants in the pathway hint to altered gene expression and hormonal response (He et al., 2003; Souter et al., 2002). Mutations in *SMT2/CVP1* and *CPI* lead to defective PIN protein endocytosis and polar localization (Men et al., 2008). Reverse genetics has established developmental defects associated with mutations in sterol biosynthetic genes and the genes that it affects, an exact mechanism of different sterol species in plants similar to the role of cholesterol and HEDGEHOG (HG) signaling for cell proliferation and growth in animals is not known (Duman-Scheel et al., 2002). However, Schrick et al. (2004) report the evolutionary conservation of steriodogenic acute regulatory-related lipid transfer protein (START) domain (Ponting and Aravind, 1999) proteins in animals and plants suggesting a possibility of lipid/sterol binding for function. Protein examples of START containing domains are transcription factors of the homeodomain-leucine zipper class (HD-ZIP) acting in the developmental pathway in plants. Well known examples include *GLABRA2* (*GL2*) involved in epidermal patterning in leaves and roots of *Arabidopsis*, *PHABULOSA* (*PHB*) and *PHAVOLUTA* (*PHV*) involved in radial patterning in *Arabidopsis* shoots (Szymanski et al., 1998; McConnell et al., 2001). Additionally, expression for genes responsible for cellular expansion or division (*TCH-4*, *Meri-5*, β -*TUBULIN* and *KORRIGAN*) were distinctly affected in different sterol and brassinosteroid mutants (He et al., 2003). Thus, suggesting the relevance of different sterol species having specific functions for plant development.

Using reverse genetics DeBolt et al. (2009) revealed the consequences of depleting SGs via mutation in *UGT80B1*. The most dramatic phenotypes of the *ugt80B1* are evident in the developing embryo and testa (DeBolt et al., 2009). These symptoms result in slower radical emergence in the developing seedling, but are no longer evident 7 days after germination. The aim of this study was to understand how the plant responded to removal of the most abundant membrane sterol derivative via transcriptomics.

2.2 Results

Analysis of transcriptional change in *ugt80B1*

Ten day old *ugt80B1* seedlings were used for transcriptional profiling. We used the Affymetrix ATH1 GeneChip to compare the expression profiles of wild-type and *ugt80B1* plants. Total RNA from the seedling samples was used in all microarray experiments. The simple experimental design whereby mutant sample were compared with wild type samples involved RNA extraction which was hybridized, processed, and scanned in parallel. LOESS normalization using the mean across the chips as the baseline (Dudoit and Fridlyand, 2002) was applied directly to the probe data because of its higher reproducibility (Chu et al., 2006). After normalization, the correlation coefficients of perfect match probes between chips ranged from 0.89 to 0.98, with a mean value of 0.93. The expression data was exported to Microsoft Excel and analyzed by T-TEST and the resulting *P* values were used to determine a false discovery rate (Storey and Tibshirani, 2003). Genes with signal intensity values that suggested genes were absent in

both mutant and wild-type were removed. The stringency of the P value was varied between 1 and >0.005 to identify responsive transcripts with varied statistical constraints. The goal of this filter was the removal of false positives within the dataset. Based on 2 –fold shift in gene expression to qualify as differentially expressed with no statistical limitation there were 583 RNAs differentially expressed in *ugt80B1* versus wild-type Arabidopsis seedlings in our experimental system. Of the 583 differentially expressed genes, 83 RNAs were reduced and 500 were elevated in *ugt80B1* relative to wild-type. Using a P value cutoff of 0.1 there were 85 genes downregulated and 480 genes upregulated in the mutant relative to wild-type. Using a P-value of 0.01 this number fell to 41 downregulated and 283 upregulated genes. Using a P-value of 0.005 as a cutoff we identified 38 genes that were differentially downregulated and 202 genes that were upregulated in the mutant based on 2-fold gene expression from wild-type plants. Hence, by knocking out UGT80B1 in seedlings of Arabidopsis a total of 240 genes were differentially expressed relative to wild-type using the most stringent statistical cutoff.

Functional Categorization of Differentially Expressed Genes

To gain insight into the differences between categories, genes were grouped into annotation classes based on putative function. The classifications were produced using homology to known gene functions and GO terms for biological processes and each category was compared with the total number of annotations in each category. Genes were broken into 19 categories: metabolism, photosynthesis, protein modification and processing, circadian rhythm, flavanoid biosynthesis, metal chelators, cell fate and patterning, P450's, embryogenesis, transposons, transcription factors, stress response genes, hormone regulatory genes, signaling, transport/trafficking, cytoskeleton, cell wall, lipid membrane/storage and SG responsive genes of unknown function. Genes were functionally categorized prior to T-Test refinement and after P-value <0.005 refinement (**Table 2.1-** Downregulated and **Table 2.2-** Upregulated). The proportion of genes that fell into each category among upregulated genes highest for SG responsive genes of unknown function (14%) and signaling (14%), followed by stress response (11 %), cell wall (10 %), transport and trafficking (8%), lipid membrane processing (7%), transcription factors (7%), and hormone associated transcripts (7%)(**Figure 2.1A**). Downregulated genes, which generally had 6 fold fewer genes in total, displayed the highest proportion of genes among the stress response category (18%), signal transduction (18%), lipid membrane processing (with several genes annotated as lipid raft protein)(12%), SG responsive genes of unknown function (8%) and cell wall associated transcripts (7%)(**Figure 2.1B**). Several functional categories, such as hormone regulation and cell fate and patterning, had fewer genes among each category, but may play a role in regulating numerous genes. Among the genes functionally categorized as hormone associated, *auxin response genes* and *IAA-amido synthetase* were up and down regulated respectively. Moreover, by loosening the statistical stringency there were 19 auxin response genes upregulated in the

ugt80B1 background (**Table 2.3**). Based on functional categories of genes, we propose the exclusion of SG as a key membrane diversification element in Arabidopsis caused a defined pattern of shifts among genes associated with membrane organization and cell wall synthesis (**Table 2.1 and 2.2**). Despite subtle changes in morphology and plant phenotype in *ugt80B1* (DeBolt et al., 2009) gene expression among stress response, hormone regulation, transcription factors and signal transduction were suggestive of a role for membrane homeostasis, specifically sterol composition, in regulating stress responsive signal transduction.

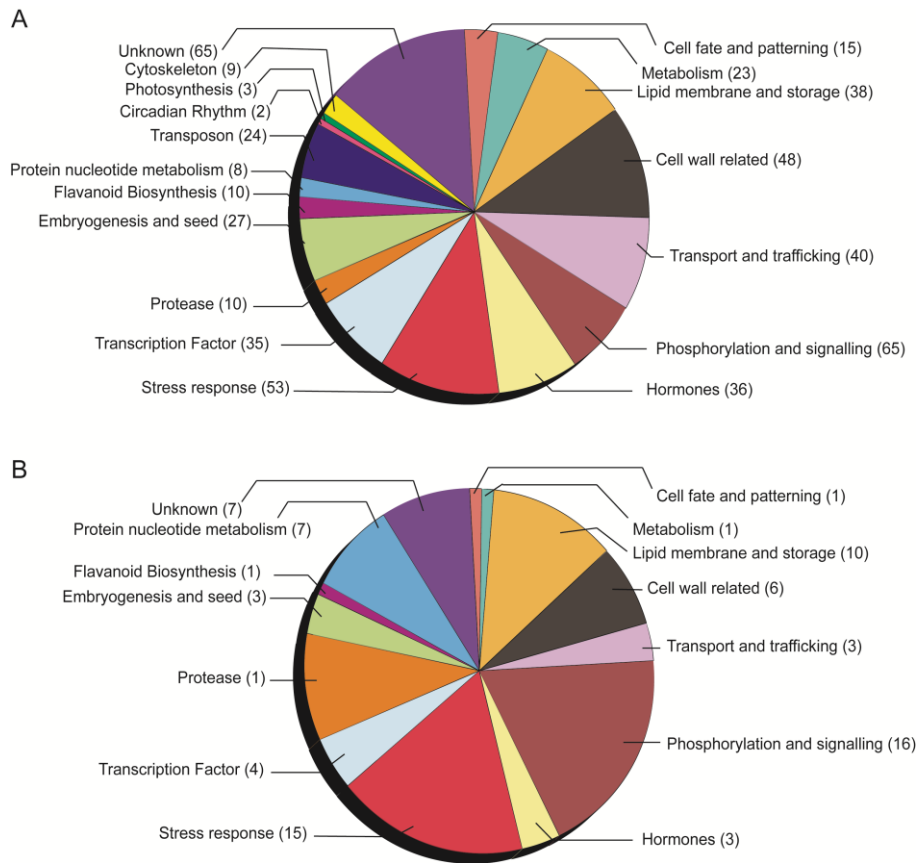


Figure 2.1 565 genes were differentially expressed in *ugt80B1* compared to wild-type. The differentially expressed genes are divided into up and down regulated genes that are represented as pie charts. (A) 480 upregulated and (B) 85 downregulated genes are divided according to their functional annotations based on TAIR and DAVID online tools. The classifications were produced using homology to known gene functions and GO terms for biological processes and each category was compared with the total number of annotations in each category. The numbers against each category represents the number of genes in the category among the list of genes. Of downregulated genes the most abundant classifications were lipid membrane and storage, signaling and stress

response. A pattern of differentially expressed lipid biosynthetic genes revealed numerous components of the sterol biosynthetic pathway, suggesting transcriptional attempts to compensate for loss of the glycosylated moiety (noted in red under *lipid, membrane and storage*- **Table 2.2**). By contrast, the most abundant upregulated classifications were transport and trafficking, cell wall modification and stress response.

Table 2.1 Downregulated genes in *ugt80B1*, fold change expressed as wild-type versus *ugt80B1*. P-value<0.005

Functional category	Annotation	Fold Change	P-Value
UGT80B1			
At1g43620	<i>UGT80B1</i> (A in KO, P in control)	9.40	1.90E-05
SG responsive genes of unknown function			
At5g01350	<i>unknown protein</i>	3.96	1.11E-05
At4g04330	<i>unknown protein</i>	2.02	4.47E-04
At2g35290	<i>unknown protein</i>	2.01	1.12E-03
At2g41990	<i>unknown protein</i>	2.55	2.06E-03
At3g21080	<i>unknown protein</i>	2.25	4.53E-03
Stress response			
At4g33630	<i>EXECUTER1 (EX1)</i>	2.05	6.61E-06
At4g25200	<i>AtHSP23.6-mito</i>	3.84	9.38E-04
At2g38390	<i>peroxidase (salt stress)</i> <i>O-methyltransferase (Biotic stress responsive)</i>	2.08	9.04E-04
At1g21100	<i>ATMYB74 (drought)</i>	2.54	9.79E-04
At4g05100	<i>ATMYB74 (drought)</i>	2.01	1.94E-03
At1g53680	<i>Glutathione-S- transferase</i>	2.21	8.89E-04
At2g43535	<i>Defensin-like protein</i>	2.13	2.08E-03
At1g72930	<i>Flax rust resistance protein</i>	2.20	2.58E-03
At4g39070	<i>Zinc finger salt-tolerance protein</i>	2.46	2.26E-03
Signal transduction			
At5g62920	<i>ARR6- response regulator 6</i>	2.20	1.65E-04
At5g24470	<i>APRR5- response regulator protein</i>	2.17	5.62E-04
At5g48250	<i>CONSTANS homolog</i>	2.36	5.83E-04
At1g21270	<i>WAK2</i>	2.08	3.97E-03
At2g17230	<i>Protein kinase</i>	2.27	1.55E-04
Membrane/ raft			
At1g62510	<i>Lipid transfer protein</i> <i>Lipid raft protein: RING finger domain E3</i>	2.00	2.66E-04
At4g08950	<i>ligase</i> <i>Lipid raft protein: RING finger domain E3</i>	2.55	1.43E-03
At5g10380	<i>ligase</i>	3.09	1.32E-03
Cell wall			
At5g57560	<i>Xyloglucan:xyloglucosyl transferase</i>	2.76	7.16E-04
At3g45970	<i>EXPANSIN (EXPL-1)</i>	2.47	7.91E-04

Table 2.1 Continued

At5g44130	<i>FLA13- Fasciclin-AGP</i>	2.75	2.81E-04
At3g57520	<i>Alkaline alpha galactosidase</i>	3.49	8.87E-04
Transporter			
At4g15620	<i>Integral membrane family protein (MIP)</i>	2.93	1.42E-03
At2g37330	<i>ABC transporter</i>	2.41	2.28E-03
At1g64780	<i>Ammonium transporter</i>	2.52	9.31E-05
Hormone			
At1g22690	<i>gibberellin-responsive protein 12-oxophytodienoate reductase-</i>	2.20	2.35E-03
At1g76690	<i>Jasmonate synthesis</i>	2.68	8.56E-04
At1g59500	<i>IAA-amido synthase</i>	2.77	1.80E-03
Cytoskeleton			
At3g10780	<i>emp24/gp25L/p24 family protein</i>	2.01	3.96E-03
At5g02150	<i>Armadillo/beta-catenin repeat</i>	2.01	5.55E-05
Wax			
At1g70850	<i>Major latex protein (MLP28)</i>	3.07	3.87E-03
At3g51970	<i>Wax synthase</i>	2.02	1.37E-03
Emrbyogenesis			
At3g59220	<i>Cupin protein</i>	2.02	3.21E-04
Cell fate and patterning			
At1g35140	<i>EXORDIUM</i>	3.38	1.36E-03

Table 2.2 Upregulated genes in *ugt80B1*, fold change expressed as *ugt80B1* versus wild-type. P-value<0.005

Functional Category	Annotation	Fold Change	P- value
SG responsive genes of unknown function			
At3g15760	<i>unknown protein</i>	2.08	4.39E-03
At3g29370	<i>unknown protein</i>	2.48	4.03E-03
At1g65090	<i>unknown protein</i>	2.47	4.24E-03
At4g31330	<i>unknown protein</i>	3.49	4.94E-03
At2g25890	<i>unknown protein</i>	3.35	4.28E-03
At4g09890	<i>unknown protein</i>	2.79	1.40E-03
At2g41260	<i>unknown protein</i>	4.05	3.33E-06
At5g02580	<i>unknown protein</i>	2.17	1.10E-04
At5g19520	<i>unknown protein</i>	2.21	1.17E-04
At2g47780	<i>unknown protein</i>	7.42	1.20E-04
At5g19340	<i>unknown protein</i>	2.33	1.24E-04
At1g55210	<i>unknown protein</i>	3.55	1.30E-04
At1g23070	<i>unknown protein</i>	2.97	3.06E-04
At3g08030	<i>unknown protein</i>	2.01	3.06E-04
At3g19920	<i>unknown protein</i>	2.07	3.34E-03

Table 2.2 Continued

At4g27530	<i>unknown protein</i>	3.07	3.54E-03
At3g12960	<i>unknown protein</i>	3.37	3.72E-03
At2g27740	<i>unknown protein</i>	3.07	3.92E-03
At5g06190	<i>unknown protein</i>	2.13	4.01E-04
At1g64490	<i>unknown protein</i>	2.03	5.74E-04
At1g02700	<i>unknown protein</i>	2.24	6.36E-04
At5g02020	<i>unknown protein</i>	2.48	7.30E-04
At2g40475	<i>unknown protein</i>	2.00	2.91E-03
At5g01015	<i>unknown protein</i>	4.52	2.94E-03
At4g14200	<i>unknown protein</i>	2.27	3.13E-03
At5g07330	<i>unknown protein</i>	2.11	3.23E-03
At4g18920	<i>unknown protein</i>	3.08	2.01E-03
At1g22600	<i>unknown protein</i>	2.16	2.24E-03
At1g16850	<i>unknown protein</i>	2.41	2.80E-03
At1g61840	<i>DC1 domain-containing protein</i>	3.03	3.25E-03
At1g05320	<i>unknown protein</i>	2.13	8.67E-04
At1g16730	<i>unknown protein</i>	3.49	1.83E-03
At2g23640	<i>reticulon family protein</i>	2.23	1.89E-03
At2g07739	<i>unknown protein</i>	4.16	1.50E-04
At5g62490	<i>HVA22-LIKE PROTEIN K</i>	2.77	3.02E-03
Lipid membrane			
At5g14180	<i>MYZUS PERSICAE-INDUCED LIPASE 1</i>	2.33	4.67E-03
At4g12510	<i>Lipid transfer protein</i>	3.62	4.18E-03
At5g02100	<i>Oxysterol-binding protein *</i>	2.52	4.46E-04
At1g71250	<i>GDSL-motif lipase/acylhydrolase</i>	2.54	1.01E-04
At1g06350	<i>Delta 9 desaturase</i>	3.82	3.81E-04
At5g01870	<i>Lipid-transfer protein-</i>	3.94	1.21E-03
At4g11030	<i>Acyl-CoA synthetase acyl-CoA synthetase *</i>	2.48	2.99E-03
At3g48460	<i>Lipase Arab-1,</i>	2.41	7.87E-04
At3g04290	<i>GDSL-motif lipase/acylhydrolase</i>	3.24	2.61E-03
At4g34650	<i>SQUALENE SYNTHASE 2 *</i>	2.97	9.69E-04
	<i>MD-2-related lipid recognition domain-</i>		
At5g23820	<i>containing protein</i>	2.63	1.46E-03
At2g02850	<i>GDSL-motif lipase/hydrolase</i>	3.38	1.88E-03
At1g28650	<i>Lipase</i>	2.61	3.86E-03
Stress response			
At2g38530	<i>pathogenesis-related protein</i>	2.17	4.43E-03
At3g54510	<i>ERD- early-responsive to dehydration protein</i>	2.15	1.54E-04
At4g07820	<i>Pathogenesis-related protein</i>	2.44	3.71E-04
At5g47060	<i>senescence-associated protein</i>	2.32	6.59E-06
At4g10270	<i>Wound-induced protein</i>	3.21	4.57E-03
At5g51890	<i>peroxidase</i>	2.61	4.22E-03
At1g11130	<i>SCRAMBLED</i>	2.02	2.63E-04
At2g15010	<i>Pathogenesis related protein</i>	2.43	3.45E-04

Table 2.2 Continued

At1g47980	<i>Dessication-response protein</i>	3.51	4.62E-04
At1g17020	<i>Ascorbate oxidase</i>	5.29	3.21E-03
At1g78780	<i>pathogenesis-related family</i>	2.90	1.53E-03
At3g01190	<i>Peroxidase</i>	2.12	1.67E-03
At5g67400	<i>peroxidase (emb CAA66967.1)</i>	4.00	2.02E-03
At4g26010	<i>Peroxidase</i>	3.80	3.30E-03
At5g60220	<i>Senescence-associated protein - TETRASPANIN family</i>	2.37	3.83E-03
At2g46790	<i>ARABIDOPSIS PSEUDO-RESPONSE REGULATOR 9</i>	2.53	3.37E-03
At1g01520	<i>MYB-type HTH- Salt response</i>	2.34	1.67E-03
At2g29380	<i>Glutathione S-transferase</i>	3.39	5.78E-04
At1g48130	<i>1-CYSTEINE PEROXIREDOXIN 1</i>	3.00	5.10E-04
At2g31380	<i>SALT TOLERANCE HOMOLOGUE</i>	2.16	1.10E-03
At2g43510	<i>defensin-like (DEFL) family</i>	2.88	7.97E-04
At1g17010	<i>Stress induced ascorbate oxidaseSRG1-like protein</i>	2.96	1.04E-04
At5g09980	<i>ELICITOR PEPTIDE 4</i>	3.10	1.33E-03
Calmodulin and Calmodulin binding			
At4g00820	<i>IQ-DOMAIN 18</i>	2.21	6.04E-04
At5g35670	<i>IQ-domain 33 (iqd33)- Calmodulin</i>	3.47	4.83E-04
At2g32460	<i>Calmodulin-like protein</i>	2.64	2.08E-03
At2g34020	<i>calcium-binding EF hand family protein</i>	3.79	2.24E-03
Hormone			
At2g18010	<i>Auxin-responsive family protein</i>	2.17	2.73E-03
At1g29500	<i>Auxin-induced protein</i>	2.69	3.09E-03
At3g48700	<i>ARABIDOPSIS THALIANA CARBOXYESTERASE 13</i>	2.13	1.13E-03
At1g75580	<i>AUXIN-INDUCED PROTEIN X10A</i>	7.96	1.93E-03
At1g29430	<i>Auxin-induced protein</i>	2.18	4.25E-03
At3g58450	<i>Ethylene-responsive protein ER6</i>	2.39	6.76E-04
At5g54000	<i>Ethylene-forming-enzyme-like dioxygenase</i>	2.55	1.57E-03
At1g67100	<i>LOB DOMAIN-CONTAINING PROTEIN 40</i>	2.58	1.88E-04
At4g38850	<i>small auxin up RNA (SAUR-AC1)</i>	3.67	1.56E-03
At1g78390	<i>9-cis-epoxycarotenoid dioxygenase</i>	13.34	5.43E-04
At2g21200	<i>auxin-responsive protein</i>	2.67	1.21E-03
P450			
At3g28740	<i>CYP81D1</i>	3.00	1.15E-04
At5g25180	<i>CYP71B14</i>	2.93	4.55E-04
At1g11600	<i>CYP77B</i>	2.60	9.53E-04
Proteinase			
At2g31980	<i>Cysteine proteinase</i>	7.27	4.87E-05
At3g54940	<i>Cysteine proteinase</i>	2.67	8.58E-04
At4g35350	<i>Cysteine protease XCP1</i>	2.86	1.53E-03

Table 2.2 Continued

Signaling			
At4g29270	<i>Acid phosphatase</i>	3.54	4.90E-04
At4g29690	<i>nucleotide pyrophosphatase - like protein</i>	2.56	9.77E-04
At1g07430	<i>Protein phosphatase 2C,</i>	2.30	3.04E-03
At5g65890	<i>AtACR1- ACT domain</i>	2.26	7.63E-04
At1g14700	<i>Purple acid phosphatase</i>	2.21	2.95E-03
At5g61350	<i>receptor-like kinase RLK/Pelle</i>	3.16	3.83E-03
Metabolism			
At5g03860	<i>Malate synthase</i>	3.79	1.00E-03
At1g32900	<i>Starch synthase</i>	2.23	5.80E-04
At4g21490	<i>NADH dehydrogenase</i>	2.10	5.10E-04
At1g14120	<i>2-oxoglutarate-dependent dioxygenase</i>	3.38	2.46E-04
At5g44360	<i>FAD-binding domain-containing protein</i>	2.83	1.63E-03
At2g19900	<i>ATNADP-ME1</i>	2.34	1.39E-03
At5g64210	<i>alternative oxidase 2</i>	2.38	3.32E-03
At5g52570	<i>CAROTENOID HYDROXYLASE 2</i>	2.01	3.67E-03
Metals			
At1g71050	<i>Copper chaperone (CCH)</i>	2.93	1.03E-03
At2g23240	<i>EC metallothionein-like family 15 protein;</i>	2.36	1.63E-03
At2g02210	<i>C2H2-type zinc finger protein</i>	3.60	4.64E-05
At1g32740	<i>Zinc binding protein</i>	2.46	4.20E-04
Flavanoid			
At4g35150	<i>Caffeic acid O-methyltransferase</i>	2.70	2.19E-04
At3g51240	<i>Flavanone 3-hydroxylase (FH3)</i>	2.25	9.64E-04
At3g53140	<i>Caffeic acid O-methyltransferase - homt1</i>	3.14	1.30E-03
Cell wall			
At1g78210	<i>hydrolase, alpha/beta fold family protein</i>	2.29	3.87E-03
At5g48900	<i>pectate lyase</i>	2.98	4.03E-03
At2g42840	<i>PROTODERMAL FACTOR 1</i>	2.29	3.51E-03
At5g55730	<i>FASCICLIN-LIKE ARAB INOGALACTAN 1</i>	2.53	1.11E-03
At1g60090	<i>BETA GLUCOSIDASE 4</i>	3.27	2.29E-03
At1g80280	<i>Hydrolase</i>	2.06	2.39E-03
At1g67750	<i>Pectate lyase</i>	4.25	7.30E-04
At1g64390	<i>Endo-beta-1,4-glucanase</i>	2.88	2.95E-03
At1g32100	<i>Pinoresinol-lariciresinol reductase</i>	2.33	4.59E-03
At4g26320	<i>ARABINOGALACTAN PROTEIN</i>	7.05	7.60E-04
At5g59170	<i>proline rich protein</i>	2.36	7.63E-04
At5g40730	<i>Arabinogalactan</i>	7.36	2.33E-03
At2g20750	<i>BETA-EXPANSIN</i>	6.08	2.42E-03
At5g03760	<i>Cellulose synthase like-A9</i>	2.19	9.84E-05
At3g44990	<i>XTH31</i>	4.63	1.65E-06
At5g66460	<i>Mannan endo-1,4-beta-mannosidase</i>	2.93	1.39E-04
At1g31750	<i>proline-rich family protein;</i>	2.46	4.41E-04

Table 2.2 Continued

At1g26770	<i>expansin 10</i>	2.09	3.15E-03
At3g42850	<i>arabinose kinase</i>	3.07	3.23E-03
At5g02260	<i>expansin precursor</i>	2.55	3.51E-03
At5g10430	<i>AtAGP4</i>	3.41	4.93E-03
At2g44740	<i>CYCLIN</i>	2.41	4.64E-03
At3g21370	<i>beta-glucosidase,</i>	2.46	2.66E-03
Trafficking			
	<i>SEC14 phosphoglyceride transfer family protein</i>		
At1g30690	<i>protein</i>	2.07	3.92E-03
At5g65020	<i>Annexin</i>	2.18	1.84E-04
At4g19400	<i>Actin binding protein</i>	2.49	3.52E-04
At1g75780	<i>Tubulin beta-1 chain</i>	2.95	1.25E-03
At1g73190	<i>Alpha-TIP</i>	2.58	5.00E-04
At4g27370	<i>Myosin heavy chain ATM2'</i>	2.13	5.02E-04
Cell fate and patterning			
At1g11130	<i>SCRAMBLED</i>	2.02	2.63E-04
At1g72970	<i>HOTHEAD</i>	2.38	2.41E-03
At5g14750	<i>Werewolf (WER)/ MYB66</i>	2.31	3.95E-04
At3g13840	<i>SCARECROW</i>	4.29	4.38E-03
Embryogenesis			
At3g51810	<i>embryonic abundant protein AtEm1</i>	2.63	4.84E-03
At3g50980	<i>DEHYDRIN XERO 1 (XERO1)</i>	2.37	4.85E-03
At5g44310	<i>late embryogenesis abundant protein-like</i>	2.98	3.77E-03
At3g17520	<i>late embryogenesis abundant domain-containing protein</i>	2.24	3.28E-03
At5g55240	<i>embryo-specific protein- Ca2+-binding EF-hand protein</i>	2.41	1.97E-03
At2g28490	<i>Cupin</i>	2.58	8.65E-04
At2g35300	<i>late embryogenesis abundant</i>	4.27	1.91E-04
At1g32560	<i>late-embryogenesis abundant protein</i>	3.13	5.95E-04
At3g53040	<i>late embryogenesis abundant protein</i>	2.53	1.19E-03
At4g26740	<i>embryo-specific protein 1 (ATS1)</i>	2.42	1.34E-03
At2g36640	<i>phosphotyrosine protein -LEA</i>	2.70	1.93E-03
Transport			
At3g59140	<i>ABC transporter</i>	2.44	3.33E-03
At4g23700	<i>Na⁺/H⁺ antiporter family</i>	3.06	4.06E-03
At1g64110	<i>AAA-type ATPase family</i>	3.19	9.60E-04
At1g71960	<i>ABC transporter</i>	2.38	5.31E-04
At2g47490	<i>putative mitochondrial carrier protein-transporter</i>	2.21	4.62E-04
At5g40010	<i>AAA-type ATPase family protein</i>	2.88	1.52E-03
At3g03620	<i>MATE efflux family</i>	4.29	6.26E-07
At4g16160	<i>pore protein homolog</i>	2.42	9.65E-05

Table 2.2 Continued

Seed storage / maturation			
At4g27150	<i>NWMU2 - 2S albumin 2 precursor</i>	4.33	3.66E-04
At5g54740	<i>2S storage protein-like</i>	2.80	7.50E-04
At5g22470	<i>Seed maturation protein PM38</i>	2.43	8.04E-04
At4g36700	<i>globulin-like protein extA protease inhibitor/seed storage/lipid</i>	4.91	1.20E-03
At5g46900	<i>transfer protein</i>	6.20	4.23E-04
At3g27660	<i>oleosin isoform</i>	2.13	2.52E-03
At5g40420	<i>oleosin</i>	2.61	2.67E-04
At1g24020	<i>pollen allergen-like protein</i>	3.34	1.11E-03
At1g62710	<i>BETA-VPE</i>	2.45	8.49E-04
At3g20210	<i>DELTA-VPE</i>	4.97	2.33E-03
Protease			
At2g38905	<i>protease inhibitor II</i>	3.58	2.04E-03
At3g48350	<i>cysteine endopeptidase-related</i>	2.51	2.32E-03
At5g08260	<i>serine-type carboxypeptidase</i>	2.16	2.86E-03
Transcription factors			
At1g68240	<i>transcription factor</i>	2.30	3.95E-03
At1g77950	<i>MADS box transcription factor</i>	3.38	
At2g41070	<i>ATBZIP12</i>	2.50	
At4g03790	<i>Gypsy like transcription factor</i>	3.98	5.97E-04
At2g14650	<i>gypsy-like retrotransposon</i>	4.76	1.60E-04
At3g03450	<i>DELLA protein transcription factor transducin-related / WD-40 repeat protein- related</i>	2.72	1.71E-04
At1g27470		2.31	7.03E-04
At4g24660	<i>HOMEBOX PROTEIN 22 (ATHB22);</i>	2.24	3.13E-03
At4g10580	<i>gypsy-like retrotransposon</i>	4.43	1.49E-03
At5g32430	<i>transposable element gene</i>	4.80	1.23E-03
At3g31970	<i>gypsy-like retrotransposon</i>	2.79	1.06E-03
At4g22450	<i>Transposable element</i>	2.61	5.14E-04
At4g03900	<i>CACTA-like transposase</i>	6.69	2.37E-04
Misc			
At1g03880	<i>NBD-like protein</i>	2.52	4.74E-06
At4g07670	<i>Protease</i>	2.29	5.48E-04
At1g48470	<i>GLUTAMINE SYNTHETASE 1</i>	2.19	6.20E-04
At1g03790	<i>SOMNUS (SOM)</i>	2.65	2.67E-04
At5g19100	<i>Dermal glycoprotein precursor</i>	2.27	3.11E-04
At1g12130	<i>Flavin-containing monooxygenase</i>	3.20	3.51E-04
At2g46830	<i>putative RNA-binding protein</i>	2.13	4.64E-04
At5g01300	<i>Phosphatidylethanolamine-binding</i>	2.23	7.88E-04
At5g60020	<i>Laccase - LAC2-4</i>	4.05	4.97E-04
At4g28680	<i>tyrosine decarboxylase, ribosomal protein S12 mitochondrial family protein</i>	2.22	2.90E-03
At2g07675		2.70	4.03E-03

Table 2.2 Continued

At5g17540	<i>acetyl CoA:(Z)-3-hexen-1-ol acetyltransferase</i>	2.33	4.05E-03
At3g25900	<i>homocysteine S-methyltransferase AtHMT-1</i>	2.09	4.76E-03

*Red in **Table 2.2** indicates genes in sterol biosynthetic pathway differentially expressed in *ugt80B1*.

Table 2.3 Auxin responsive genes upregulated in *ugt80B1* P<0.1 based on T-TEST

Auxin	Target Description	Fold Change
	<i>SAUR51, SMALL AUXIN UPREGULATED RNA</i>	
At1g75580	<i>51</i>	7.96
At3g03840	<i>SAUR27</i>	4.91
At1g48660	<i>Auxin-responsive GH3 family protein</i>	3.92
At4g38850	<i>small auxin up RNA (SAUR-AC1)</i>	3.67
At5g18060	<i>SAUR23</i>	3.46
At4g34770	<i>SAUR1</i>	3.20
At1g29490	<i>SAUR68</i>	3.06
At1g29460	<i>SAUR65</i>	3.04
At1g29510	<i>SAUR67</i>	2.74
At1g29500	<i>SAUR66</i>	2.69
At5g66260	<i>SAUR11</i>	2.68
At2g21200	<i>SAUR7</i>	2.67
At1g29440	<i>SAUR63</i>	2.66
At1g56150	<i>SAUR71</i>	2.56
At4g36110	<i>SAUR9</i>	2.48
At1g29430	<i>SAUR62</i>	2.18
At2g18010	<i>SAUR10</i>	2.17
At4g31320	<i>SAUR37</i>	2.15
At3g12955	<i>SAUR74</i>	2.04

Differential genes expression linked to phenotypes of *ugt80B1*

Both flavanoid biosynthesis and defective embryogenesis were striking phenotypes of the *ugt80B1* single mutant (DeBolt et al., 2009). At P<0.005 level of significance, there were no genes associated with flavanoid biosynthesis downregulated and 3 genes were upregulated, *Caffeic acid O-methyltransferase* (At4g35150), *Flavanone 3-hydroxylase (FH3)*(At3g51240) and *Caffeic acid O-methyltransferase – (homt1 At3g53140)* (**Table 2.2**). However, loosening the statistical stringency to P<0.01 showed that a single gene was downregulated in *ugt80B1* that was associated with flavanoid biosynthesis, which was putative *flavonol 3-O-glucosyltransferase* (At2g29630). Moreover, 12 genes were upregulated in the mutant background that were putatively involved in flavanoid biosynthesis (**Table 2.4**)(*SRG1-like protein*, *UDP glucose:flavonoid-3-o-glucosyltransferase*, *Flavonol-7-O-rhamnosyltransferase*, *Chalcone synthase*,

Flavanone 3-hydroxylase (FH3), *Caffeic acid O-methyltransferase*, *Caffeic acid O-methyltransferase*, *SRG1-like protein Strong homology to SRG1 protein*, *WRKY* transcription factor). Given that seeds had transparent testa phenotype (*tt15*) due to a membrane defect, it was previously postulated that the effect of *ugt80B1* on flavanoid biosynthesis was indirect and may result from altered precursor transport (DeBolt et al., 2009). The data provided herein suggests that transcriptional feedback is occurring in the pathway, and lack of flavanoid accumulation in *ugt80B1* is coupled with a compensatory upregulation of several key steps in the pathway including *chalcone synthase* (the first committed step (Schmelzer et al., 1988)), *Flavanone 3-hydroxylase* and *Caffeic acid O-methyltransferase*.

Embryogenesis was defective in *ugt80B1* and analysis of transcript abundance herein revealed genes both up and down regulated that are central to embryogenesis. There were 11 genes upregulated in *ugt80B1* that were embryogenesis proteins (**Table 2.2**). Embryonic abundant protein (At3g51810) is an ABA inducible protein that is also responsive to heat stress. Two additional late embryogenesis abundant (LEA) proteins were ABA induced (At3g17520, At4g26740) and one LEA protein was induced by osmotic stress (At5g44310).

Another phenotype of the *ugt80B1* mutant was an ablation of the electron dense cuticular accumulation of aliphatic monomers (DeBolt et al., 2009). In the WT, the cuticle appeared in micrographs as a regular darker-colored layer on the outer surface of seed epidermal cell walls. Compared to wild-type, the cuticle in the *ugt80B1* mutant was largely ablated. The observed upregulation of *HOTHEAD* (At1g72970) was noted because it too displayed defective electron-dense structures in floral structures (petals and at the inner epidermis of the pistil) (Kurdyukov et al., 2006). Furthermore, two genes, wax synthase (At3g51970) and *MAJOR LATEX PROTEIN28* (At1g70850) were both significantly downregulated in *ugt80B1* and may be linked to export defects due to SG deficiency (**Table 2.1**).

Table 2.4 Upregulated genes putatively involved in Flavanoid biosynthesis in *ugt80B1*.

Flavanoid biosynthesis	Target Description	Fold Change
At1g17010	<i>SRG1-like protein</i>	2.96
At1g30530	<i>UDP glucose:flavonoid 3-o-glucosyltransferase</i> ,	2.21
At1g06000	<i>Flavonol-7-O-rhamnosyltransferase</i>	2.12
At5g13930	<i>Chalcone synthase</i>	2.61
At3g51240	<i>Flavanone 3-hydroxylase (FH3)</i>	2.25
At3g53140	<i>Caffeic acid O-methyltransferase</i>	3.14
At4g35150	<i>Caffeic acid O-methyltransferase</i>	2.69
At1g17020	<i>SRG1-like protein Strong homology to SRG1 protein</i> ,	5.28
At2g37260	<i>ATWRKY44</i>	2.95

Table 2.4 Continued

At1g63650	<i>ENHANCER OF GLABRA 3 (EGL3)</i> <i>S-adenosyl-L-methionine-dependent</i>	3.09
At1g24735	<i>methyltransferase</i>	2.16
At4g27250	<i>Dihydrokaempferol 4-reductase</i>	2.13

Transcriptional and proteomic analysis of seed storage proteins in *ugt80B1*

There were several other seed related genes differentially expressed and these almost exclusively fell into the seed storage protein (SSP) category. For instance, *NWMU2 - 2S albumin 2 precursor*, *2S storage protein-like*, *Seed maturation protein PM38*, *globulin-like protein*, *extA protease inhibitor/seed storage/lipid transfer protein*, *oleosin isoform*, *oleosin*, *pollen allergen-like protein*, *BETA-VPE* and *DELTA-VPE* were all upregulated in *ugt80B1*, whereas no SSP were downregulated (**Table 2.1** and **2.2**). To further elucidate whether the SSP were altered both at the transcriptional and protein level, soluble and total membrane protein preparations from *ugt80B1* and wild-type plant siliques were made. These were run on a SDS PAGE gel to separate proteins and bands that were present or absent in the mutant relative to wild-type were sequenced. One band was visibly less abundant in the mutant and its sequence revealed high homology to CRUCIFERN seed storage protein (**Figure 2.2**). Hence, the striking transcriptional upregulation of seed storage proteins observed in the *ugt80B1* seedlings appeared to be linked to a lack of seed storage protein accumulation in the developing seed.

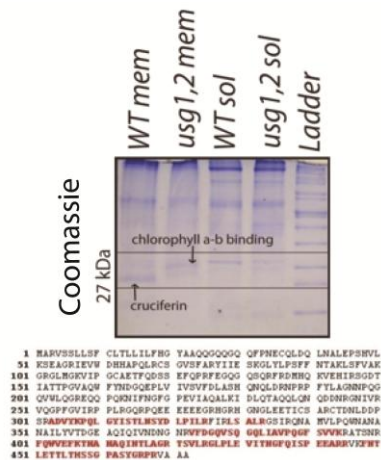


Figure 2.2 SDS-PAGE and MS results for identification of CRUCIFERIN

Mature siliques from *ugt80B1* and wild-type plants were ground in TRIS buffer prior to centrifugation to separate supernatant soluble and pellet membrane fraction from each genotype. The fractions were loaded separately on SDS-PAGE and stained with Coomassie blue stain. Two distinct bands present or absent in *ugt80B1* and wild-type respectively were sequenced via LC-MS. CRUCIFERIN protein absent in *ugt80B1* was identified via sequencing. Protein sequence given represents CRUCIFERIN with parts in red identified via MS.

Stress responsive gene expression and stress responsive UGT80B1 expression: assaying heat, cold and salt stress response using transgenic plants expressing *proUGT80B1::GUS*

Greater than one quarter of differentially expressed genes were responsive to either biotic or abiotic stress induction ($P > 0.005$). Downregulated genes were *EXECUTER1* (*EX1* At4g33630), *AtHSP23.6-mito* (At4g25200), *HSP40 DNAJ* (At5g23240), *peroxidase* (salt stress At2g38390), *O-methyltransferase* (Biotic stress responsive At1g21100), *ATMYB74* (drought At4g05100), *Glutathione-S-transferase* (At1g53680), *Defensin-like protein* (At2g43535), *Flax rust resistance protein* (At1g72930) and *Zinc finger salt-tolerance protein* (At4g39070) (**Table 2.1**). Of this cluster of genes, the identification of HSP proteins as SG responsive was consistent with previous studies that have identified that HSPs may be involved with SG mediated stress response signaling in human fibroblast cells and slime molds (Kunimoto *et al.*, 2000; Murakami-Murofushi *et al.*, 1987). A further 22 stress response genes were upregulated in the *ugt80B1* mutant including 4 *pathogenesis related proteins*, 4 *peroxidases*, 2 *ascorbate oxidase proteins* and a range of pathogen induced singletons (**Table 2.2**). Salt response, drought response, pathogen response, wound induced, defensin, and senescence induced proteins were differentially expressed, therefore SG mediated gene expression can be attributed to a broad spectrum of conditional stress. These data provide evidence that glycosylation of membrane sterols by UGT80B1 may serve as a dynamic membrane mediator of stress response.

A means to test this postulate in plants used transgenic plants expressing *proUGT80B1::GUS* to visualize and report tissue specific changes in transcript abundance. *UGT80B1* transcript responded to all the abiotic pressures applied, including sodicity (150 mM NaCl), increased solute concentration created to impose osmotic stress (2 x MS-AGAR). Temperature variation with moderately high and low temperatures were included overlapping with osmotic stress (2 x MS-AGAR). Previous analyses suggested that growth and development of *ugt80B1* was not responsive to cold stress (DeBolt *et al.*, 2009). Results that demonstrated *proUGT80B1::GUS* response to heat, cold and salt stress suggested that *ugt80B1* may be responsive to saline growth conditions as changes in transcript abundance was only noticed when temperature variations overlapped with osmotic stress (2 x MS-AGAR) (**Figure 2.3**).

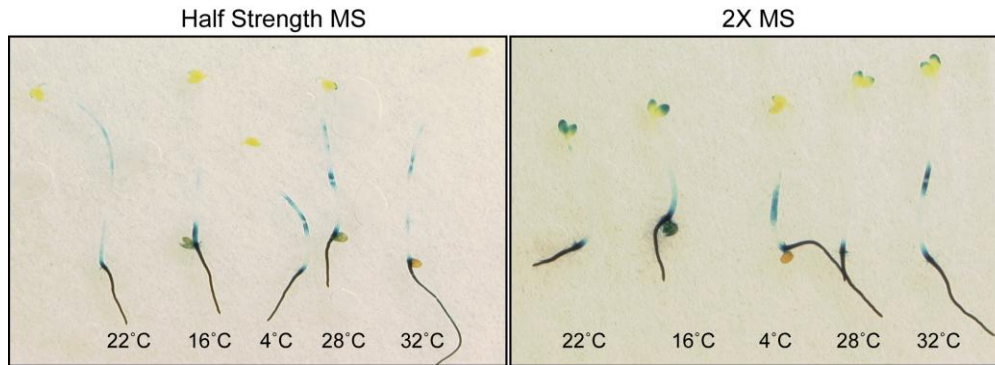


Figure 2.3 Effect of temperature variation and osmotic stress on *proUGT80B1:GUS*. *proUGT80B1:GUS* seedlings were grown in dark in half strength MS media and 2X strength MS media. Each of the plates was subjected to modest temperature variations in standard incubator for high temperatures and cold-room for low temperature. After 2 hours the seedlings were checked by GUS staining.

2.3 Discussion

This study provides evidence that glycosylation of membrane sterols by UGT80B1 may serve as a dynamic membrane mediator of stress response in *Arabidopsis* and is not redundant with free sterols (FS). Notable among the upregulated genes was the presence of genes associated with sterol biosynthesis: at the $P > 0.005$ level three genes were identified, *SQUALENE SYNTHASE 2*, *acyl-CoA synthetase* that are key enzymes in the first part of the sterol biosynthetic pathway where acetate is converted to squalene in mevalonate pathway (Nes, 1999; Holmberg et al., 2002), and *OSBP3a oxysterol binding protein*. *SQUALENE SYNTHASE* forms the putative regulatory point and first committed step towards sterol biosynthesis (Schaller, 2003). *SQUALENE SYNTHASE* is sensitive to sterol levels in plants, with increased sterols lowering the expression of this enzyme (Tansey and Shechter, 2000; Devarenne et al., 2002). Thus, with a 22-fold increase in FS, one would expect the downregulation of *SQUALENE SYNTHASE* in *ugt80B1*. But an upregulation of *SQUALENE SYNTHASE* in *ugt80B1* could be due to altered sterol sensing in these mutants. In addition the trafficking of sterols could be aberrant in *ugt80B1* background as an upregulation of a putative sterol binding and trafficking protein, *OSBP3a OXYSTEROL BINDING PROTEIN* is upregulated. Although the literature is scarce on the Oxysterol binding protein family, studies in other organisms point to sterol trafficking function among other functions such as lipid sensing, transport and trafficking and signaling (Raychaudhuri and Prinz, 2010). *Arabidopsis* ORP3a, one of the 12 members of the oxysterol binding proteins (Umate, 2011) binds to sitosterol and oxysterol and is present in the ER pointing to trafficking function at the site of sterol synthesis (Saravanan et al., 2009). Perhaps *ugt80B1* lacks the lipid sensing due to aberrant expression in *OXYSTEROL BINDING PROTEIN* genes leading to a feedback in the sterol biosynthesis. Alternatively, reducing sterol end product glycosylation caused upregulation of sterol biosynthetic genes.

UGT80B1 and SG act as transport mediator for SSP, flavanoids, aliphatic monomers and stress response

Phenotypes of *UGT80B1* deficient plants included altered accumulation of a diverse set of proteins and metabolites such as SSP, flavanoids and aliphatic monomers. Transport and accumulation of these metabolites involve the endoplasmic reticulum, tonoplast and plasma-membranes (Ibl and Stoger, 2012; Petrusa et al., 2013; Pollard et al., 2008). As integral membrane components, we hypothesized that SG composition may influence transport of precursors that are vital to each of these disparate pathways. These gene expression studies showed that a range of transporters were both down-regulated and upregulated in *ugt80B1* (**Table 2.1** and **2.2**). Several of these genes occur in families of transporters that could influence flavanoid, SSP or aliphatic monomers. For instance, ATP-bind cassette (ABC) transporters were both downregulated (At2g37330- *ALUMINUM SENSITIVE 3* (Larsen et al., 2005)) and upregulated (At3g59140- *MULTIDRUG RESISTANCE-ASSOCIATED PROTEIN 14* (Kolukisaoglu et al., 2002), At1g71960) in *ugt80B1*. Moreover, there were four additional ABC transporters that were excluded by $P > 0.005$ statistical cutoff, but present at the $P > 0.01$ cutoff (**Table 2.5**). ABC transporters have been identified that are critically involved cutin and wax export (for example Panikashvili et al., 2007). Furthermore, ABC and MATE transporters (multidrug and toxic compound extrusion) are both involved in transporting flavanoids into the vacuole in Arabidopsis. For instance, *transparent testa12* encodes a MATE transporter (Debeaujon et al., 2001) and in grapevines an ABC transporter is implicated in transporting flavanoids across the vacuole (Frangne et al., 2002). Therefore a plausible explanation for both the ablated aliphatic monomers transport to the cell wall and lack of flavanoid accumulation in the vacuole (DeBolt et al., 2009) could be a consequence of ineffective transporter activity due to defective membrane integrity. Alternatively, since SG diversifies liquid ordered microdomains in plants (Laloi et al., 2007) the possibility of lipid raft associated transporter function for transporting these macromolecules across the PM cannot be ruled out; especially since lipid rafts in plants are associated with proteins for signaling, stress, trafficking and cell wall metabolism (Grennan, 2007) (*genes associated with these functions can be found in Table 2.1 and 2.2*).

Reduction in CRUCIFERIN (**Figure 2.2**), one of the most abundant 12S globulins (Wan et al., 2007) in Arabidopsis implies either a defect in trafficking from their processing site, the ER to Protein storage vacuoles (PSV) (Otegui et al., 2006) or a defect in the ER itself. Where defects in ER would have manifested itself as more severe defects in plant growth (Stefano et al., 2012), the phenotypes of *ugt80B1* are modest at best; which points to the possibility of a defect in trafficking. However, the presence of transcripts involved in the trafficking being differentially expressed leaves a possibility for investigation in this direction. Among the notable transcripts were an *armadillo* homolog (At5g02150), *emp24/gp25L/p24* (At3g10780) and an *E3 ligase* orthologous to the mammalian lipid raft protein (At5g10380) (**Table 2.1**) that were downregulated. The E3 ligases putatively modify and regulate membrane protein trafficking

(d'Azzo et al., 2005). The armadillo homolog and emp24/gp25L/p24 homolog are annotated according to their sequence homology to known trafficking proteins. Upregulated genes associated with trafficking were identified as a SEC14 phosphoglyceride transfer family protein, Annexin, Actin binding protein, Tubulin beta-1 chain, Alpha-TIP and a myosin heavy chain ATM2 (Table 3). Associations between sterol rich microdomains and trafficking components have been well described (Slimane et al., 2003). Hence, these data suggest that altering the SG content of membranes influenced secretion and trafficking in Arabidopsis. The phenotypes of the seed and embryo associated with *ugt80B1* were the most severe (DeBolt et al., 2009). We have discovered herein the *ugt80B1* displayed defective seed storage protein accumulation and remobilizing these protein supplies may provide a developmental delay.

To further the investigation into existing phenotypes and matching transcriptional data, SGs are proposed to be lipid activators of stress responsive signal transduction in human fibroblast cells (Kunimoto et al., 2000). However, DeBolt et al., (2009) were unable to show hypersensitivity to cold stress using a *ugt80A2 ugt80B1* double mutant. Perhaps the difference in organisms and sterol species could be the reason for these results. However several osmolyte transporters, ammonium transporter (At1g64780), Na⁺/H⁺ antiporter family (At4g23700), AAA-type ATPase (At1g64110, At5g40010), mitochondrial carrier protein- transporter (At2g47490), MATE efflux family (At3g03620) and a pore protein homolog (At4g16160) were differentially expressed in *ugt80B1*. MATE efflux family proteins are also known to export malate and citrate in Arabidopsis (Lui et al., 2009) and may reflect an imbalance of osmolytes in *ugt80B1* cells. Metabolic changes overlap in some stresses specially drought, salt and low temperatures (Krasensky and Jonak, 2012). Furthermore, upregulation of the Na⁺/H⁺ antiporter family *AtCHX17* (At4g23700, Maresova and Sychrova, 2006) in *ugt80B1* was consistent with salt stress mediated transcription of *proUGT80B1::GUS* (**Figure 2.3**). Hence, it is plausible that altered transcription of the *AtCHX17* and MATE is a regulatory means to balance osmotic stress implicating SG in mediating stress response. Previous studies have shown that Na⁺/H⁺ antiporter family is a vacuolar cation/proton antiporter of Arabidopsis and plays an important role in salt tolerance, ion homeostasis and development (Blumwald et al., 2000). Transcriptional variation of *proUGT80B1::GUS* was prominent with increased salinity as compared to elevated or decreased temperatures (**Figure 2.3**), suggesting a role of SG in salt stress.

Table 2.5 Upregulated ABC transporters excluded for T-TEST at P<0.005 but included in P<0.01 in *ugt80B1*.

ABC transporters	Target Description	Fold Change
At3g28345	ATP-BINDING CASSETTE B15 (ABCB15)	3.11
At3g21080	ABC transporter phloem-localized ABC-type transporter-like	2.25
At2g37330	protein (AtALS3)	2.41
AT2g34660	ABC transporter (AtMRP2)	2.69

Transcription factors and Cell Fate Patterning

Transcription factors were also only upregulated in *ugt80B1* when compared to wild-type, and included a *DELLA*, *HOMEBOX*, *MADS BOX*, *CACTA*, *BZIP* and *WD-40* transcription factors (**Table 2.2**). Broadly, DAVID analysis and TAIR9 Gene Ontology (GO) descriptions were employed to categorize genes corresponding to a specific cellular and developmental program (Huang et al., 2008). This tool interpreted the global transcript data as a transcriptional signature linked to ‘epidermal cell development’. Based on the epidermal patterning genes defined in the DAVID analysis as well as described in established literature (Hochholdinger and Zimmermann, 2008; Kwak and Schiefelbein, 2008), several characterized regulators and genes expressed in epidermal cell layers were identified including *SCRAMBLED* (*SCM*), *WEREWOLF* (*WER*), *ENHANCER OF GLABRA3* (*EGL3*) and *EXTENSINS* (**Table 2.6**). The epidermal cell layer in Arabidopsis roots comprises two types of cells, trichoblast, or root hair cells (H-cell), and atrichoblast or non-root hair cells (N-cells), that are arranged in an alternating radial fashion. The mechanism by which this patterning is accomplished relies on positional information, whereby epidermal cells that lay on top of anticlinal cell walls of two underlying cortical cells take on the fate of H-cell and others become N-cells. Various factors such as transcription factors, hormones, cell-to-cell signaling as well as many non-transcription factor genes have been uncovered in addition to the positional requirement for epidermal cell patterning (Bruxet et al., 2012; Dolan L., 2006; Ishida et al., 2008; Schiefelbein et al., 2009). The *SCRAMBLED* (*SCM*) leucine-rich receptor-like kinase (LRR-RLK) is key to relaying positional information underlying this pattern (Dolan, 2006; Kwak and Schiefelbein, 2008). Signaling through *SCM* is required for the downstream repression of the R2R3-MYB transcription factor *WEREWOLF* (*WER*) in H cells. In turn, the repression of *WER* in H cells leads to an increase in the levels of *WER* in N cells and thereby in the levels of a transcriptional regulatory complex consisting of *WER-GLABRA3* (*GL3*)/*ENHANCER OF GLABRA3* (*EGL3*)-*TRANSPARENT TESTA GLABRA1* (*TTG1*). The output of these events leads to activation of direct targets such as the N-cell determinant and homeodomain-leucine-zipper transcription factor *GLABRA2* (*GL2*) (Kwak and Schiefelbein, 2008). Simultaneously the H-cell factor *CAPRICE* (*CPC*) is transcriptionally activated in N-cells that move sympastically

via membranous channels plasmodesmata (PD) to H cell, thereby activating H-cell fate (Bernhardt et al., 2005; Kurata et al., 2005a; Kurata et al., 2005b). Higher plant PD have a highly constricted proteinaceous endoplasmic reticulum (ER) called a desmotubule that is located in the PD pore (Kragler et al., 1998; Lee et al., 2011; Maule et al., 2011) and a cytoplasmic sleeve between the plasma membrane and the desmotubule allows for movement of molecules such as proteins, metabolites, ions, RNA and virus's (Ruiz-Medrano et al., 2004; Zambryski and Crawford, 2000).

The presence of critical sterols downstream in the pathway has been suggested to play a role in plant root development (Carland et al., 2010; Diener et al., 2000). Perhaps SG via UGT80B1 plays a role in epidermal cell layer for root development either directly influencing the transcription factors found in this study or via influencing PD membrane structure thereby indirectly affecting developmental programs such as root epidermal patterning. Surprisingly several of the genes in our transcriptional profiling have been found to be directly associated with PD proteome. Taking advantage of the Arabidopsis PD proteome (Fernandez-Calvino et al. (2011), we cross-referenced differentially expressed transcripts for those corresponding to putative PD association. Results indicated several receptor like kinases (RLK) that were putatively PD enriched and differentially expressed (**Table 2.7**). A class III peroxidase, *AtPer44*, *GERMIN-LIKE PROTEIN10*, *TETRASPANIN4* and *RETICULAN LIKE PROTEINB13* were also found in both lists (**Table 2.7**). It is of interest to note the presence of *SCRAMBLED* receptor like kinase in the list overlapping with the studies on plasmodesmata proteome. A transient localization in plasmodesmata cannot be ruled out since the plasmodesmata membrane forms a unique platform for the enrichment of receptor like kinases/proteins. *SCRAMBLED* has been shown to be required for epidermal patterning in the Arabidopsis and its positional accumulation in H-cells combined with an accumulation of an unknown positional cue leads to the differentiation of the particular epidermal cell into a root hair cell. Apart from this we also note the presence of the Class III peroxidase family genes *AtPer44* and *TETRASPANIN4*. Proteins related to cell wall loosening or modifications such as the peroxidases are found to be enriched in and around plasmodesmata due to their requirement in *de novo* plasmodesmata formation, while tetraspanins have been thought to form tetraspanin enriched microdomains analogous to animals. Thus the role of steryl glycosides as a specialized membrane structural component at the plasmodesmata that can support proteins of particular nature cannot be denied. This creates a segway into critically analyzing the role of UGT80B1 and its implicated SG in root epidermal patterning.

Table 2.6 List of genes that are related to cell fate and patterning

Tair ID	Gene name	Δ	Functional annotation	Ref.
At2g37260	<i>WEREWOLF</i>	+ 2.95	Transcription factor, epidermal cell fate specification, seed coat development	
At1g11130	<i>SCRAMBLED</i>	+ 2.02	Signal transduction, Regulates expression of <i>GLABRA2</i> , <i>CAPRICE</i> , <i>WEREWOLF</i> , and <i>ENHANCER OF GLABRA3</i>	
At1g63650	<i>ENHANCER OF GLABRA3</i>	+ 3.10	Epidermal cell fate	(Dinneny et al., 2008)
At3g13840	<i>SCARECROW</i>	+ 4.29	Regulation of transcription	(Dinneny et al., 2008)
At5g35190	<i>EXTENSIN - LIKE PROTEIN</i>	+ 2.24	Cell wall organization, proline-rich extension-like family protein	
At3g10710	<i>PECTINESTERASE FAMILY PROTEIN</i>	+ 3.37	Cell wall modification	(Won et al., 2009)
At3g56980	<i>BHLH039/ORG3</i>	+ 3.77	Transcription factor	
At5g60520	<i>LATE EMBRYONIC ABUNDANT PROTEIN - I</i>	+ 2.33	Late embryogenesis abundant protein-related	
At4g19690	<i>Fe(II) TRANSPORT PROTEIN</i>	+ 6.28	Cellular iron ion homeostasis, response to bacterium and ion transport (Iron, Cadmium, manganese and zinc)	
At3g58060	<i>CATION EFFLUX FAMILY PROTEIN</i>	+ 2.31	Cation transport membrane	
At4g37070	<i>PATATIN-LIKE PROTEIN</i>	+ 2.40	Lipid metabolic process, Acyl transferase/acyl hydrolase/lysophospholipase	(Won et al., 2009)

Table 2.6 Continued

At4g23690	<i>PUTATIVE DISEASE RESISTANCE PROTEIN</i>	+ 2.32	Defense response, ligand biosynthetic process, disease resistance-responsive family protein / dirigent family protein	(Won et al., 2009)
At5g67400	<i>PEROXIDASE</i>	+ 4.00	Oxidative stress response	(Won et al., 2009)
At3g01190	<i>PEROXIDASE 27</i>	+ 2.12	Oxidative stress response	(Won et al., 2009)
At2g39690	<i>UNKNOWN PROTEIN</i>	+ 2.19	Unknown, mitochondrion	(Won et al., 2009)
At1g64780	<i>AMMONIUM TRANSPORTER</i>	- 2.51	Transporter	(Won et al., 2009)

Table 2.7 List of genes associated with plasmodesmata.

TAIR ID	Gene Description	Fold-Change	Reference
At3g62020	<i>GERMIN-LIKE PROTEIN (GLP10)</i>	+2.05	(Ham et al., 2012)
At4g26010	<i>AtPER44 (Class III peroxidase)</i>	+3.81	(Burch-Smith and Zambryski, 2012; Fernandez-Calvino et al., 2011)
At5g22460	<i>ALPHA/BETA-HYDROLASES SUPERFAMILY PROTEIN</i>	+3.23	(Fernandez-Calvino et al., 2011)
At1g11130	<i>SCRAMBLED (SCM)</i>	+2.02	(Fernandez-Calvino et al., 2011)
At5g60220	<i>TETRASPANIN4</i>	+2.38	
At2g23640	<i>RETICULAN LIKE PROTEIN B13 (RTNLB13)</i>	+2.23	
At5g44130	<i>FASCICLIN-LIKE ARABINOGALACTAN PROTEIN 13 PRECURSOR (FLA13)</i>	-0.36	(Fernandez-Calvino et al., 2011)

Table 2.7 Continued

At5g06860	<i>POLYGALACTURONASE INHIBITING PROTEIN 1 (ATPGIP1)</i>	-0.49	(Fernandez-Calvino et al., 2011)
At4g16563	<i>ASPARTYL PROTEASE FAMILY PROTEIN</i>	-0.24	(Fernandez-Calvino et al., 2011)
At3g57520	<i>RAFFINOSE SYNTHASE 2 (ATSIP2)</i>	-0.29	(Fernandez-Calvino et al., 2011)
At3g45970	<i>EXPANSIN-LIKE A1 (ATEXLA1)</i>	-0.4	(Fernandez-Calvino et al., 2011)

2.4 Methods

Generation and growth of *Arabidopsis thaliana* plants and mutant *ugt80B1* line

For the gene profiling studies, we grew *ugt80B1* and wild-type in *Arabidopsis* ecotype Columbia (Col-0) in liquid culture. 100mg of seeds for *ugt80B1* and wild-type were surface sterilized with 30% household bleach solution and moist chilled at 4°C. The seeds were then inoculated in exactly 100 mL of half strength MS media in 250 mL conical flask in triplicate to eliminate secondary effects due to development and environment. These plants were grown under long-day conditions (16-h/8-h photoperiod) for 10 days and all experiments were harvested within 5 minutes to avoid secondary effects of circadian clock related transcripts (Schaffer et al., 2001). Consistent with this approach, only two genes associated with circadian rhythm were identified as differentially expressed between the mutant and wild type (**Table 2.8**). The approach used also ensured adequate seedling material (100 mg = approximately 5500-6000 seedlings) for each RNA extraction, added experimental robustness by the large number of individuals in each sample and minimized any minor developmental transition effects that would have complicated the analysis.

Table 2.8 Circadian rhythm genes differentially regulated in *ugt80B1* versus wild-type

Circadian rhythm	Target Description	Fold Change
At2g46830	<i>CIRCADIAN CLOCK ASSOCIATED 1</i>	2.12
At2g46790	<i>Pseudo-response regulator PRR9. I</i>	2.52

Systematic and integrative analysis of genes responding to depletion of SG

A simple microarray experiment measuring transcript abundance from seedlings depleted in SG was used in our studies to identify genes responding to SG depletion. RNA was extracted from all the replicates using QUIGEN RNeasy mini kit for RNA extraction. These were sent to Microarray Core facility on University of Kentucky campus for microarray hybridization using Affymetrix Arabidopsis Genome Array and data collection. Normalization was performed per gene and per gene chip of the log₂ values for three replicates for *ugt80B1* and wild-type using the flags, “present”, “absent” and “marginal”. The transcripts absent in both *ugt80B1* and wild-type were eliminated and the ones present and marginal in both were retained. Based on a cutoff of 2-fold change in expression the genes differentially expressed in both were retained and further separated into up-regulated and down-regulated genes. These genes were further grouped under the biological process they take part in, according to annotations given by TAIR. However, a simple microarray experiment like this can generate a large amount of data, with genes that are differentially expressed over a range of biological processes. To overcome this we used DAVID bioinformatics resource tool (Huang et al. 2008). DAVID utilizes enrichment analysis to systematically map genes in the given list to the associated biological annotation and highlight the most enriched or overrepresented biological annotation (Huang et al. 2008). With the use of DAVID functional annotation chart enriched annotation terms associated with the gene lists were identified. This made use of P-Value (EASE score or modified Fisher’s exact test) and enrichment scores, thus the terms with higher enrichment values and significant P-value (default cutoff 0.1) were further analyzed.

Chapter 3: A Membrane-Associated UDP-Glc:Steryl Glucosyltransferase 80B1 (UGT80B1) is Required for Plasmodesmata Function and Morphogenesis Underlying Cell Fate Determination in the *Arabidopsis* Root Epidermis

3.1 INTRODUCTION

In multicellular organisms, the machinery comprising cell layers that are functional units requires that the cells conform themselves to a regular pattern during development. In plants an array of complex genetic factors, cell-to-cell communication and hormonal gradients play a role in cell patterns leading to the formation of plant organs (Sachs, 1991; Van Norman et al., 2011). One such system in *Arabidopsis* is root epidermal patterning, which is highly predictable and extensively studied. The alternating emergence of root hair or trichoblast cells (H) versus non-root hairs or atrichoblast cells (N) relies on positional information, whereby epidermal cells that contact anticlinal cell walls of two underlying cortical cells take on the H cell fate and others become N cells (Dolan, 2006). The SCRAMBLED (SCM) leucine-rich receptor-like kinase (LRR-RLK) is key to relaying positional information underlying this pattern (Dolan, 2006; Kwak and Schiefelbein, 2008). Signaling through SCM is required for the downstream repression of the R2R3-MYB transcription factor WEREWOLF (WER) in H cells. In turn, the repression of WER in H cells leads to the increase in the levels of WER in N cells and thereby in the levels of a transcriptional regulatory complex consisting of WER-GLABRA3 (GL3)/ENHANCER OF GLABRA3 (EGL3)-TRANSPARENT TESTA GLABRA1 (TTG1). The output of these events leads to activation of direct targets such as the N-cell determinant and homeodomain-leucine-zipper transcription factor GLABRA2 (GL2) (Kwak and Schiefelbein, 2008).

Other transcription factors (TF), hormones, cell-to-cell signaling as well as many non-TF components have been uncovered in addition to the positional requirement for epidermal cell patterning (Bruex et al., 2012; Ishida et al., 2008). The interplay between positional requirements and the underlying molecular machinery involves cell-to-cell communication (Dolan, 2006; Lee and Schiefelbein, 2002; Schiefelbein et al., 2009) plausibly via active recruitment and passage through symplastic connections known as plasmodesmata (PD) (Kragler et al., 1998). In support of this postulate, there is some indirect evidence suggesting that PD are utilized for cell-to-cell movement of CAPRICE (CPC), a small single-repeat R3-MYB transcription factor that is required for epidermal patterning and cell-type differentiation of H cells (Kurata et al., 2005a).

Symplastic continuity is especially important in multicellular organisms for the regulated movement of proteins and macromolecules between cells (Kragler et al., 1998). PD are plasma membrane (PM) lined channels that span plant cell walls. Desmotubules, which are compressed endoplasmic reticulum (ER) structures, lie in the central axes of PD. Proteins move between cells via the thin cytoplasm between the PM and desmotubule and also via desmotubule membranes (Maule et al., 2011). Owing to their unique function, PD membranes

are likely to contain proteins and membrane components that differ from the rest of the PM (Maule et al., 2011). A handful of studies have examined this specialized membrane, such as the work by Fleurat-Lessard et al., (1997) in which immunogold labeling demonstrated exclusion of H⁺-ATPase from PD PM, suggesting specific targeting and/or active exclusion. Additionally, proteomic studies on isolated PD membranes indicate the enrichment of membrane microdomain (also known as lipid raft) associated proteins, such as REMORIN and GPI-anchored proteins (Fernandez-Calvino et al., 2011). However, experimental evidence linking lipid membrane components, such as sterols or sphingolipids, to PD structure and function are lacking. Technical difficulties arise in studying such hydrophobic environments, and uncovering PD phenotypes in genetic screens is laborious.

Mutations in genes involved in sterol biosynthesis cause severe developmental phenotypes in *Arabidopsis* (Lindsey et al., 2003; Schaller, 2003). Loss of epidermal cell file organization in the root was observed in mutants for *FACKEL/HYDRA2* (*FK/HYD2*) encoding sterol C-14 reductase (Schrick et al., 2000; Souter et al., 2002), as well as in *STEROL METHYLTRANSFERASE 1* (*SMT1*) and the double mutant for *SMT2* and *SMT3* (Carland et al., 2010; Diener et al., 2000). The epidermal patterning defect was not rescued by the addition of downstream sterols or brassinosteroids, suggesting that other critical sterols could play specific roles in plant root development. One striking feature of membrane sterols in plants is the degree to which they are glycosylated (Uemera and Steponkus, 1994). In *Arabidopsis*, the Carbon-3 (C3) hydroxyl of membrane sterols and acyl sterols are commonly decorated with a glucose (Glc) residue (Schrick et al., 2012; Wewer et al., 2011). Borner et al., (2005) have shown the enrichment of sterol glycosides (SG) in membrane microdomains.

Despite glycosylated sterols comprising a significant percentage of membrane sterols in plants (up to 40% (Grille et al., 2010)), their biological function has remained elusive. Two genes in the *Arabidopsis* genome have been found to encode UDP-Glc:sterol glucosyltransferases, *UGT80A2* and *UGT80B1*. The corresponding enzymes are required for the accumulation of SGs and thus for the diversification of sterol versus SG composition in membranes (DeBolt et al., 2009). In the present report, we investigated membrane sterol glycosylation via *UGT80B1*. We show that *ugt80B1* mutants display impaired cell fate determination in the root epidermis underpinned by aberrant PD morphogenesis, suggesting a model in which *UGT80B1* provides the membrane environment required for intercellular movement of key R3-MYB transcription factors in epidermal patterning. Live imaging also reveals that *UGT80B1* activity affects targeted localization of the SCM receptor protein to the PM of H cells in the epidermis. A mechanistic role for specific sterol and SG composition in supporting membrane specialization and architecture underlying cell-type differentiation is proposed.

3.2 RESULTS

Randomized cell files in *ugt80B1* roots

Two genes are implicated in membrane sterol glycosylation in *Arabidopsis*, *UGT80A2* (At3g07020) and *UGT80B1* (AT1g43620) (DeBolt et al., 2009). We found that *UGT80B1* was highly expressed in root tissue as visualized by a promoter fusion to the reporter beta-glucuronidase (GUS) (**Figure 3.1**). Homozygous recessive mutations in *UGT80B1* (T-DNA insertion alleles SALK_021175C, SALK_103581C and the double mutant allele described in (DeBolt et al., 2009)(**Figure 3.2**) caused visible alterations in root epidermal patterning (**Figure 3.3; Table 3.1**). The *ugt80A2* mutant was indistinguishable from wild-type, and *ugt80A2,B1* double mutants failed to show more severe defects in root patterning than *ugt80B1*. The root epidermis of *ugt80B1*, in comparison to wild-type, displayed fewer H cells (30 ± 1.6 wild-type versus 17 ± 1.4 for *ugt80B1*; **Figure 3.3A**: Both SALK insertion alleles were examined and the results are summarized in **Table 3.2**).

In comparison to wild-type, *ugt80B1* mutants exhibited an increase in the distance between root hairs (wild-type; $172 \pm 5 \mu\text{m}$ versus *ugt80B1*; $257 \pm 10 \mu\text{m}$) (**Figure 3.3B, C**). The trichoblast cell areas were significantly greater for wild-type ($3451 \pm 282 \mu\text{m}^2$) than for *ugt80B1* ($2780 \pm 306 \mu\text{m}^2$) (**Figure 3.3D**), indicating that the reduced hair frequency could not be explained by excessive trichoblast cell elongation. Furthermore, in contrast to the predictable arrangement of alternating H and N cell files in wild-type (Bruex et al., 2012; Ishida et al., 2008) an increased frequency of N relative to H files was observed in *ugt80B1* (**Figure 3.3E,F**). Adding to this variability in *ugt80B1* was the observation of H and N cells within the same cell file (**Figure 3.3E,F, Table 3.1**). Taken together, these results illustrated an altered cell fate pattern in *ugt80B1* mutants, which was associated with an increase in N cell files.

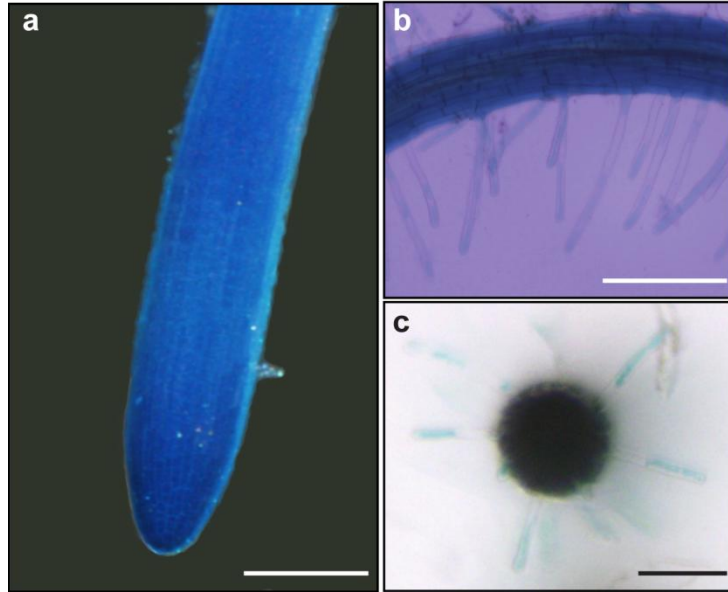


Figure 3.1 *UGT80B1* expresses ubiquitously in *Arabidopsis* roots. GUS staining of *ProUGT80B1:GUS* expressing *Arabidopsis* showing expression in epidermal layer of roots (A) and root hairs (B). Cross-section shows GUS expression in all root cell layers (C). Bar represents 100 μ m.

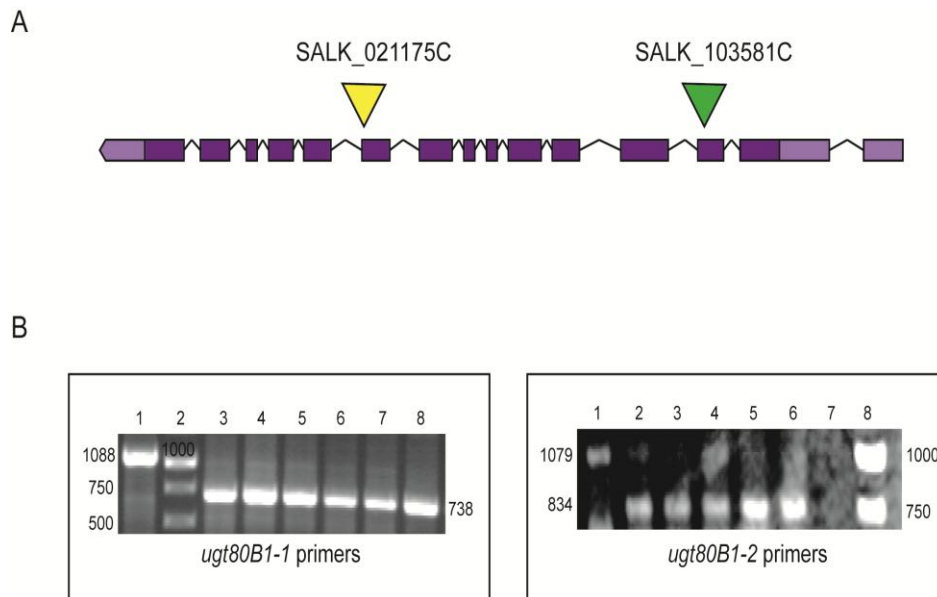


Figure 3.2 T-DNA insertion alleles for *UGT80B1*. **A)** Indicates the position of the T-DNA insertion in *UGT80B1* alleles SALK_021175C and SALK_103581C respectively. **B)** Homozygosity of the T-DNA insert was confirmed by polymerase chain reaction: Left panel follows the order of 1 (WT band), 2 (ladder), 3-8 (single band in the homozygous allele at 738); Right panel has 1 (WT band), 2-6 (single band in the homozygous allele at 834), 7 empty lane and 8 (ladder).

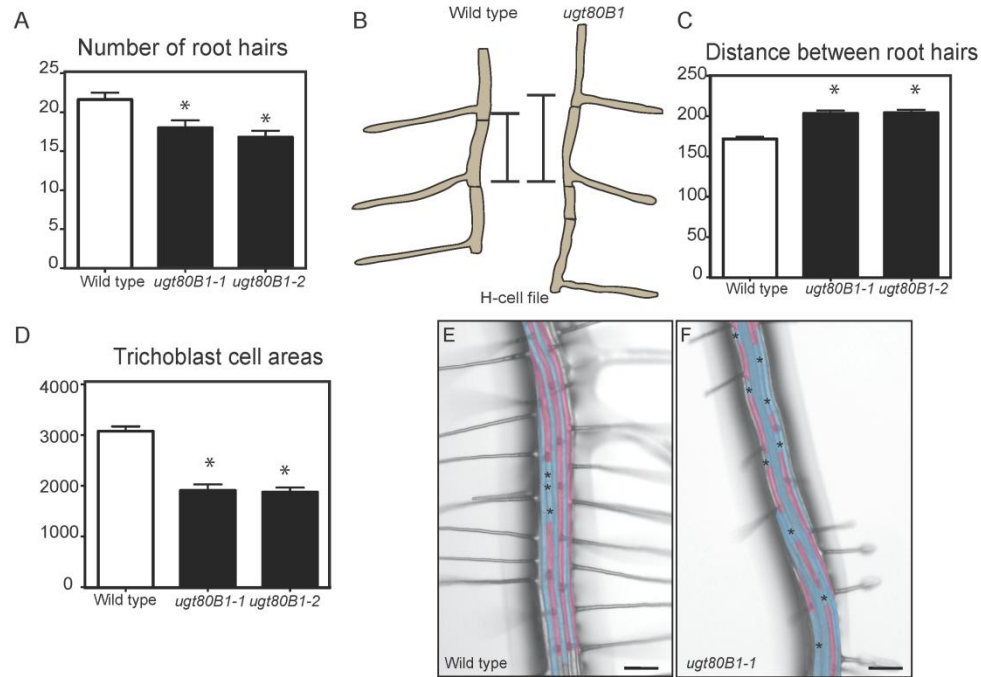


Figure 3.3 Mutations in *UGT80B1* cause aberrant epidermal root hair distribution. Number of root hairs for wild-type and *ugt80B1* alleles per 1.6 mm root length (**A**) ($P < 0.001$, Student T-test, $n = 423$). Distance between adjacent root hairs in an H-cell file measured between root hairs (**B**, Scale bar = 100 μm) per 1.6 mm root length for wild-type and *ugt80B1* ($P < 0.001$, Student T-test, $n = 32$)(**C**). Trichoblast cell area measurements for wild-type and *ugt80B1* (**D**) ($P < 0.05$, Student T-test, $n = 19$). Error bars indicate SE in (A,B,C). Stereomicroscopy images with false coloration to show randomization of H and N-cell files in *ugt80B1* versus wild-type (**E**, **F**). False color cyan shows N-cell files and false color magenta shows H-cell files. Black asterisk marks ectopic N-cell in an otherwise H-cell file. Scale bar = 200 μm

Table 3.1 Percentage emergence of hair and non-hair cells in H and N cell files for wild-type and *ugt80B1* alleles. Averages and SE are indicated for each genotype. Asterisk represents $P < 0.05$ based on Mann Whitney U test, $n = 40$.

Genotype	Cells in H position		Cells in N position	
	Hair cells (%)	Non Hair cells (%)	Hair cells (%)	Non Hair cells (%)
Wild type	94.0 \pm 2.0	6.0 \pm 0.8	0	100
<i>ugt80B1-1</i>	64.3 \pm 2.0*	35.7 \pm 3.1*	9.0 \pm 1.6*	91.1 \pm 3.0*
<i>ugt80B1-2</i>	70.0 \pm 1.8*	30.0 \pm 2.5*	6.0 \pm 1.3*	94.2 \pm 2.5*

Table 3.2 Number of root hairs, distance between adjacent root hairs and trichoblast cell areas in both *ugt80B1-1* and *ugt80B1-2*.

Genotype	No. Of root hairs (N=20)	Distance between root hairs (μm) (N=76)	Trichoblast cell Area (μm^2) (N=200)
Wild type	22 \pm 1	171.8 \pm 2.6	3076 \pm 96.05
<i>ugt80B1-1</i>	18 \pm 1*	203.4 \pm 3.4*	1905 \pm 121.0*
<i>ugt80B1-2</i>	17 \pm 0.8*	204.2 \pm 3.7*	1872 \pm 92.3*

* P < 0.05 based on Bonferroni's multiple comparison test.

Aberrant expression of root epidermal cell TFs in *ugt80B1*

Given the defect in epidermal patterning in the *ugt80B1* root, we explored global gene expression patterns in wild-type and *ugt80B1* 10-day-old seedlings grown hydroponically in the light to enrich for root tissue (**Figure 2.3**). We used the interactive genomic software DAVID combined with TAIR9 Gene Ontology (GO) description (Huang et al., 2008), for dataset interpretation, which revealed a transcriptional signature described as 'epidermal cell development' associated with *ugt80B1*. Several characterized regulators of epidermal cell layers were identified including *EGL3*, *WER*, and *SCM* (**Table 2.6**). To further investigate these epidermal patterning regulators that were differentially expressed in *ugt80B1* roots (**Table 2.6**), we introduced transgenic reporter lines into the *ugt80B1* mutant background (**Figure 3.4**). We chose the GL2 reporter because of its role as a downstream target of the transcriptional regulatory complex that determines epidermal cell fate in the root. Expression of the *ProGL2:GUS* reporter is normally observed in a position-dependent pattern in developing non-hair cells in the N position (Masucci et al., 1996). Consistent with the above-described epidermal patterning defects, the *ProGL2:GUS* reporter was expressed in an abnormal manner in *ugt80B1*, with a significant fraction of H-cells exhibiting *ProGL2:GUS* expression and N-cells lacking expression (**Figure 3.4; Table 3.3**). These data support the conclusion that *ugt80B1* displays randomized cell files and aberrant cell type pattern formation due to early defects in cell-type specific transcriptional regulation.

We also examined the expression of *WER*, a member of the R2R3-MYB family and constituent of the *WER-GL3/EGL3-TTG1* central transcriptional regulatory complex involved in the root epidermal patterning pathway (Bruex et al., 2012; Lee and Schiefelbein, 1999) in *ugt80B1*. In wild-type roots, the *WER* protein preferentially accumulates in the nuclei of differentiating N cells in the epidermal cell layer where it acts as a positively regulator in opposition to single-repeat R3-MYB TFs such as *CPC*, *TRIPTYCHON* (*TRY*) and *ENHANCER OF TRIPTYCHON1* (*ETC1*) to direct cell fate (Ishida et al., 2008; Lee and Schiefelbein, 2002; Ryu et al., 2005). Examination of the functional translational reporter *ProWER:WER:GFP* in the *ugt80B1* root epidermis, revealed *WER:GFP* accumulation in both N and H positions, consistent with abnormal GL2 promoter activity (**Figure 3.4**). One possibility is that the observed epidermal phenotypes

arise from inefficient symplastic trafficking of the regulatory R3-MYB TFs, (e.g. CPC, TRY, ETC1) that establish the epidermal patterns. Alternatively or in addition, abnormal expression of the WER transcription factor, and consequentially its target GL2, could plausibly arise due to dysfunctional transcriptional regulation via the upstream SCM receptor protein as described below.

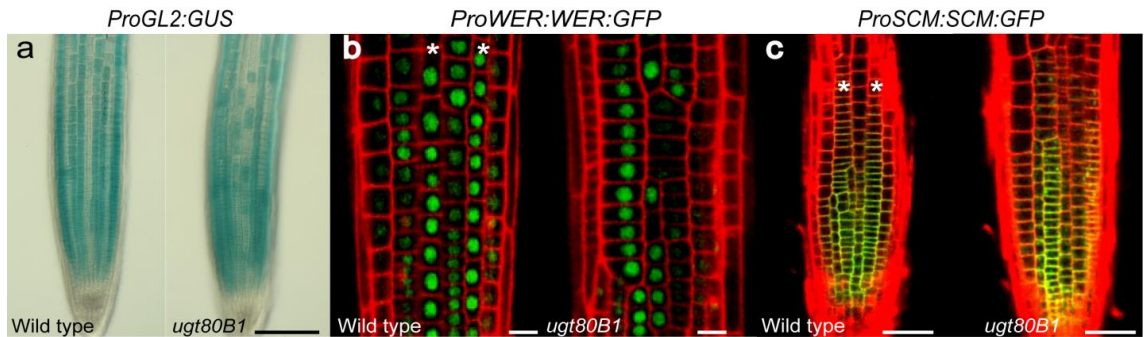


Figure 3.4 Localization of the *pGL2::GUS*, *pWER::WER:GFP* and *pSCM::SCM:GFP* reporter fusions in four-day-old *ugt80B1* versus wild-type roots. Roots of *ugt80B1* mutant and wild-type seedlings expressing *pGL2::GUS* were analyzed for GUS expression (A). *WER::WER:GFP* (B) and *SCM::SCM:GFP* (C) reporter fusions were examined in *ugt80B1* and wild-type by confocal microscopy counter-stained with propidium iodide to visualize the cell wall (red) and WER:GFP and SCM:GFP accumulation (green) in a longitudinal view. WER:GFP preferentially accumulates in the N cell nuclei (white asterisks and inset) in wild-type, whereas in *ugt80B1*, WER:GFP is found in both N and H cells (inset) (B). Preferential localization of SCM-GFP at PM in maturing epidermal cells at H cell positions in wild-type (white asterisk). SCM:GFP is visible at the PM and in the cytosol as punctae of various sizes in *ugt80B1* (C). Scale bar (A) = 200 μm , (B) = 50 μm , (C) = 100 μm .

Table 3.3 Pattern of the *GL2::GUS* expression in the root epidermis

Genotype	H Cell Position		N Cell Position	
	GUS Non-Expressing Cells (%)	GUS-Expressing Cells (%)	GUS Non-Expressing Cells (%)	GUS-Expressing Cells (%)
<i>GL2::GUS</i> (WT WS)	95.0 ± 1.0	5.0 ± 1.0	0 ± 0	100 ± 0
<i>GL2::GUS</i> (<i>ugt80B1</i>)	79.3 ± 1.9 ^a	20.7 ± 1.9 ^a	11.2 ± 2.0 ^a	88.8 ± 2.0 ^a

At least 20 5-day-old seedlings were examined for each line. Values represent mean ± standard deviation.

^a Differs significantly from wild-type ($P < 0.05$; Student's t-test).

Subcellular localization defects of the SCM receptor in *ugt80B1*

SCM is a membrane-associated LRR-RLK that functions by mediating positional information from the underlying cortical cells to the epidermal cells to establish and reinforce N versus H cell identities (Kwak and Schiefelbein, 2008). Signaling through SCM results in transcriptional repression of *WER* in H cells. Additionally, there is feedback regulation by the *WER-GL3/EGL3-TTG1* complex on *SCM* expression in N cells (Kwak and Schiefelbein, 2008). Therefore we reasoned that the SCM receptor protein should respond to abnormal *WER* expression, and additionally could be the cause of aberrant *WER* expression (**Figure 3.4**). Fitting with either or both ideas, the *SCM* mRNA was identified as differentially expressed in *ugt80B1* mutants (**Table 2.6**). Wild-type expression of *SCM:GFP* is found in both H and N cell peripheries in the meristematic zone of developing *Arabidopsis* roots. However in the early elongation zones the expression was preferentially in H cells. Consistent with wild-type, in *ugt80B1* mutants bearing a *ProSCM:SCM:GFP* construct, we observed a relatively normal distribution of *SCM:GFP* marking the periphery of both N and H cell in the meristematic zone (**Figure 3.4**). However in contrast to wild-type, H cell plasma membrane preference of *SCM:GFP* in early elongation zone was lost in *ugt80B1*. Additionally an unexpected increase in *SCM:GFP* punctate-like structures of varying sizes was seen in the cytoplasm of *ugt80B1* mutants in comparison to wild-type (**Figure 3.4**). Since enzymatic activity for sterol glycosylation has been observed in both the PM and endomembranes (Grille et al., 2010), these observations suggest that a depletion of glycosylated sterols interferes with SCM targeting to the plasma membrane.

UGT80B1 protein is localized to ER, PM and PD in root epidermal cells

To further examine the subcellular localization of UGT80B1 in the root epidermis, we utilized a translational fusion of UGT80B1 to GFP. Complementation of *ugt80B1* with *Pro35S:UGT80B1:GFP* rescued its transparent testa phenotype (DeBolt et al., 2009). The fusion protein was detected as a single 95 KDa band in a Western blot using an Anti-GFP antibody (**Figure 3.5A**). Laser scanning confocal microscopy enabled live imaging of *UGT80B1:GFP* in epidermal cells of the *Arabidopsis* root (**Figure 3.5B**). UGT80B1:GFP was found localized to ER (endomembrane), PM and PD (**Figure 3.5C-F**). The ER was identified based on structural and morphological dynamics similar to that previously reported for this compartment (Cutler et al., 2000) (**Movie 3.1**) with tubular and cisternae ER structures being highly dynamic. By focusing on UGT80B1:GFP labeled ER tubules at cell-to-cell junctions, we observed specific signals consistent with desmotubules spanning the PD (**Figure 3.6A**). Tubules from adjacent epidermal cells, marked by UGT80B1:GFP, were dynamic and appeared to display coordinated movements (**Movie 3.2**). Consistent with these observations, dye-loading experiments using an ER-specific dye showed intimate coupling of ER between cells through the PD desmotubules (Cantrill et al., 1999; Grabski et al., 1993; Martens et al., 2006). Fluorescence signal from UGT80B1:GFP was seen to be distributed in dynamic punctate at the PM focal plane of the root epidermis (**Movie 3.3; Figure 3.5F**).

To distinguish UGT80B1:GFP subcellular localization in the cell wall versus the PM, cotyledons (**Figure 3.7**) and roots (**Figure 3.6B**) from transgenic plants expressing *UGT80B1:GFP* were plasmolysed and counter-stained with propidium iodide. We found that the UGT80B1:GFP signal was localized in the PM as well as at the cell wall, where discrete punctae were observed (**Figure 3.6B; Figure 3.5E,F**). Strikingly, time-lapse imaging during plasmolysis revealed that the majority of cell-wall-associated punctae were tethered by Hechtian strands to the protoplast, providing a site for cell-to-cell symplastic association (**Figure 3.6B,C; Movie 3.4**). Previous reports have linked cell wall punctae to PD (Raffaele et al., 2009). In agreement with previous studies on the symplastic continuity of epidermal cells through the PD (Duckett et al., 1994; Kragler et al., 1998; Zhu et al., 1998), UGT80B1:GFP labeled membranes that traverse PD, connecting adjacent root epidermal cells.

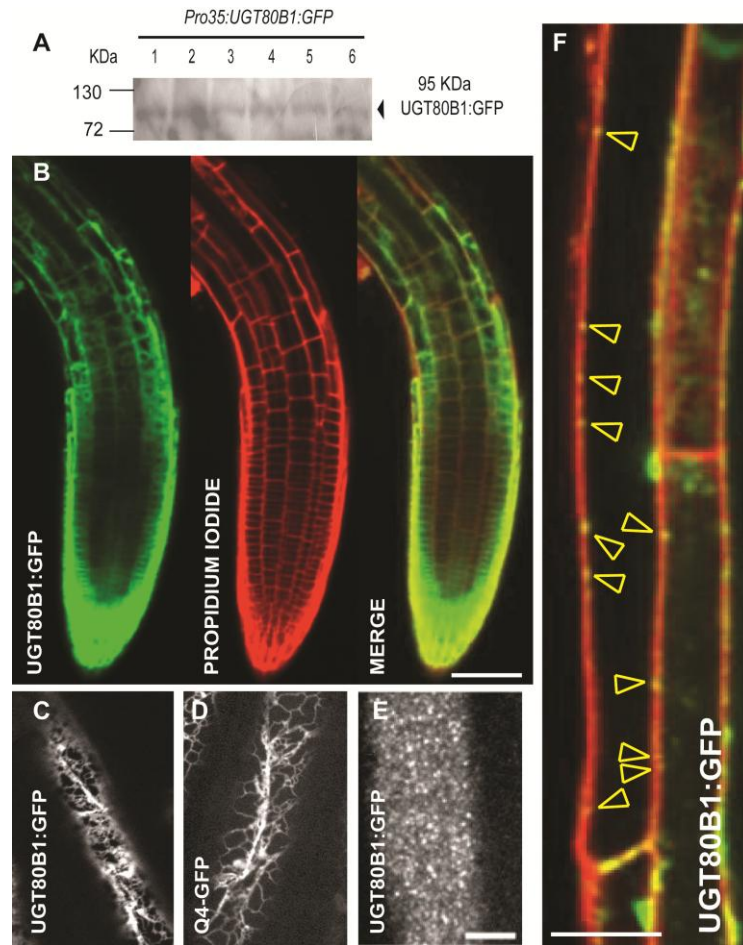


Figure 3.5 Localization of UGT80B:GFP reporter fusion in the root epidermis. Western blot analysis of Arabidopsis plants expressing *Pro35S::UGT80B1:GFP*. UGT80B1:GFP detected as a 95kDa band (arrow) using Anti-GFP antibody (**A**). Three-day-old roots indicate UGT80B1:GFP protein (green) partially overlapping with propidium iodide counter-staining (red) (**B**). Subcellular localization to the ER of UGT80B1:GFP (**C**) similar to the ER marker Q4:GFP localization (**D**) and PM (**E**). The punctate distribution of UGT80B1:GFP at the PM focal plane was consistent with PD (**F**) and counter-stained root cells revealed discrete foci along cell wall – PM interfaces (yellow carats - **F**).

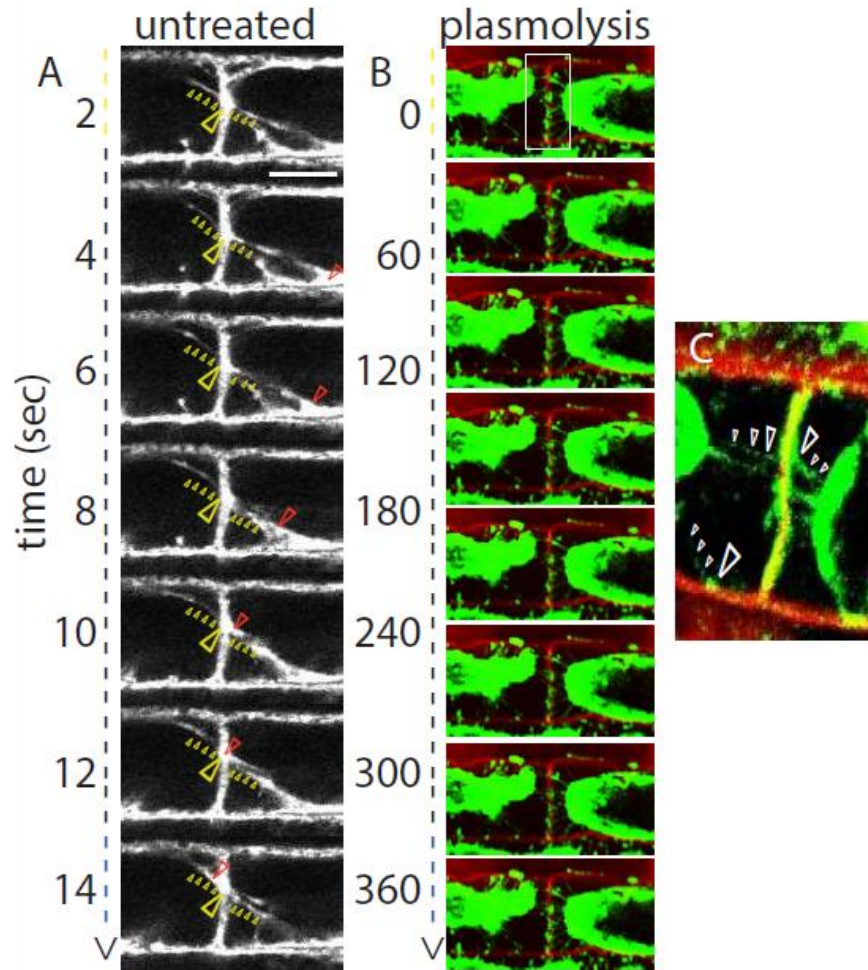


Figure 3.6 Desmotubule localization of UGT80B:GFP reporter fusion in the root epidermal cells. Laser scanning confocal microscopy of *Arabidopsis* epidermal root cells expressing UGT80B1:GFP reveals coordinate behavior of ER tubules (yellow carats) (A). Each frame was taken at 2 sec intervals and demonstrates punctate accumulation of UGT80B1:GFP passing symplastically from the basal to apical cell (magenta carat). Plasmolysis with 0.8 M mannitol (B,C) demonstrates static cell-to-cell attachment sites. A confocal microscopy time series of epidermal root cells expressing UGT80B1:GFP (green) stained with propidium iodide (red) to visualize the cell wall (B). Enlarged section indicated by white box in (B) shows cell-to-cell attachment of UGT80B1:GFP labeled ER (yellow carats) (C). During the 6 min interval the coordinate cell-to-cell alignment of Hechtian strands (white carats) was evident in a static manner (C). Bar = 10 μ m (A,B) 5 μ m (C).

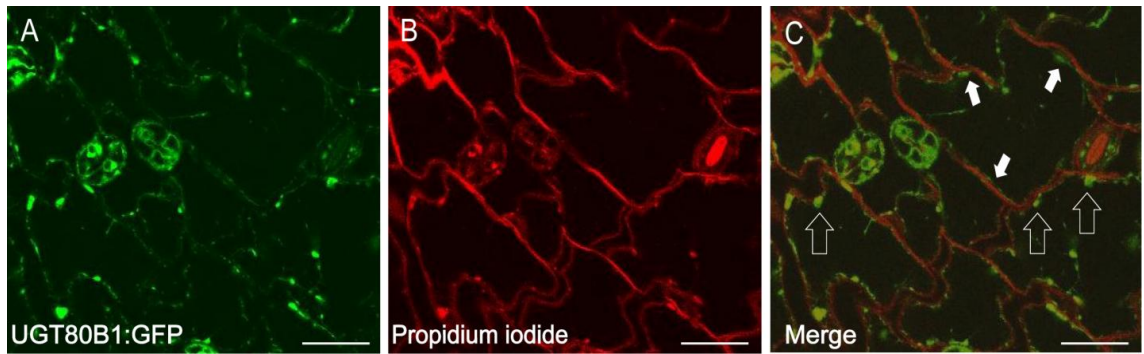


Figure 3.7 Localization of UGT80B1:GFP reporter in four-day-old Arabidopsis cotyledon cells. A confocal microscopy image of fluorescent accumulations (green) of UGT80B1:GFP at the cell wall-PM interface of cotyledon cells after plasmolysis with 0.8 M mannitol (A). Fluorescent image of cell wall stained with propidium iodide (red) of the same cotyledon cells as in A (B). Merged image of UGT80B1:GFP (green) and cell wall (red) showing the large punctate UGT80B1:GFP at the cell-wall-PM interface (open white arrows) and the plasmolysed PM labeled with UGT80B1:GFP away from the cell wall (white arrows) (C). Bar represents 50 μm .

[Movie 3.1.mov](#)

Movie 3.1 UGT80B1:GFP localizes to the ER. A confocal microscopy movie stacks of the ER in epidermal cells of dark grown hypocotyl regions in *Pro35S:UGT80B1:GFP* expressing plants. Static cortical ER is seen in the background as a meshwork and highly dynamic cisternae and tubular ER strands are visualized in the foreground. Images captured at every 10 second was stacked using ImageJ and movie played at 7 frames per second. Scale bar 10 μm .

[Movie 3.2.mov](#)

Movie 3.2 UGT80B1:GFP labeled ER tubules show symplastic continuum. Focusing on the tubular ER structures from root epidermal cells of 5-day-old seedlings expressing *Pro35S:UGT80B1:GFP* CLSM images of ER tubules from adjacent cells show coordinated movement at the cell boundaries. Images captured every 8 seconds and stacked using ImageJ. The movie plays at 7 frames per second. Scale bar 50 μm .

[Movie 3.3.mov](#)

Movie 3.3 UGT80B1:GFP localizes as a punctate at the PM. Confocal microscopy focusing on the PM focal plane in the root epidermal cells of 5-day-old *Pro35S:UGT80B1:GFP* expressing plants. UGT80B1:GFP shows highly dynamic punctate of different sizes localized at the PM. Larger punctate structures are fairly static when compared to smaller highly dynamic structures. Images captured at every 10 seconds, stacked using ImageJ and played at 7 frames per second. Scale bar 10 μm .

[Movie 3.4.mov](#)

Movie 3.4 UGT80B1:GFP labeled ER tubules show symplastic continuum during plasmolysis. Confocal microscopy of 5-day-old seedlings expressing *Pro35S:UGT80B1:GFP* after plasmolysis with 0.8 M mannitol. Focusing on the tubular UGT80B1:GFP (green) labeled ER structures movie stacks show coordinated movement from adjacent cells. Cell wall counter stained with propidium iodide (red) to add contrast. Images captured every 12 seconds, stacked using ImageJ and plays at 7 frames per second. Scale bar 50 μm .

Aberrant PD structure and morphology in *ugt80B1*

The epidermal patterning defects and abnormal expression patterns of the *GL2*, *WER* and *SCM* regulatory components in *ugt80B1* roots could result, at least in part, from a defect in symplastic transport of key non-cell autonomous R3-MYB TFs, e.g. *CPC*, *TRY*, and *ETC1*. Moreover, the live cell imaging data in which UGT80B1:GFP marks desmotubules and forms cell-to-cell continuum at the PD led us to propose a role for UGT80B1 in the maintenance of PD structure. We examined the ultrastructure of PD using ultrathin sections of fixed and resin embedded seedlings via transmission electron microscopy (TEM). By visual comparison of PD structures were categorized as simple, complex or incomplete (Ehlers and Kollmann, 1996) (**Figure 3.8A,B**). In our analysis we refer to all non-simple structures as complex, including branched structures such as the H, V, X and Y forms as well as the highly-branched structures. Complex PD also included twinned PD, where PD occur in pairs <100 nm apart (Burch-Smith and Zambryski, 2010; Burch-Smith et al., 2011) (**Figure 3.8A,B**). Simple PD that form a single channel between cells are the predominant form in immature tissues (Burch-Smith and Zambryski, 2010). Consistent with previous reports, we found that in wild-type, ~63% of PD were simple. In contrast, for both *ugt80B1* mutant alleles analyzed we observed a ~2-fold decrease in simple PD (**Figure 3.8A,B**). Since we analyzed immature tissue, relatively low percentages of complex (both branched and twinned) forms of PD were expected (Burch-Smith and Zambryski, 2010). Wild-type maintained the expected outcome for complex PD with ~15% branched and ~7% twinned (**Figure 3.8A**). In contrast we observed a ~2-fold increase in branched PD (~31%) and ~3-fold decrease in twinned PD (~2%) in the two *ugt80B1* alleles (**Figure 3.8A**). In addition, we observed ~15% of PD to be incomplete in wild-type while the *ugt80B1* alleles displayed a ~2-fold increase in incomplete PD (~30%) (**Figure 3.8A,B**).

Detailed analysis of PD morphology revealed that the middle aperture and neck regions of the PD in *ugt80B1* mutants were aberrant. PD aperture is highly dynamic, changing with various factors such as tissue age and interactions with viral proteins (Burch-Smith et al., 2011; Duckett et al., 1994; Kragler et al., 1998; Oparka et al., 1999; Stonebloom et al., 2009). Consistent with prior studies on PD ultrastructure, we found wild-type PD with middle aperture regions dilated ($98.0 \mu\text{m} \pm 2.1$) in comparison to visible constrictions at the neck regions (47.3 ± 0.6) (**Figure 3.8C-E**). For both *ugt80B1* alleles we measured a significant reduction in middle aperture ($73.2 \mu\text{m} \pm 1.7$ and $70.0 \mu\text{m} \pm 2.1$ for *ugt80B1-1*, -2

respectively) and a small but significant increase in the neck aperture ($51.8 \mu\text{m} \pm 1.0$ and $60.6 \mu\text{m} \pm 1.1$ for *ugt80B1-1*, *-2* respectively) (**Figure 3.8C-E**).

To test whether the PD abnormalities in *ugt80B1* are a manifestation of a generalized defect associated with a collapsed membrane architecture due to imbalance in sterol species, or alternatively due to a unique requirement for UGT80B1, we examined PD morphology in a sterol biosynthesis mutant. Defects in root epidermal patterning were uncovered in several of the sterol biosynthesis mutants, including *fk/hdy2* (Souter et al., 2002). Due to the severe cell division phenotypes associated with the *fk* loss-of-function mutant for sterol C-14 reductase (Schrack et al., 2000), a weak allele was utilized, *fk-J3158* (Qian et al., 2013). TEM revealed PD defects in the *fk-J3158* mutant with small but significant ($P < 0.0001$) increases in neck region aperture in the mutant ($63.3 \text{ nm} \pm 1.9$) that were similar to those for *ugt80B1* when compared to wild-type ($47.3 \text{ nm} \pm 0.6$) (**Figure 3.9A**). Quantification of middle apertures revealed a significant ($P < 0.0001$) reduction in middle aperture of *fk-3158* ($80.7 \text{ nm} \pm 2.7$) as compared to wild-type ($98.0 \text{ nm} \pm 2.1$) (**Figure 3.9A**). The overall ratios of simple, branched, twinned and incomplete forms of PD in *fk-3158* match that of wild-type (**Figure 3.9B**). However, an increase in branched PD (~22%) and a decrease in simple PD (~49%) structures was observed (wild-type branched, ~15%; simple, ~63%). Taken together, *fk-J3158*, similar to *ugt80B1*, displayed PD with abnormal morphologies. Reduction in downstream sterols and accumulation of unusual sterols in *fk-3158* could lead to SG depletion causing an effect on PD structure.

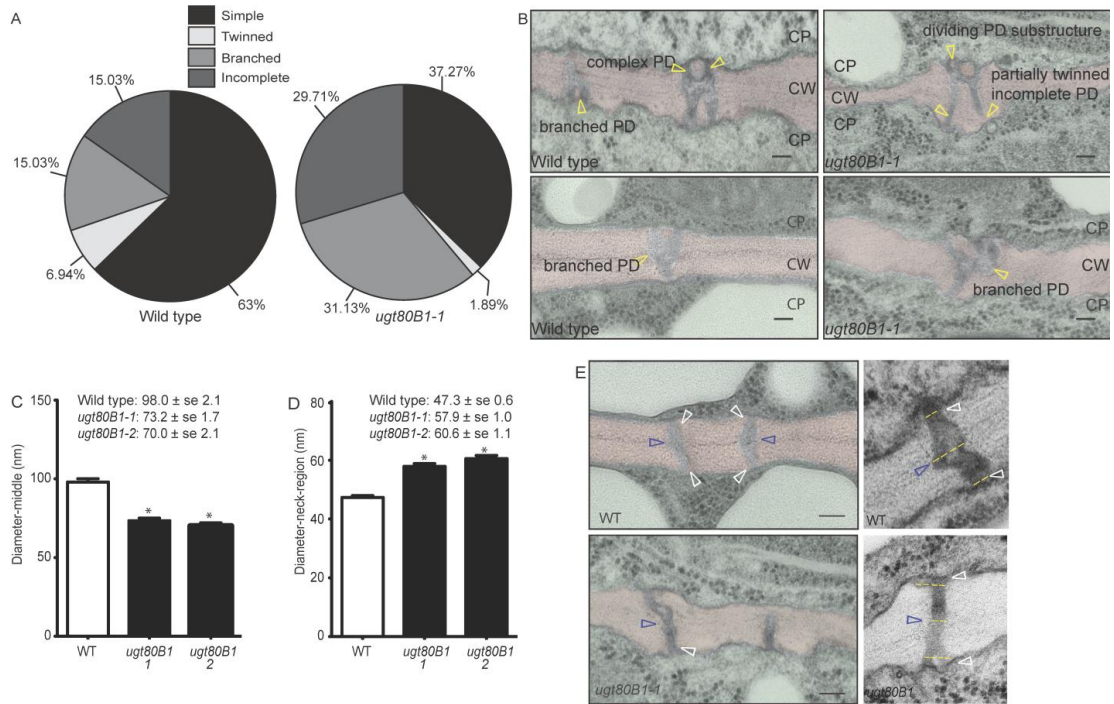


Figure 3.8 *ugt80B1* mutant is impaired in PD morphology. Quantitative assessment of PD structures using ultrathin TEM sections (**A**) (at least 250 PD from a minimum of two non-serial sections were analyzed for PD morphology). Decreases in simple and twinned PD and an increase in branched PD structures were found in *ugt80B1* in comparison to wild-type (Chi-Square test of independence, $X^2(2, N=1059)=61.9275, P<0.0001$). Examples of complex PD structures (twinned, H and Y forms) imaged using TEM (**B**). Cell wall (CW) is indicated by false color pink, Cytoplasm (CP) is indicated by false color green, Scale bar = 100 nm). TEM images were used to take diameter measurements from middle (**C**) and neck regions (**D**) of the PD from wild-type and both *ugt80B1* alleles ($n \geq 250$). Images illustrate the regions chosen for the measurements (**E**) (white carats mark the neck and purple carats mark the middle). Scale bar = 100 nm.

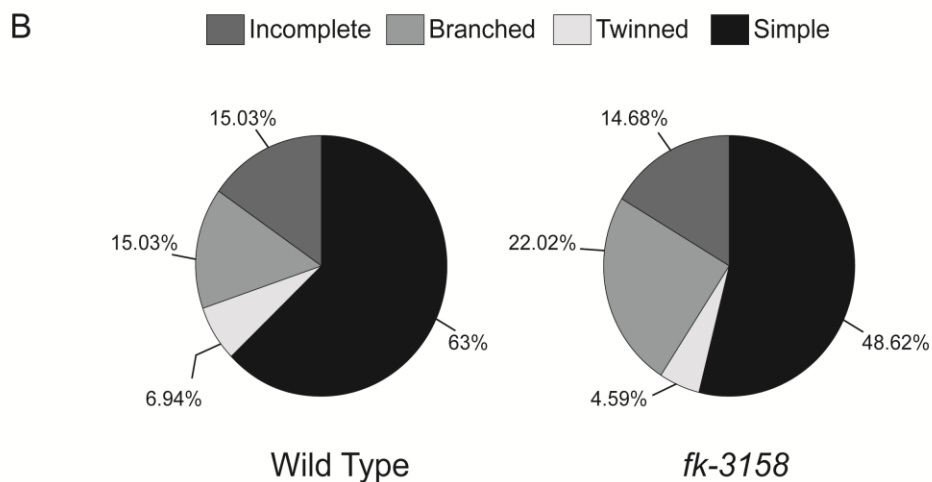
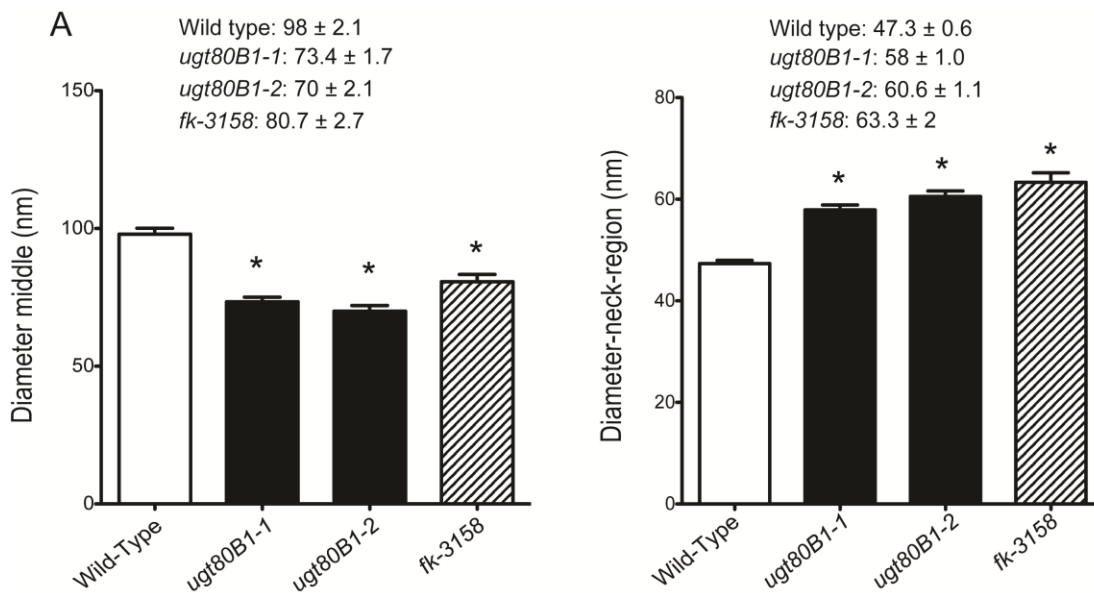


Figure 3.9 PD phenotype is present in the *fackel* allele *fk-3158*. A) The plasmodesmata diameter phenotypes observed in the *ugt80B1* alleles were also evident in *fackel fk-3158*. B) Branching structure of the PD was also altered in the *fackel fk-3158* compared with wild-type. * indicates significant difference from the mean established at $P = 0.05$ (Student T-test), with standard error and mean values added in A.

Sterol glucoside profiling reveals reduction of stigmasteryl glucosides in *ugt80B1* roots

To probe the relationship between the PD phenotype and SG composition, we quantified SG levels in roots from *ugt80B1* and *fk-J3158* mutants in comparison to wild-type. We also included *ugt80A2,B1* double mutants as well as *ugt80A2* single mutants as controls in our analysis. The *ugt80A2,B1* double mutants had previously been shown to exhibit a significant reduction in SG levels in seeds (Schrick et al., 2012), and other aerial tissues (DeBolt et al., 2009). Lipids extracted from roots were examined for SG composition by direct infusion electrospray ionization tandem mass spectrometry (ESI-MS/MS) (**Figure 3.10**; **Table 3.4**). The results show that in wild-type roots, the most common SG is sitosteryl glucoside (~76%), followed by campesteryl (~13%), stigmasteryl (~10%), brassicasteryl (~0.4%) and cholesteryl (0.1%) glucosides, similar to the SG composition observed in seeds (Schrick et al. 2012).

The SG profiles from *ugt80B1* mutant roots indicate a significant reduction in stigmasteryl glucosides (~56% of wild-type levels), but not in the other types of SG detected in the analysis (**Figure 3.10A**; **Table 3.4**). In contrast, *ugt80A2* mutant roots exhibited an overall decrease in total SG (~42% of the wild-type levels), and similar decreases in sitosteryl, campesteryl, and stigmasteryl glucosides (~41, 39 and 46% of wild-type levels, respectively) (**Figure 3.10A**; **Table 3.4**), suggesting that *UGT80A2* accounts for most of the SG production in roots. Consistent with functional redundancy for the two *UTG80* enzymes, *ugt80A2,B1* double mutants displayed an enhanced reduction in SG levels (~15% of wild-type levels) (**Figure 3.10A**; **Table 3.4**). SG profiling indicated that *fk-J3158* mutants also display a reduction in total SGs (58% of wild-type levels), with significant decreases in both sitosteryl and campesteryl glucosides (~54% and ~44% of the wild-type levels, respectively) (**Figure 3.10A**; **Table 3.4**). There was also a trend indicating a reduction in stigmasteryl glucosides in *fk-J3158*. Since ASGs are synthesized from SGs, we expected to observe reductions of several of these compounds in roots from the affected mutants. However, only the *ugt80A2,B1* double mutants exhibited a significant decrease in total ASGs, an average of ~66% of the wild-type level (**Figure 3.10B**; **Table 3.4**).

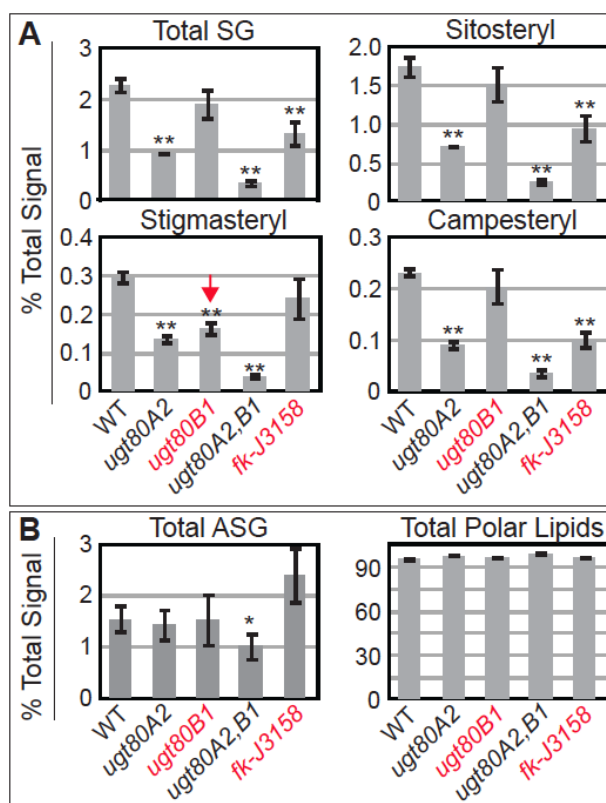


Figure 3.10 Steryl glucoside (SG) and acyl steryl glucoside (ASG) content in wild-type and mutant roots. (A) Total steryl glucosides (SG), and sitosteryl, stigmasteryl, and campesteryl glucosides, and (B) Acyl steryl glucosides (ASG) and total polar lipids were quantified as percent total signal by ESI-MS/MS for wild-type (WT), *ugt80A2*, *ugt80B1*, *ugt80A2,B1* and *fk-J3158*. (A) Arrow points to a reduction in stigmasteryl glucosides in *ugt80B1*. Error bars indicate SD for n=4. Significant differences from WT are indicated by a single asterisk ($P \leq 0.05$) or double asterisk ($P \leq 0.001$).

Table 3.4 SG and ASG quantification in roots. Mass spectral signals are shown as percentages of the total signal that included >95% total routine polar lipids for each sample. Averages are indicated for n=4, with standard deviations in parentheses. Significant decreases from Col wild-type (WT) are indicated by a single asterisk ($P \leq 0.05$) or double asterisk ($P \leq 0.001$).

	WT Col	<i>ugt80A2</i>	<i>ugt80B1</i>	<i>ugt80A2,B1</i>	<i>fk-J3158</i>
Total SGs	2.283 (0.170)	0.948** (0.058)	1.900 (0.305)	0.348** (0.086)	1.322** (0.268)
sitosteryl	1.745 (0.148)	0.714** (0.034)	1.521 (0.246)	0.263** (0.066)	0.951** (0.193)
stigmasteryl	0.296 (0.019)	0.136** (0.014)	0.165** (0.021)	0.039** (0.008)	0.242 (0.058)
campesteryl	0.231 (0.010)	0.091** (0.011)	0.204 (0.036)	0.036** (0.011)	0.101** (0.019)
brassicasteryl	0.008 (0.000)	0.005** (0.001)	0.007 (0.001)	0.003** (0.001)	0.019 (0.004)
cholesteryl	0.002 (0.000)	0.002 (0.001)	0.003 (0.001)	0.007 (0.003)	0.009 (0.003)
Total ASGs	1.525 (0.281)	1.421 (0.333)	1.527 (0.538)	1.004* (0.295)	2.384 (0.569)
Total 16:0	0.598 (0.085)	0.582 (0.088)	0.614 (0.256)	0.242* (0.036)	0.849 (0.235)

Table 3.4 Continued

16:0 sitosteryl	0.451 (0.068)	0.409 (0.053)	0.480 (0.198)	0.157* (0.024)	0.563 (0.138)
16:0 stigmasteryl	0.049 (0.009)	0.050 (0.007)	0.033 (0.013)	0.020* (0.005)	0.132 (0.046)
16:0 campesteryl	0.086 (0.012)	0.112 (0.028)	0.092 (0.041)	0.040** (0.007)	0.113 (0.044)
16:0 brassicasteryl	0.005 (0.001)	0.005 (0.002)	0.003 (0.002)	0.007 (0.005)	0.023 (0.015)
16:0 cholesteryl	0.007 (0.003)	0.006 (0.001)	0.006 (0.003)	0.018 (0.008)	0.018 (0.006)
Total 18:3	0.238 (0.057)	0.259 (0.069)	0.236 (0.069)	0.099* (0.035)	0.376 (0.051)
18:3 sitosteryl	0.174 (0.040)	0.192 (0.050)	0.180 (0.054)	0.044* (0.013)	0.230 (0.050)
18:3 stigmasteryl	0.027 (0.010)	0.028 (0.007)	0.018 (0.004)	0.008* (0.004)	0.057 (0.012)
18:3 campesteryl	0.029 (0.005)	0.032 (0.010)	0.030 (0.010)	0.030 (0.010)	0.064 (0.015)
18:3 brassicasteryl	0.003 (0.001)	0.003 (0.001)	0.003 (0.000)	0.004 (0.004)	0.009 (0.002)
18:3 cholesteryl	0.005 (0.003)	0.004 (0.001)	0.005 (0.002)	0.013 (0.006)	0.016 (0.002)
Total 18:2	0.343 (0.068)	0.272 (0.079)	0.360 (0.112)	0.242 (0.082)	0.560 (0.136)
18:2 sitosteryl	0.257 (0.046)	0.204 (0.056)	0.283 (0.086)	0.142* (0.042)	0.389 (0.110)
18:2 stigmasteryl	0.029 (0.006)	0.029 (0.009)	0.024 (0.007)	0.016* (0.004)	0.071 (0.025)
18:2 campesteryl	0.044 (0.014)	0.031 (0.010)	0.042 (0.015)	0.046 (0.017)	0.061 (0.011)
18:2 brassicasteryl	0.002 (0.001)	0.003 (0.001)	0.004 (0.001)	0.006 (0.002)	0.013 (0.002)
18:2 cholesteryl	0.011 (0.009)	0.005 (0.002)	0.008 (0.004)	0.032 (0.020)	0.026 (0.007)
Total 18:1	0.259 (0.080)	0.237 (0.087)	0.216 (0.071)	0.199 (0.086)	0.369 (0.105)
18:1 sitosteryl	0.183 (0.038)	0.173 (0.062)	0.162 (0.053)	0.084* (0.029)	0.200 (0.064)
18:1 stigmasteryl	0.026 (0.021)	0.016 (0.005)	0.011 (0.004)	0.036 (0.022)	0.060 (0.019)
18:1 campesteryl	0.032 (0.010)	0.037 (0.015)	0.028 (0.010)	0.024 (0.010)	0.053 (0.015)
18:1 brassicasteryl	0.008 (0.011)	0.004 (0.002)	0.004 (0.002)	0.020 (0.011)	0.022 (0.010)
18:1 cholesteryl	0.010 (0.005)	0.008 (0.003)	0.010 (0.004)	0.035 (0.018)	0.033 (0.009)
Total 18:0	0.086 (0.033)	0.071 (0.028)	0.102 (0.034)	0.223 (0.074)	0.231 (0.009)
18:0 sitosteryl	0.037 (0.011)	0.035 (0.013)	0.049 (0.019)	0.072 (0.028)	0.059 (0.019)
18:0 stigmasteryl	0.007 (0.003)	0.006 (0.002)	0.005 (0.002)	0.011 (0.006)	0.015 (0.008)
18:0 campesteryl	0.014 (0.008)	0.011 (0.004)	0.017 (0.010)	0.080 (0.028)	0.086 (0.019)
18:0 brassicasteryl	0.003 (0.001)	0.003 (0.001)	0.003 (0.001)	0.008 (0.004)	0.011 (0.004)
18:0 cholesteryl	0.025 (0.014)	0.017 (0.008)	0.028 (0.008)	0.052 (0.018)	0.060 (0.028)
Total Routine Polar Lipids	95.638 (1.206)	97.595 (0.389)	96.354 (0.965)	98.581 (0.347)	96.224 (0.843)

3.3 DISCUSSION

UGT80B1 is a novel membrane component required for epidermal cell fate in the root.

In this report we present a suite of evidence linking UGT80B1, an enzyme that mediates sterol glycosylation, to the cell fate determination pathway in the root epidermis. Epidermal patterning defects are apparent in *ugt80B1* (**Figure 3.3**), and were further confirmed by misexpression of the *ProGL2:GUS* reporter in both H and N cells from *ugt80B1* roots (**Figure 3.4; Table 3.3**). Moreover, in *ugt80B1* mutants, WER transcripts corresponding to the R2R3-MYB transcription

factor were abnormally upregulated (**Table 2.6**) and aberrant accumulation of *WER:GFP* occurred at both N and H positions (**Figure 3.4**). In addition to the similar misexpression of *WER* and its target *GL2*, the *SCM* mRNA was identified as differentially expressed in *ugt80B1* mutants (**Table 2.6**). *SCM* signaling relays positional information from the underlying cortical cells to establish and reinforce epidermal cell fates (Kwak and Schiefelbein, 2008). In the meristematic zone, *ugt80B1* displayed a normal distribution of *SCM:GFP* marking the PM in both N and H cells (**Figure 3.4**). However in the early elongation zone, *SCM* was not preferentially localized to H cells as it is in wild-type. In addition to the loss of cell-type specific expression in *ugt80B1*, *SCM:GFP* appeared to decrease at the PM and instead was found in punctate-like structures (**Figure 3.4**). This abnormal cytoplasmic aggregation of *SCM* indicates that *UGT80B1* is required for subcellular targeting of *SCM* to the PM.

A major finding described here was that the *UGT80B1* protein, like *SCM*, is localized within the PM, where it is presumably involved in glycosylation of specific membrane sterols. A translational fusion to *GFP* indicated that *UGT80B1* is targeted to ER, PM and cell wall-associated punctae identified as PD (**Figure 3.6**). Indeed, in living cells we visualized *UGT80B1:GFP* in ER tubules that spanned the PM and cell wall, displaying coincident behavior between adjacent cells (**Movie 3.2**). Time-lapse observation revealed *UGT80B1* at sites of cell-cell association. The data indicate that *UGT80B1* localized in a non-uniform manner and additionally provides direct evidence for an ER continuum between cells in the root epidermis.

Membrane modules at PM and PD are required for root epidermal patterning

Collectively, the data presented here support the notion that both PM and PD membranes in association the cell walls are dysfunctional in the *ugt80B1* mutant. *SCM*-mediated signaling requires high protein concentrations of the *SCM* receptor to preferentially accumulate in H cells in order to establish the H cell fate (Kwak and Schiefelbein, 2009). As described above, the aberrant cytoplasmic aggregation of *SCM* in *ugt80B1* mutants, coupled with reduced levels of expression at cell boundaries points to a role for *UGT80B1* in anchoring the *SCM* receptor at the PM. We propose that *UGT80B1* and a specific sterol glycoside composition support a defined membrane environment at the PM for targeted localization of *SCM* and possibly other yet unidentified membrane-associated proteins that act together with *SCM* in epidermal patterning.

UGT80B1 function is also necessary for the cell-type-specific expression of *SCM*. In the early elongation zones of root epidermis, *ugt80B1* mutants abnormally display expression of *SCM:GFP* in both H and N cells (**Figure 3.4**). *SCM* signaling requires positional cues from the underlying cortical cells to initiate downstream transcriptional events. At later stages a bias towards accumulation of *SCM* in H-cells occurs as a result of transcriptional repression of *SCM* by the *WER-GL3/EGL3-TTG1* complex in N cells (Kwak and Schiefelbein 2009). The small single-repeat R3-MYB transcription factor *CPC* is a positive

regulator of SCM in H cells (Kwak and Schiefelbein, 2008; Ryu et al., 2005). Although WER negatively regulates CPC expression in N cells, the mobility of CPC into neighboring H cells inhibits WER and its own expression. Competition between CPC and WER in binding to the EGL3/GL3-TTG1 complex in H cells feeds into the auto-regulatory network resulting in SCM accumulation in H cells. CPC mobility is likely to be aberrant in *ugt80B1*, based on *GL2:GUS* and WER:GFP reporter lines that show expression in both H and N cell files in *ugt80B1*. Like *ugt80B1* mutants, loss-of-function mutants in *CPC* display reduced numbers of H cells in the root epidermis (Wada et al., 1997). Moreover, *cpc* and *ugt80B1* mutants exhibit similar expression patterns for both *GL2* and WER reporter lines ((Lee and Schiefelbein, 2002); **Figure 3.4**). We propose that UGT80B1, through its sterol glycosylation activity, provides a conducive membrane environment at PD to facilitate the regulated cell-to-cell movement of R3-MYB transcription factors like CPC, TRY and ETC1.

***ugt80B1* mutants provide evidence for the role of plasmodesmata in the root epidermal patterning**

The abnormal morphology of PD seen in *ugt80B1* mutants, characterized by constricted middle aperture and flared neck regions (**Figure 3.8**) indicates that sterol versus SG composition determines the 3D structure and architecture of this specialized membrane. Membrane composition is thought to be critical in the functional scaffolding to support PD structure and morphology. Indeed, the unique membrane curvature and specialized proteins that reside in PD (Maule et al., 2011; Tilsner et al., 2011) point towards a role for membrane microdomains (Tilsner et al., 2011). Strikingly, various proteins associated with the PD proteome (Fernandez-Calvino et al., 2011) overlap with those identified from membrane microdomains (Kierszniowska et al., 2009; Lefebvre et al., 2007). Several such predicted PD-associated proteins including SCM itself (Fernandez-Calvino et al., 2011) were also uncovered as being differentially expressed in *ugt80B1* (**Table 2.7**). However, the SCM receptor has not previously been localized as PD. Consistent with reports of membrane microdomains functioning as signaling platforms (Lefebvre et al., 2007) as well as enrichment of microdomains at the PD (Tilsner et al., 2011) it is possible that a transient localization of SCM to the PD exists supported by its existence in Arabidopsis PD proteome (Fernandez-Calvino et al., 2011). Additionally, TETRASPANINS and RETICULONS, two PD-resident proteins implicated in the maintenance of PD structure (Maule et al., 2011; Tilsner et al., 2011) were found to be up-regulated in *ugt80B1* (**Table 2.7**). This observation suggests that self-regulating transcriptional feedback could arise from PD dysfunction.

Of the small single-repeat R3-MYB transcription factors that are thought to participate in cell-to-cell movement in the root epidermis, CPC has been studied most extensively (Kurata et al., 2005a). In addition to the results provided here, several lines of evidence support of the notion that PD are the passage ways that allow CPC to move from N cells where the transcript is synthesized to H cells where the protein becomes nuclear localized (Kurata et al., 2005a). It was

previously found that Brefeldin A (BFA) treatment was not able to inhibit CPC movement, nor was expression in the secretion mutant *rhd3* (Kurata et al., 2005a), arguing against secretion-internalization dependent apoplastic transport. Additionally, the regulation of CPC movement was found to be tissue specific and CPC was shown increase the size exclusion limit between epidermal cells, characteristic of proteins that are transported via PD in a regulated manner (Kurata et al., 2005b).

Targeting to the PD membranes is likely to be mediated by specific interactions. It is plausible that such interactions involve a unique lipid environment that is specific to the cell type and its developmental stage. Movement of the homeodomain transcription factor KNOTTED, for example, depends on the developmental state of the tissue (Kim et al., 2003). If competency is dependent upon developmentally regulated factors, these might also include the specific lipid architecture of the PD. Therefore lipid composition, including ratios of sterols to SGs, could be quantitatively or qualitatively regulated to determine the structure and function of specialized membranes, such as those found in PD.

Common mechanisms underlying epidermal patterning in the root and leaf

The results presented here provide evidence for the role of glycosylated sterols in regulating epidermal cell fate in the root (**Figure 3.11**). A deficiency in specialized steryl glucosides (ie. stigmasteryl glucosides) in both the *fk-J3158* and *ugt80B1* mutants may explain their similar defects in PD morphogenesis and structure (**Figure 3.8, Figure 3.9**). The *fk-J3158* allele (Qian et al., 2013) was originally identified in a genetic screen for stomatal patterning mutants. In *fk-J3158* mutants, abnormal stomatal clusters form, presumably due to aberrant asymmetric cell divisions coupled with a suspected lesion in cell-to-cell signaling (Qian et al., 2013). Stomatal patterning relies on both asymmetric divisions and cell-to-cell communication for cell fate decisions. Similar to root epidermal cell patterning, stomatal patterning within the leaf epidermis follows a pattern in which at least one pavement cell forms between a pair of guard cells (Dong and Bergmann, 2010). Positive regulators of stomatal cell development include a set of basic helix-loop-helix (bHLH) TFs (FAMA, SPEECHLESS (SPCH), MUTE, ICE1/SCREAM, SCREAM2) (Kanaoka et al., 2008; MacAlister et al., 2007; Ohashi-Ito and Bergmann, 2006; Pillitteri et al., 2007). Negative regulation involves receptor-mediated signaling that prevents the neighboring cells from adopting the stomatal cell fate (Lee et al., 2012). Mutations in any of the regulators result in the formation of clusters of stomata on leaves.

A connection to PD comes from the characterization of mutations in *GLUCAN SYNTHASE-LIKE 8 (GSL8)*, which encodes a putative callose synthase that is required for callose deposition at the cell plate, cell wall and PD. It was suggested that abnormal stomatal clusters found in *gs/8* mutants are caused by an increased permeability of PD between adjacent cells (Guseman et al., 2010). Opposite to what is observed in the root epidermal cells, in stomatal patterning, the restriction of symplastic movement is required for the proper

segregation of cell fates. However, the commonality of the involvement of PD membrane channels in both stomatal and root epidermal cell patterning systems presents an opportunity to study the convergence of a specific role for a defined sterol versus SG environment in the formation of this specialized membrane compartment.

In conclusion, a major finding reported here is that disruption of *UGT80B1*, which encodes an enzyme implicated in the production of SGs, results in aberrant epidermal cell fate determination in the *Arabidopsis* root (**Figure 3.1**). SG profiling of root tissues indicated that in comparison to wild-type, *ugt80B1* mutants have a significant decrease in stigmaterol glucosides, but not in other sterol derivatives that were analyzed (**Figure 3.10**), suggesting that a specific SG deficiency may be responsible for the observed *ugt80B1* phenotypes. UGT80B1 may also be required for the synthesis of additional critical sterol glycosides that were not detected in our analysis. It is plausible that specific cell types in *ugt80B1* mutants, such as differentiated H cells, have localized deficiencies that were missed by analysis of lipid extracts from whole roots. Since UGT80B1 catalyzes the glycosylation of existing membrane sterols, its functional recruitment to sites of membrane specialization, such as PD, illustrates the capacity for plant cells to diversify local membrane environments in a spatially discrete manner (**Figure 3.6**). The differentiation of epidermal cells in the root likely represents a highly dynamic biological process. Taken together, the present study provides evidence for a model in which localized concentrations of specific SG compounds in cell-wall associated membranes, such as PD and PM, orchestrate the dynamic molecular events underlying epidermal patterning.

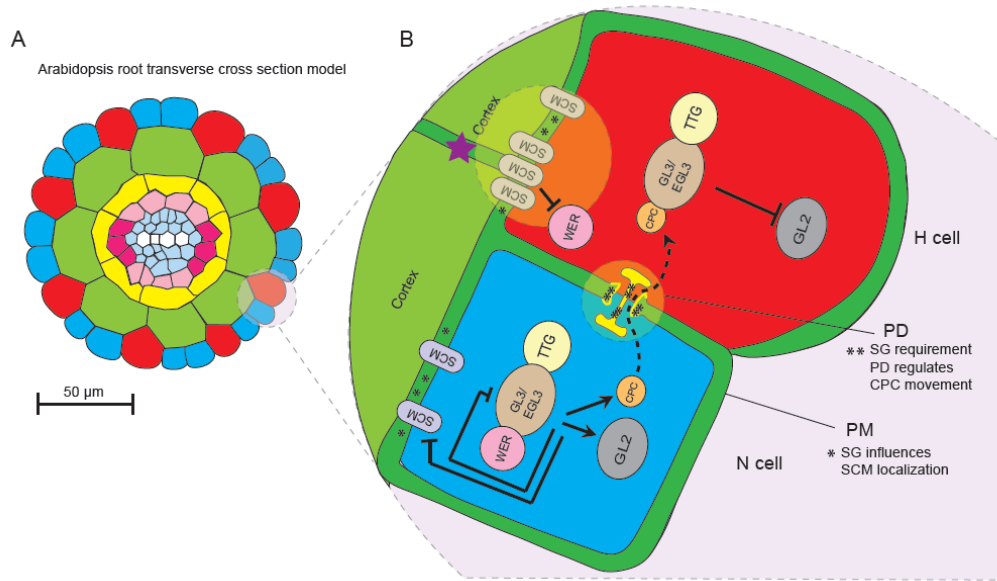


Figure 3.11 Model illustrating membrane SG requirement for epidermal patterning. A diagram depicting all the cell layers in a transverse section of Arabidopsis root. Focus is placed on the outermost epidermal cell layer with alternating N (non-root hair) cell (blue) and H (root-hair) cell (red) (A). Signaling pathway for the formation of alternating H and N cell epidermal pattern (B). SG influences localization of SCM receptor kinase at H and N cell PM. This localization marks the beginning of N versus H cell patterning. Epidermal cells located over the underlying cortical cell receive less of the positional cue required to switch on SCM mediated signaling. This leads to expression of GL2 and CPC and repression of SCM. GL2 influences maintenance of N cell fate. Epidermal cells located on the anticlinal walls of underlying cortical cells receive enough positional cue (purple star) to switch on SCM signaling and repression of WER. CPC moves from to adjacent N cell to developing H cell via PD. SG influences this movement by maintaining PD structure and morphology.

3.4 METHODS

Plant material and growth conditions *Arabidopsis thaliana* lines used in this study were of the Columbia ecotype (Col-0). T-DNA insertion alleles for *ugt80B1-1* (SALK_021175), *ugt80B1-2* (SALK_021175), and *ugt80A2* (SALK_020939) were obtained from the Salk collection (Alonso et al., 2003). The homozygous *ugt80A2,B1* double mutant was constructed by crossing. The *fk-J3158* allele was previously described (Qian et al., 2013). DeBolt et al., (2009) documented the *ugt80B1* and *ugt80A2* mutants in the Wassilewskija (Ws-0) background. Homozygosity for the Col-0 T-DNA insertions was confirmed by PCR. The transgenic line expressing *ProUGT80B1:GUS* was previously described (DeBolt et al., 2009). Reporter lines for genetic crosses have been described previously: *ProGL2:β-glucuronidase (GUS)*, *ProWER:WER-green fluorescent protein (GFP)*, *ProSCM:SCM-GFP* (Kwak and Schiefelbein, 2008; Lee and Schiefelbein, 1999;

Masucci et al., 1996). Reciprocal crosses were performed with *ugt80B1-1* and transgenic lines carrying reporter constructs. Progeny genotypes were confirmed among the F2 by screening for the transparent testa seed phenotype and fluorescence microscopy/GUS staining for reporters and/or PCR with primers for GFP and GUS. Seeds were sterilized using 30% household bleach solution and chilled for 3 days in 0.15% agar at 4°C in dark prior to planting.

Constructs To generate the CaMV-35S promoter GFP reporter line, the open reading frame for UGT80B1 was amplified from wild-type Col-0 genomic DNA using a DNeasy Plant Mini Kit (QIAGEN) with 5'-ggggacaagtttgatacaaaaagcaggcttcATGGCTAGTAATGTATTTGATCATCC-3' and 5'-ggggaccactttgtacaagaaagctgggtCACGCCACCACATGGAAGACAACACT-3' forward and reverse primers and cloned directly into the destination vector pMDC83 (Curtis and Grossniklaus, 2003). The GFP:UGT80B1 reporter line with its native promoter was constructed by PCR amplification using the following: 5'-TCCCCCTGCAGGCCACCCTAATGTTTGGTCATTTGATGT-3' and 5'-CGGGGTACCCACCTTTAAAACTGAATTCAACTAACAGC-3'. The PCR product was digested with *Sbf*I and *Kpn*I and ligated into the pMDC43 vector at matching sites to replace the CaMV-35S promoter. The UGT80B1 coding sequence was PCR amplified from Col-0 cDNA using 5'-GCTTGGCGCGCCCATGGCTAGTAATGTATTTGATC-3' and 5'-GGCCTTAATTAATCACACGCCACCACATGGAAGAC-3'. The PCR product was sequenced and digested with *Asc*I and *Pac*I and cloned at the respective sites fusing the cDNA to a C-terminal GFP in the pMDC43 vector containing proUGT80B1 resulting in the *ProUGT80B1:GFP:UGT80B1* construct. Both constructs were sequence verified using promoter and gene flanking primers and three nested primers: 5'-CACTGTCCCGTCATTTTG-3', 5'-GTGCCATTCTTTGGGGAT-3' and 5'-CGATGTGCAGCCTTTTCT-3'. The destination constructs were transformed into *ugt80B1* plants by *Agrobacterium tumefaciens*, mediated floral dip (Clough and Bent, 1998). Complementation of *ugt80B1* was monitored by restoring testa color (DeBolt et al., 2009). UGT80B1:GFP seedlings examined for subcellular localization were bright homozygous lines identified from the T2 and analyzed in subsequent generations.

Laser scanning confocal microscopy and fluorescence stereomicroscopy

Seeds were germinated on plates containing sterilized 0.5X Murashige and Skoog (MS) (Murshige and Skoog, 1962) agar for 7–14 d in light conditions at 21°C in a Conviron Adaptis1000 environmental chamber fitted with a Conviron *Arabidopsis* light kit (Conviron). For stereomicroscopy, individual seedlings were visualized either in MS agar without removing them from plates and employed both brightfield and fluorescence modes. For confocal microscopy of seedlings, a custom built U-shaped parafilm sandwich was made from 2 layers of parafilm cut with a razor blade to a microscope slide (75 by 25 mm) width and immobilized with vacuum grease to a microscope slide. The U-shaped regions were filled with 0.5x MS media containing 1% agar and sterilized seeds were planted at the open

end of the U prior to covering the sandwich with a cover slip and allowing the agar to solidify at a 10° angle. Once mounted, seeds were germinated by placing the mounted slides in a sterilized plate containing a moistened kimwipe to limit water loss from the slide for 4-7 days in continuous light. Imaging of seedlings in the dark was performed on an Olympus MVX-10 Macro/Stereo fluorescence microscope with a Prior light source and GFP filter (Olympus) and 1X objective employing internal 2X zoom, or an Olympus FV1000 laser scanning confocal microscope using a 20x, 40x or 60x N.A. water-immersion objective equipped with lasers for excitation wavelengths ranging from 405–633 nm. EGFP and ERFP were excited using the 488 nm and 543 nm, respectively and emission spectra were at 509 and 584nm respectively. Initial image processing was performed using Olympus Fluoview software (Olympus). All further image analysis was performed using ImageJ (W. Rasband, National Institute of Health, Bethesda, MD) software.

Plasmolysis 5-day-old transgenic seedlings expressing *Pro35S:UGT80B1-GFP* were treated with 0.8M mannitol for 2 hours with gentle shaking. The seedlings were stained with 10µg/ml propidium iodide prior to imaging the cotyledons.

Quantification of epidermal patterning All measurements were performed at the 'root hair zone' as defined earlier (Schiefelbein and Somerville, 1990). This area was approximately one vertical mm from the root tip and all measurements in this area were examined in 5-day old light grown seedlings. Area measurements for each trichoblast cell used area measurement output after tracing the polygon via the freehand selection tool (ImageJ) and pixel number² converted to µm². Measurements were made using ImageJ and statistical analysis was done using Prism4 (GraphPad) to obtain frequency distributions and significance using Students T-test. The distance measurements between trichoblast cells were calculated for wild-type and mutant using ImageJ for 6 seedlings each over 1.6 mm length of the root. The measurement was taken between centers of the base of one root hair to the next in the same trichoblast cell file. Percentage emergence of hair and non-hair cells in H and N cell file was calculated after manually analyzing the cell files for a minimum of 40 seedlings. Statistical analysis and significance was tested using Mann Whitney U test on Prism4 (GraphPad).

Resin Embedding and Sectioning In order to investigate radial patterning in the roots of *ugt80B1*, two day old seedlings from wild-type and mutant were harvested from 0.5% MS agar square plates and fixed in 3.4% glutaraldehyde and 4% paraformaldehyde in 0.1M Cacodylate buffer, pH 6.8 overnight at 4°C. Subsequently the seedlings were washed in the same buffer with 5% sucrose and post fixed with osmium tetroxide for 2 hours at 4°C. Gradual dehydration was performed in 50%, 70%, 80% and 90% graded ethanol on ice, followed by 2X 100% ethanol on ice and 2X propylene oxide at room temperature. Infiltration and embedding in LX112 (Ladd Research Industries) was achieved according to manufacturer's instructions. Ultrathin sections were cut on a Reichert-Jung ultracut microtome (Leica) with custom made glass knives.

TEM of 5-day-old Arabidopsis seedling roots

Resin embedding of *ugt80B1* mutants was done as mentioned above. Ultrathin sections were cut on a Reichert-Jung ultracut microtome (Leica) with custom made glass knives and collected on 300 mesh uncoated copper grids. After double staining with 2% aqueous uranyl acetate and lead citrate for 15 and 10 minutes, the sections were examined using a Philips BioTwin 12 transmission EM operated at 100 kV. Images were captured by a Gatan ES 1000W CCD camera. The PD aperture diameters were measured using the line tool in ImageJ. Middle and neck regions of individual PD were chosen for measurement and line length measured in pixels was converted to nm. Significance of measurements was computed through Bonferroni's multiple comparison test. To classify different PD structure; simple, complex and incomplete, PD structures were visually counted among the TEM micrograms modeled after work by Ehlers and Kollmann (1996). In order to separate PD structures that were incomplete and branched criteria was placed on branched structures whereby all structures classified as branched were complete. Independence of observations for types of PD were established through Chi-Square tests using SAS (SAS Institute, Cary, NC).

Global analysis of genes responding to *ugt80B1* *ugt80B1* and wild-type seeds were germinated and grown in liquid culture with 100 mg of seed in 100 ml of half strength MS media in each 250 ml conical flask in triplicate to eliminate secondary effects due to development and environment. Plants were grown under long-day conditions (16-h/8-h photoperiod) for 10 days and tissue was harvested within 5 minutes to avoid secondary effects of circadian clock related transcripts. The approach ensured adequate seedling material (100 mg = approximately 5500-6000 seedlings) for each RNA extraction, added experimental robustness by the large number of individuals in each sample and minimized any minor developmental transition effects. mRNA was extracted using an RNeasy Plant Mini Kit for RNA extraction as per manufacturer's instructions (QIAGEN). Since *UGT80B1* is expressed in all plant tissues (see eFP-analysis of At1g43620 (Winter et al., 2007)), 10-day post germination (dpg) seedlings were used for transcriptional profiling. Hybridization and gene chip analysis was performed at the University of Kentucky Microarray Core Facility. The data was then LOESS normalized. A 2-fold cutoff was used to qualify genes as differentially expressed (P-Value < 0.01). We applied DAVID analysis to the dataset to systematically map genes to associated biological annotations and highlight the most enriched or overrepresented biological annotation. The methods used for the DAVID analysis are defined (Huang et al., 2008).

Lipid Extraction and Electrospray Ionization Tandem (ESI-MS/MS) Mass Spectrometry

Seeds were surface-sterilized and sown onto 1.5% plant tissue culture grade agar containing 0.5X Murashige and Skoog medium (Murashige and Skoog, 1962), followed by stratification for 3 days at 4°C and transfer to continuous light at 23°C. At 4-5 days, seedling roots were harvested by cutting with a razor blade

and rapid transfer to hot isopropanol (75°C). Lipids were extracted using a protocol described previously (Schrick et al., 2012), a modification from the method by (Bligh and Dyer, 1959). The amount used for mass spectral analysis was 300 µl for *ugt80A2* and *ugt80B1* mutants, and the entire 1 ml sample for the *ugt80A2,B1* and *fk-J3158* mutants. Samples were dried under nitrogen, and a precise amount of standard mix was added. The samples were dissolved in 1.2 ml solvent comprised of chloroform/methanol/300 mM ammonium acetate in water (300/665/35). The internal standard mixture was comprised of 0.3 nmol di12:0-PC, 0.3 nmol di24:1-PC, 0.3 nmol 13:0-lysoPC, 0.3 nmol 19:0-lysoPC, 0.15 nmol di14:0-PE, 0.15 nmol di23:0-PE, 0.15 nmol 14:0-lysoPE, 0.15 nmol 18:0-lysoPE, 0.15 nmol di14:0-PG, 0.15 nmol-di20:0(phytanoyl)-PG, 0.15 nmol 14:0-lysoPG, 0.15 nmol 18:0-PG, 0.15 nmol di14:0-PA, 0.15 nmol di20:0(phytanoyl)-PA, 0.1 nmol di14:0-PS, 0.1 nmol di20:0(phytanoyl)-PS, 0.12 nmol 16:0-18:0-PI, 0.08 nmol di18:0-PI, 0.75 nmol 16:0-18:0-MGDG, 0.65 nmol di18:0-MGDG, 0.18 nmol 16:0-18:0-DGDG, 0.47 nmol di18:0-DGDG. Unfractionated lipid extracts were introduced by continuous infusion into the ESI source on an API 4000 electrospray ionization (ESI) tandem mass spectrometer (Applied Biosystems, Foster City, CA). Samples were introduced by an autosampler (LC MiniPAL, CTC Analytics AG, Zwingen, Switzerland), fitted with an injection loop for the acquisition time, and presented to the ESI needle at 30 µl per min. Targeted methods were employed for analysis of the di20:0(phytanoyl)-PG internal standard, SG, and ASG lipid molecules. Internal standard was detected with a scan for neutral loss of the head group moiety, NL 189.04 (C₃H₉O₆P + NH₃) in the positive mode. Routine polar lipids were detected as previously described (Xiao et al., 2010). For SG detection, a scan for neutral loss of the hexose moiety (NL 197.09, C₆H₁₂O₆ + NH₃) was used. ASG lipids were detected with neutral loss scans for the hexose moiety acylated with specified fatty acids (16:0, 18:3, 18:2, 18:1, and 18:0) + NH₃. Sample runs, mass spectra detection, and data analysis were performed as described (Schrick et al., 2012).

Chapter 4: Steryl glycoside biosynthesis is necessary for sustained root hair growth during *Arabidopsis* development

4.1 Introduction

The fundamental building blocks for development of a multicellular organism are based on the diversity of cell shapes and morphogenic forms. Polarity is a central theme of cellular differentiation and morphogenesis that span all taxa. A mechanism for controlling the polarity of membrane proteins in yeast and animal cells is via modulating the membrane sterol composition and in turn regulating their intracellular trafficking or lateral diffusion (Beh et al., 2009; Fischer et al., 2006; Keller et al., 1998; Porter et al., 1996; Slaughter et al., 2009). In plants too, sterols play a major role in morphogenesis, cell differentiation, cell polarity and patterning (Lindsey et al., 2003) and can be divided into two primary metabolic fates; one branch forming membrane sterols (primary sitosterol, stigmasterol and campesterol) and the other branch forming the plant hormone brassinosteroid. Herein, focus is placed on the membrane sterols branch. Mutations in genes involved in sterol biosynthesis such as *FACKEL* (sterol-C-14 reductase), *CEPHALOPOD* (sterol methyltransferase), *HYDRA1* (sterol $\Delta 8$ - $\Delta 7$ isomerase) and *COTYLEDON VASCULAR PATTERN1* (C-28 methyltransferase) all were found to cause severe developmental phenotypes (Topping et al., 1997; Schaller, 2003; Schrick et al., 2000; Schrick et al., 2002). Further, by live cell imaging, sterols have been shown to be central to the acquisition of cell polarity by modulating PIN protein localization (Willemsen et al., 2003) or via modulating endocytosis after cell division in root cells of *Arabidopsis* (Jaillais et al., 2008; Men et al., 2008). Yet, one of the interesting features of membrane sterols in plants is the degree to which they are glycosylated (Uemura and Steponkus, 1994; Yoshida and Uemura, 1986). Despite glycosylated sterols comprising a significant percentage of membrane sterols in plants (10-40% Grille et al., 2010), the functionality of steryl glycosides remains entirely unexplored with respect to development and patterning.

Steryl glycosides and acyl steryl glycosides are abundant constituents of the cellular membranes of higher plants (Warnecke and Heinz, 1994; Warnecke et al., 1997; Warnecke et al., 1999). Decorating the 3-hydroxy group of a sterol with a sugar moiety greatly expands the hydrophilic part of the lipid, which by theory would result in biophysical alteration of the membrane. These metabolites are generated by the catalytic activity of membrane-bound UDP-glucose:sterol glucosyltransferase proteins UGT80A2 and UGT80B1 (Warnecke et al., 1997). UDP-glucose:sterol glucosyltransferase activity has been found primarily in the plasma membrane (PM), Golgi vesicles and the endoplasmic reticulum (ER) membrane (Hartmann-Bouillon et al., 1987; Ullmann et al., 1993; Warnecke et al., 1997; Yoshida and Uemura, 1986) but the proteins themselves have yet to be localized for intracellular dynamics. There are no biomarkers specific for the glycosylated forms of sterol within the cell, but they have been isolated in abundance in the abovementioned membranes as well as recent reports of composing a large fraction of detergent resistant plasma membrane (DRM)

fractions (Laloi et al., 2007). The role of UGT80B1 in sterol glycoside biosynthesis was characterized genetically in respect to its putative role in priming cellulose biosynthesis (Peng et al., 2002), and found to have no impact on cellulose biosynthesis, but was important for flavanoid accumulation during seed development and the transport of macromolecules such as suberin and cutin across the plasma membrane (DeBolt et al., 2009). Hence, glycosylation modification of membrane sterols by UGT80B1 has a marked impact on membrane performance, including macromolecule transport. To explore the possibility that glycosylation of membrane structural sterols by UGT80B1 would be required to facilitate cellular morphogenesis and polarized growth, we conducted a reverse genetic analysis of *ugt80B1* focused on regions of the plant where developmental defects have been linked to sterol biogenesis (Men et al., 2008); the Arabidopsis root. Analyses of *ugt80B1* action, reported here, suggest that UGT80B1 is a root hair tip localized protein required for anisotropic root hair expansion in the root of *Arabidopsis thaliana*.

4.2 Results

***UGT80B1* is required for correct root hair elongation**

Examination of roots compared between wild-type Col-0 and *ugt80B1* documented that the length of root hairs was ablated in *ugt80B1* (**Figure 4.1**). To delineate the functional significance of UGT80B1 for root hair development, we grew plants containing T-DNA insertion in *UGT80B1* (SALK_021175 (*ugt80B1-2*) and *ugt80B1* (DeBolt et al., 2009)) vertically on 0.5% MS-agar plates for 7-14 days and examined the epidermal cell layer by stereomicroscopy (**Figure 4.1B** and **Figure 4.1C**). In order to not disturb the morphology or the overall phenotype of root hair positioning, roots were examined in the MS-agar plate. A distinct loss of root hair elongation was observed throughout the root in *ugt80B1* relative to wild-type controls (**Figure 4.1C**). In the *ugt80B1* plants, the degree to which root hairs elongated displayed some variation; this variability ranged from extreme truncation, whereby root hairs initiated at the bulge stage, but failed to elongate to instances where root hair anisotropy was maintained for partial root hair elongation (**Figure 4.1C**). Nevertheless, root hair length was significantly shorter in *ugt80B1* compared to wild-type (40% of wild-type)(**Figure 4.1B**). To address the postulate that the UGT80B1 transcript was accumulating in the root hair cells, we grew plants expressing a *proUGT80B1:: β -glucuronidase* (GUS) fusion and examined fixed and stained roots by light microscopy. Whole fixed plants were stained with x-glucuronide and optically examined by light microscopy revealing transcript accumulation throughout the root hair development process (**Figure 4.2**). No phase of root hair development showed a distinguishable spike in transcript abundance (**Figure 4.2A**). We interpret these events to be consistent with UGT80B1 gene expression at a steady state from the onset of root hair development and support findings of altered root hair phenotype.

Quantitative comparison between wild-type and *ugt80B1* was made for both length and width dimensions of individual root hairs. Due to the occasional

abortion of root hair formation in *ugt80B1* after bulge initiation stage, we measured only root hairs that expanded beyond the initial bulge formation (approximately 20 μm) for length and width measurements. On the basis of these criteria, root hair length perpendicular to the root epidermis was significantly lower in *ugt80B1* when compared to wild-type ($469 \pm 8.6 \mu\text{m}$ (SE) in wild-type seedlings to $187 \pm 4.6 \mu\text{m}$ (SE) in the *ugt80B1* root hairs $n=428$; ($P<0.001$ Mann–Whitney U test))(Figure 4.1D). Width of root hairs was measured by examining the cross sectional diameter of the base, middle and tip (at the most apical point before the root hair cap hemisphere). No significant difference in the diameter of the *ugt80B1* base and mid section, but a significant decrease in diameter was found at the tip when compared to wild-type (wild-type; base 10 ± 0.6 , mid 10 ± 0.6 , tip $8.5 \pm 0.6 \mu\text{m}$)(*ugt80B1*; base 10 ± 0.6 , mid 9 ± 0.8 , tip $7 \pm 0.6 \mu\text{m}$)(Figure 4.1E).

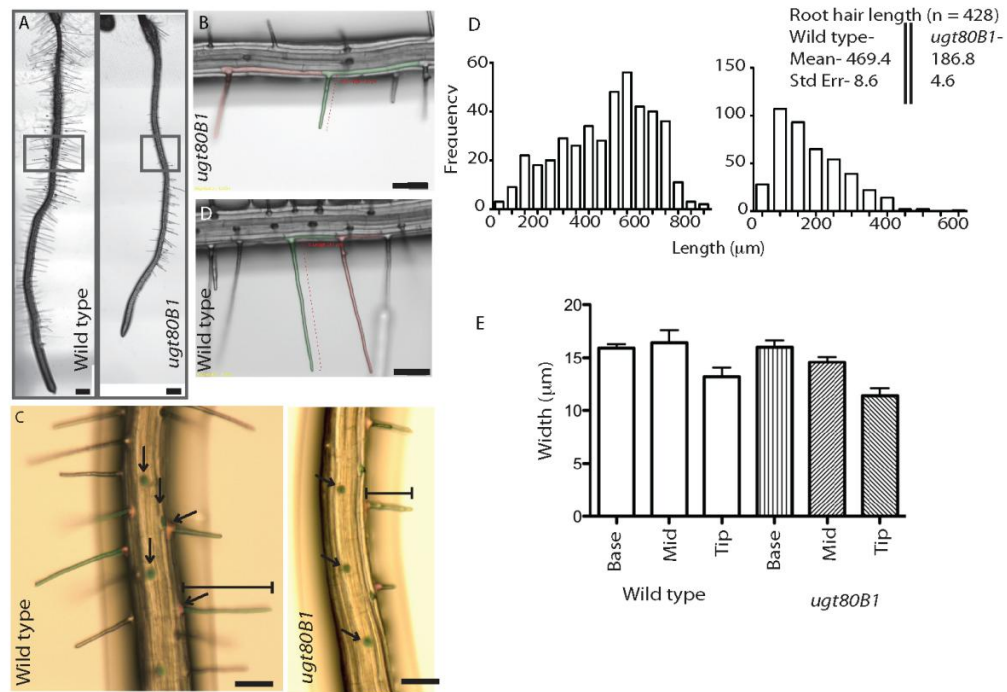


Figure 4.1 UGT80B1 is required for correct elongation of root hairs in Arabidopsis. (A–C) Stereomicroscopic examination of mutant *ugt80B1* Arabidopsis plants revealed suppression of root hair growth and development. Quantitative assessment of root hair elongation potential (D) compared between wild-type plants and those with genetic lesion in UGT80B1 ($n=428$)(A–C) showed a 2.5-fold reduction in length, which was deemed significant based on Mann-Whitney Test $P<0.0001$. By contrast, quantitative comparison of root hair width dimensions (E) between wild-type and *ugt80B1* (A–C) revealed no significant difference in width at the base or mid root hair, but a significant reduction in root hair tip width was observed ($P<0.05$) based on a Student T-Test. Scale Bars Represent = 100 μm .

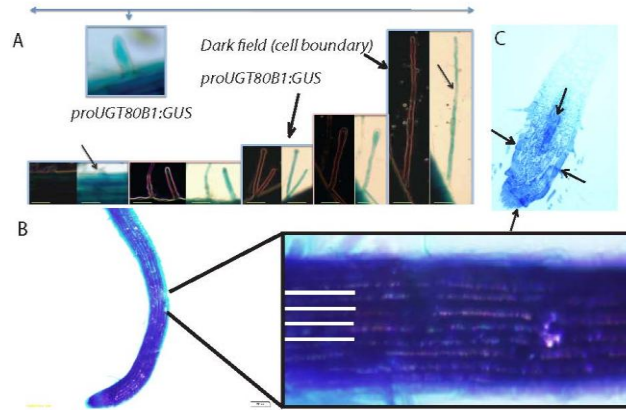


Figure 4.2 GUS expression data: **Histochemical analysis of *b*-glucuronidase**

Histochemical staining of β -glucuronidase (GUS) was performed according essentially to Bergmann et al. (2004). Briefly, seedlings expressing pro::UGT80B1- β -glucuronidase were immersed in 0.2 mL of cold staining solution containing 0.05 M sodium phosphate buffer pH 7.2, 0.2% Triton X-100, 2 mM potassium ferrocyanide, 2 mM potassium ferricyanide and 2 mM X-Gluc (5-bromo-4chloro-3-indolyl glucuronide) in 6-well cell culture plates kept on ice. Note: the X-Gluc was made up as 1M stock in dimethyl formamide. The culture plates were then incubated in darkness at room temperature with slight shaking on a rotary shaker overnight. The staining solution was then removed and seedlings were fixed and cleared using 70% and 95% ethanol solutions in series. The localization of GUS stain to developing root hairs (A) revealed consistency of *UGT80B1* expression in root hairs. Within epidermal root cells, no observed cell file specificity was determined for *UGT80B1* expression (B), based on uniform GUS staining. Gluteraldehyde fixed and longitudinally sectioned seedlings that were stained with GUS prior to fixation show increased GUS in epidermal cells and the meristematic tissue (C). Bar = 10 mm in A, 100 mm in B and C.

UGT80B1::GFP localizes to the growing tip of root hairs

Because genetic disruption of steryl glycoside synthesis by UGT80B1 caused a dramatic reduction in root hair growth, we sought to visualize the distribution of UGT80B1 in living root hair trichoblast cells by laser scanning confocal microscopy. To achieve this we developed two reporter constructs containing UGT80B1 fused to a green fluorescent protein (GFP) at the amino or carboxy termini and driven by the endogenous UGT80B1 promoter or the 35S-CaMV constitutive expression promoter. To reveal the localization of UGT80B1 without disturbing the root hair structures, which are highly sensitive to physical disturbance (Preuss et al., 2004), the root of UGT80B1::GFP was imaged first using stereo-fluorescence microscopy in sterile MS-agar media via a Z-series to account for depth of field (**Figure 4.3A**). Root hairs appeared decorated at the growing tip by distinct foci of fluorescence. Using confocal microscopy, a punctae of UGT80B1::GFP fluorescence was observed to mark the pre-bulge stage in the trichoblast cell developmental program. Subsequently, during bulge initiation,

UGT80B1 signal was concentrated within the early root hair structure (**Figure 4.3B**)(**Movie 4.1**). As the developmental program proceeded into root hair elongation, UGT80B1::GFP localized as a spatially discrete fluorescence accumulation at the growing tip (**Figure 4.3A** and **Figure 4.3C**). The plasma membrane was unevenly labeled with UGT80B1::GFP along the longitudinal axis of the developing root hair (**Figure 4.3A inset**, **Figure 4.3D**, **Figure 4.3E**). Spatially discrete tip localized fluorescence of UGT80B1 partially overlapped with the internal polarity of the cytoplasm (**Figure 4.3B**). Intriguingly, careful examination of UGT80B1::GFP at the initial stages of root hair development in a trichoblast cell file showed dynamic intercellular coordination events at the basal lateral cell interface (**Movie 3.2**). To illustrate and quantify this behavior, the midpoint of the apical basal intercellular association was mapped by fluorescence profiling revealing a spike in fluorescence that moved across the apical basal boundary (**Movie 4.2**). The dynamic behavior of the intracellular structure displayed behavior consistent with the ER (**Movie 3.1**). The coordinate behavior was observed as an ER tubule displayed extreme flexing dynamics and rapid spatial displacement velocity. This result was interpreted as the ER, labeled by UGT80B1, in adjacent epidermal trichoblast cells displaying a degree of network coordination.

To further explore the spatial association between UGT80B1, which glycosylates membrane sterols at the C3 position (DeBolt et al., 2009) and a gross picture of sterol distribution, we colocalized the sterol-binding dye filipin with UGT80B1::GFP (**Figure 4.3D**). During preparation of this manuscript, Ovecka and coworkers (2010) elegantly reported the detailed localization of filipin to the plasma membrane and internal globular structures at the very tip and subapical regions of the root hair in the plasma membrane and vesicle-like particles (Ovecka et al., 2010). UGT80B1::GFP displayed a strong degree of spatial overlap with filipin in the elongating root hair (**Figure 4.3D**). Using the fluorescent properties of filipin (RFP channel), we quantified this result by generating a fluorescence distribution plot for UGT80B1::GFP in the GFP channel and overlaying this with the filipin distribution pattern using the RFP channel in an individual root hair. Both filters revealed a fluorescence spike co-aligned with the growing tip of the hair (**Figure 4.3D**).

Laser scanning confocal microscopy showed that fluorescence appeared in a half-circumference at the very tip of the root hair (**Figure 4.3E-F**). To quantify the transverse fluorescence distribution of UGT80B1::GFP at the tip, a series of three simple fluorescence plots were generated, which revealed that the majority of fluorescence concentrated at the boundaries of the root hair cap in stage a and b, and was uniform at the cap (stage c)(**Figure 4.3F**). The distribution of UGT80B1 in the apical zone was examined based on morphology and motility revealing distinguishable particles (**Figure 4.3G**). Apart from tip localization a thin band of fluorescence was observed at the base of the growing root hair (**Figure 4.3A inset**, **yellow arrow**). This has been interpreted as basal membrane fluorescence marking the site of root hair formation in a trichoblast cell in line with internal polarity of the cell and adding to the speculation of the role of secretion in

forming the apical punctae observed. Discreet subapical punctae were detected in the growing tip of the root hair (**Figure 4.3G, white arrows**). These were similar in distribution to sub-apical endocytic compartments described by Ovecka et al. (2010) that were labeled by filipin but were not as prominent. Using both *pro35S::UGT80B1::GFP* and *pro::UGT80B1::GFP::UGT80B1* reporter fusions to assay protein localization allowed us to test whether localization was post transcriptionally controlled. *UGT80B1* driven by both the endogenous and constitutive promoters resulted in no distinguishable differences in protein localization in the cell types assayed. It is possible that localization in the constitutively expressed fusion was present in other areas of the cell, but that residence time was too brief for detection by confocal microscopy. In this scenario, the coincidence between the *pro35S::UGT80B1::GFP* and *pro::UGT80B1::UGT80B1::GFP* might occur simply due to the resident time and concentration of UGT80B1 at the site of sterol (substrate) accumulation. Regardless, both reporter lines showed consistent intracellular localization.

Since intracellular localization of UGT80B1 was not previously characterized in root epidermal cells we examined the UGT80B1::GFP reporter by laser scanning confocal microscopy along with a gross localization of the developing root using stereofluorescence (**Figure 4.3A, Figure 4.4**). Live cell imaging by confocal microscopy showed a polarized localization of UGT80B1 in the root cap (**Figure 4.4A**) and revealed an apical-basal fluorescence distribution in individual epidermal cells (**Figure 4.4A, arrows**). Fluorescence stereomicroscopy of the root cap and lateral root showed increased fluorescence in the vasculature as well as the root cap (**Figure 4.4B, Figure 4.4C**). Consistent with biochemical studies (Hartmann-Bouillon and Benveniste, 1978; Hartmann-Bouillon et al., 1987; Ullmann et al., 1993; Yoshida and Uemura, 1986), UGT80B1 was localized to the ER (**Movie 3.1**), where sterol biosynthesis primarily occurs. Plasma membrane localization was also established, based on fluorescence distribution at the cell perimeter and short-term plasmolysis experiments, which revealed the presence of hechtian strands (**Figure 4.4D-F**). ER localization was determined based on morphology and motility of the intracellular signal being highly consistent with previously documented studies, such as the ER-mGFP5–HDEL (Men et al., 2008)(**Movie 3.1**). Overall, we interpreted these data to suggest that residence time of UGT80B1::GFP was highest in the ER and plasma membrane.

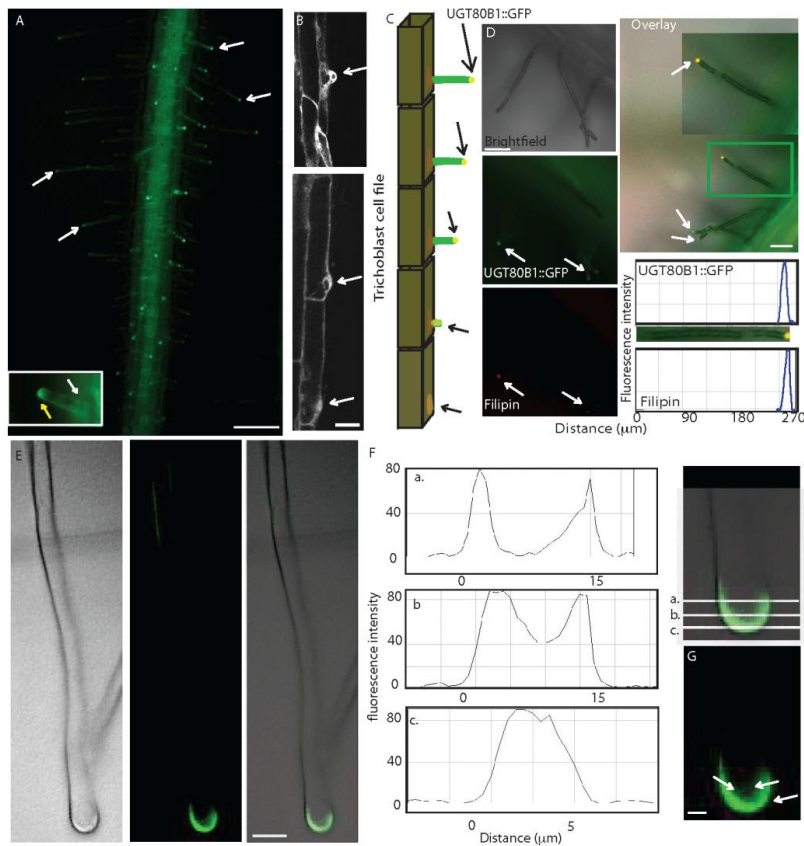


Figure 4.3 Fluorescence localization of UGT80B1::GFP in Arabidopsis root by stereomicroscopy and laser scanning confocal microscopy. (A) Global analysis of UGT80B1::GFP by stereofluorescence microscopy across the Arabidopsis root zone reveals spatially discrete punctate localization at the growing tip of root hairs (inset documents tip focused fluorescence distribution during early stages of root hair elongation). Whole cell view by laser scanning confocal microscopy documents UGT80B1::GFP accumulation at the pre-bulge stage in trichoblast cells and its discrete localization during root hair formation (B). A schematic overview of UGT80B1::GFP localization (C) within a trichoblast cell file (arrow indicated maxima of fluorescence during tip growth- not to scale). Spatially discrete localization of UGT80B1::GFP at the growing tip of root hairs colocalized with the sterol-binding dye filipin (D). Both filipin reactive sterols and UGT80B1::GFP fluorescence distribution over the length of an individual root hair showed coincident accumulation at the very tip of the hair. Live cell imaging of a root hair by confocal microscopy revealed a semi-dome shaped localization pattern at the growing tip of root hairs in UGT80B1::GFP expressing Arabidopsis plants (E-F). Fluorescence distribution quantification was consistent with fluorescence detection at the apical cap of the root hair (F). A minor degree of subapical fluorescence particles were detected (G). Scale Bars Represent = 100 μ m in (A) 10 μ m in (B and D), 20 μ m in (E), 5 μ m in (G).

[Movie 4.1.mov](#)

Movie 4.1: Documents a time lapse confocal examination of Figure 4.3B. Here, the pro::UGT80B1-GFP::UBT80B1 marks the site of root hair initiation accumulation during bulge stage. Laser scanning confocal microscopy was used for live cell imaging in seven day old light grown epidermal root cells, approximately 1 mm above the cell division zone. Bar = 10 mm

[Movie 4.2.mov](#)

Movie 4.2: Fluorescence plot of the entire apical basal division between trichoblast cells mapped using PLOT PROFILE add on to ImageJ (vis. 10 mm). Each image was separately uploaded coincident with a frame in the corresponding Movie 3.2. Each frame was merged into a movie file to show spatial distribution and fluorescence intensity over time.

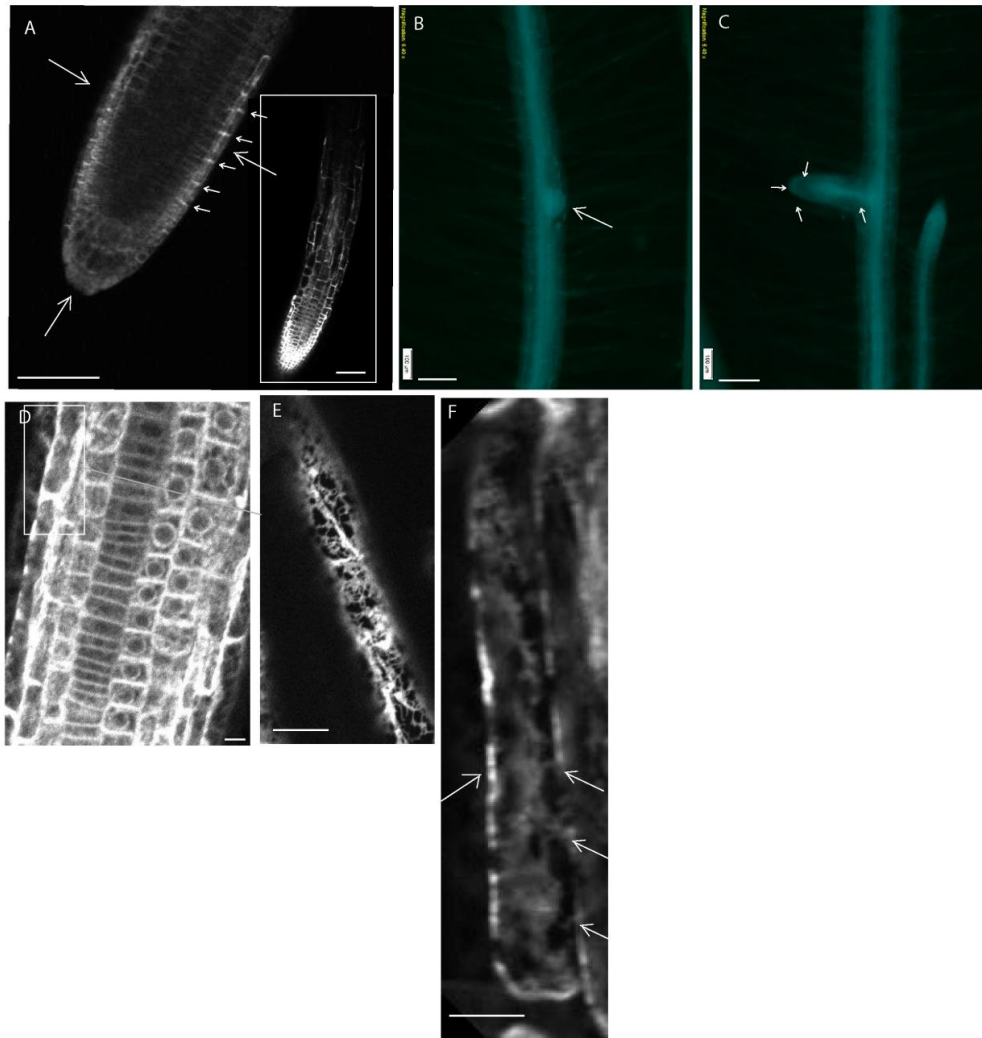


Figure 4.4 UGT80B1::GFP localization in epidermal cell types. Confocal live cell imaging of the root cap of plants expressing UGT80B1::GFP show root cap localized fluorescence and increased epidermal cell fluorescence (A). White arrows (A) indicate the increased fluorescence at the root cap extending laterally along the epidermis. Small white arrow indicate the position of the basal-apical cell interface between epidermal cells. The lateral root showed increased fluorescence in the vasculature as well as a distinct cap of fluorescence at the root cap (B-C). In the root expansion zone, approximately 1 cm above the cap, the localization of UGT80B1::GFP showed cell boundary (membrane) and endoplasmic reticulum (ER) association (D,E). (E) Confocal images of ER labeled with UGT80B1::GFP labeled in epidermal root cells of 3-d light grown *Arabidopsis* seedlings. Plasmolysis of epidermal cells using short-term treatment with aqueous NaCl solution showed the formation of Hechtian strands (F). Bar = 50 μ m in A, 100 μ m in B-C and 10 μ m in D-F.

Perturbation of actin disrupts root hair development and pre-bulge localization of UGT80B1

Pharmacological inhibition was used to examine the interaction between polarized UGT80B1::GFP localization and cell wall synthesis, polar auxin transport and an intact actin cytoskeleton. Plants expressing the UGT80B1::GFP reporter were grown vertically in the light in half strength MS media for seven days on sub-lethal doses of isoxaben (4 nM; cellulose inhibitor) and dichlorobenzonitrile (DCB; 500 nM; cellulose inhibitor) for cellulose inhibition, sucrose (2% in media) to cause synergistic effects on expansion, TIBA (1 μ M in media) as an auxin polar transport inhibitor, oryzalin for microtubule depolymerization (1 μ M in media) and latrunculin-B (lat-B 25-250 nM) to induce actin depolymerization. Radical elongation was used as a metric of expansion defect and then the pattern of UGT80B1::GFP localization documented (**Figure 4.5**). All drug treatments caused expansion defect in radical elongation, consistent with prior experimental data (Baluska et al., 2000; Chen et al., 1998; DeBolt et al., 2007; Favery et al., 2001). Root hair length was suppressed in plants grown on 2% sucrose and ablated in 250 nM Lat-B (**Figure 4.5**). By contrast, the cellulose inhibitor isoxaben increased root hair elongation and TIBA and DCB had mild effect on anisotropy. All drugs with the exception of Lat-B failed to cause mislocalization of the UGT80B1::GFP reporter from the growing tip of root hairs (**Figure 4.5**). The auxin polar transport inhibitor TIBA was documented to cause increased sub-apical fluorescence across the length of the root hair. Here, the reporter was maintained in the growing tip despite increased subapical fluorescence. Plants grown on 250 nM Lat-B produced a viable radical but failed to produce root hairs. Under Lat-B treatment, the UGT80B1::GFP reporter did not localize to the plasma membrane in epidermal root cells and was never observed to mark the basal-lateral site of root hair initiation as had occurred without drug treatment (**Figure 4.5**).

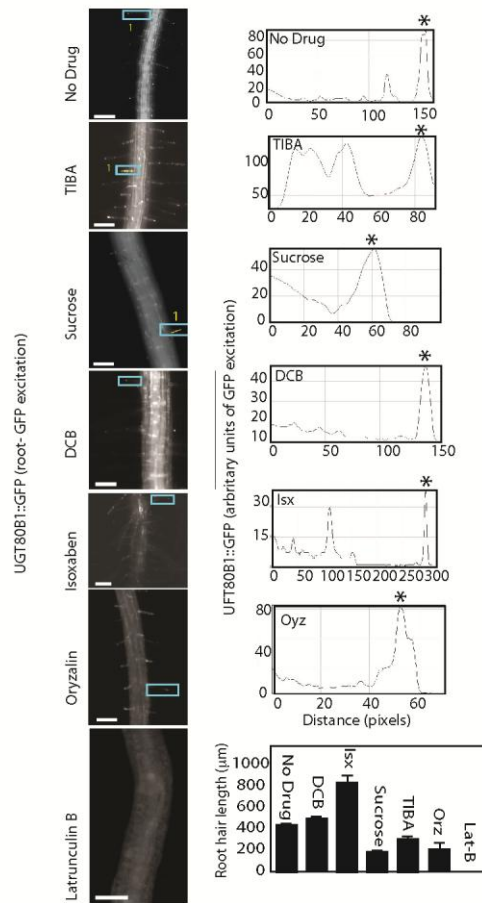


Figure 4.5 Depolymerization of actin cytoskeleton perturbs pre-bulge and root hair tip localization of UGT80B1::GFP. Transgenic plants expressing UGT80B1::GFP were subjected to sterile growth media containing Latrunculin-B (250 nM; Lat-B in DMSO), oryzalin (Orz, 1 µM in DMSO), isoxaben (ISX, 4 nM in DMSO), dichlorobenzonitrile (DCB 500 nM in DMSO), sucrose (2% in media), TIBA (triodobenzoic acid in DMSO) and no drug mock control (0.01% DMSO). Seedlings were grown in sterile conditions for 4-7 days, vertically in the light and then imaged by stereofluorescence microscopy. Root hairs were then longitudinally divided for fluorescence distribution analysis revealing tip localization in all treatments with the exception of Lat-B, which depolymerizes the actin cytoskeleton. The asterisk in each panel marks the spatial location of the root hair tip. After 250 nM Lat-B treatment UGT80B1::GFP failed to localize to pre-bulge sites of root hair initiation at any site on the developing root and failed to develop root hairs, consistent with actin dependent localization. Quantification of root hair length under each pharmacological treatment showed that Lat-B (250 nM) completely suppressed root hair elongation.

4.3 DISCUSSION

Membrane sterols play numerous essential roles in eukaryote biology by forming a key architectural element of cellular membranes. Lipids such as the glycerolipids and sphingolipids mediate membrane processes through imparting charge and structural properties, while membrane sterols structurally impose their rigidity on membrane dynamics (Dufourc, 2008). Despite their biophysical role, the function of sterols in plant biology is far from being fully elucidated, and recent genetic and molecular studies have shown that sterols mediate the transport and targeting of proteins central to hormone signaling (Men et al., 2008) and dynamics of embryonic cell differentiation, polarity, morphogenesis and patterning (Lindsey et al., 2003; Ovecka et al., 2010; Schrick et al., 2000). The vast majority of plants and fungi, as well as specific cases of animals and bacteria, modify their endogenous sterol environment by glycosylation, creating steryl glycoside derivatives. Despite the fact that at least 10% and up to 40% of membrane sterols among plant genera are steryl glycoside derivatives (Grille et al., 2010), almost nothing is known about the functionality of this modification. Steryl glycosides are synthesized by the action of membrane-bound UDP-glucose:sterol glucosyltransferase and our prior work suggested that steryl glycosides are important to macromolecule transport in the developing seed (DeBolt et al., 2009). Herein, we utilized reverse genetics in combination with cell biology to uncover a surprising role for steryl glycoside biosynthesis, via UGT80B1 action, in polarized root hair tip growth in the developing root of *Arabidopsis*.

Tip growth of plant root hairs is an extreme example of cellular polarity whereby the cell shape is many times longer than it is wide and plays important roles for the plant in nutrient acquisition by enhancing root surface area (Preuss et al., 2004). Elegant genetic and cellular studies have shown that a complex interaction between F-Actin cytoskeletal dependent trafficking, endocytic recycling and structural sterols is necessary to drive and maintain lateral tip growth (Araujo-Bazán et al., 2008; Baluska et al., 2000; de Graaf et al., 2005; Ovecka et al., 2005; Ovecka et al., 2010; Preuss et al., 2004; Voigt et al., 2005). A common feature of many of these required components is a polarized spatial distribution at the growing tip of the root hair. The intracellular localization of UGT80B1::GFP was assayed herein by laser scanning confocal microscopy. Interestingly, we found that most of the protein was optically coincident with the very tip of the growing root hair (**Figure 4.3**). Using the sterol binding dye filipin, we colocalized UGT80B1::GFP and filipin (RFP channel) to a region consistent with reports of the vesicle rich zone of root hairs (Preuss et al., 2004). Based on the suppressed root hair growth and tip localized UGT80B1::GFP, our data suggests a role for steryl glycosides in establishment and or maintenance of polarity cues during tip growth. At least two plausible mechanisms exist to explain this data. Firstly, a biophysical model whereby steryl glycosides are a lipid mediator of the molecular machinery needed for root hair tip growth and polarity establishment. Here, glycosylation of membrane sterols might create a

necessary lipid modification that results in altered endomembrane or plasma membrane properties (**Figure 4.5**), which in turn impacts the rate of delivery of proteins necessary for tip expansion. The secondly plausible hypothesis is that sterol glycosides, as membrane elements, might interact with and preferentially organize proteins and cytoskeletal elements necessary for root hair tip growth in a targeted manner. It is very likely that these two mechanisms are not necessarily mutually exclusive. For instance, in *Aspergillus nidulans* membrane sterols are biophysically necessary for the formation of microdomains, which in turn mark cell end factor destinations in hyphae, akin to tip localization, which mislocalize upon disturbance of sterols documenting biochemical interaction (Takeshita et al., 2008). Given the precedence of sterols as lipid markers of root hair tip growth (Ovecka et al., 2010), our studies provide genetic and cellular evidence supporting glycosylation modification of membrane sterols as a necessary spatial and/or temporal cue for root hair elongation.

Careful examination of differentially expressed genes in the *ugt80B1* background revealed an ensemble of cell wall and expansion mediators as well as genes involved in protein secretion, trafficking and cytoskeletal elements (**Table 2.1** and **2.2**). Cytoskeleton components were predominantly actin associated and contained three differentially expressed myosin subunits, two actin-binding proteins and an Ankyrin actin adapter protein (**Table 4.1**) leading to a speculation that feedback between actin and sterol glycosides is plausible. Consistent with transcriptional profiling data, F-Actin cytoskeletal dependent trafficking drives lateral tip growth (Baluska et al., 2000; Preuss et al., 2004; Voigt et al., 2005). Coordination between the location and timing of UGT80B1::GFP within the root hair (**Figure 4.3**) was also highly consistent with actin mediated tip growth (Baluska et al., 2000), yet due to the tissue sampling for microarray analysis it may be a more global occurrence than solely root hair. Further, UGT80B1 localization was found to be dependent on an intact actin cytoskeleton in its capacity to form laterally discrete punctae at the site of root hair initiation in a basal lateral position on trichoblast cells. Likewise, plasma membrane localization was displaced in epidermal root cells under conditions of actin depolymerization (**Figure 4.5**). By contrast, ablation of auxin transport by TIBA addition or inhibition of cell wall biosynthesis via isoxaben or DCB failed to mislocalize UGT80B1 from the growing root hair tip. Hence, live cell imaging data showed that sterol glycosides exist as an actin dependent polarized membrane modification in root hair development that when genetically ablated resulted in decreased elongation.

Our data supports the postulate that the membrane lipid environment is essential for establishing and maintaining cellular polarity and shows, through the use of genetics and cell biology that in *Arabidopsis* the glycosylation modification of structural membrane sterols represents a polarity cue. A previously defined mechanism for an upstream polarity marker is the presence of sterol-rich domains often defined as lipid rafts (Takashita et al., 2008; Wachtler and Balasubramanian, 2006) and in plants, sterol-rich domains have shown

significant enrichment of steryl glycoside derivatives (Laloi et al., 2007). A mechanism may be presented that this lipid modification causes preferential association between the membrane and polarity markers. While this is a plausible mechanism (Takeshita et al., 2008), and one that should not be ignored, the evidence we provide herein only concludes that genetic lesions in UGT80B1 caused aberrant elongation of root hairs and that UGT80B1::GFP displayed actin dependent pre-bulge localization and tip growth association. Further studies with greatly enhanced resolution must be developed to test its validity.

Table 4.1 List of cytoskeleton genes upregulated in *ugt80B1*, P<0.01

Cytoskeleton components	Target Description	Fold change
At2g31900	<i>ATMYO5</i> , Encodes a novel myosin isoform.	3.21
At5g23910	<i>microtubule motor</i>	2.62
At4g27370	<i>myosin heavy chain - like protein ATM2</i>	2.13
At4g19400	<i>actin binding</i>	2.49
At5g15600	<i>SPIRAL1-LIKE4</i>	2.69
At1g14690	<i>similar to ATMAP65-6, microtubule binding</i>	2.46
At1g75780	<i>tubulin beta-1</i>	2.94
At1g62045	<i>Ankyrin repeat family protein Actin regulation</i>	2.25
At1g05320	<i>Myosin related protein</i>	2.13

4.4 METHODS AND MATERIALS

Plant material and growth conditions *Arabidopsis thaliana* lines used in this study were of Columbia (Col-0) (SALK_021175 *ugt80B1-2*) and Wassilewskija (WS-0) ecotypes (*ugt80B1-1* DeBolt et al., 2009). Due to the inherent wavy root phenotype of WS-0, the *ugt80B1-2* was primarily used. SALK_021175C, which is Col-0 mutant with T-DNA insertion in the exon of *UGT80B1* and *ugt80B1-2* presented all the same phenotypes as documented in DeBolt et al. (2009) including transparent testa phenotype. Homozygosity for the Col-0 T-DNA was confirmed by PCR and cross-referenced with phenotypes previously described for *ugt80B1-1* in WS-0 (DeBolt et al., 2009). The transgenic plant expressing proUGT80B1:: β -glucuronidase was as described in DeBolt et al. (2009). All seeds were sterilized using 30% household bleach solution and vernalized for 3 days in 0.15% agar at 4 °C in dark prior to planting.

Constructs To generate the constitutively expressed GFP reporter line, the open reading frame for UGT80B1 was amplified from wild-type Col-0 genomic DNA using a QIAGEN plant gDNA extraction kit (QIAGEN) using ggggacaagtttgtaaaaaagcaggcttcATGGCTAGTAATGTATTTGATCATCC and ggggaccactttgtacaagaagctgggtCACGCCACCATGGAAGACAACACT forward and reverse primers and then cloned directly into the destination vector pMDC83 (Curtis and Grossniklaus, 2003). GFP::UGT80B1 reporter line with

endogenous promoter was constructed whereby proUGT80B1 was PCR amplified using primers: proUGT80B1/SbfI/F-TCCCCCTGCAGGCCACCCTAATGTTTGGTCATTTGATGT and proUGT80B1/KpnI/R-CGGGGTACCCACCTTTAAAACTGAATTCAACTAAACAGC. The resulting PCR product was digested with SbfI and KpnI enzymes and ligated (DNA-ligase- Fermentas) into the pMDC43 vector at the vector specific SbfI and KpnI sites replacing the excised CaMV-35S promoter sequence. The UGT80B1 coding sequence was PCR amplified from the cDNA made from wild-type Col-0 total RNA using primers: UGT80B1/AscI/F: GCTTGGCGCGCCCATGGCTAGTAATGTATTTGATC and UGT80B1/PacI/R GGCCTTAATTAATCACACGCCACCATGGAAGAC. The amplified PCR product was sequenced and digested with AscI and PacI and cloned at the respective sites fusing with in-frame GFP in the pMDC43 vector containing proUGT80B1 resulting in the proUGT80B1::GFP:UGT80B1 construct. Both constructs were sequence verified using the promoter and gene flanking primers and three nested primers CACTGTCCCGTCATTTTG, GTGCCATTCTTTGGGGAT and CGATGTGCAGCCTTTTCT. The destination construct was transformed by electroporation into *Agrobacterium tumefaciens*, which was used to transform flowering *ugt80B1* plants (Clough and Bent, 1998). Single gene genetic complementation of *ugt80B1* was examined by restored testa color (based on transparent testa phenotype documented for *ugt80B1* DeBolt et al., 2009) in UGT80B1::GFP (*ugt80B1*). All UGT80B1::GFP seedlings used were bright homozygous lines screened in the T2 and analyzed in subsequent generations.

Laser scanning confocal microscopy and fluorescence stereomicroscopy

Seeds were germinated on plates containing sterilized 0.5 X MS agar for 7–14 d in light conditions at 21°C in a Conviron Adaptis1000 environmental chamber affixed with a Conviron Arabidopsis light kit (Conviron). In the case of stereomicroscopy, individual seedling were visualized either in MS agar without removing them from plates and employed both brightfield and fluorescence modes. For confocal microscopy, a custom built U-shaped parafilm sandwich was created for growing seedlings. Here, 2-layers of parafilm were cut with a razor blade to a microscope slide width U-shape and then sandwiched with vacuum grease on a microscope slide. The U-shaped regions was filled with 0.5 x MS Agar media slide and sterilized seeds were planted at the open end of the U prior to covering the sandwich with a cover slip and allowing the agar to set on a 10° gradient. Once mounted, specimens were grown in a sterilized plate containing a moistened kimwipe to limit water loss from the slide for 4-7 days in 24 hr light. Seedlings were then carefully placed on the confocal microscope stage and imaged in darkness. Imaging was performed on an Olympus MVX-10 Macro/Stereo fluorescence microscope with a Prior light source and GFP filter (Olympus) and 1X objective employing internal 2X zoom, or an Olympus FV1000 laser scanning confocal microscope using a 20x, 40x or 60x N.A. water-immersion objective. The microscope is equipped with lasers for excitation wavelengths ranging from 405–633 nm and EGFP and ERFP were excited using the EGFP (488 nm) and ERFP (543 nm) setting in the Olympus Fluoview

software (Olympus). Initial image processing was performed by using Olympus Fluoview software (Olympus). All further image analysis was performed by using ImageJ (W. Rasband, National Institute of Health, Bethesda, MD) software. Fluorescence quantification was analyzed using the 'Plot Profile' feature under the built-in image analysis tools in ImageJ.

Quantification of root hair phenotype All measurements were performed at the 'root hair zone' defined by Schiefelbein and Somerville (1990). This area was approximately one vertical mm from the root tip and all measurements in this area were examined in 5-day old light grown seedlings. Root hair length was quantified for 10 seedlings each from wild-type and *ugt80B1* mutant covering 1.6 mm of root length. Length measurement was made via the freehand line tool in ImageJ and pixel number was converted to mm or μm . Statistical analysis was done using Prism4 (GraphPad) to obtain frequency distributions and significance using Mann-Whitney *U* test. Root width measurements were done similarly with measurements taken at the base, middle and tip of the growing root hair from root hair zones from 6 different seedlings of wild-type and mutant covering 1.6 mm length of the root. Statistical analysis was performed as described above.

Drug treatments The following chemical probes were employed for cell biology assays: latrunculin-B (25-250 nM derived from 2.5 mM stock in dimethylsulfoxide (DMSO)(Lat-B) and then made to the concentration required in the MS-agar media- used for actin depolymerization; isoxaben (4 nM *N*-[3-(1-ethyl-1-methylpropyl)-1,2-oxazol-5-yl]-2,6-dimethoxybenzamide- made from 1 mM stock in DMSO), dichlorobenzonitrile (DCB 500 nM from 5 mM stock in DMSO); sucrose (2% in media); TIBA (triodobenzoic acid; made fresh in carrier DMSO for auxin inhibitor- polar transport inhibitor). Transgenic plants expressing *proUGT80B1* or *pro35S::UGT80B1* were grown in the presence of each drug at the precise dose rates noted above. Quantification of root hair length and fluorescence plots were performed as described above.

Chapter 5: Membrane proteomics in steryl glycoside mutants reveals alteration in GPI anchored proteins

5.1 Introduction

In plants, the addition of a sugar moiety to membrane sterols in the C3 position occurs in >40% of membrane sterols (Potocka and Zimowski, 2008) (**Figure 1.1**). Membrane sterol glycosylation occurs by the action of two proteins UGT80A2 and UGT80B1 (Grille et al., 2010). Reverse genetic analyses have revealed a diverse set of phenotypes that are linked to null mutations in UGT80B1 yet no obvious phenotypes are associated with UGT80A2 (DeBolt et al., 2009). Most prominent, was a syndrome of defective macromolecule transport. Additionally, embryogenesis defects in *ugt80B1* were consistent with phenotypes associated with genetic knockout of other components of the sterol biosynthetic pathway (Clouse, 2000; Schaller, 2003; Schrick et al., 2000; Souter et al., 2002). However feedback between end product glycosylation and sterol biosynthesis was pronounced, since a net increase in membrane sterols in the *ugt80B1* null background did not overcome the lack of glycosylation. Positive feedback between end-product glycosylation and biosynthesis (DeBolt et al., 2009) implied a required homeostasis and a mechanism to regulate this membrane sterol balance.

Sterols and SGs are components of the plant cell membrane architecture. The distribution of sterols and SGs in the membrane may be of functional significance. A thorough lipid analysis for instance, of detergent resistant membranes (DRM) from higher plants such as tobacco (*Nicotiana tabacum*) and *Arabidopsis thaliana* revealed enrichment of sterols (Borner et al., 2005; Mongrand et al., 2004). Furthermore, characterization of DRM composition in *A. thaliana*, *N. tabacum* and Leek (*Allium ampeloprasum* var. *porrum* (L.)) membranes showed that SGs were significantly enriched in DRM fractions (Laloi et al., 2007; Lefebvre et al., 2007; Mongrand et al., 2004). Thus it is plausible that like sterols, SGs may further diversify membrane architecture. The concept of membranes having uneven distribution of certain components has been developing for 40 years since Singer and Nicholson (1972) gave a gross explanation of how the cell membranes are structured. Lipid rafts, also defined as DRMs, emerged as a possible explanation to the asymmetry in the lipid species in the apical and basal membranes of the bilayer (Lingwood and Simons, 2010; Simons and Ikonen, 1997). In these recent studies, the authors based their definition of DRMs on their insolubility in non-ionic detergents such as Triton-X 100 under cold conditions. Due to their low density they were further isolated by floating them on a density gradient (Simons and Ikonen, 1997). This property arises due to the tight packing of sphingolipids that contain saturated acyl chains and the packing of sterols (and SGs (Laloi et al., 2007; Lefebvre et al., 2007; Mongrand et al., 2004)) between them on the apical side of the membrane (Bhat and Panstruga, 2005; Lingwood and Simons, 2010; Munro, 2003; Simons and Ikonen, 1997). Previous studies have analyzed the proteomic element of DRMs.

Peskan *et al.* (2000) extracted DRMs from tobacco and showed an overlap of proteins studied previously from mammalian cell types, namely GPI-anchored proteins and heterotrimeric G proteins. DRMs and their functional significance in the cell membrane are looked upon with caution. This is partly due to the extraction procedures involved in extracting microdomains from cell membranes. It was pointed out as early as the idea emerged in early 1990's that sterols and sphingolipids have the tendency to clump together under cold conditions and detergent treatment (Bhat and Panstruga, 2005; Borner *et al.*, 2005; Grennan, 2007; Kierszniowska *et al.*, 2009; Simons and Ikonen, 1997). Studies performed in plant cells on DRMs have been using these conditions to report associated proteins however the actual dependence on sterols for these proteins is missing (Kierszniowska *et al.*, 2009). Thus, Kierszniowska *et al.* (2009) depleted the cells of sterols using a drug methyl- β -cyclodextrin used in animal systems to deplete cholesterol to study raft-associated proteins. They found no differences in the signaling proteins in contrast to previous studies but an enrichment of cell wall associated, lipid modifying and vesicular transport proteins in sterol-enriched lipid rafts. These data leave a need to characterize proteins associated with the membrane in a genetic background where a putative DRM enriched component was altered.

Herein, we aimed to characterize the abundance of proteins in two genetic backgrounds relative to wild-type plants: one with overexpression of UGT80B1 and the other knockout of UGT80B1. To cast as broad a net as possible in our proteomic studies, we decided not to extract DRMs from genetic lines depleted in SG or overexpressing SG but rather use the whole membrane proteome to probe any changes in abundance of certain proteins due to a change in SG species in their membrane. This gave us the ability to search for proteins that are responding to SG, keeping in mind the genetic complexity of SG depleted background where sterols are up by 40 fold in certain tissues (DeBolt *et al.*, 2009). This study was done keeping in mind the difficulties associated with separating membrane proteins using 2-DGE (Santoni *et al.*, 2000) however with the confidence that change in membrane architecture brought about in the genetic backgrounds used, would bring about defects in recruiting certain proteins only responding to SG and might even be unknown in their function. Total membrane extracts from *ugt80B1* and CaMV-35S::UGT80B1 lines were subjected to 2DGE and the proteins were documented by means of mass spectral peptide identification; twenty-two proteins were found to be responding to an imbalance in sterol to SG ratio.

5.2 Results and discussion

Proteomics analysis of UGT80B1 mutants

Proteomics can be a powerful means by which to identify key components of a cellular system (Borner *et al.*, 2005). Combined with reverse genetics in a model organism system such as *Arabidopsis*, it is now possible to compare the proteome of genotypes separated by a single gene mutation. In the case of SG, we recently characterized UGT80B1 and found a broad range of phenotypes

associated with its knockdown (DeBolt et al., 2009). SG, being key components of plant membrane architecture, represents an intriguing scenario to probe by proteomics. Because UDP-glucose:sterol glucosyltransferase activity has been detected in the PM, Golgi, ER and tonoplast (Hartmann-Bouillon and Benveniste, 1978; Ullmann et al., 1993; Warnecke et al., 1997; Yoshida and Uemura, 1986) we chose to assay total membrane protein extracts in the 2DGE system. Our experimental design used approximately 2500 seedlings grown in liquid culture for each genotype and each replicate, and thus allowing us to eliminate false positives by averaging. This experimental strategy was performed in duplicate 2DGE format. Spots selected were deemed significantly different based on a P value of <0.05 between the mutant and wild-type. A total of 51 proteins (spots) were differentially abundant (**Table 5.1**) and successful sequence identification of 22 was achieved by mass spectroscopy (**Table 5.2** and **Table 5.3**).

Table 5.1 Differentially expressed spots from 2D gel comparison of Arabidopsis COL-O WT versus Arabidopsis 35S:UGT80B1 and UGT80B1 KO. Reference spot numbering, pI, and MW are given for changing polypeptide spots analyzed in samples Arabidopsis total membrane fractions from COL-O wild type, 35S:UGT80B1 and *UGT80B1* knockout line seedlings (**Figure 5.1**). Also shown are fold increases or decreases (difference) of the polypeptides for COL-O WT vs 35S:UGT80B1 and *UGT80B1* KO. The differences are calculated from spot percentages (individual spot density divided by total density of all measured spots). Polypeptide spots **increased** in COL-O WT vs 35S:UGT80B1 or *UGT80B1* KO by a fold increase of > 1.7 and p value < 0.05 are highlighted in **blue** in the difference column, while spots **decreased** in COL-O WT vs 35S:UGT80B1 or *UGT80B1* KO with a fold decrease of ≤ -1.7 and p value < 0.05 are highlighted in **red**. All differences were visually verified using the montage images found on the following pages. Spot percentages are given to indicate relative abundance. Note that the p values are for n= 2 gels/sample.

Spot #	Averaged	Averaged	Averaged	WT	WT	WT	WT	Montage Image Page #
	WT Spot %	35S Spot %	KO Spot %	vs 35S Difference	vs 35S T-test (p)	vs KO Difference	vs KO T-test (p)	
2	0.022	0.002	0.014	10.3	0.032	1.5	0.399	10
4	0.066	0.006	0.062	10.6	0.061	1.1	0.833	11
7	0.219	0.089	0.148	2.4	0.022	1.5	0.123	12
13	0.121	0.035	0.079	3.4	0.050	1.5	0.239	13
24	0.023	0.011	0.018	2.0	0.013	1.3	0.627	14
34	0.031	0.010	0.015	3.1	0.044	2.1	0.039	15
47	0.038	0.013	0.039	3.0	0.242	-1.0	0.942	16

Table 5.1 Continued

52	0.017	0.003	0.012	6.7	0.010	1.4	0.148	17
79	2.158	1.299	1.486	1.7	0.033	1.5	0.083	18
81	0.010	0.002	0.002	5.4	0.047	nc	0.043	19
84	0.047	0.023	0.022	2.0	0.001	2.2	0.002	20
114	0.040	0.016	0.016	2.5	0.006	2.5	0.016	21
154	0.041	0.023	0.022	1.8	0.008	1.8	0.132	22
155	0.015	0.004	0.005	3.4	0.221	2.8	0.132	23
186	0.078	0.036	0.060	2.2	0.003	1.3	0.313	24
225	0.214	0.114	0.145	1.9	0.027	1.5	0.059	25
289	0.077	0.028	0.038	2.8	0.024	2.1	0.015	26
355	0.045	0.027	0.023	1.7	0.002	2.0	0.025	27
361	0.155	0.081	0.125	1.9	0.005	1.2	0.037	28
373	0.166	0.063	0.117	2.6	0.010	1.4	0.110	29
379	0.085	0.043	0.091	2.0	0.050	-1.1	0.361	30
392	0.299	0.030	0.050	9.9	0.004	5.9	0.002	31
407	0.102	0.024	0.010	4.2	0.017	9.9	0.007	32
63	0.011	0.037	0.020	-3.4	0.020	-1.9	0.149	33
175	0.021	0.044	0.043	-2.1	0.023	-2.1	0.021	34
300	0.005	0.016	0.020	-3.2	0.002	-3.9	0.001	35
326	0.028	0.098	0.100	-3.5	0.108	-3.6	0.102	36
334	0.013	0.049	0.029	-3.9	0.006	-2.3	0.081	37
349	0.032	0.087	0.080	-2.7	0.047	-2.5	0.053	38
418	0.022	0.178	0.029	-8.0	0.081	-1.3	0.631	39
420	0.153	0.258	0.162	-1.7	0.015	-1.1	0.726	40
432	0.886	2.522	2.084	-2.8	0.000	-2.4	0.061	41
447	0.012	0.088	0.140	-7.2	0.057	-11.4	0.072	42
448	0.022	0.071	0.063	-3.2	0.025	-2.9	0.153	43
449	0.030	0.125	0.105	-4.2	0.024	-3.5	0.081	44
450	0.012	0.042	0.023	-3.5	0.087	-1.9	0.122	45
452	0.014	0.092	0.057	-6.6	0.091	-4.1	0.041	46
29	0.010	0.005	0.004	1.9	0.060	2.7	0.039	47

Table 5.1 Continued

72	0.082	0.028	0.038	2.9	0.069	2.2	0.008	48
284	0.019	0.010	0.004	2.0	0.120	5.2	0.041	49
337	0.086	0.077	0.052	1.1	0.274	1.7	0.028	50
340	0.081	0.062	0.049	1.3	0.099	1.7	0.050	51
50	0.004	0.001	0.012	nc	0.121	-3.1	0.026	52
182	0.023	0.028	0.040	-1.2	0.277	-1.7	0.036	53
194	0.030	0.043	0.054	-1.5	0.257	-1.8	0.000	54
275	0.279	0.379	0.474	-1.4	0.150	-1.7	0.050	55
301	0.105	0.170	0.195	-1.6	0.078	-1.9	0.037	56
304	0.131	0.337	0.399	-2.6	0.224	-3.0	0.249	57
312	0.195	0.288	0.357	-1.5	0.039	-1.8	0.008	58
316	0.242	0.346	0.415	-1.4	0.136	-1.7	0.024	59
325	0.007	0.014	0.035	-2.2	0.108	-5.3	0.006	60
426	0.071	0.130	0.419	-1.8	0.505	-5.9	0.015	61
453	0.187	0.455	0.562	-2.4	0.171	-3.0	0.036	62

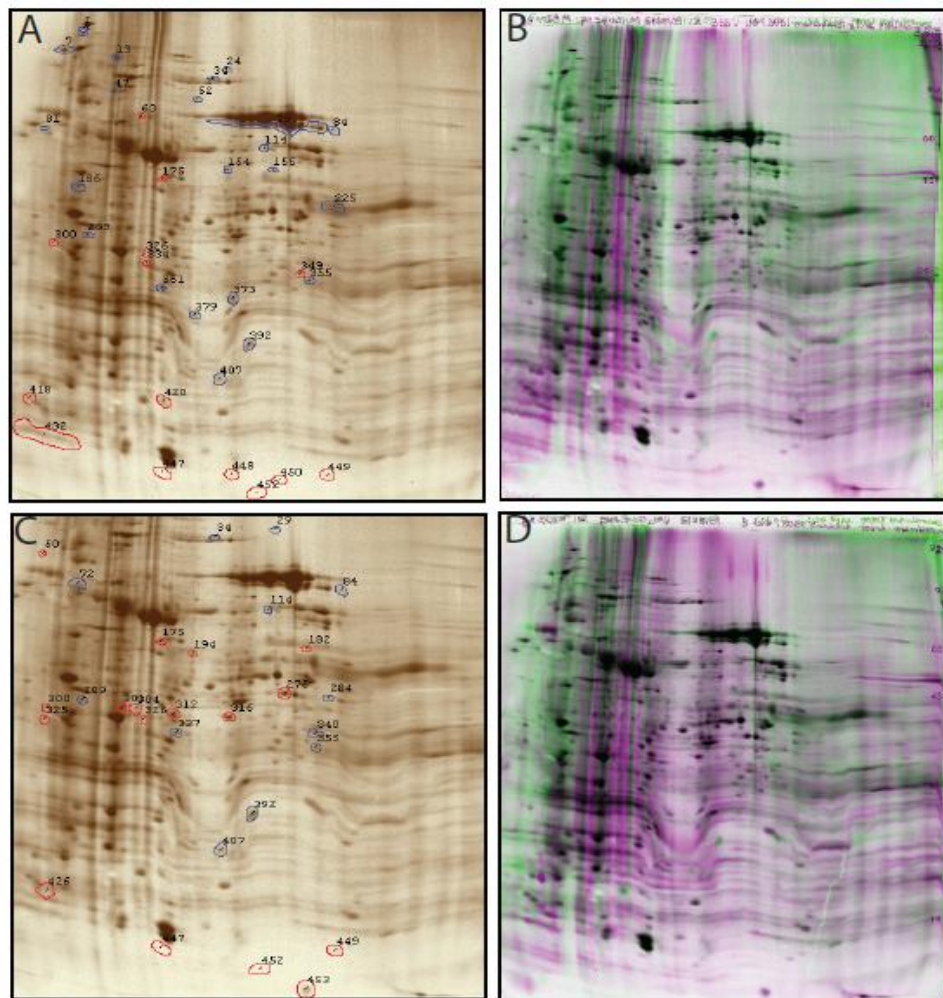


Figure 5.1 2-dimensional gel electrophoresis (silver stain and false color overlay for protein identification) of the membrane proteome derived from wild-type and SG mutant genetic backgrounds. A) COL-O wild type seedlings versus 35S:UGT80B1 overexpressing line seedlings. Polypeptide spots *Increased* in COL-O WT vs 35S:UGT80B1 by 1.7-fold or greater difference and p values < 0.05 are outlined in **Blue**, while spots *Decreased* in COL-O WT vs 35S:UGT80B1 by a -1.7-fold or greater difference and p values < 0.05 are outlined in **Red**. **B)** Overlay image showing sample Arabidopsis total membrane fractions from COL-O wild type seedlings in green overlaying sample Arabidopsis total membrane fractions from 35S:UGT80B1 overexpressing line seedlings in magenta. Image appears black where spots overlay each other. **C)** COL-O wild type seedlings versus Arabidopsis total membrane fractions from *UGT80B1* knockout line seedlings. Color coding of polypeptide spots are the same as A. **D)** Overlay image showing sample Arabidopsis total membrane fractions from COL-O wild type seedlings in green overlaying sample Arabidopsis total membrane fractions from *UGT80B1* knockout line seedlings in magenta.

TABLE 5.2 Core list of proteins identified as steryl glycoside responsive in at least two biological replicate experimental datasets. Arabidopsis gene identification numbers and functional protein annotations were derived from X!Tandem and these were verified in ARAMEMNON (<http://aramemnon.botanik.uni-koeln.de/>) (Sherameti et al., 2008). Domain and motif analysis included transmembrane spanning regions, TMD (transmembrane domain), TMDL (transmembrane domain length) and predicted lipid modifications were also characterized in ARAMEMNON (<http://aramemnon.botanik.uni-koeln.de/>) (Sherameti et al., 2008).

NOTE: TMD (transmembrane domain), TMDL (transmembrane domain length), GPI (glycosylphosphatidylinositol), PALM (palmotylation), Myr (myristoylation)












Spot #	Arabidopsis gene ID#	Functional Annotation	Transmembrane spanning regions	TMD	TMDL	Predicted lipid modifications
2	At1g2250	PATL2 (PATELLIN 2)		0		
4	At1g72150	PATL1 (PATELLIN 1)		0		
13	At3g0980	AICDC48A (CELL DIVISION CYCLE 48); ATPase		0		
72	At1g7600	vacuolarATP synthase subunit B		0		
81	At1g5630	AICRT1 (CALRETICULIN 1); calcium ion binding		1	20	
186	At4g2030	AtRabE1b (ARABIDOPSIS RAB GTPASE E1B)		1	20	GPI anchor
194	At3g0920	AIPYK10 (beta-glucosidase)		1	20	
225	At1g5400	myosinase-associated protein, putative		1	20	
284	At2g3870	AnnAt4 (ANNEXIN ARABIDOPSIS 4); calcium ion binding		0		
289	At3g1640	jacalin lectin family protein		0		GPI anchor
300	At4g04020	AIFB1a		1	20	GPI anchor
301	At3g16420	AtPBP1 (PYK10-BINDING PROTEIN 1); copper ion binding		0		
325	At4g2220	plastid lipid associated protein		1	20	GPI anchor
326	At5g1400	mitochondrial phosphate transporter (AtPHT3-1)		5	20	
334	At3g0120	band7 family protein		0		Palm.
349	At1g4720	GAMMA CA2 (GAMMA CARBONIC ANHYDRASE 2)		0		GPI anchor; Myr.
355	At5g1500	AtVDAC3 (VOLTAGE DEPENDENT ANION CHANNEL 3)		1		
379	At5g1920	Uncharacterized GPI anchored protein		3	20	GPI anchor
418	At2G47170	AtARFA1c; small GTP binding protein		0		Myristoylation
426	At5g1660	membrane protein of unknown function		1		GPI anchor; Palm.
432	At1g12310	calmodulin		0		
447	At4g02620	vacuolarATPase subunit F family protein		1		

TABLE 5.3 Core metrics for proteins identified as steryl glycoside responsive in at least two biological replicate experimental datasets. Spot number represents the protein identifier code from all identified proteins on the silver stained gel. Average spot intensity was quantified using Progenesis software (Nonlinear Dynamics, Durham, NC). Significant difference was calculated between mutant and wild-type using a cutoff of $P < 0.05$. Peptide number reflects the number of matching peptides identified by X!Tandem.

Spot No.	Averaged Spot %			Difference	T-test (p)	Difference	T-test (p)	No. of Peptides	Mw. kDa.
	WT	35S	KO	WT vs 35S	WT vs 35S	WT vs KO	WT vs KO		
2	0.022	0.002	0.014	10.3	0.032	1.5	0.399	16	91
4	0.066	0.006	0.062	10.6	0.061	1.1	0.833	17	79.8
13	0.121	0.035	0.079	3.4	0.05	1.5	0.239	15	102.8
72	0.082	0.028	0.038	2.9	0.069	2.2	0.008	4	70.2
81	0.01	0.002	0.002	5.4	0.047	nc	0.043	4	57.3
186	0.078	0.036	0.06	2.2	0.003	1.3	0.313	1	41.4
194	0.03	0.043	0.054	-1.5	0.257	-1.8	0	7	59.7
225	0.214	0.114	0.145	1.9	0.027	1.5	0.059	17	43.1
284	0.019	0.01	0.004	2	0.12	5.2	0.041	9	36.2
289	0.077	0.028	0.038	2.8	0.024	2.1	0.015	17	72.4
300	0.005	0.016	0.02	-3.2	0.002	-3.9	0.001	27	34.9
301	0.105	0.17	0.195	-1.6	0.078	-1.9	0.037	13	32.1
325	0.007	0.014	0.035	-2.2	0.108	-5.3	0.006	23	33.6
326	0.028	0.098	0.1	-3.5	0.108	-3.6	0.102	10	34.8
334	0.013	0.049	0.029	-3.9	0.006	-2.3	0.081	8	31.3
349	0.032	0.087	0.08	-2.7	0.047	-2.5	0.053	16	30
355	0.045	0.027	0.023	1.7	0.002	2	0.025	6	29.2
379	0.085	0.043	0.091	2	0.05	-1.1	0.361	1	20.5
418	0.022	0.178	0.029	-8	0.081	-1.3	0.631	1	20.6
426	0.071	0.13	0.419	-1.8	0.505	-5.9	0.015	3	18.2
432	0.886	2.522	2.084	-2.8	0	-2.4	0.061	8	16.5
447	0.012	0.088	0.14	-7.2	0.057	-11.4	0.072	6	14.3

Identification of SG regulated membrane proteins using proteomics

Peptide sequence analysis identified two Patellin proteins, three ATPase proteins, Calreticulin, RAB1B, ARF-A1c, PYK10, PBP1, Myrosinase, Annexin, Jacalin, AtFIB, Plastid lipid associated protein, phosphate transporter, voltage dependent anion channel, Calmodulin, a band 7-protein, gamma carbonic anhydrase, uncharacterized GPI anchored protein and a membrane protein of unknown function (**Table 5.2**). Broadly classifying these proteins it was evident that membrane trafficking, secretion, transport and calcium responsive proteins were the most abundant classes. Calcium associated proteins included Annexin, Calreticulin and Calmodulin. Membrane trafficking and secretion included Patellin 1 and Patellin 2, RAB1B and ARF-A1c. Three ATPase proteins were identified and associated with various functions in cell such as cell division, membrane fusions, and in proteasome-and ER-associated degradation (ERAD) (**Figure 5.2**). Two proteins, one a putative phosphate transporter (AtPHT3-1) and the other a voltage dependent anion channel (AtVDAC3) indicated that SG responsive proteins extended to both proteins with transporter and channel activities consistent with molecular phenotypes identified in reverse genetics studies

(DeBolt et al., 2009). Four out of 22 sequenced proteins were involved in process associated with the beta-glucosidase pathway. These included PYK10 (At3g09260), PBP1 (PYK10-BINDING PROTEIN 1; At3g16420), Myrosinase-associated protein At1g54010 and the Jacalin lectin family protein (At3g16460). PBP1 and PYK10 were both of greater abundance in SG mutant backgrounds (**Table 5.2** and **Table 5.3**). Finally, a class of potentially important singleton SG response proteins was identified, these included a membrane protein of unknown function (At5g16660), a band 7 family protein (At3g01290) and a GAMMA CA2 (GAMMA CARBONIC ANHYDRASE 2- At1g47260). A protein annotated as an uncharacterized GPI anchored protein (At5g19230) was identified (**Table 5.2**). Six additional proteins contained a GPI anchor making GPI anchored proteins the most highly represented class of SG responsive proteins documented herein. Identification of differentially abundant GPI anchored proteins in SG mutants was consistent with prior studies that document sterols and SGs as enriched lipid species in plant DRMs (Laloi et al., 2007; Lefebvre et al., 2007; Mongrand et al., 2004) and GPI anchored proteins as highly abundant proteins in DRMs (Borner et al., 2005). Our membrane isolation method sought to select for total membrane proteins, and therefore it was plausible that the correlation between SG mutants and GPI anchored proteins was based on association rather than membrane preparation technique.

Two of the proteins were encoded by Patellin1 (PATL1 At1g72150) and Patellin2 (PATL2 At1g22530) (**Table 5.3**; spot 2 and 4) (**Figure 5.2**), which are orthologs of Sec14p in *Saccharomyces cerevisiae*, belonging to a large superfamily found only in *Eukaryotic* organisms (Bankaitis et al., 1989; Mousley et al., 2007). It is proposed that PATL1 and PATL2 function at the intersection of lipid metabolism and membrane trafficking in cell biology (Peterman et al., 2006). Sec14 is a protein class belonging to the phosphatidylinositol transfer proteins (PITP) (Peterman et al., 2006). Sec14p plays an essential role in yeast in forming secretory vesicles and vesicle trafficking from the trans-Golgi network (TGN) by affecting the lipid microenvironment (Mousley et al., 2007). PATL1 and PATL2 displayed decreased abundance in the overexpression lines (Spot 2 and 4; **Table 5.2** and **Table 5.3**). Along with the Sec14 lipid binding domain these have a C-terminal Golgi dynamics (GOLD) domain (Peterman et al., 2006) that is suspected of mediating protein-protein interactions, Golgi dynamics and vesicle traffic (Anantharaman and Aravind, 2002). Patellin1 was localized at the cell plate and has been thought of playing a role in membrane trafficking at the later stages of cytokinesis by affecting the lipid environment as it has been found to be a novel phosphoinositide-binding protein, and its possible interaction with other proteins through the GOLD domain (Peterman et al., 2004). It is plausible that disruption in membrane processes associated with altered SG pools results in proportional shifts in lipid metabolism, shown in (DeBolt et al., 2009), which directly or indirectly reduced the abundance of lipid interacting proteins such as PATL1 and PATL2. Additional secretory proteins that displayed differential abundance in SG altered genotypes included the ARF-A1c small GTP binding protein (At2g47170) and RAB-E1B Arabidopsis RAB GTPase E1B (At4g20360). RAB GTPase-E1b proteins are known to interact with the phosphatidylinositol-4-

phosphate 5-kinase at the plasma membrane (Camacho et al., 2009). By contrast, ARF-A1c small GTP binding protein (At2g47170) (**Figure 5.2**) mediates retrograde protein transport from Golgi to the ER (Matheson et al., 2007).

It was found that CDC48 (At3g09840; **Table 5.2** and **Table 5.3**: spot 13), an AAA-type ATPase showed a lower abundance in the overexpressor genotype. CDC48A is a member of AAA ATPases (ATPases associated with various cellular activities) associated with various functions in cell such as cell division, membrane fusions, and in proteasome- and ER-associated degradation (ERAD) of proteins (Woodman, 2003). The various activities of CDC48 depend upon the adaptor proteins it is attached to. For example, when it is associated with p47 it mediates ER, Golgi and nuclear envelope assembly; and association with Ufd1-Npl4 is associated with chromatin associated nuclear envelope network, nuclear envelope reassembly and ERAD (Park et al., 2008; Woodman, 2003). Furthermore, a recent report associates CDC48 to cytokinesis and cell expansion when associated with SYP31 (Park et al., 2008; Rancour et al., 2002). These studies implied that CDC48 is functionally important to the action of NSF (N-ethylmaleimide-sensitive fusion protein) and its interacting SNAP (soluble NSF attachment protein) that disassemble the cognate SNARE proteins and make them available again for subsequent membrane vesicle transport at the cell plate (Jürgens, 2005; Park et al., 2008; Rancour et al., 2002; Woodman, 2003). Decreased CDC48 abundance could reflect a scenario whereby tipping the balance between Sterol:SG ratios in the SG mutant background, altered the overall lipid environment to become less favorable for ER fusion and ER-Golgi trafficking dynamics either at the cell plate or in the whole plant (**Figure 5.2**). Moreover, two additional vacuolar ATPase, one was a V-ATPase subunit B (At1g76030) displayed decreased abundance of 2.2-2.9 fold in *ugt80B1* and 35S:UGT80B1, the other V-ATPase F subunit (At4g02620, **Table 5.2**: Spot 447), displayed significantly increased abundance in both *ugt80B1* (11.4 fold) and 35S:UGT80B1 (7.2 fold). V-ATPases, a class of enzymes are proton pumps that localize to the membrane of endosomes, lysosomes, Golgi-derived vesicles, secretory and PMs (Toei et al., 2010). The 11 fold increase in abundance of V-ATPase subunit F (At4g02620) represents the largest fold change in membrane protein abundance in the SG mutants. Since ATPase proton pumps represented 3 out of 22 sequenced proteins, we propose that either a significant change in proton balance across intracellular membranes was driving the change in ATPase abundance or alternatively, the sterol class present in the membrane directly influenced their incorporation into the membrane. Adding weight to an imbalance in ionic balance was the identification of several proteins that function to either help maintain, respond to cellular calcium levels, or contribute to calcium signaling; these were caltreticulin, annexin and calmodulin (**Table 5.2**).

Proteins associated with beta-glucosidase, PBP1 (PYK10-binding protein 1; At3g16420) and PYK10 (beta-glucosidase complex; At3g09260) were both of greater abundance in SG mutant backgrounds (**Table 5.2**; spot numbers 301 and 194 respectively). By contrast, Jacalin lectin protein and myrosinase were of depleted abundance in the mutant backgrounds (**Table 5.3**; spot numbers 289

and 225 respectively). The upregulation of PYK10 and PBP1 have previously been shown to occur under conditions of insect attack and ablation of intracellular organelles (Sherameti et al., 2008). The ER complex sense cellular disfunction and attempts to produce glucosinilates for defense; hence, a plausible reason for increased abundance of the PYK10/PBP1 complex is that membrane alteration was sensed based on alteration of Sterol:SG ratios in the membrane (DeBolt et al., 2009). Alteration, of the Sterol:SG ratio in organelle membranes may impact membrane structure and set in motion a downstream signaling cascade that ultimately increases expression of PYK10/PBP1.

As with their parental compounds, the sterols, SGs are intrinsic membrane components (Grille et al., 2010). Knockout mutants in UGT80B1 display a breadth of phenotypes, consistent with an ablation in membrane architecture that altered the recruitment and abundance of key membrane proteins (DeBolt et al., 2009). Herein we obtained a proteomic snapshot of the membrane interacting proteins that respond to SG mutants in Arabidopsis seedlings (**Table 5.2**). Our finding revealed an unexpected overrepresentation of GPI anchored proteins among differentially abundant proteins identified, despite assaying the total membrane proteome rather than the fractionated DRM, lending support to the functional association between sterol (and their derivatives) and GPI anchored proteins.

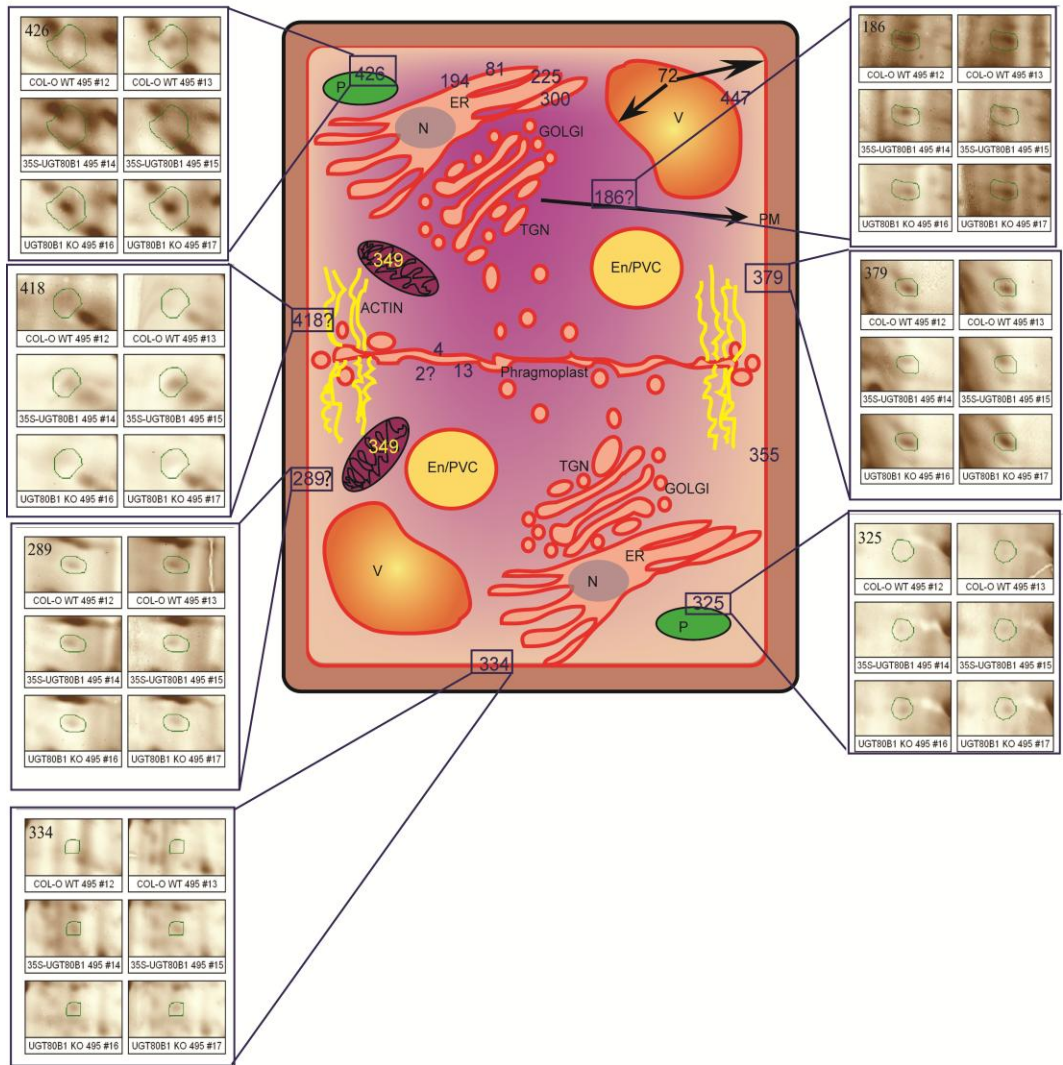


Figure 5.2 Cellular localization and quantitative assessment of SG responsive GPI anchored proteins identified by 2DGE. In the schematic representation of the cell, red represents the presence of SG previously documented (Hartmann-Bouillon and Benveniste, 1978; Hartmann-Bouillon et al., 1987; Ullmann et al., 1993; Warnecke et al., 1997; Yoshida and Uemura, 1986): N (nucleus), V (vacuole), ER (endoplasmic reticulum), PM (plasma membrane), TGN (trans-Golgi-network), P (plastid), En/PVC (endosomal/prevacuolar compartment), M (mitochondria). Surrounding the cell are magnified images of the duplicate 2DGE analysis of spot intensity in silver stained gels for each of the GPI anchored proteins. The number represents the spot count and the representative genotype was written beneath each spot. Spots were linked back to the cell schematic using blue lines. A question mark along with the spot number indicates an informational gap on subcellular localization either due to lack of supporting information or its presence in multiple locations.

5.3 Methods and Materials

Plant material and growth conditions

All *Arabidopsis* lines used in this study were of Columbia (Col-0) ecotype. Seeds were sterilized using 30 % household bleach solution and cold chilled for 3 days in 0.15 % agar at 4 °C in dark. These were then germinated and grown under continuous light (200 mmol/m²/s) in liquid media containing 0.5% Murashige and Skoog (MS) mineral salts (Sigma, St. Louis, MO). To generate plants expressing CaMV-35S:UGT80B1, the open reading frame for UGT80B1 was amplified as previously described (DeBolt et al., 2009) using the following primer pair: ggggacaagttgtacaaaaaagcaggcttcATGGCTAGTAATGTATTTGATCATCC and ggggaccactttgtacaagaaagctgggtCACGCCACCACATGGAAGACAACACT and then cloned directly into the destination vector pMDC83 (Curtis and Grossniklaus, 2003). The construct was sequence verified using the nested primers CACTGTCCCGTCATTTTG, GTGCCATTCTTTGGGGAT and CGATGTGCAGCCTTTTCT. The destination construct was transformed by electroporation into *Agrobacterium tumefaciens*, which was used to transform flowering Col-0 plants. All CaMV-35S::UGT80B1 seedlings used were T4 homozygotes. The *ugt80B1* allele described herein is SALK_021175C, which is Col-0 mutant with T-DNA insertion in the exon of *UGT80B1*. This allele was not previously described (DeBolt et al., 2009), because we sought to use a Wassilewskija (WS-0) allele rather than a Col-0 for the previous study. Homozygosity for the T-DNA was checked by PCR and further examination of phenotypes showed that these were consistent with those described for *ugt80B1* (DeBolt et al., 2009).

Total membrane protein extraction

Total membranes were prepared from *Arabidopsis* Col-0 wild-type, CaMV-35S::UGT80B1 and *ugt80B1* seedlings according to Borner et al., (2005) and Lefebvre et al., (2007) with slight modifications. Approximately, 2500 seeds (50 mg) per replicate (duplicate) from COL-0 wild-type, CaMV-35S::UGT80B1 and *ugt80B1* were surface sterilized and vernalized for 3 days at 4°C. These were then grown in liquid culture containing 0.5% Murashige and Skoog (MS) mineral salts (Sigma, St. Louis, MO) and seedlings were harvested after 13 days. Seedlings were homogenized using a mortar and pestle in liquid nitrogen and then solubilized in extraction buffer (20 mL) containing 100mM Hepes-KOH, 10% (w/v) glycerol, 5 mM EDTA, 0.6% (w/v) PVP K-25, 5 mM ascorbic acid and 200 µl protease inhibitor cocktail (Sigma Aldrich, P9599 St Louis, MO). The extract was then filtered through Mira Cloth to remove cell debris and centrifuged for 5 min at 5000 g, 4°C (Beckman Coulter centrifuge with JA 20 rotor). The supernatant collected was then centrifuged at 100,000 g for 50 minutes, 4°C (Beckman Coulter centrifuge with JA 30.50 rotor). The supernatant was discarded and the microsomal pellet was dissolved in 500 µL of buffer containing 5mM potassium phosphate pH 7.8, 5mM KCL , 0.1 mM EDTA and protease inhibitor cocktail (Sigma Aldrich, P9599 St Louis, MO). Total protein concentration was checked spectrophotometrically according to Bradford (1976).

Proteomics

Two-dimensional electrophoresis was performed using the carrier ampholine method of isoelectric focusing (O'Farrell, 1975). The total membrane preparation from each sample was done in duplicates to obtain duplicate two dimensional silver stained gels and single Coomassie blue stained gels (**Figure 5.1A-D**). For silver stained gels, the samples were precipitated for 24 hours in 5 volumes of acetone, redissolved to 2 mg/ml in SDS Boiling Buffer, and heated in a boiling water bath for 3 minutes. The samples were then diluted to 1 mg/ml in Urea Sample Buffer before loading. For Coomassie blue-stained gels, the samples were precipitated for 24 hours in 5 volumes of acetone, redissolved in 75 ul of SDS Boiling Buffer, and heated in a boiling water bath for 5 minutes. The samples were then diluted with 75 ul of Urea Sample Buffer before loading all. Isoelectric focusing was carried out in glass tubes of inner diameter 3.5 mm, using 2% pH 3.5-10 (GE Healthcare, Piscataway, NJ) for 20,000 volt-hrs. 100 ng of an IEF internal standard, tropomyosin was added to each sample prior to loading. After equilibrium in SDS sample buffer (10% glycerol, 50 mM dithiothreitol, 2.3% SDS and 0.0625 M tris, pH 6.8), each tube gel was sealed to the top of a stacking gel that overlays a 10% acrylamide slab gel (1.0 mm thick). SDS slab gel electrophoresis was carried out for about 5 hrs at 25 mA/gel. The following proteins (Sigma Chemical Co, St. Louis, MO) were added as molecular weight markers: myosin (220,000), phosphorylase A (94,000), catalase (60,000), actin (43,000), carbonic anhydrase (29,000), and lysozyme (14,000)(**Figure 5.1**). The gels were dried between cellophane sheets with the acid end to the left. Duplicate gels were obtained from each sample and were scanned with a laser densitometer (Model PDSI, Molecular Dynamics Inc, Sunnyvale, CA). The scanner was checked for linearity prior to scanning with a calibrated Neutral Density Filter Set (Melles Griot, Irvine, CA). The images were analyzed using Progenesis Same Spots software (version 3.2, Nonlinear Dynamics) and Progenesis PG240 software (version 2006, Nonlinear Dynamics, Durham, NC). The general method of computerized analysis for these pairs included image warping followed by spot finding, background subtraction (average on boundary), matching, and quantification in conjunction with detailed manual checking. 22 of the selected spots were excised from the gels for mass spectral sequence analysis (**Figure 5.1A and 5.1C**).

LC-MS/MS Analysis

Protein spots were excised from gels and digested in-gel with trypsin. Briefly, specific protein spots were washed with 50% acetonitrile in 25 mM ammonium bicarbonate (NH_4HCO_3). The gel pieces were then dehydrated with acetonitrile, rehydrated with sufficient digestion buffer (12.5 ug/mL sequencing grade modified trypsin (Promega Corp., Madison, WI) in 25 mM NH_4HCO_3) to cover, and stored for 1h at 0°C. The solution was then removed and replaced with sufficient 25 mM ammonium bicarbonate to cover the gel pieces and the samples were digested overnight (~16h) at 37°C. The digests were separated by

microflow liquid chromatography using a custom-packed 20-cm x 150-mm reversed-phase C18 column at a flow rate of 1.5 mL/min using an Ultimate 3000 high performance liquid chromatography system (Dionex Corp., Sunnyvale, CA). Mobile phase solvent A was 0.1% formic acid in water, and mobile phase solvent B was 0.1% formic acid in acetonitrile. Following equilibration of the column in 5% solvent B, 5 μ L of each digest was injected, and then the organic content of the mobile phase was increased to 60% over 60 min. The column effluent was directed to an electrospray source attached to an LTQ linear ion trap mass spectrometer (ThermoFinnigan, San Jose, CA). Peptides were analyzed in positive ion mode. MS spectra were acquired in the m/z range between 200 and 2000. Each MS acquisition was followed by 5 MS-MS experiments in a data-dependent acquisition mode. For each MS spectrum, the five most intense peaks were selected for generation of CID mass spectra. A dynamic exclusion window was applied that prevented the same m/z from being selected for 1 min after its acquisition. X!Tandem (Craig and Beavis, 2004) protein database searches were carried out using the Computational Proteomics Analysis System (CPAS) (Rauch et al., 2005).

Chapter 6: Conclusion

6.1 SG is involved in membrane processes that rely on both symplastic isolation and symplastic continuum in plant cells.

DeBolt *et al.*, (2009) demonstrated the importance of SGs in transport of macromolecules in the seeds coat of Arabidopsis plants. Transport of macromolecules across seed coat epidermal cells can be visualized as a polarized secretion. Cotton fibers are elongated single epidermal seed coat cells largely driven by changes in turgor pressure, cell wall loosening and symplastic isolation of epidermal cells from underlying cell types by gating plasmodesmata (Ruan *et al.*, 2001). Another example is tip growth of root hair cells which is dependent upon of symplastic isolation of epidermal cells is tip growth of plant root. Studies have shown that a complex interaction between F -Actin cytoskeletal dependent trafficking, endocytic recycling and structural sterols is necessary to drive and maintain lateral tip growth (Araujo-Bazán *et al.*, 2008; Baluska *et al.*, 2000; de Graaf *et al.*, 2005; Ovecka *et al.*, 2005; Ovecka *et al.*, 2010; Preuss *et al.*, 2004; Voigt *et al.*, 2005). The complex interaction of these components depends upon their polarized localization at the tip of the root hair.

Using the sterol binding dye filipin, UGT80B1::GFP colocalized with filipin (RFP channel) to a region consistent with reports of the vesicle rich zone of root hairs (Preuss *et al.*, 2004) (**Figure 4.3**). Based on the suppressed root hair growth (**Figure 4.1**) and tip localized UGT80B1::GFP, our data suggests a role for sterol glycosides in establishment and or maintenance of polarity cues during tip growth. It is plausible that SGs, as membrane elements might interact with and preferentially organize proteins and cytoskeletal elements necessary for root hair tip growth in a targeted manner. In support, in yeast *P. pastoris* SG is necessary for forming preautophagosomal structure that is required for membrane transport and fusion for micropexophagy of peroxisomes (Oku *et al.*, 2003). Consistent with the requirement of F-actin and vesicle trafficking in tip growth, data from transcriptional and proteomics profiling in SG depleted and overexpressed plants revealed genes and proteins involved in cell wall and expansion, protein secretion, trafficking and cytoskeletal elements (**Table 2.1; Table 2.2; Table 4.1; Table 5.2**). Cytoskeleton components were predominantly actin associated and consistent with these results, plasma membrane localization for UGT80B1:GFP was displaced in epidermal root cells under conditions of actin depolymerization (**Figure 4.5**). Membrane trafficking and secretion proteins from proteomics included Patellin 1 and Patellin 2, RABE1B and ARF-A1c. Specifically Patellin1, Patellin2 (**Table 5.3; spot 2 and 4**) and ARF-A1c small GTP binding protein function by forming secretory vesicles and vesicle trafficking from the trans-Golgi network (TGN) and retrograde protein transport from Golgi to the ER (Matheson *et al.*, 2007; Mousley *et al.*, 2007) (**Figure 5.2**). Given the precedence of sterols as lipid markers of root hair tip growth (Ovecka *et al.*, 2010), our studies provide genetic and cellular evidence supporting glycosylation modification of membrane sterols as a necessary spatial and/or temporal cue for root hair elongation.

Future directions will employ further genetic and cell biological studies to deduce the exact mechanism by which SGs play a role in tip growth in root hairs. Introduction of protein fusion reporters such as *TUB::RFP* into *UGT80B1::GFP* expressing background via genetic crosses will provide the opportunity to further confirm the dependence of *UGT80B1::GFP* labeled particles in growing root hair tip on cytoskeletal elements. Furthermore, genetic crosses with reporter lines *CSLD3::CFP* and *RabA4b::RFP* (that are distinctly localized at the growing root hair tip (Park et al., 2008; Preuss et al., 2004)) in *ugt80B1* mutants and *UGT80B1::GFP* expressing plants will provide insight into the membrane dynamics in SG depleted plants and its contribution to tip growth.

Another example where plasmodesmata gating play a role is the developmental pattern of epidermal cells in Arabidopsis roots. Epidermal cells are symplastically connected by membranous channels, plasmodesmata (PD), earlier in plant development. Developmental patterning where these cells form alternating rows of trichoblast (H) cells and atrichoblast (N) cells establish earlier on and by the time root hairs are visible on plant root the epidermal cells are symplastically isolated (Duckett et al., 1994). As discussed earlier this symplastic isolation is part of the driving force that is required to hold the turgor pressure needed for tip growth of root hairs (Ruan et al., 2001). An interplay between the positional requirement and cell- to- cell communication (Lee et al., 2011), via PD involving transcription factors is crucial for early pattern development (Burch-Smith et al., 2011; Lee et al., 2011; Maule et al., 2011). *UGT80B1* is localized to plasma membrane (PM) and desmotubule membrane in the PD as evident from analysis of *UGT80B1::GFP* expressing plants (**Figure 3.5; Figure 3.6; Movie 3.2; Movie 3.4**). Furthermore, defective PD aperture and development were both observed in *ugt80B1*. Based on these results it can be imagined a variation in the epidermal patterning in *ugt80B1*. Consistently, variation in distribution of trichoblast cells (H) and atrichoblast (N) cells in *ugt80B1* roots in contrast to wild-type roots was noticed (**Figure 3.3**). However, since *UGT80B1* and its SG, in this case stigmasteryl glycoside (**Figure 3.10**), also are membrane components of the PM. Thus, a more complex interplay between PM processes and PD are expected as a reason for the variation in epidermal patterning in *ugt80B1*. Apart from that, aberrant cell-to-cell communication due to transcription factors involved in the epidermal patterning process can also be imagined. In support of this assumption, mislocalization of SCM receptor protein was observed in *ugt80B1* (**Figure 3.4**). SCM relays positional information from underlying cortical cells in Arabidopsis to the developing trichoblast (H) cell (Kwak and Schiefelbein, 2007). This information is relayed via WER in H cell; whereby SCM in H cell inhibits WER action (Kwak and Schiefelbein, 2008). Inhibition of WER in H cell is seen as cell type dependent expression of *WER::GFP* in wild type plants (Ryu et al., 2005). However since SCM was mislocalized in *ugt80B1*, aberrant expression of *WER::GFP* was seen in *ugt80B1* (**Figure 3.4**). Inhibition of WER in H cell creates an imbalance in abundance of transcription factors that leads to alternate H and N cell patterning (Kwak and Schiefelbein, 2008). Furthermore, critical balance between WER and CPC transcription factors is also crucial to this patterning. With the known PD requirement for cell-cell movement of at least

CPC, we hypothesize that compromised balance between the mobile transcriptional effectors in *ugt80B1* may at least partially explain the *ugt80B1* phenotype. Thus, stigmasteryl glycosylation by UGT80B1 is critical in supporting PD and PM lipid membrane diversification needed for developmental pathway such as epidermal patterning in Arabidopsis roots (**Figure 3.11**)

Future studies will focus on real time cell to cell movement of fluorescent dyes such as fluorescein isothiocyanate (Kim et al., 2003), in its ability to move through adjacent cells throughout the development of *ugt80B1* embryo. As development continues the Arabidopsis embryo develops zones of symplastic isolation and continuum as different cell groups develop into plant organs (Kim et al., 2003). At stages of heart stage and torpedo stage in Arabidopsis development these zones are prominent. Therefore embryos from *ugt80B1* will be isolated at heart and torpedo stages and imbibed in fluorescent dyes to study their movement under confocal microscopy.

Appendix A: The involvement of J-protein AtDjC17 in root development in *Arabidopsis**

Authors: Carloalberto Petti¹, Meera Nair¹ and Seth DeBolt

*Published in *Frontiers in Plant Science*, section Plant physiology 08 October 2014

¹Equal contributing authors

A.1 Introduction

During *Arabidopsis thaliana* L. Heyne root development, the distribution of hair cells (H) has been extensively studied as a position dependent developmental program. Here, the alternating emergence of trichoblast cells or root hair (H) versus atrichoblast cells or non-root hairs (N) relies on positional information, whereby epidermal cells in direct contact with anticlinal cell walls of two underlying cortical cells acquire H cell fate and all others become N cells (Dolan, 2006). This position-dependent cell fate determination at the root epidermis is reliant on a complex regulatory pathway involving genetic cell fate determinants and mobile transcriptional regulators (Kwak and Schiefelbein, 2007). Here, SCRAMBLED (SCM), a leucine-rich receptor-like kinase (LRR-RLK) relays positional information underlying this pattern (Dolan, 2006; Kwak and Schiefelbein, 2008). Signaling through SCM establishes repression of the R2R3-MYB transcription factor WEREWOLF (WER) in H cells. As a result, the repression of WER in H cells causes increased levels of WER in N cells and in turn the levels of a regulatory complex consisting of transcriptional mediators WER-GLABRA3 (GL3)/ENHANCER OF GLABRA3 (EGL3)-TRANSPARENT TESTA GLABRA1 (TTG1). The combined effect of these factors causes activation of direct targets including the N-cell determinant and homeodomain-leucine-zipper transcription factor GLABRA2 (GL2) (Kwak and Schiefelbein, 2008). The complexity of cell fate determination in the epidermal layers is clearly evidenced by the large number of transcription regulators involved (Guimil and Dunand, 2006), as well as by an increasingly large number of additional genes e.g. auxin responsive, *AXR2*, *AXR3* (Knox et al., 2003; Nagpal et al., 2000), *KEU*, which encodes the yeast *Sec1* homologue, a key regulator of vesicle trafficking (Assad et al., 2001), *ROP2* a small Rho-plant GTPase implicated in cytoskeleton organization and cell polarity (Jones et al., 2002) and the Ethylene Oxide genes *ETO1* and *ETO2* involved in ethylene synthesis (Cao et al., 1999). Recently, a nuclear factor with homology to a heat shock factor (HSF) (ten Hove et al., 2010), which encodes the *SCHIZORIZA* gene (Mylona et al., 2002), was also linked to radial patterning. Despite the potential for heat shock protein (HSP) or HSFs to play roles in root hair development and patterning, due to the obvious exposure to changing environmental conditions, genetic evidence for key genes remains poorly characterized.

A large number of genes encode the heat shock proteins (HSPs) and heat shock factors (HSFs). HSPs were named as heat response proteins (Ritossa

1962; Tissiers *et al.*, 1974), but since have been linked to a multitude of biological processes including microtubules stabilization, anti-apoptosis, refolding of a protein in non-native status, regulation of steroid hormone receptors (Kregel, 2002), protein translocation, protein folding (reviewed by (Al-Whaibi, 2011), cell proliferation (Pechan, 1991) and at least with regard to fungi, HSPs are involved in signaling (Panaretou and Zhai, 2008). Among the HSPs the most studied are the HSP70 (Bakau and Horwich, 1998) and the DnaJ (Nakamoto and Vigh, 2007; Siddique *et al.*, 2008). DnaJ is a member of the Hsp40 family of molecular chaperones, which is also known as J-protein family (Walsh *et al.*, 2004). In Arabidopsis, the J-family encompass as many as 120 members classified in 4 sub-types (Rajan and D'Silva, 2009). J-protein type I, share all motifs found in a DnaJ a highly conserved N-terminal J-domain, followed by a glycine/phenylalanine rich region, a zinc-binding cysteine rich region and a variable C-terminal region. The remaining types display a simplified structure, with type II, missing the Zinc-finger domain and type III displaying only the J-domain. Type IV, are J-like protein with a large similarity to the J-domain but missing the recognition motif HPD (Rajan and D'Silva, 2009; Siddique *et al.*, 2008). DNAJ/ J-domain proteins are best know as co-chaperones working in association with HSP70 (Bekh-Ochir *et al.*, 2013; Jelenska *et al.*, 2010; Miernyk, 2001; Minami *et al.*, 1996; Qiu *et al.*, 2006; Summers *et al.*, 2009). During a screen of T-DNA Arabidopsis thaliana mutants for defective root hairs we identified that mutations in a type III J-protein (AtDjC17) gene and we aimed to study the transcriptional and genetic features that contribute to root development.

A.2 Results

Mutations in *Atdjc17* caused altered organization of root hair position in atrichoblast versus trichoblast cell files

In a screen for altered root hair (H-cell) occurrence, we identified a causal mutation in *Atdjc17-1-1* (At5g23240). Motif analysis showed that *AtDjC17* contained a J-domain motif and was broadly classified as a J-protein type III (Rajan and D'Silva, 2009). To further confirm the root hair phenotype, two alleles were isolated and correspond to *Atdjc17-1-1* and *Atdjc17-1-2*. Homozygosity for the insertion of a T-DNA into the *AtDjC17* exon was verified by polymerase chain reaction (PCR)(**Figure A.1**). Further, *AtDjC17* mRNA abundance was examined in wild-type (WT) as well as *Atdjc17-1-1* and *Atdjc17-1-2* plants by qRT-PCR and these data revealed no detectable *AtDjC17* mRNA for either allele. Thus, we concluded that both *Atdjc17-1-1* and *Atdjc17-1-2* were null alleles.

H-cells appeared in adjacent cell files rather than in alternating cell files in both mutant alleles (*Atdjc17-1-1* and *Atdjc17-1-2* respectively **Figure A.2** and **Figure A.3**) described as irregular root H emergence. A 31% reduction in H-cells was observed in a trichoblast cell file in *Atdjc17-1-1* (**Figure A.2B-D**). As expected, 100% of H-cells were identified in the trichoblast cell file in WT roots (n=10 seedlings) (**Figure A.2A-D**). In *Atdjc17-1-1* we observed H-cells in atrichoblast cell file (approximately 19.5% H cells), whereas no H formation was observed in atrichoblast cell files in WT. Alongside these data we also observed

a quantitative increase in the distance between adjacent H-cells in a cell file in *Atdjc17* alleles compared with WT ($217.9 \pm 6.6 \mu\text{m}$ for *Atdjc17-1-1* and $173.4 \pm 5.8 \mu\text{m}$ for WT, $P < 0.05$) (**Figure A.4H**). Accounting for this phenotype was an observed increase in trichoblast cell area for *Atdjc17* mutants (*Atdjc17-1-1*: $2916 \pm 161.6 \mu\text{m}^2$; WT: $2384 \pm 104.2 \mu\text{m}^2$, $P > 0.05$), indicative of an expansion defect.

To query whether increasing the transcript abundance for *Atdjc17* would influence root epidermal patterning phenotype, we expressed a *35S::AtDjC17* in WT plants. This resulted in a transgenic plant with 3.5 – fold increase in *AtDjC17* transcript in the roots (**Figure A.9**). Visual examination of the *35S::AtDjC17* roots also revealed irregular H-cell occurrence compared with WT. In an opposite fashion than was observed in *Atdjc17* mutants, the *35S::AtDjC17* displayed a 12.5% reduction in H-cells in a trichoblast cell file (**Figure A.2C-D**) as compared to 31% in *Atdjc17-1*. Average occurrence of H-cells in the atrichoblast file was 34% (**Figure A.2E**) compared to the 19.5% in *Atdjc17*. Additionally, *35S::AtDjC17* displayed a significant increase in the number of H-cells calculated per 0.65 mm of root length *i.e.* 19.4 ± 0.7 (**Figure A.4G**, $P < 0.05$) when compared with the values determined for the WT (**Figure A.4A-D-G**) and *Atdjc17-1-1* (**Figure A.4B-E-G**). This increase was also paralleled by a reduction of the distance between root H-cells ($135 \pm 2.9 \mu\text{m}$, $P < 0.05$; **Figure A.4H**) as compared to WT and to the *Atdjc17* mutants. These data support the requirement for *AtDjC17* in determining the correct positional distribution of H-cells among epidermis cells in the Arabidopsis root.

To further confirm that observed phenotypes in *Atdjc17* were in response to dysfunction in *AtDjC17* we complemented the T-DNA mutant with the *AtDjC17* driven by its native promoter (2000 bp upstream of initiation codon). The resulting complementation line was not discernible from the WT with respect to H-cell frequency and position (**Figure A.5**). These data were consistent with the observed phenotypes linked to *AtDjC17*.

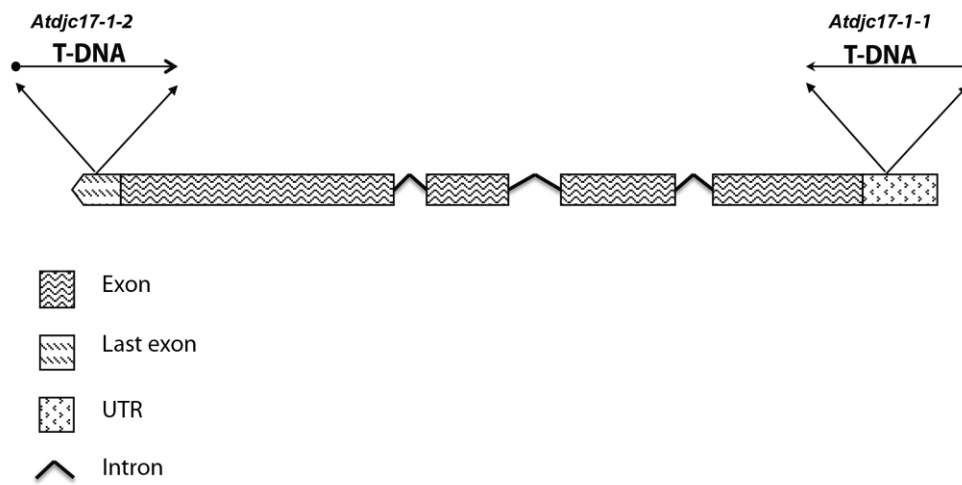


Figure A.1 Gene model and position of T-DNA insertions. Graphical representation of the gene model associated with AtDjC17 with highlighted the T-DNA insertion.

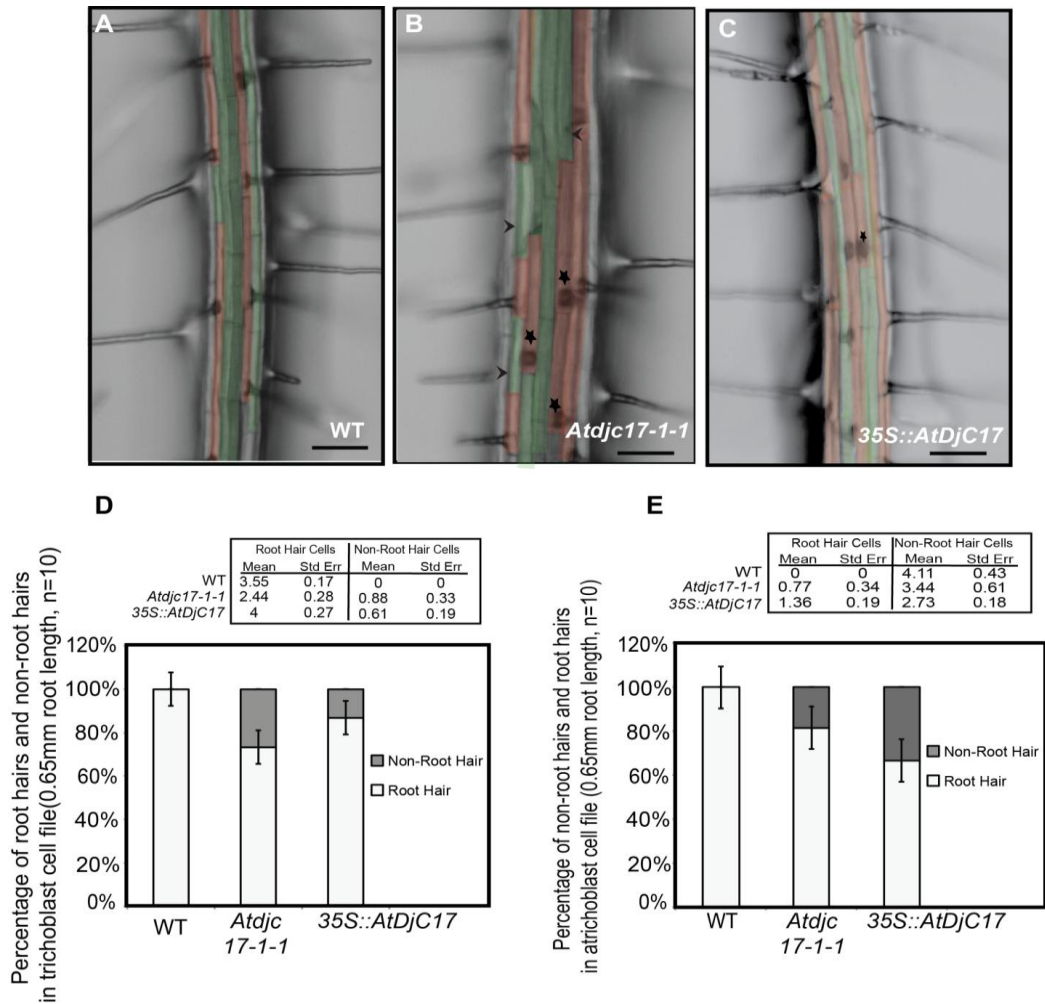


Figure A.2 Trichoblast and atrichoblast cells are arranged randomly in *Atdjc17* and overexpressor mutants. (A, B, C) False colored stereomicroscope images of WT (A), *Atdjc17-1-1* (B) and *35S::AtDJC17* (C) illustrate the patterning of root hair cells (red) and non-root hair cells (green) in cell files. Stars represent ectopic root hairs in an otherwise atrichoblast cell file. Arrowheads represent the presence of non-root hair in an otherwise trichoblast cell file in *Atdjc17-1-1*. **(D, E)** Root hair and non-root hair cells in trichoblast and atrichoblast cell files were counted in WT, *Atdjc17-1-1* and overexpressor *35S::AtDJC17*.

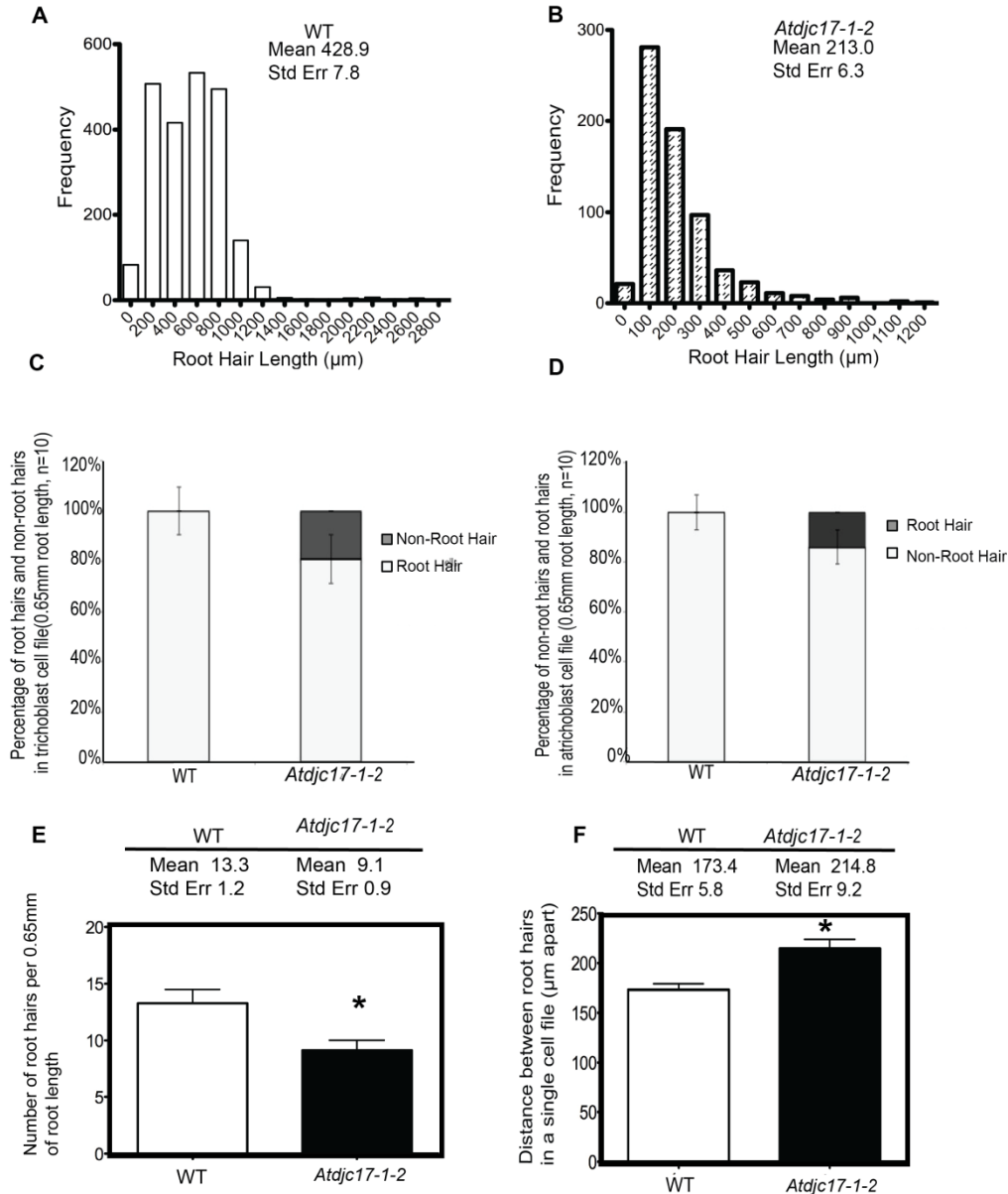


Figure A.3 Mutations in *ATDJC17* cause root hair alteration and ectopic root hair production. Histograms showing frequency of root hair length in WT (A) and *Atdjc17-1-2* (B). Whole roots of 10 seedlings were used. (C-D) Root hair and non-root hair cells in trichoblast and atrichoblast cell files were counted in WT, and *Atdjc17-1-2*. (E) Variation in number of root hairs as determined in *Atdjc17-1-2* and as compared to WT plants. An area approximately 2 mm from the root cap was chosen for the comparison covering 0.65mm root length. (F) Comparison of distance between adjacent root hairs in a single vertical trichoblast cell file in WT (A) and *Atdjc17-1-2* (E). Asterisk represents significance based on $P < 0.05$.

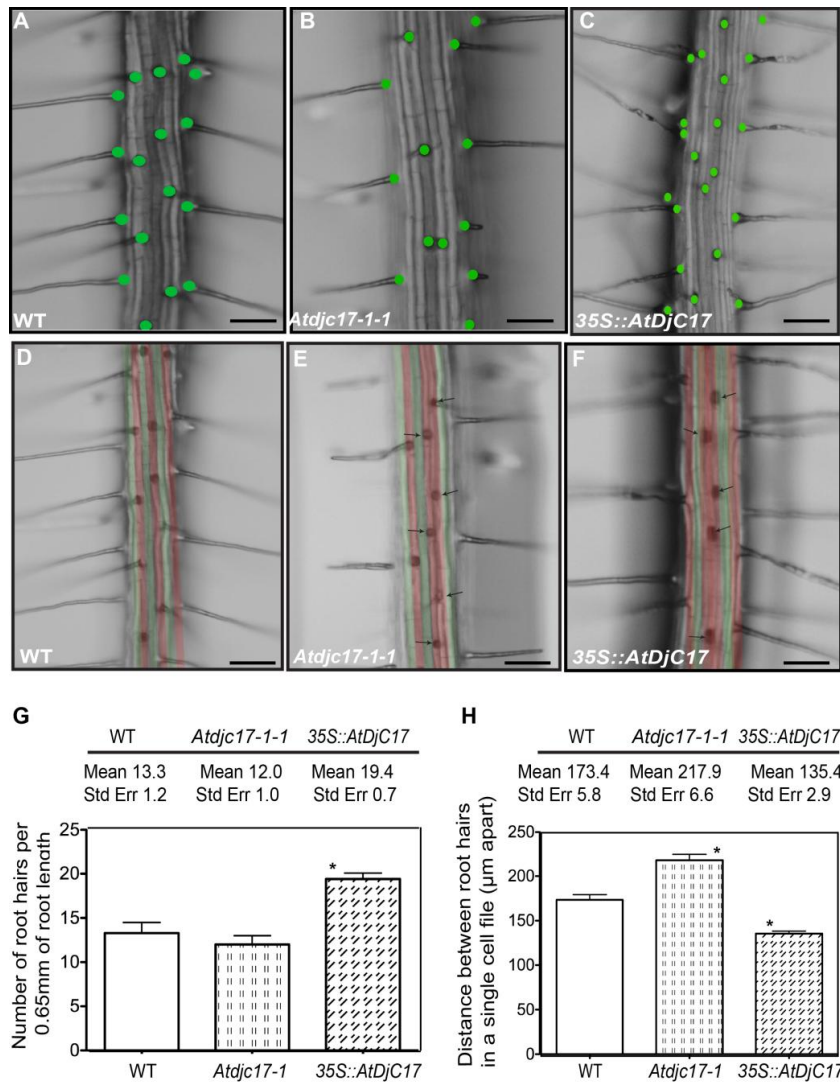


Figure A.4 Mutations and overexpression in *ATDJC17* cause root hair alteration and ectopic root hair production. (A, B, C) Variation in number of root hairs is illustrated in *Atdjc17-1-1* and *35S::AtDJC17* mutants as compared to WT plants. Green dots highlight the presence of root hair at the site. (G) Average number of root hairs determined from a total of 10 roots. An area approximately 2 mm from the root cap was chosen for the comparison covering 0.65mm root length. (D, E, F) Stereomicroscope images of WT (D), *Atdjc17-1-1* (E) and *35S::AtDJC17* (F) roots false colored to show the trichoblast (red) and atrichoblast (green) cell files. Arrows in *Atdjc17-1-1* and *35S::AtDJC17* mutant highlights the presence of 2 trichoblast cell files adjacent to each other illustrating the presence of ectopic root hair. (H) Comparison of distance between adjacent root hairs in a single vertical trichoblast cell file in WT (D) *Atdjc17-1-1* (E) and overexpressor *35S::AtDJC17* (F).

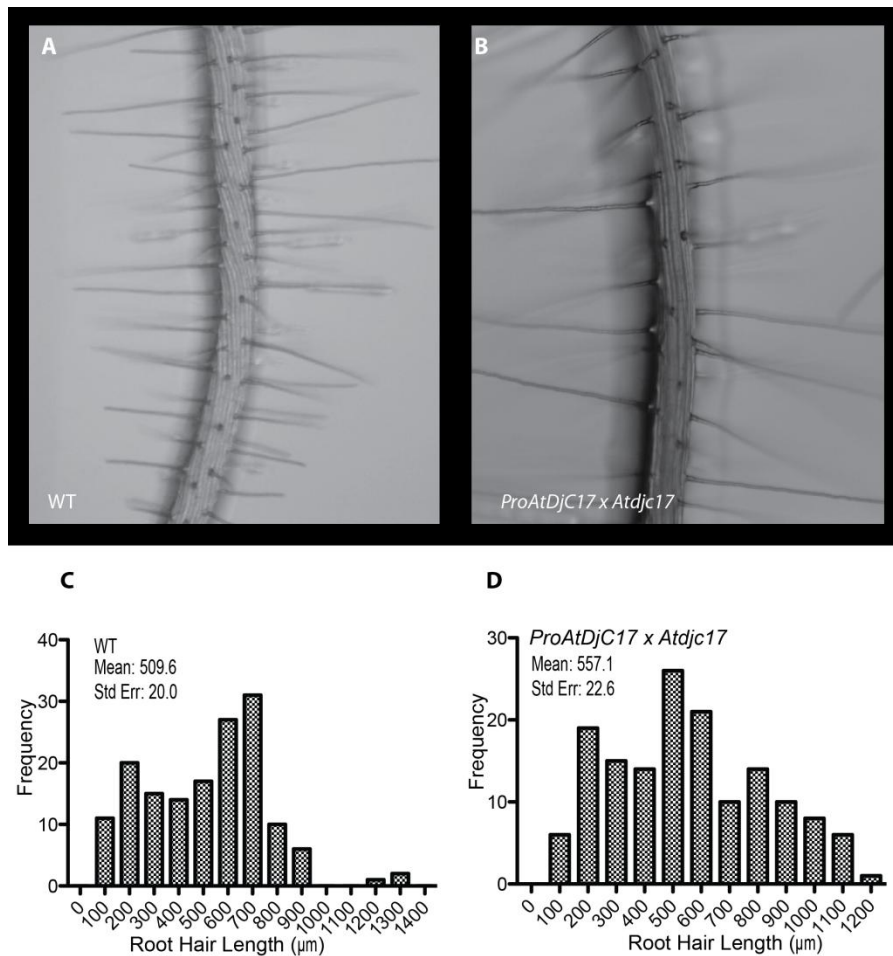


Figure A.5 Phenotypical characterization of complemented T-DNA line. The T-DNA lines were complemented by the native promoter driven *AtDjC17* overexpression. T3 lines were assed for root hair phenotypical characterization. Stereomicroscope images of WT (A) and *Atdjc17-1-1* (B) which displayed no difference in root hair positioning as compared to WT. (C-D) Histograms showing comparable frequency of root hair length in WT (C) and *ProAtdjc17 x Atdjc17-1* (D).

Visual examination of *proAtDjC17::GUS* transcript revealed localization to the stele cells

To visually determine where the *AtDjC17* transcript was expressed during root development we generated a beta-glucuronidase (GUS) reporter fused to the *AtDjC17* promoter. Microscopic examination of 7-day old seedlings indicated a spatially discreet zone of transcript coincident with the stele and no visible abundance in cortical, endodermal or epidermal cell files (**Figure A.6A-B**). Transverse sections of stained and cleared seedlings confirmed that transcript was localized principally in the stele (**Figure A.6C**). To also explore whether or not *AtDjC17* transcript abundance was stress dependent or independent in a cell

type specific manner, we imposed various stress regimes on the transgenic plants expressing *proAtDjC17::GUS*. These results revealed no shift in expression under stress.

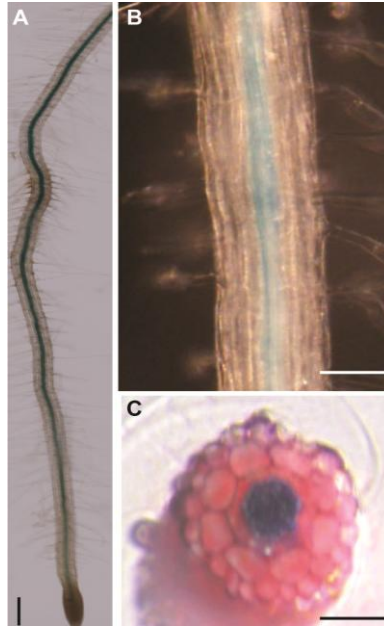


Figure A.6 GUS expression studies. (A-B) Stele-localized accumulation of *proAtDjC17::GUS* transcript in a 7-d old root. **(A)** Scale Bar 100 μ m. **(B)** Scale Bar 50 μ m. **(C)** Agarose embedded hand section of *proAtDjC17::GUS* expressing 7-d old roots displaying a clear stele accumulation of GUS, Scale Bar 50 μ m.

Transcript analysis reveals differential expression in root patterning genes in *Atdjc17-1* and *35S::AtDjC17* roots versus WT

The expression levels of known epidermal and radial patterning genes was explored. Here, we examined the leucine-rich receptor-like kinase (*SCM*), the bHLH transcription factors *GLABRA3* (*GL3*) and *ENHANCER OF GLABRA3* (*EGL3*), the R2R3-MYB transcription factor (*WER*), the small single-repeat R3-MYB transcription factor *CAPRICE* (*CPC*), the WD-repeat *TRANSPARENT TESTA GLABRA1* (*TTG1*), the WRKY transcription factor *TRANSPARENT TESTA GLABRA2* (*TTG2*), the homeodomain-leucine-zipper transcription factor *GLABRA 2* (*GL2*), the basic-leucine zipper transcription factor *SCARECROW* (*SCR*), the transcription factor *SHR*, and zinc finger proteins *JACKDAW* (*JKD*) and *MAPGPIE* (*MGP*) ((Bernhardt *et al.*, 2005; Di Laurenzio *et al.*, 1996; Galway *et al.*, 1994; Hassan *et al.*, 2010; Helariutta *et al.*, 2000; Ishida *et al.*, 2007; Ishida *et al.*, 2008; Koshino-Kimura *et al.*, 2005; Kwak and Schiefelbein 2007; Lee and Schiefelbein, 1999; Masucci *et al.*, 1996; Schellmann, *et al.*, 2002; Wada *et al.*, 1997; Wada *et al.*, 2002; Welch *et al.*, 2007; Zhang *et al.*, 2003) in *Atdjc17* alleles compared with WT. *TTG2* amongst the epidermal patterning regulators and *JKD* and *MGP* involved in radial and epidermal patterning were not

differentially expressed when compared to WT (**Figure A.7**). Results showed a significant ($P \leq 0.05$) up-regulation of *GL3*, *SCM*, *EGL3*, *WER*, *CPC*, and *TTG1* as compared to WT (**Figure A.7**). The principle exceptions were *SCR* and *SHR*, which were down-regulated ($P < 0.05$, **Figure A.7**). This trichoblast and atrichoblast specific transcripts increased abundance is consistent with both irregular H-cell development and reduced frequency of H-cells. *SCR* transcript was down-regulated in the *Atdjc17* mutant root (**Figure A.7**) moreover *SCR* has been shown to cause a loss and coupling of endodermal and cortical cell layers (Di Laurenzio *et al.*, 1996). However, mutants with loss in the *AtDjC17* gene product did not exert as dramatic effects as other characterized mutants such as *shr*, as evidenced by agarose embedded hand-sections or propidium iodide staining (**Figure A.8**). This down-regulation of *SCR* transcript likely resulted from an up or downstream regulation, such as *SHR*, which was also down-regulated in *Atdjc17*. Nevertheless, a cell division increase was quantified in cortical (Increased cell division: *Atdjc171-1/1-2*: 9 cells/section \pm 1 vs. WT 8 cells/section \pm 0, n = 15) and endodermal layers (Increase in cell frequency in endodermal layer *Atdjc171-1/1-2*: 9 cells/section \pm 1 vs. WT 8 cells/section \pm 0, n = 15) of the *Atdjc17* mutant, which was consistent with a 'scrambling' of expression among transcripts involved in epidermal patterning.

Transcriptional analyses of *AtDjC17* and 12 known regulators of root development (**Figure A.9**) were investigated in the overexpressor of *35S::AtDjC17*. As expected, *35S::AtDjC17* increased *AtDjC17* transcript levels but it was also noted a down-regulation of *GL2*, which was consistent with the ectopic root hair phenotype previously described (**Figure A.2**). In addition to *35S::AtDjC17* also the transcript levels of *GL3*, *TTG2* and *SCR* were also up-regulated. Consistently with *GL2* also *CPC* was found down-regulated along with *SHR*, whereas the remaining regulators were found to be unchanged

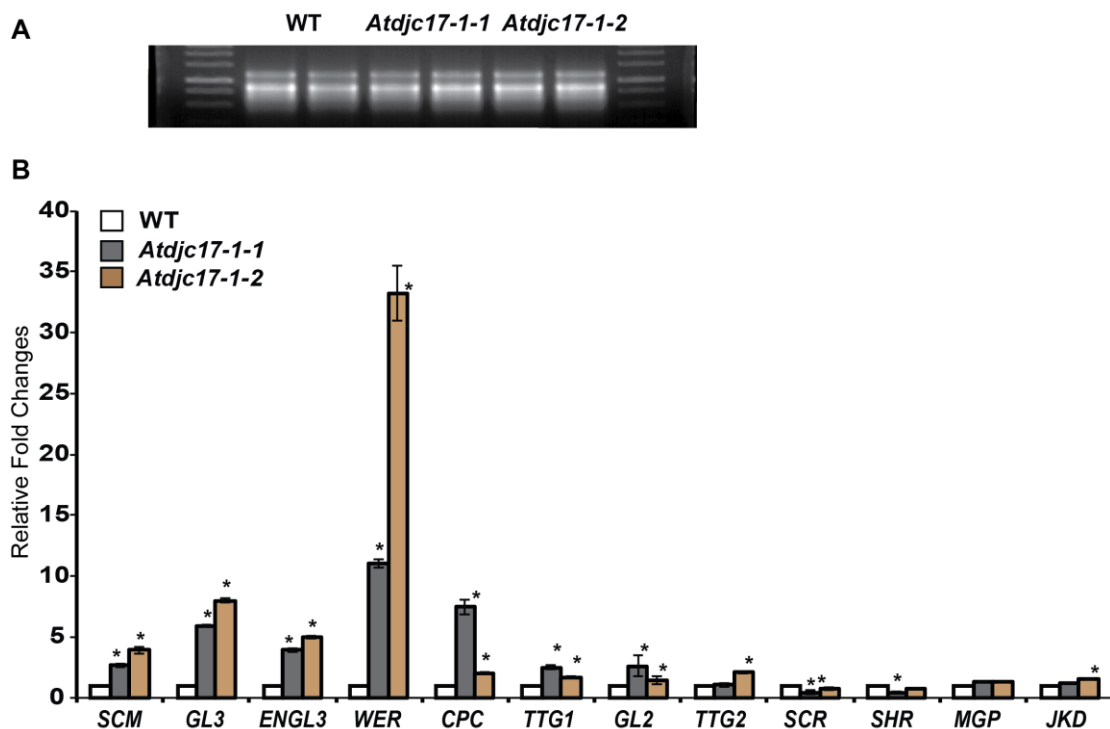


Figure A.7 Gene expression analysis for previously identified regulatory elements of root development. (A) RNA equal loading of WT and *Atdjc17* mutant lines (*Atdjc17-1-1*, *Atdjc17-1-2*). **(B)** Relative fold changes determined on whole root sample for SCRAMBLE (SCM); *GLABRA3* (GL3); *Enhancer of GLABRA3* (ENGL3); *WEREWOLF* (WER); *CAPLICE* (CPC); *TRANSPARENT TESTA 1* (TTG1); *GLABRA2* (GL2); *TRANSPARENT TESTA 2* (TTG2); *SCARECROW* (SCR); *SHORT-ROOT* (SHR); *MAGPIE* (MGP) and *JAKDOW* (JKD). Error bars indicate standard deviation. * Indicates significant difference ($P \leq 0.05$).

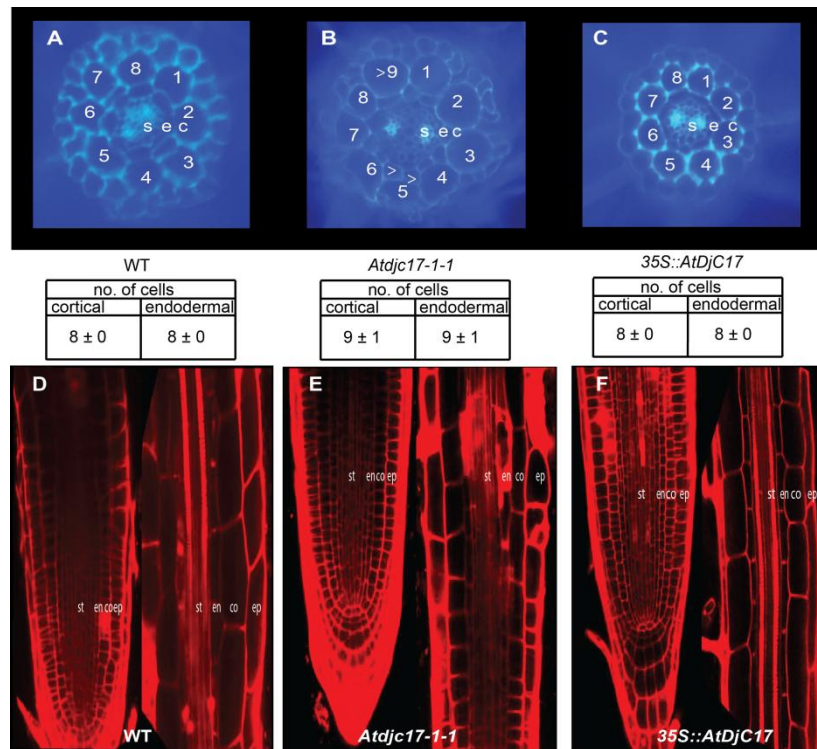


Figure A.8 Examination of cell division in WT, *Atdjc17-1-1* and *35S::AtDJC17* roots. Agarose embedded hand sections stained with calcofluor–white stained and confocal microscopic images of propidium iodide stained WT, *Atdjc17-1-1* and *35S::AtDJC17* mutant roots. **(A)** WT section. **(B)** *Atdjc17-1-1* section showing additional cell division in the cortical and endodermal layers. Note that the divisional pattern seems anticlinal in nature. Arrow heads indicate ectopic divisions. **(C)** *35S::AtDJC17* section with no evidence of altered cortical and endodermal cell numbers. **(D)** 7-day old post germination WT root tip and zone above the meristematic tip in WT root. **(E)** *Atdjc17-1-1* root tip with associated zone above the meristematic tip. **(F)** *35S::AtDJC17* root tip and elongation zone. st, stele; en, endodermis; co, cortex; ep, epidermis.

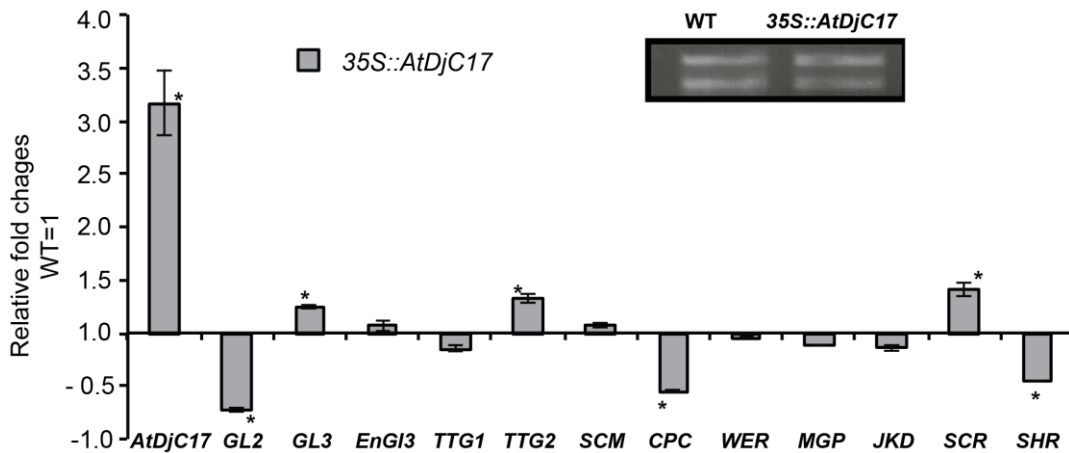


Figure A.9 Root expression analysis of the overexpressor of *AtDjC17*. Relative fold changes determined on whole root sample for 35S::AtDjC17 and 12 main regulators of root development. Error bars indicate standard deviation. * Indicates significant difference ($P \leq 0.05$).

Cortical and endodermal cell layers display aberrant divisions in *Atdjc17* but not in 35S::AtDjC17

Phenotypes associated with the dysfunction in the stele expressed *SHR*, and ground tissue stem cell expressing *MGP* and *JKD* genes include irregular pattern formation in the cortical and endodermal cell layers (Helariutta *et al.*, 2000; Koizumi *et al.*, 2011; Ogasawara *et al.*, 2011; Welch *et al.*, 2007). Although *shr* has a far more severe effect on plant growth and development than what we have documented for *Atdjc17* alleles (**Figure A.2, A.3 and A.4**) *Atdjc17* subtle phenotypes are more similar to the one documented for *mgp* and *jdw*. Using laser scanning confocal microscopy, we examined the longitudinal cell file development of *Atdjc17* and WT using propidium iodide to fluorescently label the cell walls. Here, the cortical and endodermal cell layers in *Atdjc17* root did not show obvious changes in cell division relative to WT (**Figure A.8D-F**). By contrast, when we examined cross sections of WT, *Atdjc17* and 35S::AtDjC17 seedling roots it was evident that the cortical (co) and endodermal (en) layer displayed increased frequency of cell divisions in the *Atdjc17* mutants (co: 9 cells per section ± 1 , $n = 15$; en: 9 cells per section ± 1 , $n = 15$) compared to the WT (8 cells per section ± 0 , $n = 15$ **Figure A.8A, B**). On the contrary, 35S::AtDjC17 did not show observable alteration in divisions in either cortical cells or endodermal cell layers (**Figure A.8C**). Absence of visible alteration in the longitudinal propidium iodide stained section suggests an anticlinal division alteration only identifiable through cross sections. Changes in the number of cells in the cortical layer directly influences the frequency of trichoblast cells in the epidermal layer due to the position requirement for contact with two underlying cortical cells (Kwak and Schiefelbein, 2007), which was consistent with the

observed aberrant H-cell occurrence visualized in *Atdjc17* mutants (**Figure A.2**). The modest changes in root patterning (increase cell division: *Atdjc171-1/1-2*: 9 cells/section \pm 1 vs. WT 8 cells/section \pm 0, n = 15) and development (increase in cell frequency in endodermal layer *Atdjc171-1/1-2*: 9 cells/section \pm 1 vs. WT 8 cells/section \pm 0, n = 15) displayed similarity to *mgp* and *jdk* (Welch *et al.*, 2007; Ogasawara *et al.*, 2011).

A.3 Discussion

Mutations in *AtDjC17* identified in this study, caused aberrant cell fate determination and cell divisions in ground tissue layers in Arabidopsis roots. Existing literature supports DNAJ/ J-domain family proteins functioning as co-chaperones working in association with HSP70 class proteins (Bekh-Ochir *et al.*, 2013; Jelenska *et al.*, 2010; Miernyk, 2001; Qiu *et al.*, 2006; Summers *et al.*, 2009), however, coexpression analyses and extensive pull-down assays (data not presented) have thus-far failed to reveal a candidate HSP70 to act in conjunction with *AtDjC17*. Based on the observed root phenotypes, we hypothesized that a DNAJ-HSP40 (*AtDjC17*) could plausibly be required for cell fate determination by acting with a cognate HSP70 as a protein chaperone to fortify key stage(s) in the pathway. We envisioned that chaperone function could be important, particularly at the epidermis, where exposure to the adjacent soil environment may require such a chaperone due to environmental stress. However, an unexpected feature of the *AtDjC17* was its prominent expression in restricted to stele tissue of the Arabidopsis root (**Figure A.6**). This is despite H-cell irregularity phenotypes being observed in the epidermis (**Figure A.2**). Interestingly, dysfunction in genes encoding the zinc finger proteins *JKD* and *MGP* resulted in a similar syndrome of defective epidermal cell fate determination and division defects despite transcription being localized outside of epidermal tissue. *JKD* expression is localized in ground tissue, quiescent center (QC) and to a lesser extent in mature cortical cells and is known to limit *SHR* and control cell divisions that give rise to endodermal and cortical layers (Hassan *et al.*, 2010; Welch *et al.*, 2007). *SHR*, a GRAS family transcription factor is expressed in stele tissue (Welch *et al.*, 2007) and influences root development by influencing asymmetric divisions that give rise to ground tissue as well as endodermal cell identity. It does this in part by regulating *SCR*, another GRAS family transcription factor (Helariutta *et al.*, 2000). Both *SHR* and *SCR* affect overall root development as mutations in these genes causes supernumerary and replacement of cortical/endodermal cell layer with a single ground cell layer having heterogeneous cell identity. Therefore, the prominent stele expression support a matching expression for *AtDjC17* with *SHR* and suggests possible functional influence in the same pathway. We propose a model whereby a chaperone complex involving *AtDjC17* could be influencing this pathway in a non-cell autonomous fashion that involves *SHR*, *SCR*, *JKD* and *MGP*.

Indeed, examining gene expression of *SHR* and *SCR* in *Atdjc17* supports these data. Quantitative Real Time (Q-RT) PCR revealed down-regulation of *SCR*. We anticipated that down-regulation of *SCR* in *Atdjc17* would be mirrored

by *SHR*, which was confirmed by Q-RT PCR (**Figure A.7**). By contrast, in the whole root samples from *Atdjc17*, trichoblast and atrichoblast specific expressed transcripts (atrichoblast (*WER*, *GL2*, *CPC*); trichoblast (*EGL3*, *GL3*)) both displayed increased abundance relative to WT. Considering the mixed identity among epidermal cell files observed as H-cell-fate irregularities, the observed increased transcript abundance among these cell type specific transcripts was not unexpected, but does not conclusively suggest any single element as responsive. Alternatively, Q-RT PCR on whole root samples might not be a sensitive method to uncover differences in cell type specific transcript levels. Cell type specific Q-RT PCR on *Atdjc17* may provide better understanding of the differences in gene expression for epidermal patterning specific genes.

Intriguingly, expression levels of *JKD* and *MGP*, were not differentially expressed in *Atdjc17* further suggests that *AtDjC17* functions independently of these factors. These data did not support our hypothesis of transcriptional linkage to the zinc finger proteins *JKD* and *MGP* but did identify transcriptional association to *SCR/SHR*. Given its critical requirement for root development, it is indeed plausible that molecular chaperone function for *SHR* would be important to safeguard the root developmental program. Taken together, *JKD* null mutations cause ectopic periclinal divisions in the cortical and endodermal layer but also an ectopic root hair development in a non-cell autonomous fashion (Hassan *et al.*, 2010; Welch *et al.*, 2007). Hence, while the localization of *AtDjC17* expression to stele cells partially overlapped with *SHR* the phenotype of *Atdjc17* more closely resembled *jdk*, although with a far less severe impact on cell division and whole plant morphogenic phenotypes. The position dependence needed to acquire H-cell versus N-cell fate in epidermal cells (Dolan, 2006) is such that ectopic divisions within the cortical cells observed in transverse cross sections of the *Atdjc17* root could explain the corresponding irregular pattern of H-cell emergence (**Figure A.2**). Further studies are needed to assign biochemical association between possible targets of the *AtDjC17* co-chaperone, in addition to isolation of the anticipated cognate HSP70. Although many genes have been identified in root development (Guimil and Dunand, 2006) no prior evidence supports a requirement for a DNAJ-HSP40 for epidermal cell fate determination, and results from *Atdjc17* raise the intriguing possibility of a HSP complex playing a chaperone role in root development.

A.4 Material and Methods

Plant material and Growth conditions

Arabidopsis thaliana (L.) Heynh (*Arabidopsis*) ecotype Colombia-0 was used in all experiments. The T-DNA insertional alleles [At5g23240, germplasm SALK_008678 (*Atdjc17-1-1*) and SALK_024726C (*Atdjc17-1-2*)] were obtained from the *Arabidopsis* Biological Resource Center (ABRC, Ohio State University). Seeds were surface sterilized and vernalized at 4°C for 2 days in the darkness prior to plating them on ½ strength Murashige and Skoog (MS) basal salts medium (pH 5.7) (Duchefa, Holland) solidified with 0.8% agar. Seeds were germinated under 16 h light; 8 h darkness conditions at a constant temperature

of 22°C. Seeds were plated as above described and plates were vertically positioned and incubated in dark grown (22°C) condition. The phenotypes of *Atdjc17-1-1* and *Atdjc17-1-2* were compared to that of WT during plant growth and development. Plants were grown in MetroMix 360 (SunGro Horticulture) in a temperature controlled environmental chamber (22°C)(Adaptis, Conviron).

Genotyping of the mutant lines

Homozygosity of the knockout lines *Atdjc17-1-1/Atdjc17-1-2* was verified by polymerase chain reaction (PCR)-based genotyping, primers sequences are given in **Table A.1**. Total plant DNA was extracted as previously described (Rogers and Benedich, 1985). For PCR purposes the DNA concentration was standardized to 100 ng μl^{-1} in Tris pH 8.0 (10 mM).

Microscopy

Imaging and quantitation of seedling phenotype employed fluorescence stereomicroscopy (Olympus MVX) and ImageJ (National Institute of Health, Bethesda, MD). Statistical analysis comparing *Atdjc17* and WT plants used PRISM4 (Graphpad, La Jolla, CA) and Minitab (Minitab Inc., USA). Seedling phenotypes, including root hair and epidermal patterning defects were examined consistently at 7-d post-germination. Seedlings were grown vertically in ½ strength MS agar. Root hair length measurements were averaged across the entire root. To examine the pattern of epidermal development in a uniform spatial region of the root we documented cell area in the region covering 0.65 mm of root, initiating approximately 2 mm above the root cap. Average cell length and area determinations for each trichoblast/atrichoblast cell used area measurement output after tracing the polygon via the freehand selection tool (ImageJ) and pixel-number² converted to μm^2 . Due to the 3-dimensional nature of the root structure only those root hairs visible in the optical plane were counted. Transverse root sections were made as described (Hung et. al., 1998) whereby roots were embedded in 3% molten agarose and hand sectioned using double-edged razor blade. The sections were stained with calcofluor-white (Sigma, USA) stain and visualized under fluorescence stereomicroscope (Olympus MVX; DAPI filter). For β -glucuronidase (GUS) histochemical assay, staining solution was prepared according to (Guivarc'h et al., 1996). The seedlings were cleared, sectioned as above and counter stained with 0.05% Ruthenium red according to (Hassan et al., 2010) before visualization. Propidium iodide staining was performed as described in (Nawy et al., 2005). Accordingly 7-d post-germination seedlings were stained with 10 mgL^{-1} propidium iodide for 30 seconds to 2 minutes, rinsed and mounted on water. Microscopy was performed on an Olympus FV1000 laser scanning confocal microscope using a 63 × N.A 1.4 water-immersion objective. The microscope is equipped with lasers for excitation wavelengths ranging from 405–633 nm and propidium iodide stain was excited using the DsRed setting in the Olympus Fluoview software (Olympus). All image processing was performed by using Olympus Fluoview software (Olympus) and ImageJ (W. Rasband, National Institutes of Health, Bethesda, MD) software.

Construction of reporter and overexpression lines. Selection and expression analysis of transgenic lines

The *AtDjC17* transcript accumulation was assayed by fusing the *AtDjC17* promoter to the GUS (Jefferson et al., 1987) reporter gene through a promoter::*uidA* fusion construct. A 1.5 Kb putative promoter region was PCR-amplified with the specific primers ATDJC17P-F/ ATDJC17P-R (**Table A.1**) and the PCR amplified product was cloned into pCXPGUS ZeBaTA vectors (Chen et al., 2009). For overexpression studies, the open reading frame was PCR amplified from genomic DNA using primers ATDJC17G-F/ATDJC17G-R and the amplicon (1.45 Kb) was cloned into the pCXSN vector (Chen et al., 2009) under the constitutive expression of the Cauliflower mosaic virus (CaMV)-35S promoter (35S). Sequence verified clones were transformed by electroporation into *Agrobacterium tumefaciens* hypervirulent strain GVS3101. Arabidopsis plants were transformed (Clough and Bent, 1998) and homozygous alleles selected using the selectable marker hygromycin (25 µg/ml, Duchefa). Homozygous T3 plants from independent transformants were used in subsequent studies. T-DNA lines were complemented by restoring *AtDjC17* under the control of the native promoter. The native promoter was PCR amplified and cloned within *KpnI* and *HindIII* sites of the pMDC32 vector replacing the 2X35S promoter. The full length *AtDjC17* cDNA was cloned within the *AscI* and *PacI* sites completing the fusion cassette. For complementation, T-DNA lines were floral dipped and selected for hygromycin resistance. T2/T3 generations were used for phenotypical characterization.

Gene expression studies

Sterilized *Atdjc17* and WT seed were germinated and grown vertically on ½ strength MS agar plates in 16:8 light:dark conditions for 7-d. Root was rapidly excised from batches of approximately 200 seedlings using a surgical blade in aseptic conditions and snap frozen in liquid nitrogen. Total RNA was extracted using QIAGEN RNeasy Plant mini kit and treated with DNase I (Fermentas, LifeSciences) according to the manufacturer's instructions. Up to 2 µg of the extracted total RNA was used for single stranded cDNA synthesis using High capacity cDNA reverse transcription kit (Applied Biosystems). The final volume was diluted 4-fold and 2 µl of the synthesized cDNA (100 ng) was used in the subsequent RT-PCR reactions. Quantitative real time PCR was conducted using Fast SYBR® Green Mastermix (Applied Biosystems) or HOTFIREPOL® EvAGreen® mastermix (OAK Biotechnologies LLC, USA) with StepOne™ Real-Time PCR system (Applied Biosystems). For the RT-PCR reaction the following conditions were used: 1 cycle of initial denaturation at 95°C for 10 or 15 minutes accordingly to the master mix employed, followed by 40 cycles of denaturation at 95°C for 15 seconds and annealing/extension at 60°C for 30 seconds; followed by melting curve analysis. Actin 2 was used as internal control (**Table A.1**), with 3-pooled biological replicates and 3 technical replicates. Primers for RT-PCR where possible were taken from referenced sources or designed using PRIMER3 (http://www.embnet.sk/cgi-bin/primer3_www.cgi)(**Table A.1**).

Table A.1: List of primers employed for genotyping, cloning and for Real Time-PCR

Name	Function	Sequence	Ref.
Genotyping			
<i>Atdjc17-1-1-LP</i>		5'-TATTGATTCCGTCCGCAATAC-3'	
<i>Atdjc17-1-1-RP</i>		5'-AATGATGGCCATATCATGACC-3'	
<i>Atdjc17-1-2-LP</i>		5'-GAGTCTATCGCAATCGACGAG-3'	
<i>Atdjc17-1-2-RP</i>		5'-TTACTGGAGTCCATCAAACGC-3'	
<i>LBb1-3</i>		5'-ATTTTGCCGATTTCCGGAAC-3'	
Promoter and Gene Cloning			
<i>ProAtdjc17-F</i>		5'-GGTAGTGGTGATGAGATAGTAG-3'	
<i>ProAtdjc17-R</i>		5'-ATTTTCCCCTTCTCTGTTTTGGAA-3'	
<i>Atdjc17-F</i>		5'- AGCTGTTCAACACAAGCTAGAAGA-3'	
<i>Atdjc17-R</i>		5'- AATGTTCTTTGTTACATTTGCAGGT-3'	
RT-PCR			
<i>SCM-F</i>		5'-ACATCGATGCGTTGACAAGA-3'	
<i>SCM-R</i>		5'-TATCGGCGGTCTAAATCCTG-3'	
<i>SCR-F</i>		5'-CAGTTGATGGAGCCAAATCC-3'	
<i>SCR-R</i>		5'-AACTGCCTCTCCTTTCCACA-3'	
<i>WER-F</i>		5'-TGTCAAAGCTCATGGCAAAG-3'	
<i>WER-R</i>		5'-ATCCTCTTCTTGCTCGGTGA-3'	
<i>CPC-F</i>		5'-TTGGCGACAGGTGGGAGTTGAT-3'	
<i>CPC-R</i>		5'-AACGACGCCGTGTTTCATAAG-3'	
<i>GL3-F</i>		5'- ACATTGGTGAAGGAATGCCTGGAC-3'	1
<i>GL3-R</i>		5'- TTACTATCCGCGTATGAGCGTTG-3'	1

Table A.1 Continued

EGL3-F	5'-TGAAACCGCCGATAGCAAAG-3'	1
EGL3-R	5'-CTCCAAGAAACGGGAAGCAA-3'	1
TTG1-F	5'-GCGATTTCTCCGTCTTTGG-3'	1
TTG1-R	5'-CGCTCGTTTTGCTGTTGTTG-3'	1
TTG2-F	5'-CCCCACAACCTTTCTAAGCAAACA-3'	1
TTG2-R	5'-TGCTTAGGAAGTTGTGAGTGAAG-3'	1
GL2-F	5'- ATGAAGCTCGTCGGCATGAGTGGG-3'	1
GL2-R	5'- TGGATTGCCACTGAGTTGCCTCTG-3'	1
SRT-F	5'-GGTGTGGTTCGATGGTACA-3'	
SRT-R	5'-CTCAAAGCCCATCATCAACC-3'	
MGP-F	5'-GGTTCTTTGCTTCGTTTGGA-3'	
MGP-R	5'-CCGCATTCCCAATATCAACT-3'	
JKD-F	5'-TTGCTCCATTGGGTTGATTA-3'	
JKD-R	5'-CAACCTTTGTCCCCACATTC-3'	
ACT2-F	5'-GGCTTAAAAGCTGGGGTTT-3'	
ACT2-R	5'-TTGTCACACACAAGTGCATCA-3'	

1-Ishida T, Hattori S, Sano R, Inoue K, Shirano Y, Hayashi H, Shibata D, Sato S, Kato T, Tabata S, Okada K, Wada T (2007) Arabidopsis *TRANSPARENT TESTA GLABRA2* Is Directly Regulated by R2R3 MYB

Transcription Factors and Is Involved in Regulation of *GLABRA2* Transcription in Epidermal Differentiation. *The Plant Cell Online* **19**: 2531-2543

Appendix B: Analyzing cellulose biosynthesis with confocal microscopy*

***Published as a book chapter in:** The Plant Cell Wall: Methods and Protocols

Authors: Meera Nair and Seth DeBolt

Methods in Molecular Biology Series (Series Editor: John Walker)

Edition Editor: Zoë Popper

B.1 Introduction

Once a challenging technique with limited accessibility, confocal microscopy has rapidly evolved into a robust technique providing proteome level localization data with quantitative precision (Chalfie et al., 1994; Culter et al., 2000; Heazlewood et al., 2007; Moore and Murphy, 2009; Tian et al., 2004). The capacity to visualise your target protein relies on a fused autofluorescent protein (AFP), which excites when laser activated. Classic examples are green fluorescent protein (GFP) derived from the jellyfish *Aequorea victoriae* being fused to your plant protein of interest. Since the discovery of GFP 16 years ago (Chalfie et al., 1994), numerous forms of AFP have been derived including blue fluorescent protein (BFP), cyan fluorescent protein (CFP), yellow fluorescent protein (YFP) and the mFruits collection (Shaner et al., 2004; Shaner et al., 2005; Zhang et al., 2002). Monomeric version of photoswitchable or DRONPA (Habuchi et al., 2005) and photoactivatable GFP exist (Patterson and Lippincott-Schwartz, 2004). Designing an AFP expression fusion can therefore be a daunting task as there are many considerations including; which AFP, expression vectors, the choice of where to fuse your AFP, what promoter to use, and whether to use stable or transient expression of your chimeric protein fusion. Furthermore, Fluorescence Recovery After Photobleaching (FRAP; Bates et al., 2006), Fluorescence Resonance Energy Transfer (FRET; Hink et al., 2002) and bimolecular fluorescence complementation (BiFC; Bhat et al., 2006) could be considered during experimental design depending on your application. This chapter aims to provide researchers with a generalised introduction to the materials and methods needed for performing a live cell imaging analysis of proteins in the plant cell wall.

Live cell imaging has been developed to explore the location of proteins that are fused to AFPs in living tissue by fluorescence microscopy. These tools have been developed alongside sophisticated advances in microscopy, specifically laser assisted confocal microscopy that relies on precise spectral wavelengths produced by different lasers. The morphology and motility of the protein-AFP fusion can then be used to place a protein in a particular part of the cell with the main limitation being the resolution of the focal plane of the confocal microscope. Cell wall biosynthetic proteins have been localised to the plasma membrane, cell wall, the secretory system and the endomembrane system. The central focus of this chapter is on the progression for cloning the gene, sequence checking the gene, the myriad of factors involved in selecting a vector for C or N terminal AFP

fusion, selection of a promoter to drive the fusion protein and the binary vector system to introduce the AFP tagged gene into your plant either transiently or stably. Where possible, the numerous pitfalls that must be negotiated during protein localization experiments are highlighted. Once introduced into the transgenic plant, the AFP-fusion protein can be imaged and a brief overview of imaging systems and approaches to quantification has been provided.

Vector selection

Promoter

The choice of promoter used to drive the target gene fused to an AFP in the transgenic plant must be made. The two main choices are the use of a native promoter (defined as 1–2 kb of upstream sequence from the target genes start codon), versus a *Cauliflower mosaic virus* (CaMV) 35S or double 35S constitutive promoter. If one is interested in studying a single protein and there is a requirement for the AFP fusion to function as closely as possible to the native protein with respect to localization, tissue-specificity, timing and level of expression, then it may be necessary to express the fusion in transgenic plants under control of the native promoter. Moreover, if ones protein of interest can be knocked out in a model organism, for instance in the model plant *Arabidopsis*, one can functionally complement the knockout allele with the AFP-fusion protein as a means to check that mutant phenotypes are restored to that of wild-type plants. This experiment infers functionality of the chimeric protein. At the other extreme, if there is a need to localise thousands of fusions in a relatively short period of time, then transient expression may be the most cost effective as would a high throughput approach with a constitutive promoter such as 35S using a Gateway® cloning (Invitrogen, Carlsbad, CA) system, using vectors such as pSITE (Goodin et al., 2007) or pMDC (Curtis and Grossniklaus, 2003).

Some consider that expression under the control of native promoters will be always superior to that of employing constitutive promoters. However, simply using the native promoter, or more often 1–2 kb of “upstream” sequence, ignores the fact that promoter/gene duplication may affect expression levels, as will genomic context since the AFP fusion is unlikely to be expressed from the same genetic locus as the native gene (Bhat et al., 2006). It also appears to be a common belief that expression from 35S, or even double 35S, promoters necessarily results in accumulation of fusions proteins of the levels higher than native proteins. However, all such results are highly dependent upon the protein under investigation. Fusion of an AFP to a protein may stabilise it. In systems such as *Arabidopsis*, where it is straightforward to obtain T-DNA insertion alleles for your gene of interest (Alonso et al., 2003), single gene complementation by your AFP-fusion protein provides some confidence of correct functionality of your fusion protein *in planta*.

Where to fuse your AFP: Amino (N), Carboxy (C) or internal

Where to fuse your AFP? Should one use an amino (N) or a carboxy (C) terminal fusion? While N or C terminal fusions are the most common, and easiest to construct, some proteins may not tolerate AFPs fused to a terminal end and it may be necessary to insert the AFP into an internal site. Moreover, if your target protein contains an N-terminal signal peptide it may result in mislocalisation if expressed as fusions to the C-termini of AFPs (Simpson et al., 2001). To overcome this, computational methods have been developed to predict the effect of an AFP on a particular fusion (Simpson et al., 2001). Most binary expression vector systems, sometimes referred to as destination vectors, have been developed to suite N- or C-terminal fusions (Chakrabarty et al., 2007; Earley et al., 2006; Tzfira et al., 2005). To head off any potential problems when testing an AFP fusion, both C and N terminal fusions can be made for preliminary studies using a transient expression system prior to stable transformation or detailed quantitative imaging analysis. When considering the vector system you aim to use a question is, whether the researcher will use a Gateway® cloning (Invitrogen, Carlsbad, CA) or non-gateway restriction enzyme based cloning such as pCAMBIA vectors (CAMBIA Corporation, Canberra, Australia)? Gateway® cloning technology can be particularly useful for both high throughput studies, as described above, and single protein studies due to its robust and accurate cloning and most of the current vector systems employ this technology. Both of these vector systems have C and N terminal AFP variants or versions with no AFP to allow the user to insert their AFP internally. For Gateway® cloning the pMDC and pSITE vector systems are good example and for restriction enzyme based the use of pCAMBIA is ideal for plant based expression.

Choice of AFP

The demonstration that the GFP (Chalfie et al., 1994) isolated from the jellyfish *Aequora victoriae*, could be linked to proteins of interest in order to allow *in vivo* examination of protein localization and dynamics in real-time has transformed cell biology in a manner similar to the effect of the polymerase chain reaction on molecular biology. Numerous AFP spectral variants are available in colours such as red fluorescent protein (RFP) (Matz et al., 1999), YFP (Zhang et al., 2002) and now banana, orange, cherry, tomato and plum in the mFruits collection (Shaner et al., 2004). Recently, a novel monomeric red fluorescent protein, TagRFP, has been described (Merzlyak et al., 2007). This protein is brighter and more resistant to photobleaching than mRFP and can be used in combination with GFP in FRET experiments. To this end, despite GFP being a popular AFP tag for creating fusion proteins, currently the most common FRET pair is CFP/YFP. For the case study described herein, YFP was chosen to fuse to cellulose synthase (CESA) because this allowed for cyan fluorescent protein (CFP) to be fused to TUBULIN. Spectral properties of YFP and CFP allow their excitation and thus visualization in different channels allowing the simultaneous view of two fluorophors in a single plant cell (Paredes et al., 2006).

Transformation of your AFP fusion into a plant

There is one main question for the choice of transformation for a live cell imaging experiment: are you going to use a stable transformation or a transient one? This decision is not a trivial one. In high throughput circumstances, creating stable transformations is time consuming and can be restrictive depending on laboratory resources. Therefore for proteome-scale projects transient assays are often preferred. Transient assay systems utilise agroinfiltration of your AFP fusion into *Nicotiana benthamiana* leaves. This simple technique employs injecting an *Agrobacterium* (expressing your AFP fusion) solution directly into the underside of a leaf blade, inoculating for 2–3 days and then imaging the living leaf tissue. Alternatively, stable transformation in *Arabidopsis thaliana* utilises *Agrobacterium* mediated floral dipping methods (Clough and Bent, 1998) to introduce your AFP fusion into the genome as a T-DNA insertion. The advantage of stable transformation is the capacity to localise your target protein in numerous tissues and developmental stages. The presence of the AFP fusion protein in the plant can then be checked by western blot using antibodies against your chosen AFP (readily available from common suppliers such as Sigma-Aldrich, St Louis MO).

B.2 Materials

Polymerase chain reaction (PCR) to amplify gene of interest with promoter and subcloning into an entry vector

1. Proof reading enzyme for amplification, Platinum®PfxDNA Polymerase, stored at -20°C (Invitrogen, Carlsbad, CA).
2. 5' and 3' primers specific for promoter and gene for CESA. 100 mM stock is diluted to 10 mM sub stock to be used as a working solution. These are stored at -20°C. (See **Note 1**).
3. 10X Pfx Buffer 25 mM MgSO₄, 100 mM dNTPs (Invitrogen Carlsbad, CA), stored at -20°C (See **Note 2**).
4. Template as genomic DNA (gDNA) (500 ng/μL⁻¹), stored at -20°C (See **Note 3**).
5. pENTR® dTOPO® vector system ([Invitrogen](#), Carlsbad, CA), stored at -20°C.

Cloning of your gene of interest into a compatible destination vector to make AFP fusions and introducing this into the plant by *Agrobacterium* mediated transformation

1. pSITE2NA destination vector (See **Note 4**), stored at -20°C.
2. Gateway® cloning kits (Invitrogen, Carlsbad, CA) stored at -20°C.
3. *Agrobacterium* competent cells, stored at -80°C (Invitrogen, Carlsbad, CA).

SDS-Polyacrylamide gel electrophoresis (SDS-PAGE)

1. Running buffer (5X): 125 mM Tris, 960 mM glycine, 0.5% (w/v) SDS. Store at room temperature.

2. 2X SDS sample loading buffer: 100 mM Tris-Cl pH 6.8, 4% v/v SDS, 0.2% bromophenol blue, 20% w/v glycerol, stored at room temperature.
3. Pre-stained molecular weight markers: Kaleidoscope markers (Bio-Rad, Hercules, CA).
4. 0.5 M Tris-Cl buffer pH 8.
5. 100 mM Phenylmethanesulfonyl fluoride (PMSF; Sigma Aldrich, St. Louis)) in isopropanol, stored at -20°C.

Western Blotting for YFP

1. Setup buffer: 25 mM Tris (do not adjust pH), 190 mM glycine, 20% (v/v) methanol, stored at room temperature.
2. Transfer buffer: Setup buffer with the added inclusion of 0.05% (w/v) SDS. Store in the transfer apparatus at room temperature (See **Note 5**).
3. Supported nitrocellulose membrane from Millipore, Bedford, MA, and 3MM Chromatography paper from Whatman, Maidstone, UK (See **Note 6**).
4. Tris-buffered saline with Tween (TBS-T): Prepare 10X stock solution containing 1.37 M NaCl; 27 mM KCl; 250 mM Tris-HCl, pH 7.4; 1% Tween-20.
5. Tris-buffered saline with Tween (TBS-T): Prepare 1X stock for use by diluting 100 mL of 10X stock in 900 mL water.
6. Blocking buffer: 5% (w/v) non-fat dry milk in TBS-T.
7. Primary antibody dilution buffer: TBS-T supplemented with 2% (w/v) fraction bovine serum albumen (BSA).
8. Anti-YFP monoclonal antibody (available from Sigma Aldrich, St Louis) stored at -20°C (See **Note 7**).
9. Secondary antibody: Anti-mouse IgG conjugated to horse radish peroxidase (available from Sigma Aldrich, St Louis) stored at -20°C (See **Note 7**).
10. Chemiluminescence detection kit (SuperSignal West Pico Chemiluminescent Substrate (Pierce Biotechnology, Rockford, IL) stored at 4°C.
11. Detection using Bio-Rad ChemiDoc XRS+® (BioRad, Hercules, CA).

Imaging analysis

1. Cover slips 48 × 60, 24 × 60 (Menzel, Braunschweig Germany).
2. Fine point tweezers #5 Dumont (Electron Microscopy Sciences, Hatfield, PA).
3. Dow Corning High Vacuum Grease (Specialty Fluids Co, Valencia, CA).
4. Sterile water.

B.3 Methods

Herein we describe a Gateway® cloning for tagging CESA to YFP and the use of confocal microscopy to visualise it in plants. Gateway-compatible binary vectors have greatly improved the cloning efficiency of AFP tagging projects (Curtis and Grossniklaus, 2003; Earley et al., 2006). Briefly, Gateway® cloning uses the lambda phage site-specific recombination system in order to transfer

DNA fragments between plasmids containing compatible recombination sites (Walhout et al., 2000). What makes this strategy so attractive is that once DNA clones of interest are captured into an entry vector (pENTR/pDONR), they can be mobilised into a plethora of destination vectors that permit expression in bacteria, insects, yeasts, or plants but also allow for introducing the target gene into an AFP vector with RFP, YFP, CFP or GFP fluorophors.

Numerous factors influence imaging for instance the cell type being imaged, whether your experiments is simply to determine the location of your target protein or whether you wish to track the dynamic behaviour of the your target protein by time lapse imaging. The best results have been obtained by localizing protein dynamics in upper regions of the hypocotyls of etiolated seedlings grown in a vertical position on Murashige-Skoog (MS) agar plates for 2.5– 4 days at room temperature (22°C), mounted between cover slips in water and then imaged (Gutierrez et al., 2009; Paredez et al., 2006).

Polymerase chain reaction (PCR) to amplify gene of interest and subcloning into an entry vector

1. Independent amplification of the CESA and promoter or your gene of interest achieved using a PCR reaction composed of 1.5 pmol of each primer, 0.3 mM dNTPs, 1X *Pfx* Buffer, 1mM MgSO₄ (See **Note 8**) and 1.25 units Platinum®*Pfx*DNA Polymerase (Invitrogen, Carlsbad, CA), 1 µL of gDNA, made to 20 µL with deionised H₂O (dH₂O). The following thermocycler reaction times and temperature can be used, a 3-min heating at 95°C was followed by 32 cycles of 95°C (30 s) denaturation, 55°C (30 s) annealing temp (See **Note 9**), 1 min per kilobase product size extension times, and a final extension of 7 min.
2. Gateway® cloning of the PCR product into an entry vector is then achieved based on manufacturer's instructions (Invitrogen, Carlsbad, CA).

Cloning of your gene of interest with promoter into a compatible destination vector to make AFP fusions and introducing this into the plant by *Agrobacterium* mediated transformation

1. The CESA gene in entry vector can then be cloned in to a destination vector such as pSITE2N using the manufacturer's manual for Gateway® cloning (Invitrogen, Carlsbad, CA). The double CAMV 35S promoter can be excised using compatible restriction enzymes and the amplified promoter region ligated into the vector by directional cloning. This creates an additional step in the cloning and will depend on whether you wish to examine localization of your target gene with a constitutive or native promoter.
2. At this stage a sequence verified version of your target gene (See **Note 10**), for instance pSITE2NproCESA::CESA (See **Note 11**), can then be transformed into electro or chemically competent *Agrobacterium tumefaciens* cells according to manufacturer's manual (Invitrogen, Carlsbad, CA).

3. Introducing the transgene into the plant should follow published protocols (Clough and Bent, 1998). (See **Note 12**).
4. Selection of stable transformants in *A. thaliana* will be achieved by growing the T1 progeny on sterile 0.5 strength MS media supplemented with 50 $\mu\text{g}/\text{mL}^{-1}$ Kanamycin (Kan⁵⁰). Plants able to grow on the Kan⁵⁰ media are then transferred to soil and grown.

SDS Page and Western Blotting for detection of YFP in Plant Tissue

For simplicity this method assumes the use of Criterion cell and precast gels from BioRad® (Hercules, CA) as well as the BioRad Trans-Blot® Electrophoretic Transfer Cell®.

1. Total protein from individual transformants is extracted by simply grinding 2–3 leaves using liquid nitrogen in mortar and pestle and 300 μL 0.5 M Tris-Cl buffer with 0.1 mM final concentration PMSF. 1 volume 2X SDS loading buffer is added to 1 volume of total protein and boiled for 5 minutes. It is then carefully loaded into the well of the precast gel along with molecular weight markers and the gel is run for 1 h at 80 mA in the Criterion cell system (BioRad® Hercules, CA).
2. After protein separation by SDS-PAGE the samples are transferred to a nitrocellulose membrane according to the manufacturer's instructions (assuming the use of a BioRad Trans-Blot® Electrophoretic Transfer Cell®) (See **Note 6**).
3. The coloured molecular weight markers should be clearly visible on the membrane. Nitrocellulose membrane is carefully transferred in a solution of blocking buffer for 1 h at room temperature on a shaker.
4. The nitrocellulose membrane is rinsed and then immersed in a solution of 1:10,000 dilution of anti-YFP antibody in TBST/2% BSA for 1 h on a rocking platform (See **Note 13**).
5. Washed three times for 5 min each with 50 mL TBS-T and then immerse in 1:30,000-fold dilution of the secondary antibody as above. Wash again 3 times for 10 min each with TBS-T. Then incubate in equal volumes of Pico-West (total of 4 mL) (Pierce Biotechnology, Rockford, IL) solution for 1 min, seal in a plastic sleeve and examine chemiluminescent signal in the BioRad® GelDoc. Select transgenic plants that show the presence of YFP for confocal imaging (See **Note 14**).

Preparation of plants for imaging

1. Once stable transformants expressing YFP::CESA fusion are identified and transferred to soil, the plants are grown to obtain seeds from them.
2. The seeds once ready are harvested in a newspaper piece and dried in a dry corner of the lab for 3 to 4 days. They are then sterilised using 30% bleach and 5% SDS for surface sterilisation. The seeds are washed thoroughly to remove sterilization solution using sterile water. It is then resuspended in

- 0.15% Agar and stored in dark at 4°C for vernalisation for 3 days (See **Note 15**).
3. *A. thaliana* seedlings are grown in dark for 2.5 days on 0.5 strength MS-agar plates at 22°C.

Imaging Analysis

1. Single seedlings are gently removed from 0.5 strength MS-agar plates and mounted in an aqueous solution between a 48 × 60 and a 24 × 60 cover slip.
2. The silicon vacuum grease is carefully applied to the perimeter of the 24 × 60 cover slips to avoid any water loss or evaporation over the duration of imaging and essentially avoids compression of the epidermal cells of the tissue being imaged (See **Note 16**).
3. For imaging YFP::CESA, a purpose built spinning disk confocal microscope using Leica X 63 N.A. = 1.4 oil immersion objective and Roper Cascade 512b EMCCD camera can be used (See **Note 17**).
4. The confocal plane is focused then on the plasma membrane focal plane with an exposure of 600 ms for YFP::CESA (**Figure D.1**). A method to improve the signal to background noise ratio is to average multiple frames using the frame averaging feature in the imaging software being used.
5. YFP is excited at 488 nm and data is collected through a 525.50 nm band pass filter (Chroma Technologies, Brattleboro, VT) (Paredes et al., 2006). The image can be acquired using image acquisition software and analyzed (See **Note 18**).
4. To obtain multiple frames of a single cell to provide a time-lapse series (i.e. a movie), seek the time-lapse feature in the image acquisition software being used (See **Note 18**) (select the number of frames to be acquired and the amount of time between each frame) (See **Note 19**).

B.4 Notes

1. When the primers arrive dilute them to 100 mM concentration using TE (10 nM Tris-Cl, 1 mM EDTA) buffer and make a 10 mM working solution for yourself.
2. Each of the dNTPs is available as a 100 mM stock which can be combined as a 10 mM sub stock for your use.
3. Here the cloning strategy calls for the amplification of cellulose synthesizing enzyme or CESA with the promoter thus genomic DNA needs to be used to include introns as well as exons and regulatory regions. Genomic DNA preparation can be done using the established protocols (Lukowitz et al., 2000).
4. pMDC and pSITE vectors can be requested from the authors (Curtis and Grossniklaus, 2003; Goodin et al., 2004).
5. The transfer buffer should be cooled below room temperature before you begin to do the transfer. This can be done by cooling the buffer at 4°C prior to doing western blots.

6. Nitrocellulose membranes should not be touched and should not be handled without using gloves. It would be best to use tweezers to handle the membrane at all times.
7. Primary and secondary antibodies should be aliquoted into 200 μ L aliquots and stored at -20°C . When required a vial should be retrieved and used and the remaining can then be stored at 4°C for multiple uses. This way the main stock will not be contaminated if there is a chance of doing so.
8. MgSO_4 levels can be optimised for your specific PCR reaction through a little research.
9. The annealing temperatures have to be optimised for a specific pair of primers; usually a thumb rule of 1 degree less than the melting temperature for the primers is used.
10. It is usually better to sequence your target gene for missense mutations at the DNA level that confer changes in the amino acid sequence of the target protein (Sequencing reactions such as BigDye® (Applied Biosystems, Carlsbad, CA) and nested primer design for sequencing are not covered in this chapter.
11. Amplification for C-terminal fusions (for purpose of this chapter, this refers to the AFP fusion being fused to the C-terminal end of the target gene) remove the stop codon from the target gene in the 3' primer. For N-terminal fusions, the AFP is referred to as being fused to the N-terminus of the target gene.
12. You can also do *Agrobacterium* infiltration into *Nicotiana benthamiana* (Goodin et al., 2007) for transient expression.
13. An overnight addition of primary antibody can be done in 4°C cooler with a rocking bottom or shaker.
14. If no signal is obtained for YFP in transgenic plants in stable transformants (*A. thaliana*) check for YFP in all plant samples by PCR in gDNA; if positive select additional lines for protein analysis by western blotting in the next generation or if negative retransform and proceed from there.
15. Seed sterilization should be done under the hood to minimise the chance of contamination. It is always worthwhile to use only less than half of your seed stock so that if a mistake is made in subsequent steps, there are always some transformant seeds available to begin again.
16. For transient expression, a similar strategy is employed whereby a portion of the infiltrated *N. benthamiana* is physically removed from the leaf and mounted as described above.
17. Numerous confocal microscope systems are available and are equally attractive for live cell imaging experiments. The leading companies and examples of their confocal systems as of January 2010 are Leica (Leica SP5 AOBS Point Scanning Spectral Confocal Microscope), Olympus (Olympus Fluo View FV1000MPE, a multiphoton laser scanning microscope), Yokogawa (Yokogawa CSU-10 spinning disk confocal microscope) Zeiss 780NLO Laser-Scanning Confocal Microscope.
18. Softwares for imaging analysis: Metamorph - Molecular Devices (Sunnyvale, CA), which can be used for microscope automation and image acquisition. LAS Image Analysis optional software module developed by Leica

Microsystems (Bannockburn, IL) provides sequence control assisting acquiring, detecting, and measuring multiple image features. In addition to Leica, all major companies have similar systems (see local representative). ImageJ is a Freeware software program that has numerous features developed by a worldwide community of cell biologists to streamline quantitative analysis of confocal imaging results. In addition to the numerous image analysis tools built into ImageJ, there are Plugins for tracking position over time by Kymograph, reslicing of stacks, 3D reconstruction, time-stamping, conversion of BioRad stacks to Quicktime format as well as most format conversion, 3D rendering and quantitation (ImageJ, National Institute of Health, Bethesda, MD).

19. The main pitfall for time-lapse image collection is drift (x, y or z drift). X and Y plane drift can be overcome fairly easily by allowing the drift to occur and then use the Stackreg algorithm ImageJ plugin (<http://rsbweb.nih.gov/ij/plugins>) after acquisition to correct for the drift (**Figure B.1A** compared to **Figure B.1B**). Z drift on the other hand cannot be corrected for and therefore requires manual adjustment during acquisition (**Figure B.1C**).

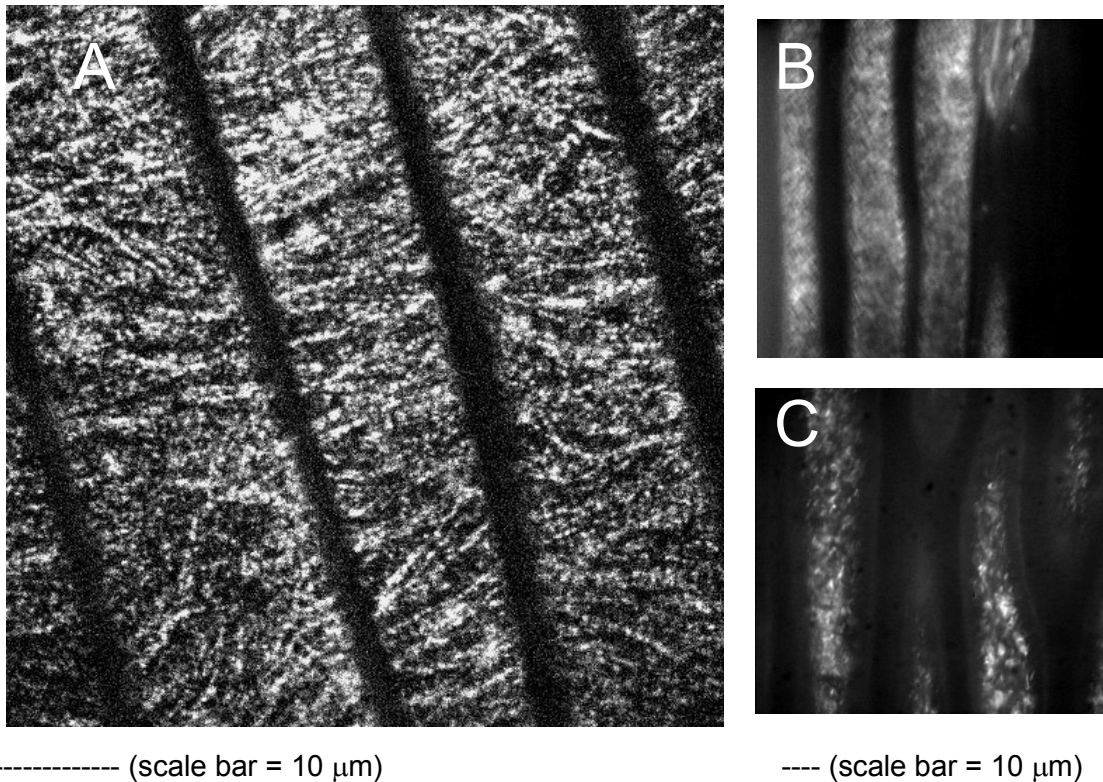


Figure B.1 Live cell imaging of cellulose synthase. A) Plasma membrane focal plane B) X and Y drift during time lapse image acquisition can reduce image quality and make it difficult to track protein dynamics C) Z drift during time lapse image acquisition can reduce image quality and distort protein dynamics analyses

Appendix C: UGT80B1 is enriched in detergent resistant membrane fraction.

C.1 Introduction

Whole genome microarray data and 2-dimension gel electrophoresis membrane proteomics in the *ugt80B1* null background was compared with that of wild-type plants containing active UGT80B1 (**Table 2.1, 2.2 and 5.2**). These data demonstrated a metabolic fingerprint indicative of association with lipid rafts, such as previously documented signaling and hormone regulation, lipid membrane processes and trafficking (Borner *et al.* 2005; Grennan, 2007; Lefebvre *et al.* 2007; Mongrand *et al.* 2004; Simons and Toomre, 2000) This network of genes contained numerous known components of mammalian lipid rafts (Brown and London, 1998) and termed detergent resistant membranes (DRM) in plants (Bhat and Pastrunga, 2005; Grennan, 2007), a term derived due to their biochemical fractionation using detergent treatment under cold conditions; and confirmed our suspicion that altering glycosylation was capable of altering the membrane sterol balance and DRM processes. These data were also supported to several recent studies of DRM composition in Arabidopsis, Tobacco and Leek membranes, that all found SGs were enriched in DRM fractions (Laloi *et al.* 2007; Lefebvre *et al.* 2007; Mongrand *et al.* 2004). Given that lipid rafts, or DRM's are formed through the cooperative interaction of proteins, sterols and sphingolipids (Lingwood and Simons, 2010) there is a conservative rationale that SGs are further diversifications of these membrane elements. This encouraged us to pursue a biochemical analysis of UGT80B1 to determine whether its localization was enriched in DRMs.

C.2 Results

Utilizing transgenic Arabidopsis plants expressing *Pro35S:UGT80B1:GFP* total membrane was extracted and biochemically fractionated using a 2-phase PEG-Dextran. This allowed for separation of plasma membrane from endomembrane and thylakoid membrane (**Figure C.1**). The purified plasma membrane was then loaded on to a sucrose gradient after treatment with 2% TRITON-X at 4°C and each fraction collected and run on a SDS-PAGE gel to allow proteins to separate based on size. Proteins were transferred to a nitrocellulose membrane and probed against an Anti-GFP monoclonal antibody revealing that the location of the UGT80B1::GFP fusion protein was in the DRM fraction. Fluorescence microscopy confirmed punctuate globules expressing UGT80B1:GFP (**Figure C.1**). Hence, both SG and the biosynthetic enzyme UGT80B1 are enriched in DRM fractions of the plasma membrane.

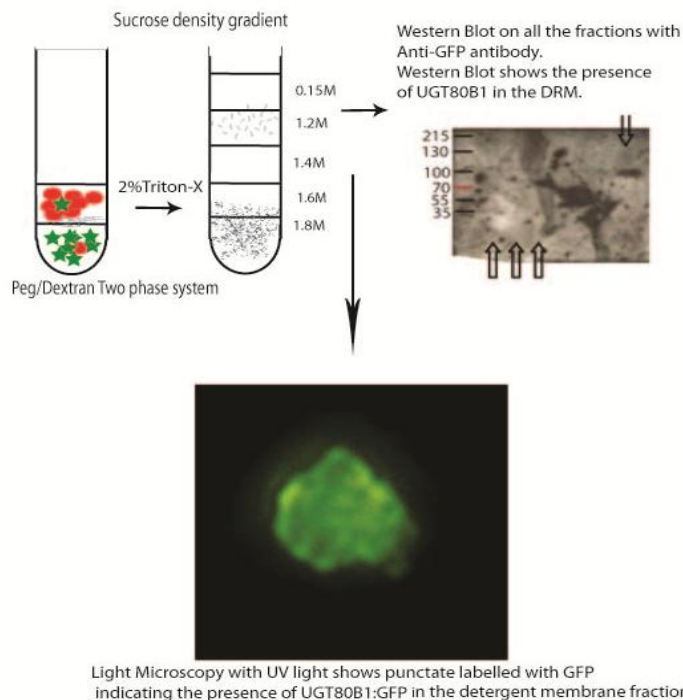


Figure C.1 Method used to detect UGT80B1:GFP in DRM fraction. Following the arrows from left to right, illustration shows the 2-phase PEG/Dextran with red circles representing PM fraction and green stars representing thylakoid membranes and other endomembranes. PM fraction was collected and treated with 2% Triton-X and loaded on a sucrose density gradient. After ultracentrifugation all fractions were collected and tested using western blot using Anti-GFP antibody. Visible band is seen corresponding to UGT80B1:GFP in documented DRM fraction from sucrose gradient. Fluorescence microscopy confirms the presence of UGT80B1:GFP labelled punctate in DRM fraction.

C.3 Method for extraction of lipid raft

50 mg *35S:UGT80B1:GFP* seeds were started on half strength MS liquid culture and seedlings harvested after 13 days. Total membrane extraction was done according to Borner et al., (2005) and Lefebvre et al., (2007) with slight variations. The seedlings are homogenized using liquid nitrogen and further homogenized using 2ml extraction buffer containing 100mM Hepes-KOH, 10% (w/v) glycerol, 5 mM EDTA, 0.6% (w/v) PVP K-25, 5 mM ascorbic acid and 200 μ l protease inhibitor cocktail (Sigma Aldrich, P9599). The extract was filtered through Mira Cloth to remove cell debris and further centrifuged for 5 minutes at 5000g at 4°C (Beckman Coulter centrifuge with JA 20 rotor). The supernatant collected was then centrifuged at 100,000g for 50 minutes, 4°C (Beckman Coulter centrifuge with JA 30.50 rotor). The supernatant was discarded and the microsomal pellet was dissolved in minimum volume (200-500 μ l) of buffer containing 5mM potassium phosphate pH 7.8, 5mM KCL, 0.1 mM EDTA and protease inhibitor cocktail (Sigma Aldrich, P9599). Plasma membranes were

separated from the microsomal fraction using a two-phase system with a final weight of 4g containing 6.4% (w/w) Dextran, 6.4% PEG and 5mM KCl in a 10 ml pyrex tube and collecting the upper phase after centrifuging at 7000 rpm for 5 min at 4°C (Beckman Coulter, JA 20 rotor). The upper phase was then diluted in excess or 3 times in buffer containing 50mM Tris-HCL pH 7.5, 3mM EDTA with protease inhibitor cocktail (Sigma Aldrich, P9599) and treated with 2% Triton-X 100 on ice for 30 min. The treated plasma membranes were then combined with cold 2.4M sucrose in TNE to a final concentration of 1.8M sucrose and was overlaid on discontinuous sucrose gradient from 1.6M to 0.15M sucrose and centrifuged at maximum speed (41000 rpm or 288,000g) for 18 hours in a swinging bucket rotor (SW 41 Beckman coulter). Four fraction of the sucrose gradient were collected and subjected to western blotting identify whether the desired protein separates in the predicted lipid raft fraction which is close to 0.15M sucrose fraction, utilizing anti-GFP antibody and chemiluminescence. All the fractions were checked for GFP expression using fluorescence microscopy.

References:

Abraham, W., Wertz, P.W., Burken, R.R., and Downing, D.T. (1987). Glucosylsterol and acylglucosylsterol of snake epidermis: structure determination. *Journal of Lipid Research* 28, 446-449.

Alonso, J.M., Stepanova, A.N., Leisse, T.J., Kim, C.J., Chen, H., Shinn, P., Stevenson, D.K., Zimmerman, J., Barajas, P., Cheuk, R., Gadrinab, C., Heller, C., Jeske, A., Koesema, E., Meyers, C.C., Parker, H., Prednis, L., Ansari, Y., Choy, N., Deen, H., Geralt, M., Hazari, N., Hom, E., Karnes, M., Mulholland, C., Ndubaku, R., Schmidt, I., Guzman, P., Aguilar-Henonin, L., Schmid, M., Weigel, D., Carter, D.E., Marchand, T., Risseuw, E., Brogden, D., Zeko, A., Crosby, W.L., Berry, C.C., and Ecker, J.R. (2003). Genome-Wide Insertional Mutagenesis of *Arabidopsis thaliana*. *Science* 301, 653-657.

Al-Whaibi, M. (2011) Plant heat-shock proteins: A mini review. *J. King Saud Univ.-Sci.* 23, 139-150.

Anantharaman, V. and Aravind, L. (2002) The GOLD domain, a novel protein module involved in Golgi function and secretion. *Genome Biology* 3, research0023.0021 - research0023.0027.

Araujo-Bazán, L., Peñalva, M.A., and Espeso, E.A. (2008). Preferential localization of the endocytic internalization machinery to hyphal tips underlies polarization of the actin cytoskeleton in *Aspergillus nidulans*. *Molecular Microbiology*. 67, 891-905.

Assaad, F., Huet, Y., Mayer, U., Jürgens, G. (2001). The cytokinesis gene *KEULE* encodes a Sec1 protein that binds the syntaxin KNOLLE. *Journal of Cell Biology*. 152, 531-543.

Bakau, B., Horwich, A.L. (1998). The Hsp70 and Hsp60 chaperone machines. *Cell* 92, 351-366.

Baluska, F., Salaj, J., Mathur, J., Braun, M., Jasper, F., Samaj, J., Chua, N.-H., Barlow, P.W., and Volkmann, D. (2000). Root hair formation: F-actin-dependent tip growth is initiated by local assembly of profilin-supported F-actin meshworks accumulated within expansin-enriched bulges. *Developmental Biology*. 227, 618-632.

Baluska, F., Wojtaszek, P., Volkmann, D. and Barlow, P. (2003). The architecture of polarized cell growth: The unique status of elongating plant cells. *BioEssays* 25, 569-576.

Bankaitis, V.A., Malehorn, D.E., Emr, S.D. and Greene, R. (1989) The *Saccharomyces cerevisiae* SEC14 gene encodes a cytosolic factor that is required for transport of secretory proteins from the yeast Golgi complex. *The Journal of Cell Biology* 108, 1271-1281.

Bates, I.R., Wiseman, P.W., and Hanrahan, J.W. (2006). Investigating membrane protein dynamics in living cells. *Biochemistry and Cell Biology* 84, 825-831.

Bergmann, D.C., Lukowitz, W., and Somerville, C.R. (2004). Stomatal Development and Pattern Controlled by a MAPKK Kinase. *Science* 304, 1494-1497.

Beh, C., Alfaro, G., Duamel, G., Sullivan, D., Kersting, M., Dighe, S., Kozminski, K. and Menon, A. (2009). Yeast oxysterol-binding proteins: sterol transporters or regulators of cell polarization? *Mol. Cell. Biochem.* 326, 9-13.

Bekh-Ochir, D., Shimada, S., Yamagami, A., Kanda, S., Ogawa, K., Nakazawa, M., Matsui, M., Sakuta, M., Osada, H., Asami, T., and Nakano, T. (2013). A novel mitochondrial DnaJ/Hsp40 family protein BIL2 promotes plant growth and resistance against environmental stress in brassinosteroid signaling. *Planta* 237, 1509-1525.

Benveniste, P. (2004). Biosynthesis and accumulation of sterols. *Annual Review of Plant Biology* 55, 429-457.

Bernhardt, C., Zhao, M., Gonzalez, A., Lloyd, A., and Schiefelbein, J. (2005). The bHLH genes GL3 and EGL3 participate in an intercellular regulatory circuit that controls cell patterning in the *Arabidopsis* root epidermis. *Development* 132, 291-298.

Bessueille, L., and Bulone, V. (2008). A survey of cellulose biosynthesis in higher plants. *Plant Biotechnology* 25, 315-322.

Bessueille, L., Sindt, N., Guichardant, M., Djerbi, S., Teeri, T.T., and Bulone, V. (2009). Plasma membrane microdomains from hybrid aspen cells are involved in cell wall polysaccharide biosynthesis. *Biochemical Journal* 420, 93-103.

Bhat, R.A., and Panstruga, R. (2005). Lipid rafts in plants. *Planta* 223, 5-19.

Bhat, R., Lahaye, T., and Panstruga, R. (2006). The visible touch: in planta visualization of protein-protein interactions by fluorophore-based methods. *Plant Methods* 2, 12.

Bligh, E.G., and Dyer, W.J. (1959). A rapid method of total lipid extraction and purification. *Canadian Journal of Biochemistry and Physiology* 37, 911-917.

Blumwald, E., Aharon, G.S., and Apse, M.P. (2000). Sodium transport in plant cells. *Biochimica et Biophysica Acta (BBA) - Biomembranes* 1465, 140-151.

Borner, G.H.H., Sherrier, D.J., Weimar, T., Michaelson, L.V., Hawkins, N.D., MacAskill, A., Napier, J.A., Beale, M.H., Lilley, K.S., and Dupree, P. (2005). Analysis of Detergent-Resistant Membranes in Arabidopsis. Evidence for Plasma Membrane Lipid Rafts. *Plant Physiology* 137, 104-116.

Bouc, P.J.D., Etsebeth, S., Liebenberg, R.W., Albrecht, C.F., Pegel, K., and Van Jaarsveld, P.P. (1996). Beta-sitosterol and beta-sitosterol glucoside stimulate human peripheral blood lymphocyte proliferation: Implications for their use as an immunomodulatory vitamin combination. *International Journal of Immunopharmacology* 18, 693-700.

Bouvier-Navé, P., Husselstein, T., Desprez, T., and Benveniste, P. (1997). Identification of Cdnas Encoding Sterol Methyl-Transferases involved in the Second Methylation Step of Plant Sterol Biosynthesis. *European Journal of Biochemistry* 246, 518-529.

Bouvier-Navé, P., Ullmann, P., Rimmelé, D., and Benveniste, P. (1984). Phospholipid-dependence of plant UDP-glucose-sterol- β -D-glucosyltransferase. I. Detergent-mediated delipidation by selective solubilization. *Plant Science Letters* 36, 19-27.

Bradford MM (1976) A rapid and sensitive method for the quantitation of microgram quantities of protein utilizing the principle of protein-dye binding. *Analytical Biochemistry* 72, 248-254.

Brady, S.M., Orlando, D.A., Lee, J.-Y., Wang, J.Y., Koch, J., Dinneny, J.R., Mace, D., Ohler, U., and Benfey, P.N. (2007). A High-Resolution Root Spatiotemporal Map Reveals Dominant Expression Patterns. *Science* 318, 801-806.

Brown, D.A., and London, E. (1998). Functions of lipid rafts in biological membranes. *Annual Review of Cell and Developmental Biology* 14, 111-136.

Bruex, A., Kainkaryam, R.M., Wieckowski, Y., Kang, Y.H., Bernhardt, C., Xia, Y., Zheng, X., Wang, J.Y., Lee, M.M., Benfey, P., Woolf, P.J., and

Schiefelbein, J. (2012). A Gene Regulatory Network for Root Epidermis Cell Differentiation in Arabidopsis. *PLoS Genet* 8, e1002446.

Burch-Smith, T., Stonebloom, S., Xu, M., and Zambryski, P. (2011). Plasmodesmata during development: re-examination of the importance of primary, secondary, and branched plasmodesmata structure versus function. *Protoplasma* 248, 61-74.

Burch-Smith, T.M., and Zambryski, P.C. (2010). Loss of INCREASED SIZE EXCLUSION LIMIT (ISE)1 or ISE2 Increases the Formation of Secondary Plasmodesmata. *Current Biology* 20, 989-993.

Bush, P.B., and Grunwald, C. (1974). Steryl Glycoside Formation in Seedlings of *Nicotiana tabacum* L. *Plant Physiology* 53, 131-135.

Camacho, L., Smertenko, A.P., Perez-Gomez, J., Hussey, P.J. and Moore, I. (2009) Arabidopsis Rab-E GTPases exhibit a novel interaction with a plasma-membrane phosphatidylinositol-4-phosphate 5-kinase. *Journal of Cell Science* 122, 4383-4392.

Cantrill, L.C., Overall, R.L., and Goodwin, P.B. (1999). CELL-TO-CELL COMMUNICATION VIA PLANT ENDOMEMBRANES. *Cell Biology International* 23, 653-661.

Cao, X.F., Linstead, P., Berger, F., Kieber, J., and Dolan, L. (1999). Differential ethylene sensitivity of epidermal cells is involved in the establishment of cell pattern in the Arabidopsis root. *Physiologia Plantarum* 106, 311-317.

Carland, F., Fujioka, S., and Nelson, T. (2010). The Sterol Methyltransferases SMT1, SMT2, and SMT3 Influence Arabidopsis Development through Nonbrassinosteroid Products. *Plant Physiology* 153, 741-756.

Carland, F.M., Fujioka, S., Takatsuto, S., Yoshida, S., and Nelson, T. (2002). The Identification of CVP1 Reveals a Role for Sterols in Vascular Patterning. *The Plant Cell Online* 14, 2045-2058.

Chakrabarty, R., Banerjee, R., Chung, S.-M., Farman, M., Citovsky, V., Hogenhout, S.A., Tzfira, T., and Goodin, M. (2007). pSITE Vectors for Stable Integration or Transient Expression of Autofluorescent Protein Fusions in Plants: Probing *Nicotiana benthamiana*-Virus Interactions. *Molecular Plant-Microbe Interactions* 20, 740-750.

Chalfie, M., Tu, Y., Euskirchen, G., Ward, W.W., and Prasher, D.C. (1994). Green fluorescent protein as a marker for gene expression. *Science* 263, 802-805.

- Chen, R., Hilson, P., Sedbrook, J., Rosen, E., Caspar, T. and Masson P.** (1998). The Arabidopsis thaliana AGRAVITROPIC 1 gene encodes a component of the polar-auxin-transport efflux carrier. *Proc. Natl. Acad. Sci.* *95*, 15112-15117.
- Chen, S., Songkumarn, P., Liu, J., and Wang, G.L.** (2009). A Versatile Zero Background T-Vector System for Gene Cloning and Functional Genomics. *Plant Physiology* *150*, 1111-1121.
- Chen, S., and Brown, I.R.** (2007). Neuronal expression of constitutive heat shock proteins: implications for neurodegenerative diseases. *Cell Stress & Chaperones* *12*, 51-58.
- Choi, H., Ohyama, K., Kim, Y.-Y., Jin, J.-Y., Lee, S.B., Yamaoka, Y., Muranaka, T., Suh, M.C., Fujioka, S., and Lee, Y.** (2014). The Role of Arabidopsis ABCG9 and ABCG31 ATP Binding Cassette Transporters in Pollen Fitness and the Deposition of Steryl Glycosides on the Pollen Coat. *The Plant Cell Online* *26*, 310-324.
- Chow, A.M., and Brown, I.R.** (2007). Induction of heat shock proteins in differentiated human and rodent neurons by celastrol. *Cell Stress & Chaperones* *12*, 237-244.
- Chu, T., Deng, S., and Wolfinger, R.** (2006). Modeling Affymetrix data at the probe level. In *DNA Microarray and Statistical Genomics Techniques: Design, Analysis, and Interpretation of Experiment*, D. Allen, G. Page, T. Beasley, and J. Edwards, eds. (Boca Raton, FL, Chapman & Hall/CRC), pp. 197–222.
- Clough, S.J., and Bent, A.F.** (1998). Floral dip: a simplified method for Agrobacterium-mediated transformation of Arabidopsis thaliana. *The Plant Journal* *16*, 735-743.
- Clouse, S.D.** (2000) Plant development: A role for sterols in embryogenesis. *Current Biology* *10*, R601-R604.
- Craig, R. and Beavis, R.C.** (2004) TANDEM: matching proteins with tandem mass spectra. *Bioinformatics* *9*, 1466-1467.
- Cruz-Aguado, R., and Shaw, C.A.** (2009). The ALS/PDC syndrome of Guam and the cycad hypothesis. *Neurology* *72*, 474-474.
- Cutler, S.R., Ehrhardt, D.W., Griffitts, J.S., and Somerville, C.R.** (2000). Random GFP::cDNA fusions enable visualization of subcellular structures in cells of Arabidopsis at a high frequency. *Proceedings of the National Academy of Sciences* *97*, 3718-3723.

Curtis, M. and Grossniklaus, U. (2003). A Gateway™ cloning vector set for high-throughput functional analysis of genes in plants. *Plant Physiol.* 133,462-469.

d'Azzo, A., Bongiovanni, A., and Nastasi, T. (2005). E3 Ubiquitin Ligases as Regulators of Membrane Protein Trafficking and Degradation. *Traffic* 6, 429-441.

Debeaujon, I., Peeters, A.J.M., Léon-Kloosterziel, K.M., and Koornneef, M. (2001). The *TRANSPARENT TESTA12* Gene of Arabidopsis Encodes a Multidrug Secondary Transporter-like Protein Required for Flavonoid Sequestration in Vacuoles of the Seed Coat Endothelium. *The Plant Cell Online* 13, 853-871.

DeBolt, S., Gutierrez, R., Ehrhardt, D.W. and Somerville, C. (2007). Nonmotile cellulose synthase subunits repeatedly accumulate within localized regions at the plasma membrane in Arabidopsis hypocotyl cells following 2,6-dichlorobenzonitrile treatment. *Plant Physiol* 145, 334–338.

DeBolt, S., Scheible, W.-R., Schrick, K., Auer, M., Beisson, F., Bischoff, V., Bouvier-Navé, P., Carroll, A., Hematy, K., Li, Y., Milne, J., Nair, M., Schaller, H., Zemla, M., and Somerville, C. (2009). Mutations in UDP-Glucose: Sterol Glucosyltransferase in Arabidopsis Cause Transparent Testa Phenotype and Suberization Defect in Seeds. *Plant Physiology* 151, 78-87.

de Graaf, B.H., Cheung, A.Y., Andreyeva, T., Levasseur, K., Kieliszewski, M. and Wu, H.M. (2005). Rab11 GTPase-regulated membrane trafficking is crucial for tip-focused pollen tube growth in tobacco. *Plant Cell* 17, 2564-2579.

Delmer, D.P. (1999). CELLULOSE BIOSYNTHESIS: Exciting Times for A Difficult Field of Study. *Annual Review of Plant Physiology and Plant Molecular Biology* 50, 245-276.

Devarenne, T.P., Ghosh, A., and Chappell, J. (2002). Regulation of Squalene Synthase, a Key Enzyme of Sterol Biosynthesis, in Tobacco. *Plant Physiology* 129, 1095-1106.

Diener, A.C., Li, H., Zhou, W.-x., Whoriskey, W.J., Nes, W.D., and Fink, G.R. (2000). STEROL METHYLTRANSFERASE 1 Controls the Level of Cholesterol in Plants. *The Plant Cell* 12, 853-870.

Di Laurenzio, L., Wysocka-Diller, J., Malamy, J.E., Pysh, L., Helariutta, Y., Freshour, G., Hahn, M.G., Feldmann, K.A., and Benfey, P.N. (1996). The SCARECROW Gene Regulates an Asymmetric Cell Division That Is Essential for Generating the Radial Organization of the Arabidopsis Root. *Cell* 86, 423-433.

Dinneny, J.R., Long, T.A., Wang, J.Y., Jung, J.W., Mace, D., Pointer, S.,

Barron, C., Brady, S.M., Schiefelbein, J., and Benfey, P.N. (2008). Cell Identity Mediates the Response of Arabidopsis Roots to Abiotic Stress. *Science* **320**, 942-945.

Dolan, L. (2006). Positional information and mobile transcriptional regulators determine cell pattern in the Arabidopsis root epidermis. *Journal of Experimental Botany* **57**, 51-54.

Dong, J., and Bergmann, D.C. (2010). Chapter Nine - Stomatal Patterning and Development. In *Current Topics in Developmental Biology*, C.P.T. Marja, ed. (Academic Press), pp. 267-297.

Duckett, C.M., Oparka, K.J., Prior, D.A.M., Dolan, L., and Roberts, K. (1994). Dye-coupling in the root epidermis of Arabidopsis is progressively reduced during development. *Development* **120**, 3247-3255.

Dudoit, S., and Fridlyand, J. (2002). A prediction-based resampling method for estimating the number of clusters in a dataset. *Genome Biology* **3**, research0036.0031 - research0036.0021.

Dufourc, E. (2008). Sterols and membrane dynamics. *J Chem Biol* **1**, 63-77.

Duman-Scheel, M., Weng, L., Xin, S., and Du, W. (2002). Hedgehog regulates cell growth and proliferation by inducing Cyclin D and Cyclin E. *Nature* **417**, 299-304.

Earley, K.W., Haag, J.R., Pontes, O., Opper, K., Juehne, T., Song, K., and Pikaard, C.S. (2006). Gateway-compatible vectors for plant functional genomics and proteomics. *The Plant Journal* **45**, 616-629.

Ehlers, K., and Kollmann, R. (1996). Formation of branched plasmodesmata in regenerating *Solanum nigrum*-protoplasts. *Planta* **199**, 126-138.

Esders, T.W., and Light, R.J. (1972). Glucosyl- and Acetyltransferases Involved in the Biosynthesis of Glycolipids from *Candida bogoriensis*. *Journal of Biological Chemistry* **247**, 1375-1386.

Favery, B., Ryan, E., Foreman, J., Linstead, P., Boudonck, K., Steer, M., Shaw, P. and Dolan, L. (2001). *KOJAK* encodes a cellulose synthase-like protein required for root hair cell morphogenesis in Arabidopsis. *Genes Dev.* **15**, 79-89.

Fernandez-Calvino, L., Faulkner, C., Walshaw, J., Saalbach, G., Bayer, E., Benitez-Alfonso, Y., and Maule, A. (2011). Arabidopsis Plasmodesmal Proteome. *PLoS ONE* **6**, e18880.

Fischer, U., Ikeda, Y., Ljung, K., Serralbo, O., Singh, M., Heidstra, R., Palme, K., Scheres, B. and Grebe, M. (2006). Vectorial information for Arabidopsis planar polarity is mediated by combined AUX1, EIN2, and GNOM activity. *Curr. Biol.* *16*, 2143-2149.

Fleurat-Lessard, P., Frangne, N., Maeshima, M., Ratajczak, R., Bonnemain, J.L., and Martinoia, E. (1997). Increased Expression of Vacuolar Aquaporin and H⁺-ATPase Related to Motor Cell Function in *Mimosa pudica* L. *Plant Physiology* *114*, 827-834.

Frangne, N., Eggmann, T., Koblischke, C., Weissenböck, G., Martinoia, E., and Klein, M. (2002). Flavone Glucoside Uptake into Barley Mesophyll and Arabidopsis Cell Culture Vacuoles. Energization Occurs by H⁺-Antiport and ATP-Binding Cassette-Type Mechanisms. *Plant Physiology* *128*, 726-733.

Furt, F., Simon-Plas, F., and Mongrand, S. (2011). Lipids of the Plant Plasma Membrane. In *The Plant Plasma Membrane*, A.S. Murphy, B. Schulz, and W. Peer, eds. (Springer Berlin Heidelberg), pp. 3-30.

Galway, M.E., Masucci, J.D., Lloyd, A.M., Walbot, V., Davis, R.W., and Schiefelbein, J.W. (1994). The TTG Gene Is Required to Specify Epidermal Cell Fate and Cell Patterning in the Arabidopsis Root. *Developmental Biology* *166*, 740-754.

Goodin, M.M., Chakrabarty, R., Banerjee, R., Yelton, S., and DeBolt, S. (2007). New Gateways to Discovery. *Plant Physiology* *145*, 1100-1109.

Grabski, S., De Feijter, A.W., and Schindler, M. (1993). Endoplasmic Reticulum Forms a Dynamic Continuum for Lipid Diffusion between Contiguous Soybean Root Cells. *The Plant Cell Online* *5*, 25-38.

Grennan, A.K. (2007). Lipid Rafts in Plants. *Plant Physiology* *143*, 1083-1085.

Grille, S., Zaslowski, A., Thiele, S., Plat, J., and Warnecke, D. (2010). The functions of steryl glycosides come to those who wait: Recent advances in plants, fungi, bacteria and animals. *Progress in Lipid Research* *49*, 262-288.

Grunwald, C. (1971). Effects of Free Sterols, Steryl Ester, and Steryl Glycoside on Membrane Permeability. *Plant Physiology* *48*, 653-655.

Guimil, S., and Dunand, C. (2006). Patterning of Arabidopsis epidermal cells: epigenetic factors regulate the complex epidermal cell fate pathway. *Trends in Plant Science* *11*, 601-609.

Guivarc'h, A., Caissard, J.C., Azmi, A., Elmayan, T., Chriqui, D., and Tepfer, M. (1996). In situ detection of expression of the gus reporter gene in transgenic plants: ten years of blue genes. *Transgenic Research* 5, 281-288.

Guo, D., Venkatramesh, M., and Nes, W.D. (1995). Developmental regulation of sterol biosynthesis in *Zea mays*. *Lipids* 30, 203-219.

Guseman, J.M., Lee, J.S., Bogenschutz, N.L., Peterson, K.M., Virata, R.E., Xie, B., Kanaoka, M.M., Hong, Z., and Torii, K.U. (2010). Dysregulation of cell-to-cell connectivity and stomatal patterning by loss-of-function mutation in *Arabidopsis* CHORUS (GLUCAN SYNTHASE-LIKE 8). *Development* 137, 1731-1741.

Gutierrez, R., Lindeboom, J.J., Paredez, A.R., Emons, A.M.C., and Ehrhardt, D.W. (2009). *Arabidopsis* cortical microtubules position cellulose synthase delivery to the plasma membrane and interact with cellulose synthase trafficking compartments. *Nat Cell Biol* 11, 797-806.

Habuchi, S., Ando, R., Dedecker, P., Verheijen, W., Mizuno, H., Miyawaki, A., and Hofkens, J. (2005). Reversible single-molecule photoswitching in the GFP-like fluorescent protein Dronpa. *Proceedings of the National Academy of Sciences of the United States of America* 102, 9511-9516.

Halling, K.K., Ramstedt, B., and Slotte, J.P. (2008). Glycosylation induces shifts in the lateral distribution of cholesterol from ordered towards less ordered domains. *Biochimica et Biophysica Acta (BBA) - Biomembranes* 1778, 1100-1111.

Ham, B.-K., Li, G., Kang, B.-H., Zeng, F., and Lucas, W.J. (2012). Overexpression of *Arabidopsis* Plasmodesmata Germin-Like Proteins Disrupts Root Growth and Development. *The Plant Cell* 24, 3630-3648.

Haque, M., Hirai, Y., Yokota, K., Mori, N., Jahan, I., Ito, H., Hotta, H., Yano, I., Kanemasa, Y., and Oguma, K. (1996). Lipid profile of *Helicobacter* spp.: presence of cholesteryl glucoside as a characteristic feature. *Journal of Bacteriology* 178, 2065-2070.

Hartmann-Bouillon, M.-A., Benveniste, P., Lester, P. and Roland, D. (1987). Plant membrane sterols: Isolation, identification, and biosynthesis. In *Methods in Enzymology* (Academic Press), 632-650.

Hartmann-Bouillon, M.-A. and Benveniste, P. (1978). Sterol biosynthetic capacity of purified membrane fractions from maize coleoptiles. *Phytochem.* 17, 1037-1042.

- Hassan, H., Scheres, B., and Blilou, I.** (2010). JACKDAW controls epidermal patterning in the Arabidopsis root meristem through a non-cell-autonomous mechanism. *Development* 137, 1523-1529.
- He, J.-X., Fujioka, S., Li, T.-C., Kang, S.G., Seto, H., Takatsuto, S., Yoshida, S., and Jang, J.-C.** (2003). Sterols Regulate Development and Gene Expression in Arabidopsis. *Plant Physiology* 131, 1258-1269.
- Heazlewood, J.L., Verboom, R.E., Tonti-Filippini, J., Small, I., and Millar, A.H.** (2007). SUBA: the Arabidopsis Subcellular Database. *Nucleic Acids Research* 35, D213-D218.
- Helariutta, Y., Fukaki, H., Wysocka-Diller, J., Nakajima, K., Jung, J., Sena, G., Hauser, M.-T., and Benfey, P.N.** (2000). The SHORT-ROOT Gene Controls Radial Patterning of the Arabidopsis Root through Radial Signaling. *Cell* 101, 555-567.
- Hillig, I., Leipelt, M., Ott, C., Zahringer, U., Warnecke, D., and Heinz, E.** (2003). Formation of glucosylceramide and sterol glucoside by a UDP-glucose-dependent glucosylceramide synthase from cotton expressed in *Pichia pastoris*. *FEBS Letters* 553, 365-369.
- Hink, M., Bisseling, T., and Visser, A.W.G.** (2002). Imaging protein-protein interactions in living cells. *Plant Mol Biol* 50, 871-883.
- Hochholdinger, F., and Zimmermann, R.** (2008). Conserved and diverse mechanisms in root development. *Current Opinion in Plant Biology* 11, 70-74.
- Holmberg, N., Harker, M., Gibbard, C.L., Wallace, A.D., Clayton, J.C., Rawlins, S., Hellyer, A., and Safford, R.** (2002). Sterol C-24 Methyltransferase Type 1 Controls the Flux of Carbon into Sterol Biosynthesis in Tobacco Seed. *Plant Physiology* 130, 303-311.
- Hou, C.T., Umemura, Y., Nakamura, M., and Funahashi, S.** (1968). Enzymatic Synthesis of Steryl Glucoside by a Particulate Preparation from Immature Soybean Seeds. *Journal of Biochemistry* 63, 351-360.
- Huang, D.W., Sherman, B.T., and Lempicki, R.A.** (2008). Systematic and integrative analysis of large gene lists using DAVID bioinformatics resources. *Nat Protocols* 4, 44-57.
- Hughes, J., and Hughes, M.A.** (1994). Multiple secondary plant product UDP-glucose glucosyltransferase genes expressed in cassava (*Manihot esculenta* Crantz) cotyledons. *Mitochondrial DNA* 5, 41-49.

Hung, C.-Y., Lin, Y., Zhang, M., Pollock, S., David Marks, M., and Schiefelbein, J. (1998). A Common Position-Dependent Mechanism Controls Cell-Type Patterning and GLABRA2 Regulation in the Root and Hypocotyl Epidermis of Arabidopsis. *Plant Physiology* 117, 73-84.

Husselstein, T., Gachotte, D., Desprez, T., Bard, M., and Benveniste, P. (1996). Transformation of *Saccharomyces cerevisiae* with a cDNA encoding a sterol C-methyltransferase from *Arabidopsis thaliana* results in the synthesis of 24-ethyl sterols. *FEBS Letters* 381, 87-92.

Ibl, V., and Stoger, E. (2012). The formation, function and fate of protein storage compartments in seeds. *Protoplasma* 249, 379-392.

Ishida, T., Hattori, S., Sano, R., Inoue, K., Shirano, Y., Hayashi, H., Shibata, D., Sato, S., Kato, T., Tabata, S., Okada, K., and Wada, T. (2007). Arabidopsis TRANSPARENT TESTA GLABRA2 Is Directly Regulated by R2R3 MYB Transcription Factors and Is Involved in Regulation of GLABRA2 Transcription in Epidermal Differentiation. *The Plant Cell Online* 19, 2531-2543.

Ishida, T., Kurata, T., Okada, K., and Wada, T. (2008). A Genetic Regulatory Network in the Development of Trichomes and Root Hairs. *Annual Review of Plant Biology* 59, 365-386.

Jaillais, Y., and Gaude, T. (2008). Plant Cell Polarity: Sterols Enter into Action after Cytokinesis. *Developmental Cell* 14, 318-320.

Jaillais, Y., Fobis-Loisy, I., Miège, C. and Gaude, T. (2008). Evidence for a sorting endosome in Arabidopsis root cells. *Plant J.* 53, 237-247.

Jang, J.-C., Fujioka, S., Tasaka, M., Seto, H., Takatsuto, S., Ishii, A., Aida, M., Yoshida, S., and Sheen, J. (2000). A critical role of sterols in embryonic patterning and meristem programming revealed by the fackel mutants of *Arabidopsis thaliana*. *Genes & Development* 14, 1485-1497.

Jefferson, R.A., Kavanagh, T.A. and Bevan, M.W. (1987). GUS fusions: B-glucuronidase as a sensitive and versatile gene fusion marker in higher plants. *EMBO Journal.* 6, 3901-3907.

Jelenska, J., van Hal, J.A., and Greenberg, J.T. (2010). *Pseudomonas syringae* hijacks plant stress chaperone machinery for virulence. *Proceedings of the National Academy of Sciences* 107, 13177-13182.

Jones, M.A., Shen, J.-J., Fu, Y., Li, H., Yang, Z., and Grierson, C.S. (2002). The Arabidopsis Rop2 GTPase Is a Positive Regulator of Both Root Hair Initiation and Tip Growth. *The Plant Cell Online* 14, 763-776.

Jones, M.A., Raymond, M.J., and Smirnov, N. (2006). Analysis of the root-hair morphogenesis transcriptome reveals the molecular identity of six genes with roles in root-hair development in Arabidopsis. *The Plant Journal* 45, 83-100.

Jürgens, G. (2005) Cytokinesis in higher plants. *Annual Review of Plant Biology* 56, 281-299.

Kanaoka, M.M., Pillitteri, L.J., Fujii, H., Yoshida, Y., Bogenschutz, N.L., Takabayashi, J., Zhu, J.-K., and Torii, K.U. (2008). SCREAM/ICE1 and SCREAM2 Specify Three Cell-State Transitional Steps Leading to Arabidopsis Stomatal Differentiation. *The Plant Cell Online* 20, 1775-1785.

Karamyan, V.T., and Speth, R.C. (2008). Animal models of BMAA neurotoxicity: A critical review. *Life Sciences* 82, 233-246.

Keller, P. and Simons, K. (1998). Cholesterol Is Required for Surface Transport of Influenza Virus Hemagglutinin. *J. Cell Biol.* 140, 1357-1367.

Khabazian, I., Bains, J.S., Williams, D.E., Cheung, J., Wilson, J.M.B., Pasqualotto, B.A., Pelech, S.L., Andersen, R.J., Wang, Y.T., Liu, L., Nagai, A., Kim, S.U., Craig, U.K., and Shaw, C.A. (2002). Isolation of various forms of sterol β -d-glucoside from the seed of *Cycas circinalis*: neurotoxicity and implications for ALS-parkinsonism dementia complex. *Journal of Neurochemistry* 82, 516-528.

Kierszniowska, S., Seiwert, B., and Schulze, W.X. (2009). Definition of Arabidopsis Sterol-rich Membrane Microdomains by Differential Treatment with Methyl- β -cyclodextrin and Quantitative Proteomics. *Molecular & Cellular Proteomics* 8, 612-623.

Kim, J.-Y., Yuan, Z., and Jackson, D. (2003). Developmental regulation and significance of KNOX protein trafficking in Arabidopsis. *Development* 130, 4351-4362.

Knox, K., Grierson, C.S., and Leyser, O. (2003). AXR3 and SHY2 interact to regulate root hair development. *Development* 130, 5769-5777.

Koizumi, K., Wu, S., MacRae-Crerar, A., and Gallagher, Kimberly L. (2011). An Essential Protein that Interacts with Endosomes and Promotes Movement of the SHORT-ROOT Transcription Factor. *Current Biology* 21, 1559-1564.

Kojima, M., Ohnishi, M., Ito, S., and Fujino, Y. (1989). Characterization of acylmono-, mono-, di-, tri- and tetraglycosylsterol and saponin in Adzuki bean (*Vigna angularis*) seeds. *Lipids* 24, 849-853.

- Kolukisaoglu, Ü., Bovet, L., Klein, M., Eggmann, T., Geisler, M., Wanke, D., Martinoia, E., and Schulz, B.** (2002). Family business: the multidrug-resistance related protein (MRP) ABC transporter genes in *Arabidopsis thaliana*. *Planta* 216, 107-119.
- Koshino-Kimura, Y., Wada, T., Tachibana, T., Tsugeki, R., Ishiguro, S., and Okada, K.** (2005). Regulation of CAPRICE Transcription by MYB Proteins for Root Epidermis Differentiation in *Arabidopsis*. *Plant and Cell Physiology* 46, 817-826.
- Kovganko, N.V., and Kashkan, Z.N.** (1999). Sterol glycosides and acylglycosides. *Chemistry of Natural Compounds* 35, 479-497.
- Kragler, F., Lucas, W.J., and Monzer, J.** (1998). Plasmodesmata: Dynamics, Domains and Patterning. *Annals of Botany* 81, 1-10.
- Krasensky, J., and Jonak, C.** (2012). Drought, salt, and temperature stress-induced metabolic rearrangements and regulatory networks. *Journal of Experimental Botany* 63, 1593-1608.
- Kregel, K.C.** (2002). Invited Review: Heat shock proteins: modifying factors in physiological stress responses and acquired thermotolerance. *J. Appl. Physiol.* 122, 189-197
- Kubo, H., Peeters, A.J.M., Aarts, M.G.M., Pereira, A., and Koornneef, M.** (1999). *ANTHOCYANINLESS2*, a Homeobox Gene Affecting Anthocyanin Distribution and Root Development in *Arabidopsis*. *The Plant Cell Online* 11, 1217-1226.
- Kunimoto, S., Kobayashi, T., Kobayashi, S., and Murakami-Murofushi, K.** (2000). Expression of Cholesteryl Glucoside by Heat Shock in Human Fibroblasts. *Cell Stress & Chaperones* 5, 3-7.
- Kurata, T., Ishida, T., Kawabata-Awai, C., Noguchi, M., Hattori, S., Sano, R., Nagasaka, R., Tominaga, R., Koshino-Kimura, Y., Kato, T., Sato, S., Tabata, S., Okada, K., and Wada, T.** (2005a). Cell-to-cell movement of the CAPRICE protein in *Arabidopsis* root epidermal cell differentiation. *Development* 132, 5387-5398.
- Kurata, T., Okada, K., and Wada, T.** (2005b). Intercellular movement of transcription factors. *Current Opinion in Plant Biology* 8, 600-605.
- Kurdyukov, S., Faust, A., Trenkamp, S., Bär, S., Franke, R., Efremova, N., Tietjen, K., Schreiber, L., Saedler, H., and Yephremov, A.** (2006). Genetic and biochemical evidence for involvement of HOTHEAD in the biosynthesis of long-

chain α -, ω -dicarboxylic fatty acids and formation of extracellular matrix. *Planta* 224, 315-329.

Kwak, S.H., Shen, R., and Schiefelbein, J. (2005). Positional Signaling Mediated by a Receptor-like Kinase in Arabidopsis. *Science* 307, 1111-1113.

Kwak, S.H., and Schiefelbein, J. (2007). The role of the SCRAMBLED receptor-like kinase in patterning the Arabidopsis root epidermis. *Developmental Biology* 302, 118-131.

Kwak, S.H., and Schiefelbein, J. (2008). A Feedback Mechanism Controlling SCRAMBLED Receptor Accumulation and Cell-Type Pattern in Arabidopsis. *Current Biology* 18, 1949-1954.

Kwak, S.H., and Schiefelbein, J.W. (2009). Regulated accumulation of the SCRAMBLED receptor and position-dependent cell type patterning in Arabidopsis. *Plant Signaling and Behavior* 4, 332-335.

Laloi, M., Perret, A.-M., Chatre, L., Melsner, S., Cantrel, C., Vaultier, M.-N., Zachowski, A., Bathany, K., Schmitter, J.-M., Vallet, M., Lessire, R., Hartmann, M.-A., and Moreau, P. (2007). Insights into the Role of Specific Lipids in the Formation and Delivery of Lipid Microdomains to the Plasma Membrane of Plant Cells. *Plant Physiology* 143, 461-472.

Larsen, P.B., Geisler, M.J.B., Jones, C.A., Williams, K.M., and Cancel, J.D. (2005). ALS3 encodes a phloem-localized ABC transporter-like protein that is required for aluminum tolerance in Arabidopsis. *The Plant Journal* 41, 353-363.

Lebrun, A.-H., Wunder, C., Hildebrand, J., Churin, Y., Zähringer, U., Lindner, B., Meyer, T.F., Heinz, E., and Warnecke, D. (2006). Cloning of a Cholesterol- α -glucosyltransferase from *Helicobacter pylori*. *Journal of Biological Chemistry* 281, 27765-27772.

Lee, J.S., Kuroha, T., Hnilova, M., Khatayevich, D., Kanaoka, M.M., McAbee, J.M., Sarikaya, M., Tamerler, C., and Torii, K.U. (2012). Direct interaction of ligand–receptor pairs specifying stomatal patterning. *Genes & Development* 26, 126-136.

Lee, J.Y., Wang, X., Cui, W., Sager, R., Modla, S., Czymmek, K., Zybaliou, B., van Wijk, K., Zhang, C., Lu, H., and Lakshmanan, V. (2011). A Plasmodesmata-Localized Protein Mediates Crosstalk between Cell-to-Cell Communication and Innate Immunity in Arabidopsis. *The Plant Cell Online* 23, 3353-3373.

Lee, M.M., and Schiefelbein, J. (1999). WEREWOLF, a MYB-Related Protein in Arabidopsis, Is a Position-Dependent Regulator of Epidermal Cell Patterning. *Cell* 99, 473-483.

Lee, M.M., and Schiefelbein, J. (2002). Cell Pattern in the Arabidopsis Root Epidermis Determined by Lateral Inhibition with Feedback. *The Plant Cell Online* 14, 611-618.

Lefebvre, B., Furt, F., Hartmann, M.-A., Michaelson, L.V., Carde, J.-P., Sargueil-Boiron, F., Rossignol, M., Napier, J.A., Cullimore, J., Bessoule, J.-J., and Mongrand, S. (2007). Characterization of Lipid Rafts from *Medicago truncatula* Root Plasma Membranes: A Proteomic Study Reveals the Presence of a Raft-Associated Redox System. *Plant Physiology* 144, 402-418.

Lepage, M. (1964). Isolation and characterization of an esterified form of steryl glucoside. *Journal of Lipid Research* 5, 587-592.

Li, Y., Baldauf, S., Lim, E.-K., and Bowles, D.J. (2001). Phylogenetic Analysis of the UDP-glycosyltransferase Multigene Family of *Arabidopsis thaliana*. *Journal of Biological Chemistry* 276, 4338-4343.

Lindsey, K., Pullen, M.L., and Topping, J.F. (2003). Importance of plant sterols in pattern formation and hormone signalling. *Trends in Plant Science* 8, 521-525.

Lingwood, D., and Simons, K. (2010). Lipid Rafts As a Membrane-Organizing Principle. *Science* 327, 46-50.

Liu, J., Magalhaes, J.V., Shaff, J., and Kochian, L.V. (2009). Aluminum-activated citrate and malate transporters from the MATE and ALMT families function independently to confer *Arabidopsis* aluminum tolerance. *The Plant Journal* 57, 389-399.

Lukowitz, W., Gillmor, C.S., and Scheible, W.R. (2000). Positional Cloning in *Arabidopsis*. Why It Feels Good to Have a Genome Initiative Working for You. *Plant Physiology* 123, 795-806.

Ly, P.T.T., Singh, S., and Shaw, C.A. (2007). Novel environmental toxins: Steryl glycosides as a potential etiological factor for age-related neurodegenerative diseases. *Journal of Neuroscience Research* 85, 231-237.

MacAlister, C.A., Ohashi-Ito, K., and Bergmann, D.C. (2007). Transcription factor control of asymmetric cell divisions that establish the stomatal lineage. *Nature* 445, 537-540.

Mackenzie, P.I., Owens, I.S., Burchell, B., Bock, K.W., Bairoch, A., Belanger, A., Gignoux, S.F., Green, M., Hum, D.W., Iyanagi, T., Lancet, D., Louisot, P., Magdalou, J., Roy Chowdhury, J., Ritter, J.K., Tephly, T.R., Schachter, H., Tephly, T., Tipton, K.F., and Nebert, D.W. (1997). The UDP glycosyltransferase gene superfamily: recommended nomenclature update based on evolutionary divergence. *Pharmacogenetics and Genomics* 7, 255-269.

Mackenzie, P.I., Walter Bock, K., Burchell, B., Guillemette, C., Ikushiro, S.-i., Iyanagi, T., Miners, J.O., Owens, I.S., and Nebert, D.W. (2005). Nomenclature update for the mammalian UDP glycosyltransferase (UGT) gene superfamily. *Pharmacogenetics and Genomics* 15, 677-685.

Martens, H.J., Roberts, A.G., Oparka, K.J., and Schulz, A. (2006). Quantification of Plasmodesmatal Endoplasmic Reticulum Coupling between Sieve Elements and Companion Cells Using Fluorescence Redistribution after Photobleaching. *Plant Physiology* 142, 471-480.

Masucci, J.D., Rerie, W.G., Foreman, D.R., Zhang, M., Galway, M.E., Marks, M.D., and Schiefelbein, J.W. (1996). The homeobox gene *GLABRA2* is required for position-dependent cell differentiation in the root epidermis of *Arabidopsis thaliana*. *Development* 122, 1253-1260.

Matheson, L.A., Hanton, S.L., Rossi, M., Latijnhouwers, M., Stefano, G., Renna, L., Brandizzi, F. (2007) Multiple roles of ARF1 in plant cells include spatially-regulated recruitment of coatamer and elements of the Golgi matrix. *Plant Physiology* 143, 1615–1627.

Matz, M.V., Fradkov, A.F., Labas, Y.A., Savitsky, A.P., Zaraisky, A.G., Markelov, M.L., and Lukyanov, S.A. (1999). Fluorescent proteins from nonbioluminescent Anthozoa species. *Nat Biotech* 17, 969-973.

Maule, A.J., Benitez-Alfonso, Y., and Faulkner, C. (2011). Plasmodesmata - membrane tunnels with attitude. *Current Opinion in Plant Biology* 14, 683-690.

Mayberry, W.R., and Smith, P.F. (1983). Structures and properties of acyl diglucosylcholesterol and galactofuranosyl diacylglycerol from *Acholeplasma axanthum*. *Biochimica et Biophysica Acta (BBA) - Lipids and Lipid Metabolism* 752, 434-443.

McConnell, J.R., Emery, J., Eshed, Y., Bao, N., Bowman, J., and Barton, M.K. (2001). Role of *PHABULOSA* and *PHAVOLUTA* in determining radial patterning in shoots. *Nature* 411, 709-713.

McFarlane, H.E., Shin, J.J.H., Bird, D.A., and Samuels, A.L. (2010). *Arabidopsis* ABCG Transporters, Which Are Required for Export of Diverse Cuticular Lipids, Dimerize in Different Combinations. *The Plant Cell Online* 22, 3066-3075.

Men, S., Boutte, Y., Ikeda, Y., Li, X., Palme, K., Stierhof, Y.D., Hartmann, M.A., Moritz, T., and Grebe, M. (2008). Sterol-dependent endocytosis mediates post-cytokinetic acquisition of PIN2 auxin efflux carrier polarity. *Nat Cell Biol* 10, 237-244.

Merzlyak, E.M., Goedhart, J., Shcherbo, D., Bulina, M.E., Shcheglov, A.S., Fradkov, A.F., Gaintzeva, A., Lukyanov, K.A., Lukyanov, S., Gadella, T.W.J., and Chudakov, D.M. (2007). Bright monomeric red fluorescent protein with an extended fluorescence lifetime. *Nat Methods* 4, 555-557.

Miernyk, J. A. (2001). The J-domain proteins of *Arabidopsis thaliana*: an unexpectedly large and diverse family of chaperones. *Cell Stress Chaperones* 6(3), 209–218.

Minami, Y., Höhfeld, J., Ohtsuka, K., and Hartl, F.U. (1996). Regulation of the Heat-shock Protein 70 Reaction Cycle by the Mammalian DnaJ Homolog, Hsp40. *Journal of Biological Chemistry* 271, 19617-19624.

Mongrand, S., Morel, J., Laroche, J., Claverol, S., Carde, J.P., Hartmann, M.A., Bonneau, M., Simon-Plas, F., Lessire, R., and Bessoule, J.J. (2004). Lipid Rafts in Higher Plant Cells: Purification and characterization of Triton x-100-insoluble microdomains from tobacco plasma membrane. *Journal of Biological Chemistry* 279, 36277-36286.

Moore, I., and Murphy, A. (2009). Validating the Location of Fluorescent Protein Fusions in the Endomembrane System. *The Plant Cell Online* 21, 1632-1636.

Mousley CJ, Tyeryar KR, Vincent-Pope P and Bankaitis VA (2007) The Sec14-superfamily and the regulatory interface between phospholipid metabolism and membrane trafficking. *Biochimica et Biophysica Acta (BBA) - Molecular and Cell Biology of Lipids* 1771, 727-736.

Mudd, J.B., and McManus, T.T. (1980). Effect of Steryl Glycosides on the Phase Transition of Dipalmitoyl Lecithin. *Plant Physiology* 65, 78-80.

Munro S (2003) Lipid Rafts: Elusive or Illusive? *Cell* 15, 377-388.

Murakami-Murofushi, K., Nakamura, K., Ohta, J., Suzuki, M., Suzuki, A., Murofushi, H., and Yokota, T. (1987). Expression of poriferasterol monoglucoside associated with differentiation of *Physarum polycephalum*. *Journal of Biological Chemistry* 262, 16719-16723.

Muramatsu, K., Maitani, Y., Machida, Y., and Nagai, T. (1994). Effect of soybean-derived sterol and its glucoside mixtures on the stability of dipalmitoylphosphatidylcholine and dipalmitoylphosphatidylcholine/cholesterol liposomes. *International Journal of Pharmaceutics* 107, 1-8.

Murashige, T., and Skoog, F. (1962). A Revised Medium for Rapid Growth and Bio Assays with Tobacco Tissue Cultures. *Physiologia Plantarum* 15, 473-497.

Mylona, P., Linstead, P., Martienssen, R., and Dolan, L. (2002). SCHIZORIZA controls an asymmetric cell division and restricts epidermal identity in the Arabidopsis root. *Development* 129, 4327-4334.

Nagpal, P., Walker, L.M., Young, J.C., Sonawala, A., Timpte, C., Estelle, M., and Reed, J.W. (2000). AXR2 Encodes a Member of the Aux/IAA Protein Family. *Plant Physiology* 123, 563-574.

Nakamoto, H., and Vigh, L. (2007). The small heat shock proteins and their clients. *Cell Mol Life Sci* 64, 294-306.

Nawy, T., Lee, J.-Y., Colinas, J., Wang, J.Y., Thongrod, S.C., Malamy, J.E., Birnbaum, K., and Benfey, P.N. (2005). Transcriptional Profile of the Arabidopsis Root Quiescent Center. *The Plant Cell Online* 17, 1908-1925.

Nes, W.D., McCourt, B.S., Marshall, J.A., Ma, J., Dennis, A.L., Lopez, M., Li, H., and He, L. (1999). Site-Directed Mutagenesis of the Sterol Methyl Transferase Active Site from *Saccharomyces cerevisiae* Results in Formation of Novel 24-Ethyl Sterols. *The Journal of Organic Chemistry* 64, 1535-1542.

O'Farrell PH (1975) High resolution two-dimensional electrophoresis of proteins. *Journal of Biological Chemistry* 250, 4007-4021.

Ogasawara, H., Kaimi, R., Colasanti, J., and Kozaki, A. (2011). Activity of transcription factor JACKDAW is essential for SHR/SCR-dependent activation of SCARECROW and MAGPIE and is modulated by reciprocal interactions with MAGPIE, SCARECROW and SHORT ROOT. *Plant Mol Biol* 77, 489-499.

Ohashi-Ito, K., and Bergmann, D.C. (2006). Arabidopsis FAMA Controls the Final Proliferation/Differentiation Switch during Stomatal Development. *The Plant Cell Online* 18, 2493-2505.

Ohashi-Ito, K., and Fukuda, H. (2003). HD-Zip III Homeobox Genes that Include a Novel Member, ZeHB-13 (*Zinnia*)/ATHB-15 (*Arabidopsis*), are Involved in Procambium and Xylem Cell Differentiation. *Plant and Cell Physiology* 44, 1350-1358.

Oku, M., Warnecke, D., Noda, T., Müller, F., Heinz, E., Mukaiyama, H., Kato, N., and Sakai, Y. (2003). Peroxisome degradation requires catalytically active sterol glucosyltransferase with a GRAM domain, Vol 22.

Oparka, K.J., Roberts, A.G., Boevink, P., Cruz, S.S., Roberts, I., Pradel, K.S., Imlau, A., Kotlizky, G., Sauer, N., and Epel, B. (1999). Simple, but Not

Branched, Plasmodesmata Allow the Nonspecific Trafficking of Proteins in Developing Tobacco Leaves. *Cell* 97, 743-754.

Otegui, M.S., Herder, R., Schulze, J., Jung, R., and Staehelin, L.A. (2006). The Proteolytic Processing of Seed Storage Proteins in Arabidopsis Embryo Cells Starts in the Multivesicular Bodies. *The Plant Cell Online* 18, 2567-2581.

Ovecka M., Berson T., Beck M., Derksen J, Samaj J., Baluska F. and Lichtscheidl, I.K. (2010). Structural Sterols Are Involved in Both the Initiation and Tip Growth of Root Hairs in *Arabidopsis thaliana* *Plant Cell* 22, 2999-3019.

Ovecka, M., Lang, I., Baluska, F., Ismail, A., Illes, P. and Lichtscheidl, I.K. (2005). Endocytosis and vesicle trafficking during tip growth of root hairs. *Protoplasma* 226, 39-54.

Palta, J.P., Whitaker, B.D., and Weiss, L.S. (1993). Plasma Membrane Lipids Associated with Genetic Variability in Freezing Tolerance and Cold Acclimation of Solanum Species. *Plant Physiology* 103, 793-803.

Panikashvili, D., Savaldi-Goldstein, S., Mandel, T., Yifhar, T., Franke, R.B., Höfer, R., Schreiber, L., Chory, J., and Aharoni, A. (2007). The Arabidopsis DESPERADO/AtWBC11 Transporter Is Required for Cutin and Wax Secretion. *Plant Physiology* 145, 1345-1360.

Panaretou, B., and Zhai, C. (2008). The heat shock proteins: Their roles as multi-component machines for protein folding. *Fungal Biology Reviews* 22, 110-119.

Paquette, S., Müller, B.L., and Bak, S. (2003). On the origin of family 1 plant glycosyltransferases. *Phytochemistry* 62, 399-413.

Paredes, A.R., Somerville, C.R., and Ehrhardt, D.W. (2006). Visualization of Cellulose Synthase Demonstrates Functional Association with Microtubules. *Science* 312, 1491-1495.

Park, S., Rancour, D.M. and Bednarek, S.Y. (2008) In Planta Analysis of the Cell Cycle-Dependent Localization of AtCDC48A and Its Critical Roles in Cell Division, Expansion, and Differentiation. *Plant Physiology* 148, 246-258.

Passardi, F., Dobias, J., Valério, L., Guimil, S., Penel, C., and Dunand, C. (2007). Morphological and physiological traits of three major Arabidopsis thaliana accessions. *Journal of Plant Physiology* 164, 980-992.

Patterson, G.H., and Lippincott-Schwartz, J. (2004). Selective photolabeling of proteins using photoactivatable GFP. *Methods* 32, 445-450.

- Pechan, P.M.** (1991). Heat shock proteins and cell proliferation. *FEBS Letters* 280, 1-4.
- Peng, L., Kawagoe, Y., Hogan, P., and Delmer, D.** (2002). Sitosterol- β -glucoside as Primer for Cellulose Synthesis in Plants. *Science* 295, 147-150.
- Peskan, T., Westermann, M., and Oelmüller, R.** (2000). Identification of low-density Triton X-100-insoluble plasma membrane microdomains in higher plants. *European Journal of Biochemistry* 267, 6989-6995.
- Peterman, T.K., Ohol, Y.M., McReynolds, L.J. and Luna, E.J.** (2004) Patellin1, a Novel Sec14-Like Protein, Localizes to the Cell Plate and Binds Phosphoinositides. *Plant Physiology* 136, 3080-3094.
- Peterman, T.K., Sequeira, A.S., Samia, J.A. and Lunde, E.E.** (2006) Molecular cloning and characterization of patellin1, a novel sec14-related protein, from zucchini (*Cucurbita pepo*). *Journal of Plant Physiology* 163, 1150-1158.
- Petrussa, E., Braidot, E., Zancani, M., Peresson, C., Bertolini, A., Patui, S., and Vianello, A.** (2013). Plant Flavonoids—Biosynthesis, Transport and Involvement in Stress Responses. *International Journal of Molecular Sciences* 14, 14950-14973.
- Pighin, J.A., Zheng, H., Balakshin, L.J., Goodman, I.P., Western, T.L., Jetter, R., Kunst, L., and Samuels, A.L.** (2004). Plant Cuticular Lipid Export Requires an ABC Transporter. *Science* 306, 702-704.
- Pike, L.J.** (2006). Rafts defined: a report on the Keystone symposium on lipid rafts and cell function. *Journal of Lipid Research* 47, 1597-1598.
- Pillitteri, L.J., Sloan, D.B., Bogenschutz, N.L., and Torii, K.U.** (2007). Termination of asymmetric cell division and differentiation of stomata. *Nature* 445, 501-505.
- Pollard, M., Beisson, F., Li, Y., and Ohlrogge, J.B.** (2008). Building lipid barriers: biosynthesis of cutin and suberin. *Trends in Plant Science* 13, 236-246.
- Ponting, C.P., and Aravind, L.** (1999). START: a lipid-binding domain in StAR, HD-ZIP and signalling proteins. *Trends in Biochemical Sciences* 24, 130-132.
- Porter, J.A., Young, K.E., and Beachy, P.A.** (1996). Cholesterol Modification of Hedgehog Signaling Proteins in Animal Development. *Science* 274, 255-259.

Potocka, A., and Zimowski, J. (2008). Metabolism of conjugated sterols in eggplant. Part 1. UDP-glucose: Sterol glucosyltransferase. *Acta Biochimica Polonica* 55, 127-134.

Power, F.B., and Salway, A.H. (1913). XLVII. - The identification of ipuranol and some allied compounds as phytosterol glucosides. *Journal of the Chemical Society, Transactions* 103, 399-406.

Power, F.B., and Tutin, F. (1908). LXXXIV.-The constituents of olive bark. *Journal of the Chemical Society, Transactions* 93, 904-917.

Prigge, M.J., Otsuga, D., Alonso, J.M., Ecker, J.R., Drews, G.N., and Clark, S.E. (2005). Class III Homeodomain-Leucine Zipper Gene Family Members Have Overlapping, Antagonistic, and Distinct Roles in Arabidopsis Development. *The Plant Cell Online* 17, 61-76.

Preuss, M.L., Serna, J., Falbel, T.G., Bednarek, S.Y. and Nielsen, E. (2004). The Arabidopsis Rab GTPase RabA4b localizes to the tips of growing root hair cells. *Plant Cell* 16, 1589-1603.

Pullen, M., Clark, N., Zarinkamar, F., Topping, J. and Lindsey, K. (2010). Analysis of Vascular Development in the hydra Sterol Biosynthetic Mutants of Arabidopsis. *PLoS ONE* 5, e12227.

Qian, P., Han, B., Forestier, E., Hu, Z., Gao, N., Lu, W., Schaller, H., Li, J., and Hou, S. (2013). Sterols are required for cell-fate commitment and maintenance of the stomatal lineage in Arabidopsis. *The Plant Journal* 74, 1029-1044.

Qiu, X.B., Shao, Y.M., Miao, S., and Wang, L. (2006). The diversity of the DnaJ/Hsp40 family, the crucial partners for Hsp70 chaperones. *Cellular and Molecular Life Sciences CMLS* 63, 2560-2570.

Raffaele, S., Bayer, E., Lafarge, D., Cluzet, S., German Retana, S., Boubekeur, T., Leborgne-Castel, N., Carde, J.P., Lherminier, J., Noirot, E., Satiat-Jeunemaitre, B., Laroche-Traineau, J., Moreau, P., Ott, T., Maule, A.J., Reymond, P., Simon-Plas, F., Farmer, E.E., Bessoule, J.J., and Mongrand, S. (2009). Remorin, a Solanaceae Protein Resident in Membrane Rafts and Plasmodesmata, Impairs Potato virus X Movement. *The Plant Cell Online* 21, 1541-1555.

Rajan, V., and D'Silva, P. (2009). Arabidopsis thaliana J-class heat shock proteins: cellular stress sensors. *Funct Integr Genomics* 9, 433-446.

Rancour, D.M., Dickey, C.E., Park, S. and Bednarek, S.Y. (2002) Characterization of AtCDC48. Evidence for Multiple Membrane Fusion

Mechanisms at the Plane of Cell Division in Plants. *Plant Physiology* 130, 1241-1253.

Rauch, A., Bellew, M., Eng, J., Fitzgibbon, M., Holzman, T., Hussey, P., Igra, M., Maclean, B., Lin, C.W., Detter, A., Fang, R., Faca, V., Gafken, P., Zhang, H., Whitaker, J., States, D., Hanash, S., Paulovich, A. and McIntosh, M.W. (2005) Computational Proteomics Analysis System (CPAS): An Extensible, Open-Source Analytic System for Evaluating and Publishing Proteomic Data and High Throughput Biological Experiments. *Journal of Proteome Research* 5, 112-121.

Raychaudhuri, S., and Prinz, W.A. (2010). The Diverse Functions of Oxysterol-Binding Proteins. *Annual Review of Cell and Developmental Biology* 26, 157-177.

Rerie, W.G., Feldmann, K.A., and Marks, M.D. (1994). The GLABRA2 gene encodes a homeo domain protein required for normal trichome development in *Arabidopsis*. *Genes & Development* 8, 1388-1399.

Ritossa, F. (1962). A new puffing pattern induced by temperature shock and DNP in *drosophila*. *Experientia* 18, 571-573.

Roche, Y., Gerbeau-Pissot, P., Buhot, B., Thomas, D., Bonneau, L., Gresti, J., Mongrand, S., Perrier-Cornet, J.M., and Simon-Plas, F. (2008). Depletion of phytosterols from the plant plasma membrane provides evidence for disruption of lipid rafts. *The FASEB Journal* 22, 3980-3991.

Rogers, S., and Bendich, A. (1985). Extraction of DNA from milligram amounts of fresh, herbarium and mummified plant tissues. *Plant Mol Biol* 5, 69-76.

Ross, J., Li, Y., Lim, E.K., and Bowles, D. (2001). Higher plant glycosyltransferases. *Genome Biology* 2, reviews3004.3001 - reviews3004.3006.

Ruan, Y.L., Llewellyn, D.J., and Furbank, R.T. (2001). The Control of Single-Celled Cotton Fiber Elongation by Developmentally Reversible Gating of Plasmodesmata and Coordinated Expression of Sucrose and K⁺ Transporters and Expansin. *The Plant Cell Online* 13, 47-60.

Ruiz-Medrano, R., Xoconostle-Cazares, B., and Kragler, F. (2004). The plasmodesmatal transport pathway for homeotic proteins, silencing signals and viruses. *Current Opinion in Plant Biology* 7, 641-650.

Ryu, K.H., Kang, Y.H., Park, Y., Hwang, I., Schiefelbein, J., and Lee, M.M. (2005). The WEREWOLF MYB protein directly regulates CAPRICE transcription during cell fate specification in the *Arabidopsis* root epidermis. *Development* 132, 4765-4775.

- Sabatini, S., Heidstra, R., Wildwater, M., and Scheres, B.** (2003). SCARECROW is involved in positioning the stem cell niche in the Arabidopsis root meristem. *Genes & Development* 17, 354-358.
- Sachs, T.** (1991). Cell polarity and tissue patterning in plants. *Development* 113, 83-93.
- Santoni V, Molloy M and Rabilloud T** (2000) Membrane proteins and proteomics: Un amour impossible? *Electrophoresis* 21, 1054-1070.
- Saravanan, R.S., Slabaugh, E., Singh, V.R., Lapidus, L.J., Haas, T., and Brandizzi, F.** (2009). The targeting of the oxysterol-binding protein ORP3a to the endoplasmic reticulum relies on the plant VAP33 homolog PVA12. *The Plant Journal* 58, 817-830.
- Schaffer, R., Landgraf, J., Accerbi, M., Simon, V., Larson, M., and Wisman, E.** (2001). Microarray Analysis of Diurnal and Circadian-Regulated Genes in Arabidopsis. *The Plant Cell Online* 13, 113-123.
- Schaller, H.** (2003). The role of sterols in plant growth and development. *Progress in Lipid Research* 42, 163-175.
- Schellmann, S., Schnittger, A., Kirik, V., Wada, T., Okada, K., Beermann, A., Thumfahrt, J., Jürgens, G., and Hülskamp, M.** (2002). TRIPTYCHON and CAPRICE mediate lateral inhibition during trichome and root hair patterning in Arabidopsis. *EMBO Journal*. 21, 5036-5046.
- Scheres, B., Wolkenfelt, H., Willemsen, V., Terlouw, M., Lawson, E., Dean, C. and Weisbeek, P.** (1994). Embryonic origin of the *Arabidopsis* primary root and root meristem initials. *Development* 120, 2475-2487.
- Schiefelbein, J., Kwak, S.H., Wieckowski, Y., Barron, C., and Bruex, A.** (2009). The gene regulatory network for root epidermal cell-type pattern formation in Arabidopsis. *Journal of Experimental Botany* 60, 1515-1521.
- Schiefelbein, J.W., and Somerville, C.** (1990). Genetic Control of Root Hair Development in Arabidopsis thaliana. *The Plant Cell Online* 2, 235-243.
- Schmelzer, E., Jahnen, W., and Hahlbrock, K.** (1988). In situ localization of light-induced chalcone synthase mRNA, chalcone synthase, and flavonoid end products in epidermal cells of parsley leaves. *Proceedings of the National Academy of Sciences* 85, 2989-2993.

Schreiber, S., Konradt, M., Groll, C., Scheid, P., Hanauer, G., Werling, H.-O., Josenhans, C., and Suerbaum, S. (2004). The spatial orientation of *Helicobacter pylori* in the gastric mucus. *Proceedings of the National Academy of Sciences of the United States of America* *101*, 5024-5029.

Schrick, K., DeBolt, S., and Bulone, V. (2012). Deciphering the molecular functions of sterols in cellulose biosynthesis. *Frontiers in Plant Science* *3*.

Schrick, K., Mayer, U., Horrichs, A., Kuhnt, C., Bellini, C., Dangl, J., Schmidt, J., and Jürgens, G. (2000). FACKEL is a sterol C-14 reductase required for organized cell division and expansion in *Arabidopsis* embryogenesis. *Genes & Development* *14*, 1471-1484.

Schrick, K., Mayer, U., Martin, G., Bellini, C., Kuhnt, C., Schmidt, J., and Jürgens, G. (2002). Interactions between sterol biosynthesis genes in embryonic development of *Arabidopsis*. *The Plant Journal* *31*, 61-73.

Schrick, K., Nguyen, D., Karlowski, W., and Mayer, K. (2004). START lipid/sterol-binding domains are amplified in plants and are predominantly associated with homeodomain transcription factors. *Genome Biology* *5*, R41.

Schulz, J.D., Hawkes, E.L., and Shaw, C.A. (2006). Cycad toxins, *Helicobacter pylori* and parkinsonism: Cholesterol glucosides as the common denominator. *Medical Hypotheses* *66*, 1222-1226.

Schwacke, R., Schneider, A., van der Graaff, E., Fischer, K., Catoni, E., Desimone, M., Frommer, W.B., Flugge, U.I. and Kunze, R. (2003) ARAMEMNON, a Novel Database for *Arabidopsis* Integral Membrane Proteins. *Plant Physiology* *131*, 16-26.

Shaner, N.C., Campbell, R.E., Steinbach, P.A., Giepmans, B.N.G., Palmer, A.E., and Tsien, R.Y. (2004). Improved monomeric red, orange and yellow fluorescent proteins derived from *Discosoma* sp. red fluorescent protein. *Nat Biotech* *22*, 1567-1572.

Shaner, N.C., Steinbach, P.A., and Tsien, R.Y. (2005). A guide to choosing fluorescent proteins. *Nat Meth* *2*, 905-909.

Sherameti, I., Venus, Y., Drzewiecki, C., Tripathi, S., Dan, V.M., Nitz, I., Varma, A., Grundler, F.M. and Oelmüller, R. (2008) PYK10, a β -glucosidase located in the endoplasmatic reticulum, is crucial for the beneficial interaction between *Arabidopsis thaliana* and the endophytic fungus *Piriformospora indica*. *The Plant Journal* *54*, 428-439.

- Shogomori, H., and Brown, D.A.** (2003). Use of Detergents to Study Membrane Rafts: The Good, the Bad, and the Ugly. In *Biological Chemistry*, pp. 1259.
- Simons, K., and Ikonen, E.** (1997). Functional rafts in cell membranes. *Nature* **387**, 569-572.
- Siddique, M., Gernhard, S., von Koskull-Döring, P., Vierling, E., and Scharf, K.D.** (2008). The plant sHSP superfamily: five new members in *Arabidopsis thaliana* with unexpected properties. *Cell Stress and Chaperones* **13**, 183-197.
- Simons K and Ikonen E** (1997) Functional rafts in cell membranes. *Nature* **387**:569-572.
- Simons, K., and Toomre, D.** (2000). Lipid rafts and signal transduction. *Nat Rev Mol Cell Biol* **1**, 31-39.
- Simpson, J.C., Neubrand, V.E., Wiemann, S., and Pepperkok, R.** (2001). Illuminating the human genome. *Histochem Cell Biol* **115**, 23-29.
- Simpson, F., Kerr, M.C., and Wicking, C.** (2009). Trafficking, development and hedgehog. *Mechanisms of Development* **126**, 279-288.
- Singer, S.J., and Nicolson, G.L.** (1972). The Fluid Mosaic Model of the Structure of Cell Membranes. *Science* **175**, 720-731.
- Slaughter B.D., Smith S.E. and Li, R.** (2009). Symmetry breaking in the life cycle of the budding yeast. *Cold Spring Harb. Perspect. Biol.* **1**, a003384.
- Slimane, T.A.t., Trugnan, G., van IJzendoorn, S.C.D., and Hoekstra, D.** (2003). Raft-mediated Trafficking of Apical Resident Proteins Occurs in Both Direct and Transcytotic Pathways in Polarized Hepatic Cells: Role of Distinct Lipid Microdomains. *Molecular Biology of the Cell* **14**, 611-624.
- Souter, M., Pullen, M., Topping, J., Zhang, X., and Lindsey, K.** (2004). Rescue of defective auxin-mediated gene expression and root meristem function by inhibition of ethylene signalling in sterol biosynthesis mutants of *Arabidopsis*. *Planta* **219**, 773-783.
- Souter, M., Topping, J., Pullen, M., Friml, J., Palme, K., Hackett, R., Grierson, D., and Lindsey, K.** (2002). *hydra* Mutants of *Arabidopsis* Are Defective in Sterol Profiles and Auxin and Ethylene Signaling. *The Plant Cell Online* **14**, 1017-1031.
- Stefano, G., Renna, L., Moss, T., McNew, J.A., and Brandizzi, F.** (2012). In *Arabidopsis*, the spatial and dynamic organization of the endoplasmic reticulum

and Golgi apparatus is influenced by the integrity of the C-terminal domain of RHD3, a non-essential GTPase. *The Plant Journal* 69, 957-966.

Stonebloom, S., Burch-Smith, T., Kim, I., Meinke, D., Mindrinos, M., and Zambryski, P. (2009). Loss of the plant DEAD-box protein ISE1 leads to defective mitochondria and increased cell-to-cell transport via plasmodesmata. *Proceedings of the National Academy of Sciences* 106, 17229-17234.

Storey, J.D., and Tibshirani, R. (2003). Statistical significance for genomewide studies. *Proceedings of the National Academy of Sciences* 100, 9440-9445.

Summers, D.W., Douglas, P.M., Ramos, C.H.I., and Cyr, D.M. (2009). Polypeptide transfer from Hsp40 to Hsp70 molecular chaperones. *Trends in Biochemical Sciences* 34, 230-233.

Szymanski, D.B., Jilk, R.A., Pollock, S.M., and Marks, M.D. (1998). Control of GL2 expression in Arabidopsis leaves and trichomes. *Development* 125, 1161-1171.

Tabata, R.C., Wilson, J.M.B., Ly, P., Zwiegers, P., Kwok, D., Van Kampen, J.M., Cashman, N., and Shaw, C.A. (2008). Chronic Exposure to Dietary Sterol Glucosides is Neurotoxic to Motor Neurons and Induces an ALS-PDC Phenotype. *Neuromol Med* 10, 24-39.

Takeshita, N., Higashitsuji, Y., Konzack, S. and Fischer, R. (2008). Apical sterol-rich membranes are essential for localizing cell end markers that determine growth directionality in the filamentous fungus *Aspergillus nidulans*. *Mol. Biol. Cell* 19, 339-351.

Tansey, T.R., and Shechter, I. (2000). Squalene synthase: Structure and regulation. In *Progress in Nucleic Acid Research and Molecular Biology* (Academic Press), pp. 157-195.

ten Hove, C.A., Willemsen, V., de Vries, W.J., van Dijken, A., Scheres, B., and Heidstra, R. (2010). SCHIZORIZA Encodes a Nuclear Factor Regulating Asymmetry of Stem Cell Divisions in the Arabidopsis Root. *Current Biology* 20, 452-457.

Testerman, T.L., McGee, D.J., and Mobley, H.L.T. (2001). Helicobacter pylori Growth and Urease Detection in the Chemically Defined Medium Ham's F-12 Nutrient Mixture. *Journal of Clinical Microbiology* 39, 3842-3850.

Tilsner, J., Amari, K., and Torrance, L. (2011). Plasmodesmata viewed as specialised membrane adhesion sites. *Protoplasma* 248, 39-60.

Tian, G.-W., Mohanty, A., Chary, S.N., Li, S., Paap, B., Drakakaki, G., Kopec, C.D., Li, J., Ehrhardt, D., Jackson, D., Rhee, S.Y., Raikhel, N.V., and Citovsky, V. (2004). High-Throughput Fluorescent Tagging of Full-Length Arabidopsis Gene Products in Planta. *Plant Physiology* 135, 25-38.

Tissi eres, A., Mitchell, H.K., and Tracy, U.M. (1974). Protein synthesis in salivary glands of *Drosophila melanogaster*: Relation to chromosome puffs. *Journal of Molecular Biology* 84, 389-398.

Toei, M., Saum, R. and Forgac, M. (2010) Regulation and Isoform Function of the V-ATPases. *Biochemistry* 49, 4715-4723.

Topping, J.F., May, V.J., Muskett, P.R. and Lindsey, K. (1997). Mutations in the HYDRA1 gene of *Arabidopsis* perturb cell shape and disrupt embryonic and seedling morphogenesis. *Development* 124, 4415-4424.

Turturici, G., Sconzo, G., and Geraci, F. (2011). Hsp70 and Its Molecular Role in Nervous System Diseases. *Biochemistry Research International* 2011, 18.

Tzfira, T., Tian, G.-W., Lacroix, B.t., Vyas, S., Li, J., Leitner-Dagan, Y., Krichevsky, A., Taylor, T., Vainstein, A., and Citovsky, V. (2005). pSAT vectors: a modular series of plasmids for autofluorescent protein tagging and expression of multiple genes in plants. *Plant Mol Biol* 57, 503-516.

Uemura, M., and Steponkus, P.L. (1994). A Contrast of the Plasma Membrane Lipid Composition of Oat and Rye Leaves in Relation to Freezing Tolerance. *Plant Physiology* 104, 479-496.

Ullmann, P., Ury, A., Rimmel, P., Benveniste, P., and Bouvier-Nav e, P. (1993). UDP-glucose sterol β -d-glucosyltransferase, a plasma membrane-bound enzyme of plants: Enzymatic properties and lipid dependence. *Biochimie* 75, 713-723.

Umate, P. (2011). Oxysterol binding proteins (OSBPs) and their encoding genes in *Arabidopsis* and rice. *Steroids* 76, 524-529.

Van Norman, J.M., Breakfield, N.W., and Benfey, P.N. (2011). Intercellular Communication during Plant Development. *The Plant Cell Online* 23, 855-864.

Voigt, B., Timmers, T., Samaj, J., M uller, J., Baluska, F. and Menzel, D. (2005). GFP-FABD2 fusion construct allows *in vivo* visualization of the dynamic actin cytoskeleton in all cells of *Arabidopsis* seedlings. *Eur. J. Cell Biol.* 84, 595-608.

Wachtler, V. and Balasubramanian, M.K. (2006). Yeast lipid rafts? An emerging view. *Trends Cell Biol.* 16, 1-4.

Wada, T., Kurata, T., Tominaga, R., Koshino-Kimura, Y., Tachibana, T., Goto, K., Marks, M.D., Shimura, Y., and Okada, K. (2002). Role of a positive regulator of root hair development, CAPRICE, in Arabidopsis root epidermal cell differentiation. *Development* 129, 5409-5419.

Wada, T., Tachibana, T., Shimura, Y., and Okada, K. (1997). Epidermal Cell Differentiation in Arabidopsis Determined by a Myb Homolog, CPC. *Science* 277, 1113-1116.

Walhout, A.J.M., Temple, G.F., Brasch, M.A., Hartley, J.L., Lorson, M.A., van den Heuvel, S., and Vidal, M. (2000). GATEWAY recombinational cloning: Application to the cloning of large numbers of open reading frames or ORFeomes. In *Methods in Enzymology*, S.D.E. Jeremy Thorner, and N.A. John, eds. (Academic Press), pp. 575-IN577.

Walsh, P., Bursac, D., Law, Y.C., Cyr, D., and Lithgow, T. (2004). The J-protein family: modulating protein assembly, disassembly and translocation. *EMBO Rep* 5(6), 567-571.

Wan, L., Ross, A.R.S., Yang, J., Hegedus, D.D., and Kermod, A.R. (2007). Phosphorylation of the 12 S globulin cruciferin in wild-type and *abi1-1* mutant Arabidopsis thaliana (thale cress) seeds. *Biochem J* 404, 247-256.

Warnecke, D., Baltrusch, M., Buck, F., Wolter, F., and Heinz, E. (1997). UDP-glucose:sterol glucosyltransferase: cloning and functional expression in Escherichia coli. *Plant Mol Biol* 35, 597-603.

Warnecke, D., Erdmann, R., Fahl, A., Hube, B., Muller, F., Zank, T., Zahringer, U., and Heinz, E. (1999). Cloning and Functional Expression of UGT Genes Encoding Sterol Glucosyltransferases from Saccharomyces cerevisiae, Candida albicans, Pichia pastoris, and Dictyostelium discoideum. *Journal of Biological Chemistry* 274, 13048-13059.

Warnecke, D.C., and Heinz, E. (1994). Purification of a Membrane-Bound UDP-Glucose: Sterol [β]-D-Glucosyltransferase Based on Its Solubility in Diethyl Ether. *Plant Physiology* 105, 1067-1073.

Welch, D., Hassan, H., Blilou, I., Immink, R., Heidstra, R., and Scheres, B. (2007). Arabidopsis JACKDAW and MAGPIE zinc finger proteins delimit asymmetric cell division and stabilize tissue boundaries by restricting SHORT-ROOT action. *Genes & Development* 21, 2196-2204.

- Wewer, V., Dombrink, I., vom Dorp, K., and Dormann, P.** (2011). Quantification of sterol lipids in plants by quadrupole time-of-flight mass spectrometry. *Journal of Lipid Research* 52, 1039-1054.
- Willemsen, V., Friml, J., Grebe, M., van den Toorn, A., Palme, K. and Scheres, B.** (2003). Cell Polarity and PIN Protein Positioning in Arabidopsis Require STEROL METHYLTRANSFERASE1 Function. *Plant Cell* 15, 612-625.
- Winter, D., Vinegar, B., Nahal, H., Ammar, R., Wilson, G.V., and Provart, N.J.** (2007). An "Electronic Fluorescent Pictograph" Browser for Exploring and Analyzing Large-Scale Biological Data Sets. *PLoS ONE* 2, e718.
- Wojciechowski, Z.A., ed.** (1991). *Biochemistry of phytosterol conjugates* (American Oil Chemists' Society, Champaign).
- Wojciechowski, Z.A., and Van Uon, N.** (1975). Intracellular localization and some properties of UDPG : sterol glucosyltransferase from *Calendula officinalis*. *Acta Biochimica Polonica* 22, 25-38.
- Wojciechowski, Z.A., and Zimowski, J.** (1975). Acyl composition and biosynthesis of acylated sterol glucosides in *Calendula officinalis*. *Biochimica et Biophysica Acta (BBA) - Lipids and Lipid Metabolism* 398, 111-117.
- Wojciechowski, Z.A., Zimowski, J., Zimowski, J.G., and Lyżnik, A.** (1979). Specificity of sterol-glucosylating enzymes from *Sinapis alba* and *Physarum polycephalum*. *Biochimica et Biophysica Acta (BBA) - Enzymology* 570, 363-370.
- Won, S.-K., Lee, Y.-J., Lee, H.-Y., Heo, Y.-K., Cho, M., and Cho, H.-T.** (2009). cis-Element- and Transcriptome-Based Screening of Root Hair-Specific Genes and Their Functional Characterization in Arabidopsis. *Plant Physiology* 150, 1459-1473.
- Wunder, C., Churin, Y., Winau, F., Warnecke, D., Vieth, M., Lindner, B., Zahringer, U., Mollenkopf, H.-J., Heinz, E., and Meyer, T.F.** (2006). Cholesterol glucosylation promotes immune evasion by *Helicobacter pylori*. *Nat Med* 12, 1030-1038.
- Woodman, P.G.** (2003) p97, a protein coping with multiple identities. *Journal of Cell Science* 116, 4283-4290.
- Yang, K.-Z., Xia, C., Liu, X.-L., Dou, X.-Y., Wang, W., Chen, L.-Q., Zhang, X.-Q., Xie, L.-F., He, L., Ma, X., and Ye, D.** (2009). A mutation in THERMOSENSITIVE MALE STERILE 1, encoding a heat shock protein with DnaJ and PDI domains, leads to thermosensitive gametophytic male sterility in Arabidopsis. *The Plant Journal* 57, 870-882.

Yoshida, S. and Uemura, M. (1986). Lipid composition of plasma membranes and tonoplasts isolated from etiolated seedlings of mung bean (*Vigna radiata* L.). *Plant Physiol.* 82, 807-812.

Zambryski, P., and Crawford, K. (2000). PLASMODESMATA: Gatekeepers for Cell-to-Cell Transport of Developmental Signals in Plants. *Annual Review of Cell and Developmental Biology* 16, 393-421.

Zhang, J., Campbell, R.E., Ting, A.Y., and Tsien, R.Y. (2002). Creating new fluorescent probes for cell biology. *Nat Rev Mol Cell Biol* 3, 906-918.

Zhang, F., Gonzalez, A., Zhao, M., Payne, C.T., and Lloyd, A. (2003). A network of redundant bHLH proteins functions in all TTG1-dependent pathways of Arabidopsis. *Development* 130, 4859-4869.

Zhu, T., O'Quinn, R.L., Lucas, W.J., and Rost, T.L. (1998). Directional cell-to-cell communication in the Arabidopsis root apical meristem II. Dynamics of plasmodesmatal formation. *Protoplasma* 204, 84-93.

Zimowski, J. (1992). Specificity and some other properties of cytosolic and membranous udpglc: 3- β -hydroxysteroid glucosyltransferases from *Solanum tuberosum* leaves. *Phytochemistry* 31, 2977-2981.

Vita

Name: Meera Nair

Place of birth: Alleppey, Kerala, India

Education:

2003 – 2007: Bachelor of Technology in Biotechnology

School of Bio Sciences and Technology

Vellore Institute of Technology University, Tamil Nadu, India

Scholastic and professional honors:

2012 and 2013: NSF Travel Fellowship

2008-2009: University of Kentucky, International Student Tuition Scholarship

Publications:

Petti C, **Nair M**, DeBolt S (2014). The involvement of J-protein AtDjC17 in root development in Arabidopsis. *Frontiers Plant Science*. **5**: 532.

Banerjee J., Magnani R., **Nair M.**, Dirk M. L., DeBolt S., Maiti B. M., and Houtz L. R., (2013). Calmodulin-mediated signal transduction pathways in Arabidopsis are fine-tuned by methylation. *Plant Cell*. **25** (4493-4511).

DeBolt S, Scheible W-Rd, Schrick K, Auer M, Beisson F, Bischoff V, Bouvier-Navé P, Carroll A, Hematy K, Li Y, Milne J, **Nair M**, Schaller H, Zemla M, Somerville C (2009) Mutations in UDP-Glucose:Sterol Glucosyltransferase in Arabidopsis Cause Transparent Testa Phenotype and Suberization Defect in Seeds. *Plant Physiology* **151**: 78-87.

Books and peer-reviewed book chapters:

Meera Nair and Seth DeBolt (2011) Analysing cellulose biosynthesis with confocal microscopy. In *The Plant Cell wall methods and protocols* (Popper ZA, ed), Springer Protocols, Humana Press.